(1)

DOT/FAA/RD-93/40, II

Research and Development
Service
Washington, D.C. 20591

Synthetic Vision Technology Demonstration

Volume 2 of 4
Sensor Tower Testing

Brian H. Hudson, GTRI
Molly J. Gary, GTRI
Malcolm A. Burgess, FAA
J. Allen Zak, Hughes-STX

Synthetic Vision Program Office
Federal Aviation Administration

December 1993

Final Report

U.S. Department of Transportation
Federal Aviation Administration

U.S. Department of Defense

NOTICE

Technical Report Documentation Page

1. Report No.	2. Government Accession No.	3. Recipient's Catalog No.
DOT/FAA/RD-93/40,, II		

4. Title and Subtitle	5. Report Date
SYNTHETIC VISION TECHNOLOGY DEMONSTRATION (4 VOLUMES) Volume II -- Sensor Tower Testing	DECEMBER 1993
	6. Performing Organization Code ARD-100
7. Author(s) Brian H. Hudson, Molly J. Gary, Malcolm A. Burgess, J. Allen Zak	8. Performing Organization Report No.
9. Performing Organization Name and Address SYNTHETIC VISION PROGRAM OFFICE FEDERAL AVIATION ADMINISTRATION 800 Independence Avenue, S. W. Washington, DC 20591	10. Work Unit No. (TRAIS) 11. Contract or Grant No. 13. Type of Report and Period Covered FINAL REPORT
12. Sponsoring Agency Name and Address RESEARCH AND DEVELOPMENT SERVICES FEDERAL AVIATION ADMINISTRATION 800 Independence Avenue, S.W. Washington, DC 20591	14. Sponsoring Agency Code ARD-1

15. Supplementary Notes

CO SPONSER: Control Systems Division
USAF Wright Laboratory
Wright-Patterson AFB, OHIO 45433-7521

16. Abstract

This report contains the description and results of a Synthetic Vision technology demonstration program conducted jointly by the Federal Aviation Administration, the Department of Defense and industry. The relevant technologies including millimeter wave radar sensors, infrared sensors, head-up displays, and computer processing were developed and tested in static tower tests and in flight tests in which the weather conditions were carefully measured and documented. The purpose of the program was to evaluate and demonstrate the performance of the imaging sensors and of the complete imaging system during aircraft approaches and landings in low-visibility conditions.

The static tower test facility used was the Avionics Tower Test Facility, located at Wright Patterson AFB, in which candidate sensors were set up at approximately 260 feet overlooking a nearby runway. The runway scene imaged by the sensors was instrumented to carefully measure the characteristics of fog, rain and snow as those conditions occurred in 1991-1992. Sensor performance and phenomenology was then fully characterized to provide a basis for further sensor development and for selection of sensors with which to proceed to flight test.

The test aircraft used was a Gulfstream II configured with a comprehensive data collection system and instrumentation to permit measurement of fog and precipitation through which the aircraft was flown as well as system and pilot performance during those operations. Millimeter wave sensors and an infrared sensor were used to provide an electronic image of the runway on both head-up and head-down displays during approach, landing and takeoff. Test and demonstration flights were flown into 27 difference airports in a wide variety of rain, fog and snow conditions during the period of May through December, 1992.

17. Key Words	18. Distribution Statement
SYNTHETIC VISION FLIGHT TEST MMW RADAR	Document of available to the public through the National Technical Information Service, Springfield, VA 22161

19. Security Classif. (of this report)	20. Security Classif. (of this page)	21. No. of Pages	22. Price
Unclassified	Unclassified	290	

Form DOT F 1700.7 (8-72) Reproduction of completed page authorized

TABLE OF CONTENTS

TABLE OF CONTENTS (CONT.)

TABLE OF CONTENTS (CONT.)

TABLE OF CONTENTS (CONT.)

LIST OF ILLUSTRATIONS

LIST OF ILLUSTRATIONS (CONT.)

LIST OF ILLUSTRATIONS (CONT.)

LIST OF TABLES

ACKNOWLEDGMENTS

The work described in this report, Sensor Tower Tests, Volume 2 of the Final Report of the Synthetic Vision Technology Demonstration Program, was accomplished by talented individuals of a number of organizations in industry and the government. The major efforts of the Sensor Tower Tests were the work of Georgia Tech Research Institute (GTRI), the Air Force Wright Laboratory, the sensor manufacturers Honeywell, Kodak, Lear Astronics, and Norden, and the FAA Synthetic Vision Program Office.

The lead engineer for the GTRI effort was Brian Hudson who developed and implemented the technical approach and led the methods of test, data acquistion and analyses. He was ably supported by Molly Gary in organizing the data base and analyses of radar performance, Morris Hetzler in analyses of IR sensor performance and modeling, and by John Trostel in analyses of meteorological data. Jeffrey Smart provided the expertise in the design and implementation of the data acquistion software. Patricia Ryan contributed the scene modeling effort while Samuel Piper developed the MMW radar performance estimation.

Captain Jeffrey Campbell of the Wright Laboratory Control Systems Development and Applications Branch ably carried out the test director's responsibilities in setting up and conducting the tests day-to-day, assisted by George Guiterrez and many others of the Laboratory staff. Ralph Guth of the Laboratory contibuted substantially in seeing to it that the technical as well as the management details were looked after.

Lieutenant Colonel Dale Dunford was assigned by the Air Force Wright Laboratory to the FAA Synthetic Vision Program Office for the duration of the Program and contributed substantially to the leadership required in organizing and carrying out the efforts of many diverse organizations in the conduct of the tests. J. Allen Zak of the Program Office was also instrumental in designing and implementing the meteorological instrumentation required for the tests and in obtaining the required meteorological data from the Air Force and National Weather Service.

Lavell Jordan and Jeffrey Radkey of the Honeywell Systems Research Center led the Honeywell team in designing, building and testing of their MMW radar sensor in record time. Yair Alon was the lead engineer for the design, development and testing of the Lear Astronics MMW sensor. Harold Hannan and Stanley Ekiert were instrumental in providing the Eastman Kodak infrared sensor for testing. Lester Kosowsky was instrumental in providing the Norden MMW radar sensor for testing.

SECTION 1
INTRODUCTION

1.1 BACKGROUND

In 1988 the Federal Aviation Administration (FAA), in cooperation with industry, the United States Air Force (USAF), the Navy, and several other government organizations initiated an effort to demonstrate the capabilities of existing technologies to provide an image of the runway and surrounding environment for pilots operating aircraft in low visibility conditions. This effort was named the Synthetic Vision Technology Demonstration (SVTD) program. Its goal was to document and demonstrate aircraft sensor and system performance achieved with pilots using millimeter wave (MMW) radar sensors, a forward-looking infrared (FLIR) sensor, and a head-up display (HUD).

There are several "windows" in the electromagnetic frequency spectrum where molecular absorption due to water vapor and other gases is lowest. One such region is the visible portion of the spectrum which we know from our visual experience. Other minimum absorption regions occur in the infrared and MMW regions. When the effects of water drops are added, such as rain and fog, then the higher frequency-short wavelength portions of the spectrum are much less useful. Two frequencies in the MMW portion of the spectrum - 35 and 94 GHz - appear to offer significant promise for the synthetic vision application and thus radar sensors operating at these frequencies were investigated under the program. A platinum silicide 3-5 micron infrared camera was also investigated.

The operational concept was that these on-board sensors would provide a real-time image of the runway to the pilot which would be combined with symbology and alphanumerics and displayed on the HUD. The pilot would then have all of the information needed on the display to land, taxi, and roll out in low visibility conditions. Two major parts of the project involved testing of the sensors in measured conditions on a tower overlooking an unused airfield, and testing sensor and pilot performance via a prototype system installed in a test aircraft.

This is Volume 2 of a four volume final report on the Synthetic Vision Technology Demonstration Program. This Volume documents the Tower Tests performed in the Program and was written largely by the Georgia Tech Research Institute participants who were enlisted to provide an independent assessment of the performance of the sensors. Volume 1 provides an Executive summary containing an overview of the work from a management perspective and a

summary of the results of the work performed. Volume 3 documents the Flight Tests performed in the program, incorporating reports from all of the participants including TRW, Georgia Tech Research Institute, the sensor and display manufacturers, the technical consultants to the program, and the Program Office. Volume 4 is a compilation of appendices containing additional detail pertaining to the Flight Tests.

1.2 TOWER TEST OBJECTIVES

In the tower test effort, selected millimeter wave (MMW) radar, and passive infrared (IR) imaging sensors were mounted on a fixed tower at Wright-Patterson Air Force Base (AFB), Ohio and used to statically image a runway area under varied meteorological conditions of clear, fog, rain, and snow. The sensor data and meteorological data recorded were then analyzed to determine the performance of the selected MMW and IR imaging sensors in a controlled test environment. The tower test objectives were to

- Calibrate the test sensors to engineering standards,
- Collect a sensor performance data base,
- Establish baseline sensor performance in clear weather,
- Analyze sensor performance in low visibility weather, and
- Determine the sensors' suitability for flight testing.

All of these objectives were met during the 12-month tower test period.

1.3 SUPPORT TASK

The Georgia Tech Research Institute (GTRI) supported the successful tower testing of six different millimeter wave (MMW) radar sensor configurations and two infrared (IR) sensors at Wright-Patterson AFB during Fiscal Year 91-92. The tests were conducted according to a published test methodology (the Test Plan is at Appendix G) and under the direction of the U.S. Air Force (USAF) technical monitor. An automated data collection system was developed to record test scene data from MMW and IR sensors. Data reduction and analysis techniques were established and implemented to extract sensor performance measures from the test sensor and meteorological data. A MMW sensor performance model was developed and exercised to contribute data for correlation with measured results. Project results were documented in monthly progress reports, thirty technical memoranda, three presentations at two Federal Aviation Administration (FAA) conferences, and papers at two industry symposia. The project schedule is shown in Figure 1.

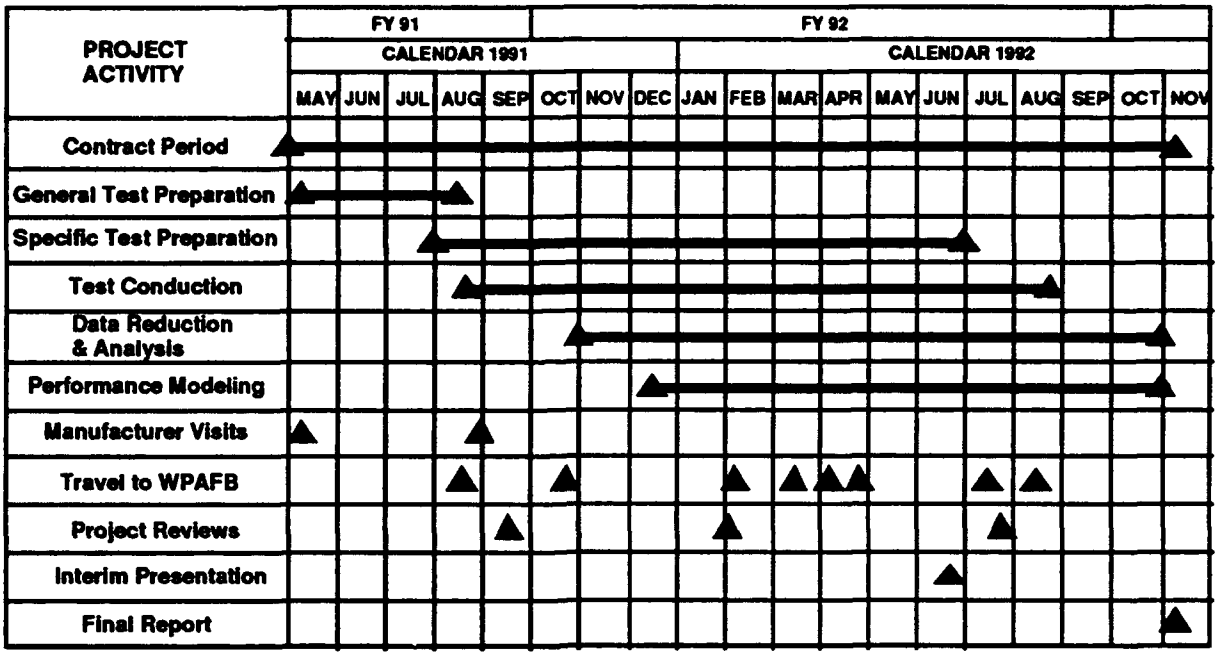

Figure 1. Project schedule.

1.4 TECHNICAL APPROACH

Sensor test data management, from collection through analysis, was the primary responsibility of the Tower Test Contractor (TTC). Figure 2 is a block diagram of the data management process. Data from the test sensors and meteorological sensors were recorded by the appropriate data acquisition system (DAS) and then made available for quick-look data analysis. In the data reduction process, the collected sensor data were calibrated against reference standards appropriate to each sensor technology. The calibrated data were correlated with meteorological and ground truth data supplied by the Air Force during the test periods, and a determination was made as to the sensor's performance under those environmental conditions. These test results will contribute to the available scientific data on adverse weather penetration by electromagnetic imaging sensors. Data items include the unprocessed (raw) and preprocessed (calibrated) sensor data, meteorological data, scene images generated from the sensor data, and performance comparison results. Data formats include computer disks and tapes, video tape recordings, evaluation tables and curves, photographs, and written reports.

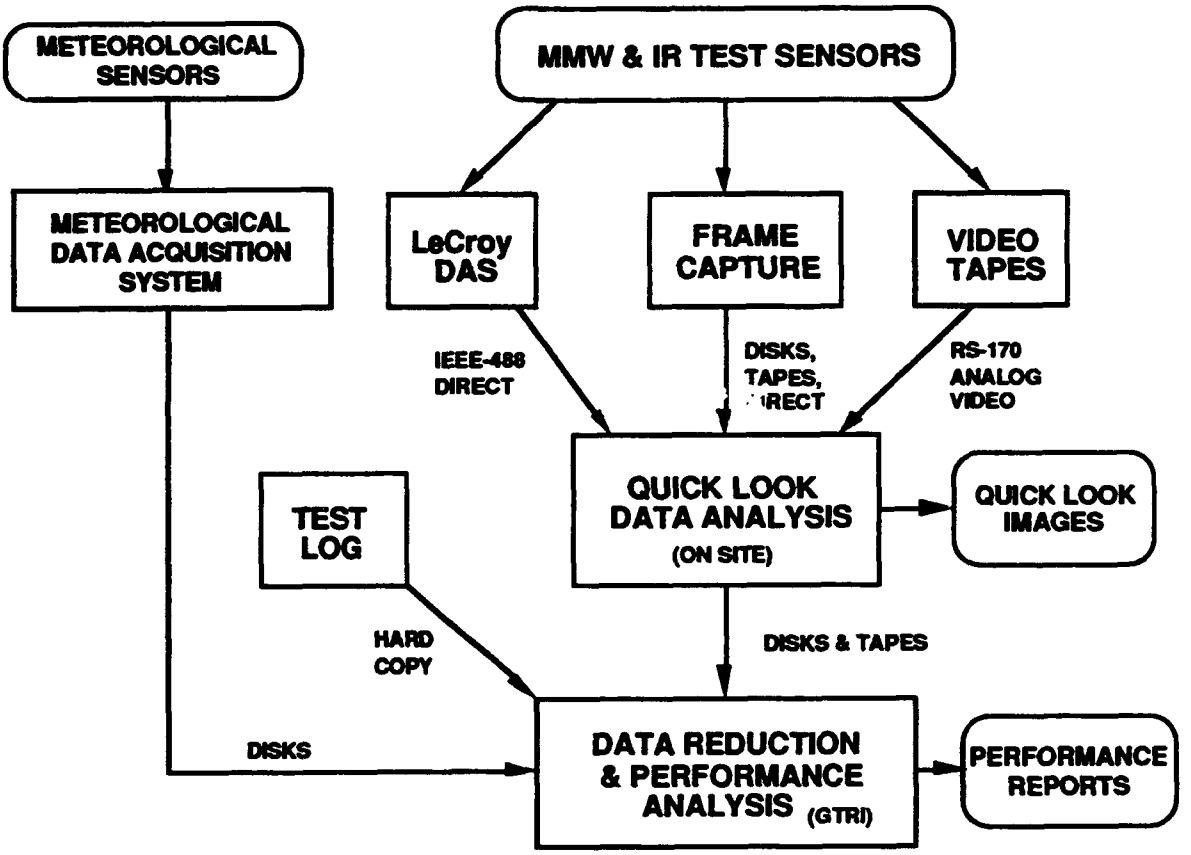

Figure 2. Data flow diagram.

SECTION 2
TASK DEVELOPMENT

2.1 PROBLEM TO BE SOLVED

The following text was taken from the Tower Test Plan (Appendix G) and defines the problem addressed in the Synthetic Vision Program.

> One of the major limitations of aircraft is the difficulty of conducting terminal area operations in adverse weather environments. Conditions involving high, gusting, or rapidly changing winds may impose almost insurmountable physical restrictions, however, operations in fog, rain, snow, smoke and haze are limited primarily by the lack of pilot vision. At established airports the visibility limitation for approach and landing operations is partially overcome by the excellent landing guidance systems now available albeit very expensive, but at unequipped facilities and for specialized missions, the pilot must still rely primarily on his ability to see. Also, aircraft taxi and ground operations are severely hampered by low visibility conditions with no current operational systems available to assist the pilot.
>
> In the recent past, several programs have undertaken to augment the pilots' vision by providing them with a real-time forward view generated by video systems such as Low Light Level Television and Infrared Cameras. One series of experiments was conducted with a millimeter wavelength (MMW) imaging system. At least one of these systems is now being applied in different forms on specialized aircraft. The advent of the Head Up Display where the images can be superimposed over the outside scene, along with new advances in imaging technology have caused renewed interest in using imaging sensors to augment pilot vision.
>
> Results from these experiments along with simulations and other studies have indicated that those imaging sensors operating in the MMW band offer the best weather penetration capability but, in practice, exhibit limited resolution (due to practical antenna aperture limits). Those operating in the Infrared (and visible) wavelengths show good resolution but appear to have comparatively poor weather penetration. Choice of the sensor system features, i.e., wavelength, for a particular application, therefore, involves compromises which are best resolved by a scientifically documented comparison of the performance of the systems in relevant weather scenarios.

2.2 TOWER TEST TASKS

The following text, also taken from the Tower Test Plan (Appendix G) further defines the Tower Test program objective.

> The program objective is to conduct a carefully documented comparative evaluation of existing brassboard or prototype imaging sensors under low visibility weather conditions and to establish a sensor performance baseline providing a benchmark of the capability for the technology state for use by the operational, manufacturing, and regulatory elements of the aviation community. This work, to be accomplished in an instrumented tower test facility and range, involves collection of sensor output data (sensor performance and imagery) and atmospheric parameters which characterize the visibility between the sensor and various targets being viewed. The data analysis and evaluation results will be based on analyses of sensor performance data (and, if available, processed image quality) and meteorological data collected by the government in low visibility weather conditions caused by fog, rain, and snow (with and without accumulation).

The objectives of sensor performance analysis were to reduce the collected imaging sensor data and corresponding meteorological data, extract performance figure of merit (FOM) data, and correlate reduced weather data with extracted FOM data to measure sensor performance in weather. Additionally, the sensor data were processed to extract basic engineering data, such as normalized radar cross section (RCS) of grass clutter, atmospheric attenuation, and volumetric RCS of precipitation. These engineering data will support future radar sensor performance estimations. Mathematical models of sensor performance in weather were exercised to predict sensor performance prior to testing and to develop modeled performance data for comparison with the measured sensor data. A computerized sensor performance data base, containing the sensor FOM and reduced weather data, was developed to automate data correlation and results presentation process.

SECTION 3
TEST PLANNING

3.1 TEST REQUIREMENTS

A Method of Test (MOT) document was prepared in July 1991 to describe the data collection, calibration, and analysis methodology for the MMW radar sensor tower tests. The Air Force added the MOT to the Tower Test Plan as Appendix A. In January 1992, a similar IR MOT, titled "Test Plan for Infrared Sensors." was added to the Tower Test Plan. The IR MOT addressed the measurement and performance data analysis requirements for the IR sensors being tested at the tower facility.

3.1.1 SENSOR SELECTION

3.1.1.1 MMW Radar Sensors

A millimeter-wave (MMW) radar sensor exploits the differences in radar cross section between paved runway and bordering grass surface areas to image a runway scene, as shown in Figure 3. Radar cross section (RCS) is a measure of a target's ability to reflect radar waves. At the low incident angles encountered by an synthetic vision (SV) radar, most of the radar illumination energy is forward scattered from the smooth, low-RCS runway, and very little is backscattered to the radar receiver. The "rougher" grass areas have medium RCS and return a higher portion of the incident radar energy. A radar reflector is designed specifically to have high RCS and backscatters a large portion of the incident radar energy.

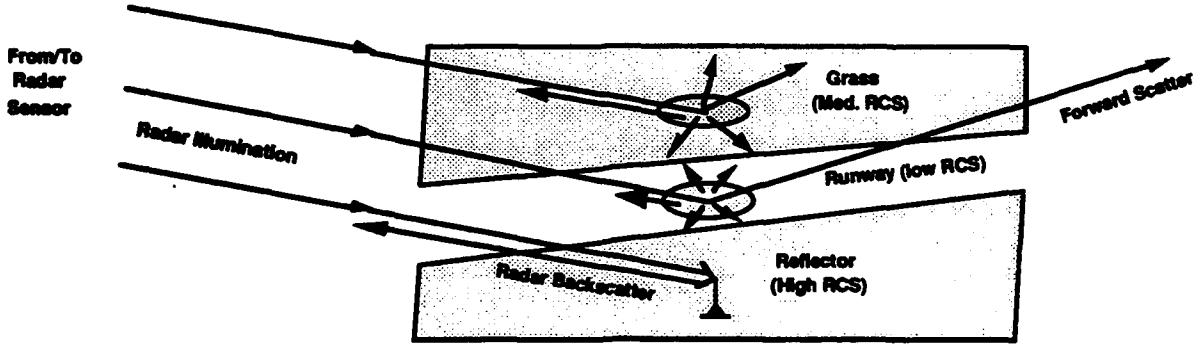

Figure 3. MMW radar detection of a runway.

MMW sensors that could image the example runway scene with sufficient resolution to demonstrate synthetic vision sensor technology were selected for tower testing. A candidate MMW test sensor initially was a 94 GHz radar developed by Lear Astronics under the Air Force

Program Research and Development Announcement (PRDA) #89-4-PMRN. Late availability of the Lear sensor for tower testing led to the inclusion of a substitute 95 GHz radar sensor from Norden Systems. The Norden TALONS radar pod was adapted from its flight test configuration to collect W-band radar performance data through the winter months. An Air Force 35 GHz radar sensor using an existing single element antenna constructed by Lockheed [30], was tested in 1990. During 1991-1992, Honeywell Incorporated developed a flight test version of the 35 GHz radar sensor with a scanning antenna that was tested in two different configurations at the tower. In the course of the tower tests, two configurations of the Lear Astronics 94 GHz radar were briefly tested.

The complete operating specifications for each test sensor were determined at least once during the testing period. Some characterization activities required partial disassembly of the test sensor and the use of special purpose test equipment, so more frequent measurement of these parameters was not practical. Some of the specifications had to be ascertained from previous off-site measurements or from manufacturer's test data. Table 1 lists radar sensor specifications and methods for measurement. The TTC used the measured radar sensor specifications to estimate performance, determine sizing and placement of calibration reflectors, and compute calibration correction factors. These specifications were also used to configure the LeCroy data acquisition system and to select an appropriate angular increment (step size) for Klinger table azimuth scanning.

The six MMW radar sensors tested at the tower and their pertinent specifications are listed in Table 2. A sensor configuration code based on the manufacturer's name and a configuration sequence number was established to label the data from each sensor tested. Two configurations of the Lear Astronics 94 GHz radar sensor, and Air Force 35 GHz radar sensor, and two configurations of Honeywell 35 GHz radar sensors were tested; the configurations differed in antenna selection, transmitter, and signal processor. The Norden Systems TALONS 95 GHz radar, although not considered a candidate Synthetic Vision sensor, provided the most extensive set of MMW radar adverse weather performance data collected on this project. Only the LA2 and HI2 radars were SVTD candidate MMW radar sensors and continued on to flight testing.

Table 1. Radar Sensor Specifications

Specification	Symbol	Units	Measurement Method	Comments
Transmit Frequency	F_t	GHz	Wavemeter	or spectrum analyzer
Transmit Power (average)	P_{ta}	W	RF Power Meter	with waveguide thermistor
Transmit Power (peak)	P_{tp}	W	RF Power Meter	Calculated from P_{ta}
Transmit Waveform	-	-	Various	Pulsed, or FMCW
Transmit Pulse Repetition Rate	PRF	kHz	Oscilloscope	or FM sweep rate
Transmit Pulse Width	τ	ns	Detector & Oscilloscope	or FM sweep width
Transmit Circuit Loss	α_t	dB	RF Power Meter	
Waveform Timing Delay	t_0	μs	Oscilloscope	For A/D synchronization
Receiver Method	-	-	Vendor	Homodyne or superheterodyne
Receiver Bandwidth	BW	MHz	Sweep Oscillator	or vendor data
Receiver Noise Figure	NF	dB	Noise Bridge	or vendor data
Receiver Circuit Loss	α_r	dB	RF Source & Power Meter	
Video Output Level	-	V	Oscilloscope	Saturated receiver level
Receiver Transfer Function	-	V/dB	Signal Injection	Receiver dynamic range
AGC/STC Factors	-	dB	Signal Injection	Dynamic variable
Antenna Beamwidths and Beam Shape	-	deg.(°)	Antenna range	(V&H) (-3 dB one-way)
Antenna Gain	G	dBi	Antenna range	Manufacturer data
Antenna Polarization	-	-	Antenna range	Manufacturer data
Antenna Scan Rate	-	Hz	Period counter	Rapid scan only
Antenna Scan Width	-	deg.(°)	Antenna Range	Vendor data
Antenna Beam Centering	-	deg.(°)	Antenna Range	Vendor data

Table 2. MMW Radar Sensors Tested at Tower

Sensor Code	Manufacturer	Frequency	Waveform	Antenna /Polarization	Signal Processor	Remarks
LA1	Lear Astronics	94 GHz	FMCW	parabolic* /circular	DSP	develop-mental
LA2	Lear Astronics	94 GHz	FMCW	parabolic** /vertical	DSP & EVS	SVTD candidate
NS1	Norden Systems	95 GHz	pulsed	parabolic /circular	none	non-candidate
HI1	U.S. Air Force	35 GHz	pulsed	slotted W/G /horizontal	none	non-candidate
HI2	Honeywell Inc.	35 GHz	pulsed	slotted W/G /circular †	DSP	SVTD candidate
HI3	Honeywell Inc.	35 GHz	pulsed	slotted W/G /horizontal	none	non-candidate

* Front-fed dual parabolic reflector with gear drive

** Cassegrain fed dual parabolic reflector with resonant scan

† Slotted waveguide fed reflector with electromechanical "Eagle scan"

Abbreviations: W/G = waveguide, DSP = digital signal processor, EVS = video processor

3.1.1.2 IR Sensors

An infrared (IR) sensor is able to image a runway scene based on the differences in temperature, emissivity, and reflectivity of the pavement areas and the bordering grass-covered areas, as shown in Figure 4. An IR camera receives thermal radiance from the scene surfaces, and a lens focuses that energy on a sensitive detector element or array of elements. The wavelength range accepted by an IR camera is based on the type of sensitive detector element used. Image contrast is developed by the differences in radiance received from the typically warmer pavement and the typically cooler grass areas within an airport scene. The actual radiance difference is a function of environmental heating and cooling during the daily cycle, grass moisture, and meteorological events.

The IR sensor systems used in the SVTD project to collect data in the 3 to 5 micron infrared band were focal plane array cameras with Stirling-cycle refrigeration for sensor cooling. Most of the infrared image data were collected with a Kodak Model KIR-310 infrared camera system. Image data were also acquired with a Mitsubishi Electric Corporation model IR-5120C infrared camera. Both of these instruments utilized platinum-silicide (PtSi) focal plane array sensors and

provided the image data in an RS-170 video signal format. Important characteristics of the two camera systems are listed in Table 3. The Kodak sensor was the only SVTD IR candidate sensor which continued on to flight testing.

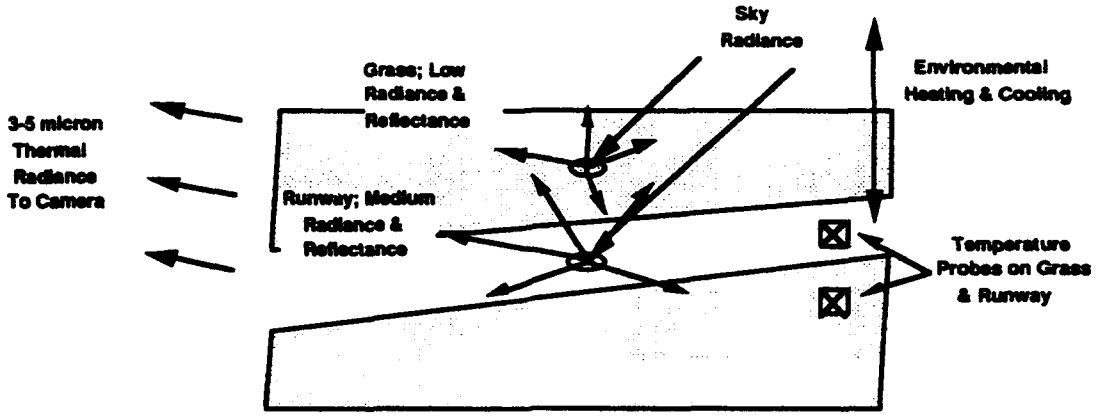

Figure 4. IR detection of a runway.

Table 3. Characteristics of Camera Systems

Characteristic	Kodak KIR-310	Mitsubishi IR-5120C
Detector	PtSi FPA	PtSi FPA
Number of array elements	640X486	512X512
Response band	3.2-4.1 microns	3-5 microns
Lens focal length	27.5 mm	50 mm
Lens aperture	f/1.7	f/1.2
Field of view	32°X25°	14°X11°
NEDT (Noise Equivalent Difference Temperature)	0.17° C	0.15° C
Cooling method	Stirling cooler	Stirling cooler
Analog output	RS-170 video	RS-170 video

3.1.2 DATA REQUIREMENTS

Data from the SV sensors under test and from weather sensors were recorded, reduced, and analyzed to produce qualitative results of imaging sensor performance in adverse weather. A flowchart of the evolution of recorded data from the sensors at the top to the processed results at the bottom is provided in Figure 5. Physical devices and processing operations are shown as rectangles, and the data in various intermediate formats are shown as rounded rectangles. There

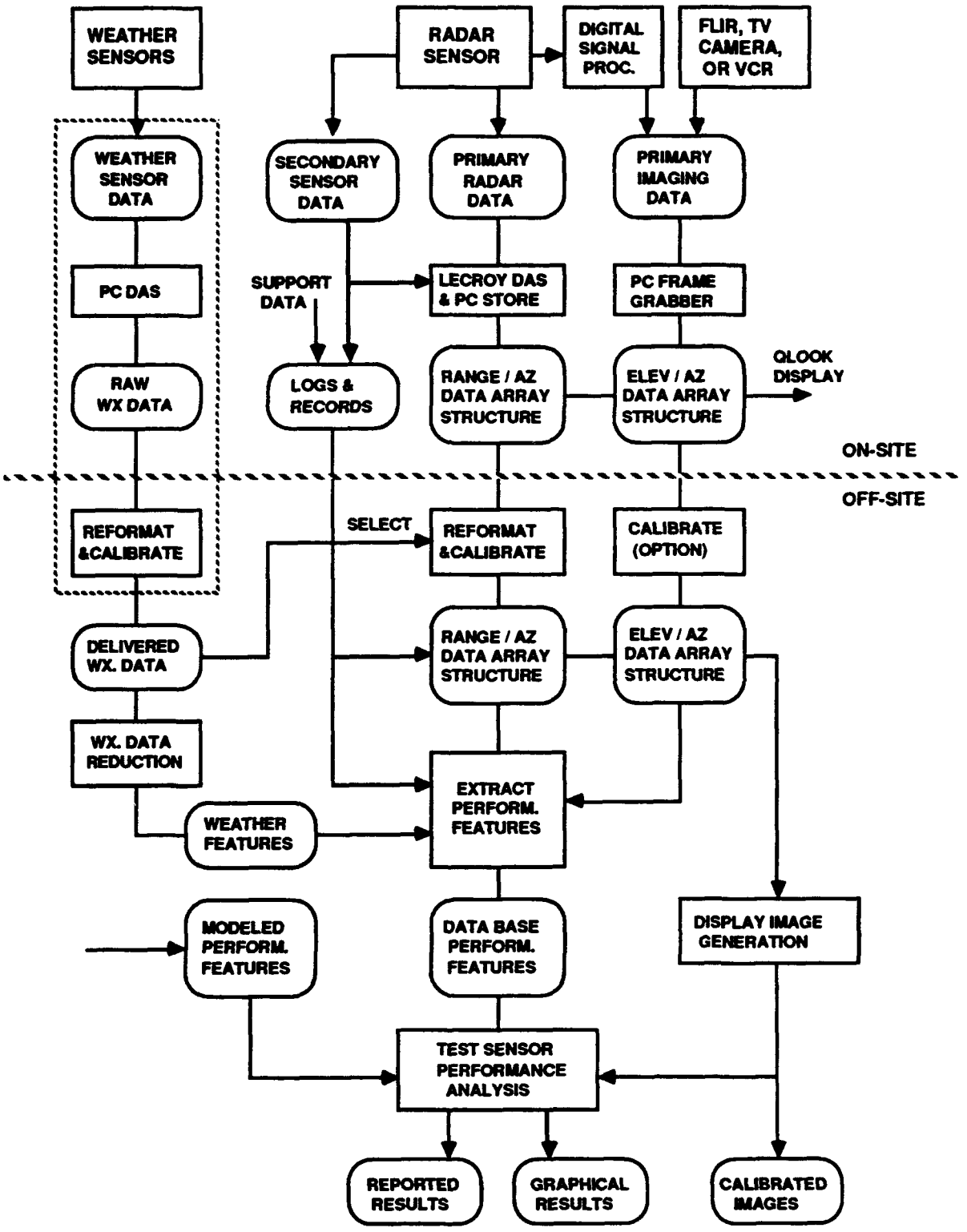

Figure 5. Flowchart of Data Evolution.

are four parallel data acquisition and processing paths that are merged during the data reduction process. The final data reduction step extracts sensor performance features and weather data into a relational data base that is exercised to develop analytical results. Sensor image data recording, processing, and display image generation enabled visual evaluation of sensor performance.

The primary data output from an electronic imaging sensor is a signal whose amplitude, frequency, polarization, or phase is a measure of the backscatter or emission from a small portion of the observed scene, called a resolution cell. To develop a two-dimensional image of the scene, the sensor system provides this output signal over a span of azimuth angles and slant ranges (or elevation angles), defined as the coverage area. Data collection equipment time-sampled, digitized, and recorded the sensor output signal with sufficient resolution to maintain the information content. Sensor data collected from the coverage area were stored in a two-dimensional data array with elements representing sensor resolution cells and dimensions equal the number of resolution cells in azimuth by the number of cells in range or elevation. Digital data filled the storage array one line at a time in a raster fashion. Radar sensor data filled each range line of the data array before the azimuth was incremented. Television format data were loaded along azimuth lines, and the elevation was incremented. The loaded data array became a recorded data file representing a single view, frame, or "snapshot" of the observed scene made by the test sensor.

Secondary data collected from an imaging sensor included parameters such as operating mode and antenna elevation that are constant over a measurement frame and dynamic system parameters such as automatic gain control and antenna azimuth that change during a frame. The data collection equipment and procedures provided for recording these additional sensor data items in registration with the primary sensor data. Constant parameters were manually entered into a data collection system computer file or entered into the Daily Test Log. Dynamic sensor parameters were imbedded with the primary sensor data or captured by an additional digital data acquisition channel. Sensor characterization measurements, including output power and receiver transfer function, or minimum detectable temperature, were performed on each sensor at least once during testing. Sensor performance measurements such as noise level or response to a calibration source were recorded through the primary sensor output and were performed daily.

Meteorological sensors, television cameras, and scene photos are examples of supporting data sources for the sensor tower testing. Results of site surveys and any important personal observations made during testing were also recorded to assist in sensor performance analysis.

These supporting data were time-marked for correlation with the primary and secondary sensor data.

Tower tests of an IR sensor were intended to demonstrate runway imaging performance under carefully documented low-visibility weather conditions for comparison with clear weather (baseline) IR performance, and for comparison with MMW sensor imaging performance. Low visibility test conditions of interest included fog, rain, and snow. Test data analysis should determine the imaging performance of the IR system as affected by atmospheric attenuation and contrast reduction under various weather conditions.

Image data were collected in both the manual gain control mode and the automatic gain control (AGC) mode. The manual gain control was desired so that the performance of the system would be that of the base system unaffected by image enhancement algorithms. In the AGC mode, the overall image quality would be optimized to cover the range of radiometric temperatures found in the scene. If IR calibration sources were placed in the scene, their emission would drive the automatic gain control; if they were not in the scene, the images could not be calibrated. The desire to collect calibrated data and the limited time available for data collection forced the data collection to be limited to the manually controlled mode.

A further goal was to compare the contrast available from IR sensors with the millimeter wave contrast data under identical weather conditions and determine the preferred system for various types of adverse weather conditions. Due to the limited time available for data collection with the IR system and the lack of occurrence of a variety of weather conditions, directly comparable conditions are not well represented in the two data sets.

Detailed descriptions of the data collection and processing are provided in Sections 6 and 7.

3.1.3 SENSOR PERFORMANCE

Sensor performance features measure a sensor's effectiveness in imaging the airport scene and are specific to the individual sensor design. Phenomenology characterizes the test scene environment in fundamental engineering values that are related to the sensor wavelength but are independent of a particular sensor design. Resolution and contrast are examples of sensor performance features. Examples of phenomenology values are radar cross section for a target or clutter area, volumetric radar cross section for precipitation, and atmospheric attenuation. Radar phenomenology values are frequency sensitive.

3.1.3.1 Performance Features

Sensor data collected during tower tests were processed to extract the specific sensor performance features listed in Table 4. These performance features were selected to apply equally well to the MMW and IR imaging sensors tested at the tower. Prior to feature extraction, the "raw" sensor data were converted into standard units of measure appropriate to each sensor technology. MMW radar sensor data were calibrated to units of equivalent received power, and IR sensor data, to units of equivalent received radiance. The term "signal" in this context refers to the amplitude values of the calibrated sensor data. The specific formulas for calculating the performance features are presented in Sections 7.1 (MMW) and 7.2 (IR) data processing.

Table 4. Sensor Performance Features

Feature Name	Abbreviation	Description
Contrast	C	Difference in received signal between runway and background (grass) areas, normalized to the background signal.
Signal-to-variability ratio	SVR	Ratio of received signal to the standard deviation of received signal.
Sharpness	S	Reciprocal of the horizontal angle between two areas of differing signal level.
Range (or elevation angle) resolution	ΔR	Smallest range or angle at which two objects can be resolved by the sensor.
Azimuth resolution	ΔA	Smallest horizontal angle at which two objects can be resolved by the sensor within 3 dB.

3.1.3.2 Phenomenology

Phenomenology is the science of observing physical events. Radar and IR phenomenology observe the responses of the environment to an electromagnetic sensor. The measured responses are normalized to units of distance, area, or volume, so that the results can be expressed in values independent of the specific test sensor used to make the measurements. Phenomenology values are useful for predicting the performance of other MMW or IR sensors in a similar operating environment. The phenomenology features that were extracted from the MMW radar sensor data are listed in Table 5, along with a brief description. The formulas and procedures for performing the MMW phenomenology calculations are included in Appendix A. There are equivalent phenomenology features for IR sensors, but limitations in the tower test methodology precluded direct measurements of those IR features. IR phenomenology features are discussed as part of the Section 8.3.

Table 5. MMW Phenomenology Features

Feature Name	Abbreviation	Description
Normalized RCS	σ^0	Radar cross section per unit area of surface.
Atmospheric attenuation	α	Reduction of apparent target RCS due to airborne material (liquid water).
Volumetric RCS	σ_v	RCS of the airborne water, normalized to volume.

A calibrated radar sensor can measure the RCS of a target or clutter area by substituting received power values into the radar range equation and solving for RCS. The resulting RCS is expressed in units of square meters or decibels relative to one square meter of RCS. This RCS measure is appropriate for characterizing a "point" target such as a vehicle. A target is an object that can be detected and characterized with a radar. Clutter is a collection of objects, either natural or man-made, that produce undesired radar returns which compete with the desired target return. Radar clutter can be localized, such as a single tree, or distributed over relatively homogeneous extended surface areas, such as pavement or grass. Area clutter RCS can be normalized to unit area (1 square meter) by dividing the RCS by the resolution cell area. A radar resolution cell is the surface area or volume bounded by the antenna elevation and azimuth beamwidths (ϕ, θ) and the range resolution (r). Volumetric RCS can be normalized to unit volume (1 cubic meter) by dividing by the resolution cell volume.

Conditions in the intervening atmosphere between a MMW radar and a target can degrade the radar's ability to detect and image that target, as shown in Figure 6. Airborne moisture due to fog and precipitation (rain, sleet, or snow) causes scattering and diffusion of the radar's electromagnetic waves. Atmospheric effects are separated into attenuation and volumetric backscatter. Section 7.4.5 describes the atmospheric physics that cause attenuation and backscatter and presents modeled values based on the size and density of airborne water droplets. A third effect of precipitation, especially snow, is a change in the RCS of the clutter surfaces.

Attenuation is the loss of apparent target RCS due to the intervening atmosphere and is expressed in decibels per kilometer (dB/km). Atmospheric attenuation applies over the entire radar propagation path, from the radar to the target and back to the radar, or twice the target slant range for a monostatic radar (i.e., one with the transmitter and receiver collocated). Attenuation reduces the range at which a radar can resolve runways from bordering grass areas, due to a reduction in apparent grass clutter RCS and runway clutter RCS.

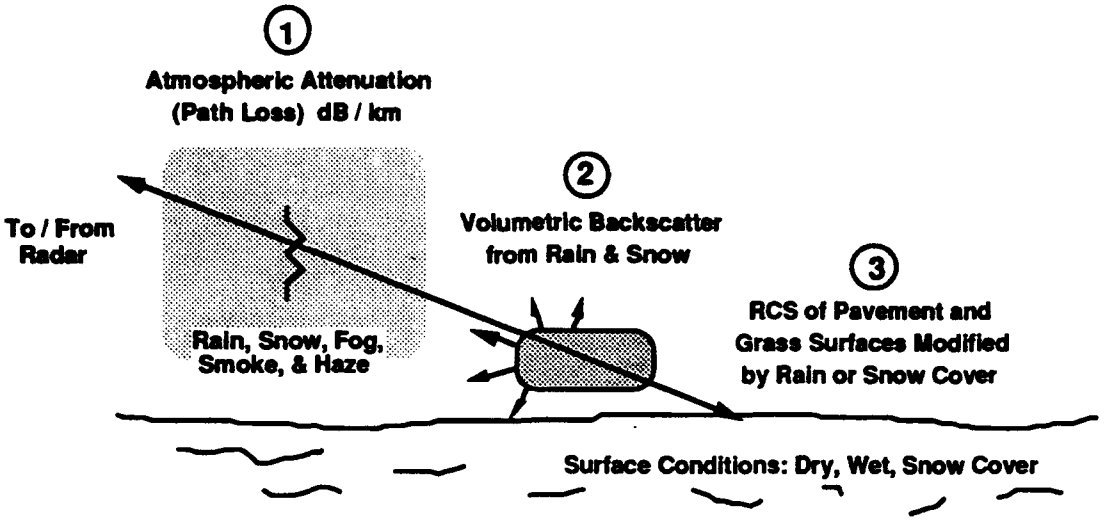

Figure 6. Meteorological effects on MMW radar sensors.

Volumetric reflectivity is the RCS of airborne particles within the radar beam per unit volume. Volumetric reflectivity is expressed in decibels relative to one square meter RCS per cubic meter of volume ($dBsm/m^3$). The atmospheric volume of an SV radar resolution cell increases with the square of range. The equivalent RCS of the precipitation can be computed at any range by adding the volume, in dB relative to one cubic meter, to the normalized volumetric RCS. MMW volumetric reflectivity is very low for fog, is relatively low for snow, but can be significant for rain.

3.1.4 TEST SCHEDULE

Eight sensor tower tests were conducted at Wright-Patterson Air Force Base between August 1991 and August 1992, as shown in the tower test schedule, Figure 7. During a one to two week "baseline test" period, the sensor was installed, calibrated, and prepared for an extended test period. A data collection system and other test support equipment were also installed. The sensor manufacturer's field team was assisted with installation of their sensor system in the 10th floor tower laboratory. Once the sensor system was made operational, it was connected to the U.S. Air Force data collection system, and the configuration parameters and test procedures were optimized. A series of specialized tests was then conducted to establish a performance baseline for the sensor. These tests measured the sensor's ability to image the runway and bordering grass areas of the test scene in clear weather conditions. Also measured were range and angular resolution, transmitter power, receiver sensitivity, ar . n.. ximum detection range.

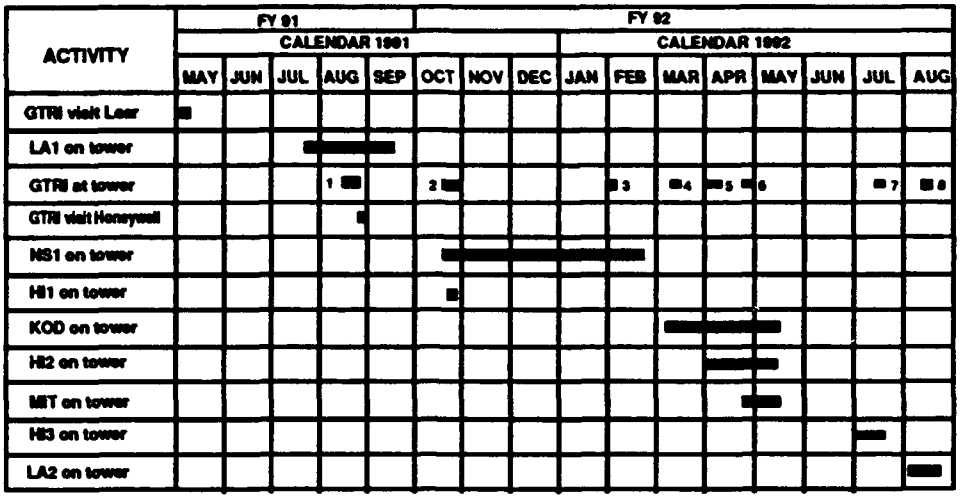

Figure 7. Tower test schedule.

After the baseline test period, the sensor and support equipment were left in a state of readiness, so that test measurements could be conducted whenever adverse weather conditions occurred. In the case of the Norden Systems MMW sensor (NS1), this extended test period lasted through four months of winter. The U.S. Air Force tower test director utilized weekly and daily weather predictions to initiate tower test activity. The intermittent nature of these tests made full-time field staffing by the manufacturer and GTRI too expensive and impractical. The successful alternative was to train U.S. Air Force personnel to operate the test sensor and support equipment on an as-needed basis. Additionally, a trained technician from the GTRI Dayton Office was available within a few hours notification to support sensor testing. Operator training, refined test procedures, and an automated data collection system were key elements to the success of this approach. Data quality could be monitored daily from images generated with the quick-look image processing software.

Some uncalibrated infrared image data which included images in falling snow were collected with the Kodak camera during the setup phase of the measurement program. Calibrated baseline infrared data were collected with the Kodak system in clear weather over 24-hour periods on March 12/13 and on May 27/28 of 1992. The Kodak system was used to collect calibrated infrared image data during adverse weather conditions on March 18, March 30, April 18, and April 21 of 1992. The weather conditions during these measurements were recorded as mixtures of fog and rain.

Isolated calibrated image data were collected with the Mitsubishi IR camera during clear weather on April 29, 1992. Concurrent weather data were not available, and the camera was not available later for adverse weather measurements. The differences in field-of-view between the Mitsubishi

camera (14° x 11°) and Kodak camera (32° x 25°) complicated the processing of Mitsubishi camera images. For these reasons the Mitsubishi IR images collected were not analyzed.

3.2. SENSOR PERFORMANCE ESTIMATION

3.2.1 MMW TEST SENSORS

GTRI preparations for tower testing the MMW radar sensors included performance estimation for the expected scene clutter and reflector targets. These performance estimations provided a valuable reference to determine if the MMW sensors were operating correctly when installed on the tower. MMW performance estimations were based on the radar sensor specifications and the radar range equation. The normalized clutter RCS (σ^0) was estimated, so that the expected target-to-clutter (T/C) and clutter-to-noise (C/N) ratios could be calculated. The effects of volumetric RCS (σ_v) for precipitation and atmospheric attenuation (α) were included in the performance estimations, using available formulas for those radar phenomenology (Appendix A). The information which follows includes calculation of the received target, clutter, rain, and noise power for the Honeywell Incorporated radar sensor, configuration 2, (HI2) along with an analysis of the pulsed waveform and the effect of the Doppler frequency shift on the system.

3.2.1.1 Target, Clutter, Rain, and Noise Power

This section describes the target, clutter, rain, and noise signal power levels. Figure 8 shows the target, clutter, rain, and noise power as a function of range for 4 mm/hr rainfall rate. This is the single pulse, predetection received power referenced to the antenna port. Post-detection signal processing such as video filtering may reduce the effective noise and rain return power. Figure 9 shows the received power for clear weather. Table 6 lists the target, clutter, rain, and noise power for 2 km range, along with the target-to-clutter, target-to-rain, and target-to-noise ratios for both rain and clear weather cases. Table 7 summarizes the radar, clutter, rain, and processing parameters used in this analysis.

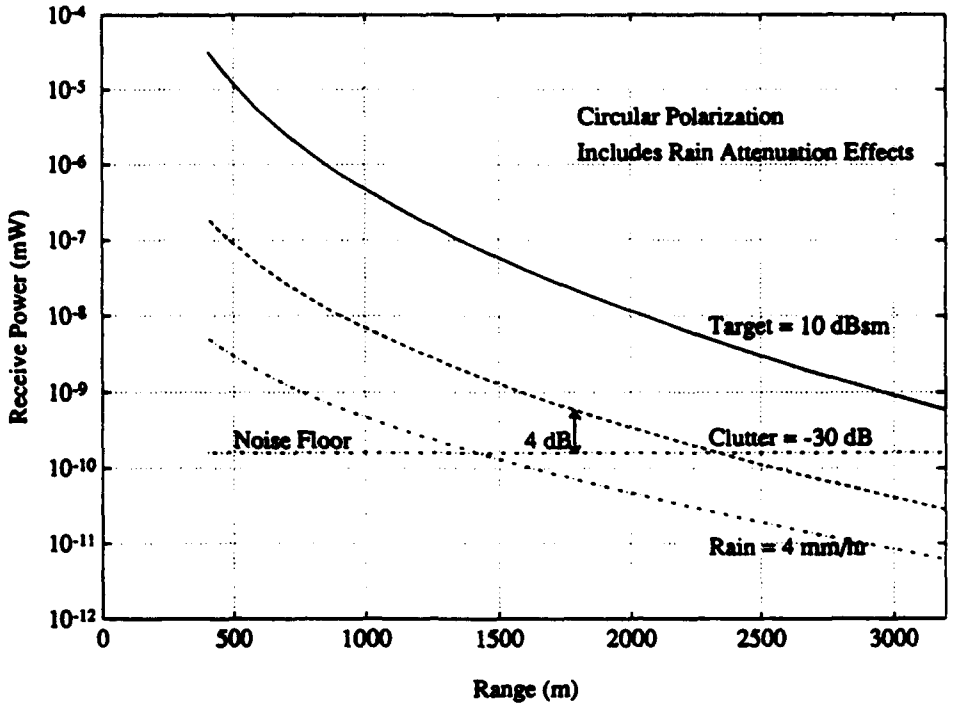

Figure 8. Received Signal Power as a Function of Range Showing Target, Clutter, Rain, and Noise Components for 4 mm/hr Rainfall Rate.

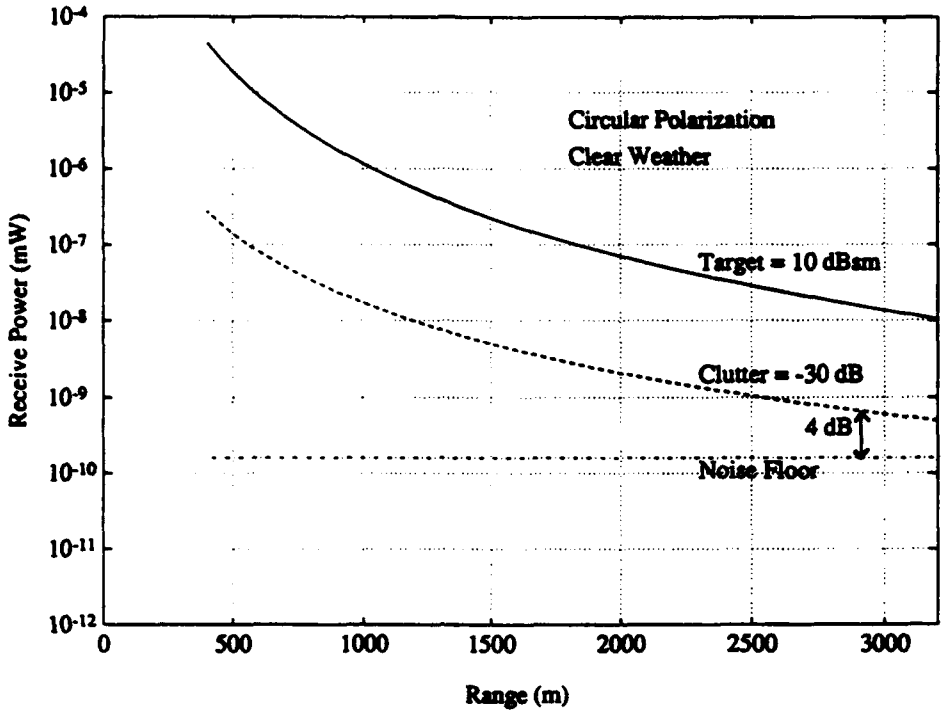

Figure 9. Received Signal Power as a Function of Range Showing Target, Clutter, and Noise Components for Clear Weather.

Table 6. Target, Clutter, Rain, and Noise Single pulse, predetection Power, Power ratios, and Radar Cross Section for 2 KM Range

	For 4 mm/hr rainfall rate	For clear weather
Target Return Power	-79.4 dBm	-71.6 dBm
Clutter Return Power	-94.7 dBm	-86.9 dBm
Rain Return Power	-103.4 dBm	
Noise Power	-98.0 dBm	-98.0 dBm
Target-To-Clutter Ratio	+15.3 dB	+15.3 dB
Target-To-Rain Ratio	+24.0 dB	
Target-To-Noise Ratio	+18.6 dB	+26.4 dB
Clutter-To-Rain Ratio	+8.7 dB	
Clutter-To-Noise Ratio	+3.3 dB	+11.1 dB
Clutter RCS	-5.3 dBsm (0.029 m^2)	-5.3 dBsm (0.029 m^2)
Rain RCS	-14.0 dBsm (0.04 m^2)	

The radar target return signal power, P_t, is given by the following radar equation

$$P_t = \frac{P G^2 \lambda^2 \sigma E}{(4\pi)^3 R^4 L_\alpha} \qquad (1)$$

where
- P = radar average transmit power
- G = radar transmit and receive antenna power gain
- λ = wavelength
- s = target radar cross section
- R = slant range
- L_α = atmospheric attenuation [9]
- E = number of radar pulses integrated.

As shown in Table 8, the target return power is -79.4 dBm at a range of 2 km.

Table 7. Summary of Parameter Assumptions

Parameter	Value	Unit	Source
Transmit Power (peak)	800	W	Honeywell
Antenna Power Gain	33	dBi	Honeywell
Frequency	35.4	GHz	Honeywell
Wavelength	8.5	mm	GTRI calculated
Target RCS	10	m^2	GTRI
Clutter Reflectivity	-30	dB	GTRI estimate
Antenna Beamwidth in Azimuth	0.8	degree	Honeywell
Antenna Beamwidth in Elevation	5.5	degree	Honeywell
Polarization	Circular		Honeywell
Range Resolution	15	m	Honeywell
Antenna Elevation	83.5	m	WPAFB
Atmospheric Attenuation			
clear weather	0.05	dB/km	GTRI
4 mm/hr rainfall rate	2.0	dB/km	GTRI
Rain Reflectivity (4 mm/hr rainfall rate)	-47	dBm-1	GTRI estimate
Reduction in rain return due to circular polarization	10	dB	GTRI estimate
Receiver Equivalent Noise Bandwidth	10	MHz	Honeywell
System Noise Figure	6	dB	Honeywell
Antenna Scan Frequency	12	Hz	Honeywell
Antenna Scan Amplitude	±15	degree	Honeywell
Antenna Scan Rate	400	deg/ s	GTRI calculated
Dwell Time	2.53	ms	GTRI calculated
Pulse Length	100	ns	Honeywell
Pulse Repetition Frequency	13.7	kHz	Honeywell
Pulse Repetition Interval	73	s	GTRI calculated
Duty Factor	0.00137		GTRI calculated
Maximum Unambiguous Range	10.9	km	GTRI calculated
Maximum Unambiguous Velocity	29	m/s	GTRI calculated

Table 8. Target Return Power Calculation

P	= Transmit power (peak)	= 800 W	=	59.0 dBm
G^2	= (Antenna power gain)^2	= $(10^{3.3})^2$	=	66.0 dBi
λ^2	= Wavelength^2	= (8.5 mm)^2	=	-41.4 dBsm
σ	= Target RCS	= 10 m^2	=	+10.0 dBsm
$(4\pi)^3$	= 1984	= 1984	=	(-) 33.0 dB
R^4	= (Slant range)^4	= (2 km)^4	=	(-) 132.0 dBmeter^4
L_α	= Atmospheric attenuation	= 2.0 dB/km	=	(-) 8.0 dB
P_t	= Target return power			-79.4 dBm

The peak transmit power for the HI2 radar is 800 W at the antenna port. This analysis used an antenna power gain value of 33 dBi. The effect of the cosecant squared elevation beam shape is ignored here. The wavelength is 8.5 mm for the 35 GHz frequency. This analysis used a target radar cross section (RCS) of 10 m^2 which is representative for vehicle targets. The measured atmospheric attenuation for 35 GHz and 4 mm/hr rainfall rate is 2.0 dB/km each way. In clear weather, the attenuation is 0.05 dB/km, so that the clear weather target return power is -71.6 dBm.

As shown in Table 9, the clutter RCS is 0.29 m^2, or -5.3 dBsm, at 2 km range, which yields a +15.3 dB target-to-clutter ratio.

$$\text{Clutter RCS} = R\,\theta_a \sqrt{\frac{1}{2}\delta R}\,\frac{1}{\cos(\psi)}\,\sigma 0 \quad [9] \tag{2}$$

The azimuth antenna beamwidth is 0.8 degree, or 14.0 milliradians. The slant range resolution for the 100 ns pulse length is 15 m. The test tower is 83.5 m above the runway area at the Wright Patterson Air Force Base, OH, test area, so that the grazing angle at 2 km slant range is 2.4 degrees [30]. The clutter reflectivity is estimated to be approximately -30 dBsm in the test area [30]. Table 10 shows the calculation of -94.7 dBsm clutter return power for 2 km range. In clear weather, the clutter return, P_c, will be -86.9 dBm an calculated by

$$P_c = \frac{P\,G^2\,\lambda^2\,R\,\theta_a\,\sqrt{\frac{1}{2}\delta}\,R\,\frac{1}{\cos(\psi)}\,\sigma^0}{(4\pi)^3\,R^4\,L_a} \tag{3}$$

Table 9. Clutter RCS

R	=	Slant range	=	2 km	=	33.0 dB meter
θ	=	Azimuth beamwidth				
	=	0.8 degree	=	14.0 mrad	=	-18.6 dB
$\sqrt{\frac{1}{2}}$	=	0.707	=	0.707	=	-1.5 dB
δR	=	Slant range resolution	=	15 m	=	11.8 dB meter
$\frac{1}{\cos(\psi)}$	=	secant of 2.4 degree				
		grazing angle	=	1.0	=	0.0 dB
$\sigma 0$	=	Normalized clutter reflectivity	=	0.001	=	-30.0 dB
		Clutter RCS	=	0.29 m2		-5.3 dBsm

Table 10. Clutter Return Power Calculation

P	=	Transmit power	=	800 W	=	59.0 dBm
G^2	=	(Antenna power gain)^2	=	$(10^{3.3})^2$	=	66.0 dBi
λ^2	=	Wavelength^2	=	(8.5 mm)^2	=	-41.4 dBsm
R	=	Slant rar ge	=	2 km	=	33.0 dB meter
θ	=	Azimuth beamwidth = 0.8 degree	=	14.0 mrad	=	-18.6 dB
$\sqrt{\frac{1}{2}}$	=	0.707	=	0.707	=	-1.5 dB
δR	=	Slant range resolution	=	15 m	=	11.8 dB meter
$\frac{1}{\cos(\psi)}$	=	secant of 2.4 degree grazing angle	=	1.0	=	0.0 dB
σ^0	=	Normalized clutter reflectivity	=	0.001	=	-30.0 dB
$(4\pi)^3$	=	1984	=	1984	=	(-) 33.0 dB
R^4	=	(Slant range)^4	=	(2 km)^4	=	(-) 132.0 dB meter^4
L_α	=	Atmospheric attenuation	=	2.0 dB/km	=	(-) 8.0 dB
P_c	=	Clutter return power				-94.7 dBm

Table 11 shows the rain RCS of 0.04 m^2, or -14.0 dBsm, as calculated by [9]

$$\text{Rain RCS} = R\,\theta_a\,\sqrt{\frac{1}{2}}\,R\,\theta_e\,\sqrt{\frac{1}{2}}\,0.5\,\delta R\,0.1\,\eta \tag{4}$$

Table 11. Rain RCS Calculation

R	= Slant range	=	2 km	= 33.0 dB meter
θ_a	= Azimuth beamwidth = 0.8 degree	=	14.0 mrad	= -18.6 dB
$\sqrt{\frac{1}{2}}$	= 0.707	=	0.707	= -1.5 dB
R	= Slant range	=	2 km	= 33.0 dB meter
θ_e	= Elevation beamwidth = 5.5 degree	=	96 mrad	= -10.2 dB
$\frac{1}{\cos(\psi)}$	= 0.707	=	0.707	= -1.5 dB
0.5	= Half of beam is below horizon	=	0.5	= -3.0 dB
δR	= Slant range resolution	=	15 m	= 11.8 dB meter
0.1	= Circular polarization reduction	=	0.1	= -10.0 dB
η	= Normalized rain reflectivity	=	0.00002	= -47.0 dB
	Rain RCS	=	0.04 m^2	-14.0 dBsm

The elevation antenna beamwidth is 5.5 degree, or 96 milliradians.[30] This analysis assumes that half of the elevation beamwidth is below the horizon. The measured normalized rain reflectivity is -47 dBm^2/m^3 for 4 mm/hr rainfall rate. An additional 10 dB reduction in rain reflectivity is approximated because the system uses circular polarization. Table 12 shows the rain return power of -103.4 dBm as calculated by

$$P_r \frac{P\,G^2\,\lambda^2\,R\,\theta_a\,\sqrt{\frac{1}{2}}\,R\,\theta_e\,\sqrt{\frac{1}{2}}\,0.5\,\delta R\,0.1\,\eta}{(4\pi)^3\,R^4\,L_\alpha} \tag{5}$$

The noise power (N = k T B F) in a 10 MHz bandwidth for a 6 dB noise figure is -98.0 dBm, as shown in Table 13.

The 10 MHz receiver noise bandwidth is based on matching the inverse of the 100 ns pulse length. The 6 dB noise figure is based on the 4.5 dB double sideband noise figure of the mixer preamplifier with an additional 1.5 dB to account for other system noise contributors.

Table 12. Rain Return Power Calculation

P	=	Transmit power	=	800 W	=	59.0 dBm
G^2	=	(Antenna power gain)^2	=	$(10^{3.3})^2$	=	66.0 dBi
λ^2	=	Wavelength^2	=	(8.5 mm)^2	=	-41.4 dBsm
R	=	Slant range	=	2 km	=	33.0 dB meter
θ_a	=	Azimuth beamwidth = 0.8 degree	=	14.0 mrad	=	-18.6 dB
$\sqrt{\frac{1}{2}}$	=	0.707	=	0.707	=	-1.5 dB
R	=	Slant range	=	2 km	=	33.0 dB meter
θ_e	=	Antenna beamwidth = 5.5 degree	=	96 mrad	=	-10.2 dB
$\frac{1}{\cos(\psi)}$	=	0.707	=	0.707	=	-1.5 dB
0.5	=	Half of beam is below ground	=	0.5	=	-3.0 dB
δR	=	Slant range resolution	=	15 m	=	11.8 dB meter
0.1	=	Circular polarization reduction	=	0.1	=	-10.0 dB
η	=	Normalized rain reflectivity	=	0.00002	=	-47.0 dB
(4π)	=	1984	=	1984	=	(-) 33.0 dB
R^4	=	(Slant range)^4	=	(2 km)	=	(-) 132.0 dB meter
L_α	=	Atmospheric attenuation	=	2.0 dB/km	=	(-) 8.0 dB
P_r	=	Rain return power				-103.4 dBm

Table 13. Noise Power Calculation

k	=	Boltzmann's constant	=	1.38×10^{-20} mW/(Hz·K)	=	-198.6 dBm/(Hz·K)
T	=	Reference temperature	=	290 K	=	24.6 dBK
B	=	Receiver noise bandwidth	=	10 MHz	=	70.0 dBHz
F	=	System noise figure	=	4	=	6.0 dB
N	=	Noise Power referenced to the antenna port				-98.0 dBm

3.2.1.2 Doppler Effects

Doppler effects are introduced when there is relative motion between a radar and the target, as when an airplane mounted radar illuminates the ground in the direction of flight. Since the MMW radars were stationary for the tower tests, Doppler effects were not an issue. Doppler effects were estimated, however, to assist in determining a MMW sensor's suitability for flight testing.

The Doppler frequency shift, f_d, is given by

$$f_d = 2\,V / \lambda \tag{6}$$

where: V = relative velocity between radar and target, and λ = wavelength = 8.5 mm, so that

$$f_d = 236\ \text{Hz} / \text{m/s}. \tag{7}$$

Figure 10 shows the Doppler frequency shift as a function of relative velocity for the 35 GHz frequency. For example, with platform velocity of 100 m/s, the resulting Doppler shift is 23.6 kHz. If the Doppler shifted is to zero Hz, the system can unambiguously process ±29 m/s for the 13.7 kHz PRF.

The receiver bandwidth is 10 MHz. For the 0.8 degree azimuth beamwidth and 400 degree per second antenna scan rate, the antenna dwell time is 2.53 ms which corresponds to a minimum video bandwidth of 395 Hz. This will permit integration gain of 22,500, or 43.5 dB relative to the noise.

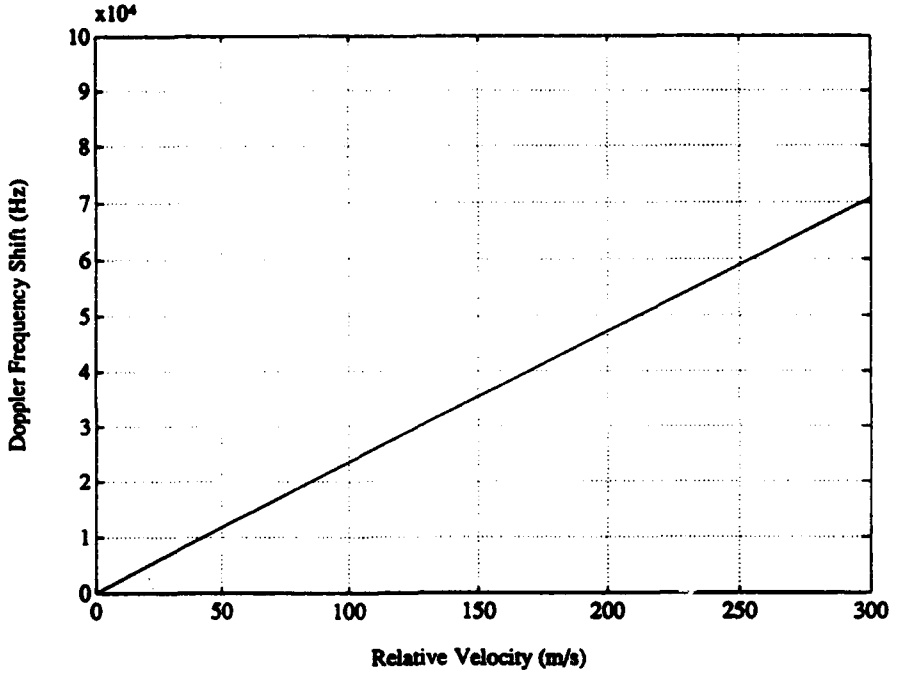

Figure 10. Doppler Frequency Shift as a Function of Velocity.

Since the Honeywell receiver is noncoherent, Doppler processing is not performed. There is no distortion or loss of performance introduced by the inevitable Doppler frequency shift of received signals due to aircraft forward velocity. This is not the case with the Lear Astronics 94 GHz FMCW radar which requires a coherent receiver. The Doppler frequency is 625 Hz / m/s, or 40.6 kHz for an approach ground speed of 65 m/s (130 knots). The 2.4 kHz frequency bin size of the fast fourier transform (FFT) process translates to one range bin, so a Doppler frequency offset of 40.6 kHz introduces a range offset error of 65 range bins. Maximum instrumented range is be reduced by 65/511, or 13%. FM1 mode (100 MHz) has a range bin size of 6.6 m, so 65 bins equals 429 m range. Range zero would be offset out in range by that distance. This range offset must be combined in processing, along with the altitude, to provide the correct perspective presentation in the head-up display (HUD) video images.

3.2.1.3 Conclusions

The target, clutter, rain, and noise power projections show that the 35 GHz system will have good performance in clear weather out to 3.2 km. In rain with 4 mm/hr rainfall rate the system should operate out to approximately 2 km. These calculations can be modified to include the effect of video signal processing or to project the signal characteristics at a specific test point when more information about the IF and video processing is available. Verification of the range

resolution of the system is important, because both the clutter RCS and rain return RCS are proportional to the range resolution.

3.2.2 IR TEST SENSORS

3.2.2.1 Drop Size Distributions and IR System Performance in Fog

Drop size distributions of typical fogs were used for the purpose of estimating the possible effects of fog on the apparent scene radiance in the camera passband. Drop size distributions for fog aerosol models for limiting cases of large and small drop size were generated in a form suitable for the computation of droplet scattering and absorption from the Mie scattering equations. [49] [13] [54] Extinction was computed for fog droplets with these two representative size distributions as a function of wavelength in the visible and IR bands. The effects of molecular band absorption and of the path radiance over the path from scene to sensor would have to be included in a complete modeling effort, but the effects of fog droplets alone on the transmission of radiation from the source is well described by the extinction coefficient computed from Mie theory.[13]

Figure 11. shows the size distribution for fog with drop sizes in the smallest size ranges. These sizes are typical of developing or "Radiation" fog with the droplet radii concentrated in the 1 to 4 micrometer range. Figure 12. shows the large drop size case of size distribution common in mature or "Advection" fog where the dominant particle radii fall in the 5 to 15 micrometer range.

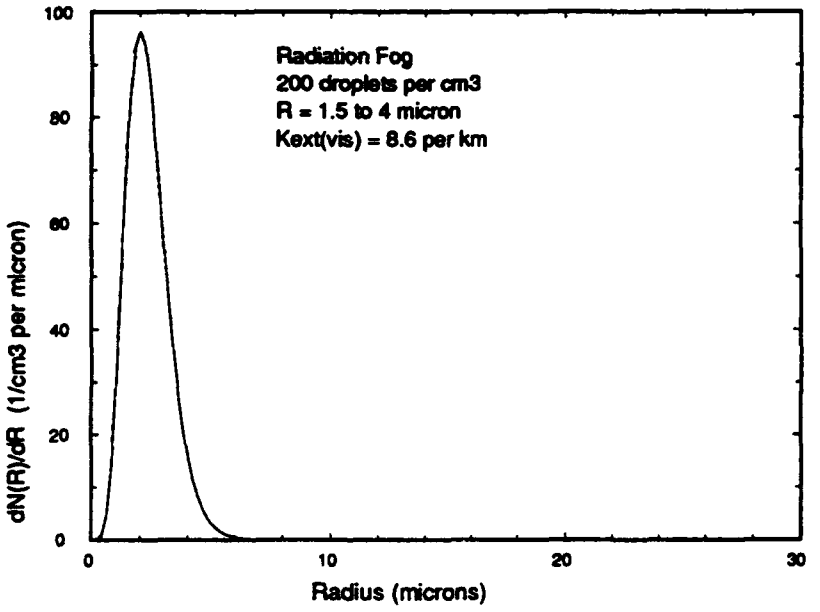

Figure 11. Drop size distribution for "Radiation" fog model.

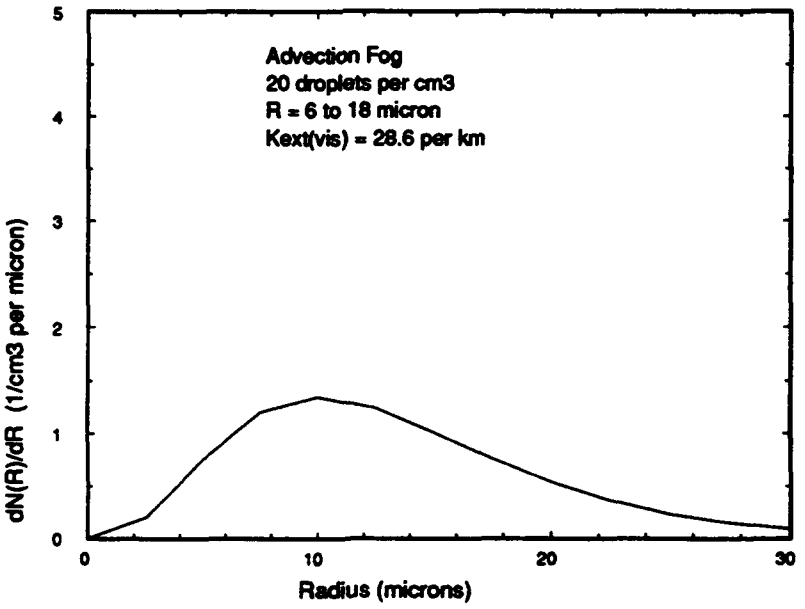

Figure 12. Drop size distribution for "Advection" fog model.

The distributions shown above as functions of drop radius were processed by a computer program to compute Mie scattering parameters and to derive extinction coefficients at visible and infrared wavelengths. The results of the extinction calculations are shown in Figures 13 and 14 for the two drop size cases at wavelengths in the visible, 3-5 micron, and 8-12 micron bands.

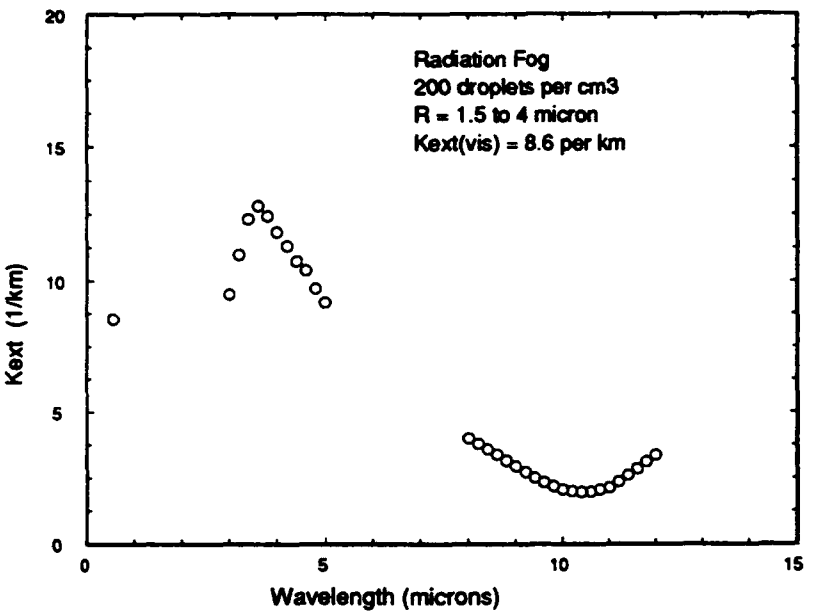

Figure 13. Fog droplet extinction coefficient plotted against wavelength for the small drop size distribution.

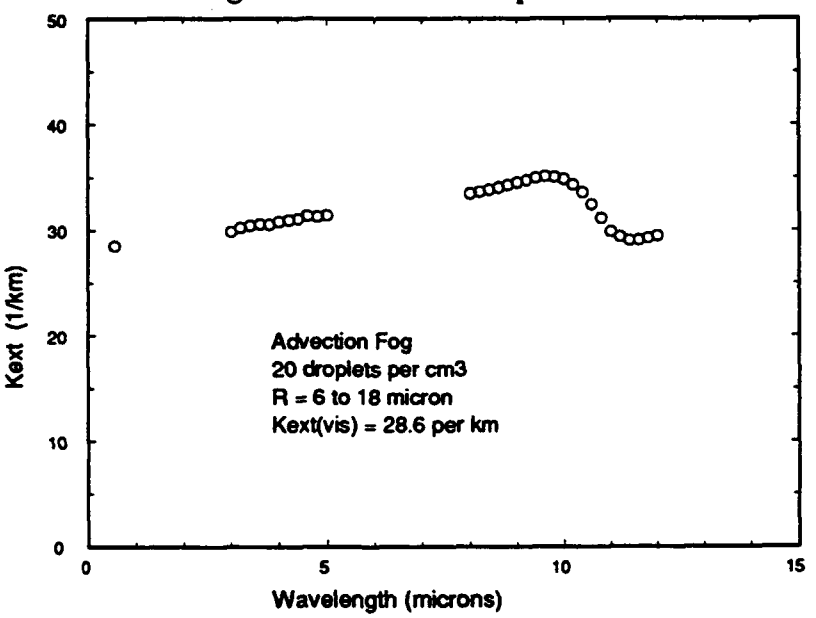

Figure 14. Fog droplet extinction coefficient plotted against wavelength for the large drop size distribution.

The corresponding path lengths at which 98% extinction by the fog droplets is reached for specific wavelengths of 0.55, 4.0, and 11.0 microns are listed in Table 14. This serves as a rough indication of the relative ability of the sensor to penetrate fog in the various bands.

Table 14. Range for 98% extinction BY FOG VERSUS WAVELENGTH

Fog Type	Wavelength 0.55 μm (Visible)	4.0 μm (3-5 μm IR)	11.0 μm (8-12 μm IR)
Advection (larger droplets)	0.137 km	0.127 km	0.107 km
Radiation (smaller droplets)	0.455 km	0.343 km	1.947 km

Note that the extinction range at both IR wavelengths is as short as that at visible wavelengths. The exception is the 8-12 micron band with the small drop size model (radiation fog), where droplet radii are around 2 micrometers. IR emissions at wavelengths in the 8-12 micron band should be attenuated less than visible light in radiation fog, but will be attenuated more than visible light in avection fog. IR emissions in the 3-5 micron band, however, will be attenuated more than visible light in both types of fog. The conclusion to be drawn from this analytical result is that an IR sensor operating in the 3-5 micron band offers no improvement in penetrating fog over sensors operating in the visible wavelengths. The 3-5 micron IR sensor does show an improvement factor when the attenuation model is run for droplet sizes smaller than 2 microns (radiation fog). The Kodak IR camera system and the Mitsubishi camera both operate in the 3-5 micron wavelength band. Therefore, their ability to provide detection at greater ranges than visible detection will depend critically on the range of droplet sizes present in the fog (or cloud). Smoke and haze particles are generally in the smaller size ranges (< 2 μm), so a 3-5 micron IR sensor would offer improved detection range over a visible light sensor under smoke or haze conditions.[22]

Drop sizes even smaller than the 2 micron radius for the "Radiation Fog" droplets must dominate in order for the infrared sensor to provide better performance than a visible light sensor in fog. Fogs with visibilities less than 1 kilometer studied at Otis AFB in 1980 and reported by B. Kunkel all had mean particle radius larger than 2 microns.[34] In general, fogs with small particle sizes have low liquid water content, and a number of studies have reported a strong correlation between liquid water content and visible light extinction in fogs.[14] This means that small drop sizes might be expected to correspond to greater visibility.

Raindrops are much larger than fog particles; hence, the attenuation due to rain is expected to be the same for infrared as for visible light sensors. Approximations of relationships between rain rate and radiation extinction by raindrops would indicate that the extinction is independent of wavelength well beyond the infrared bands used here. Similar expectations can be supported for IR extinction by snow.[49] [54] [39]

3.2.2.2 Scene Radiance at Zero-range

The apparent contrast in the scene as detected by a camera system depends on the source signal as well as the effects of the path between the observer and the scene. For infrared cameras in the 3-5 micron band, the source signal is the radiance of the scene. The source radiance is largely driven by temperatures of scene elements. Small temperature differences will result in low contrast. In adverse weather conditions, the presence of significant amounts of fog or snow eliminates much of the heating of the scene elements from solar radiation as well as the cooling effects of radiation to space. The effect of rain on scene temperatures includes cooling or heating by the rain; this tends to drive all temperatures to that of the rain droplets. The equalizing effects of such weather conditions on the temperatures of scene elements along with the effects on atmospheric path transmission and radiant emissions must be taken into account when predicting IR sensor performance in fog, rain, or snow.

The scene brightness at visible light wavelengths is primarily a measure of the reflection of ambient lighting by passive scene elements. The adverse weather conditions described above all effect the visible source signal by decreasing the illumination of the scene. Active visible band sources such as lights are affected by adverse weather to a much smaller degree than passive scene elements.

The complexity of weather effects on source signal intensity of infrared and visible scenes is too great to make any quantitative predictions of effects on apparent contrast without additional calculations that are beyond the scope of this contract. The basic characteristics of the infrared camera systems can still be used to assess some relevant limitations.

SECTION 4
GROUND TRUTH PREPARATION

4.1 MEASUREMENT SCENE DEFINITION

As specified in the Tower Test Plan, tests conducted under this contract were carried out at the Air Force Avionics Directorate, Wright-Patterson AFB, on the tenth floor of Building 620.[51] This location for the sensors allowed them to "view" an area which encompassed a variety of terrain and structure types, principally including the runway reserved for the USAF Museum. Figure 15 shows an elevation view of the scene. A top view drawing of the area with some of the key landmarks is provided in Figure 16.

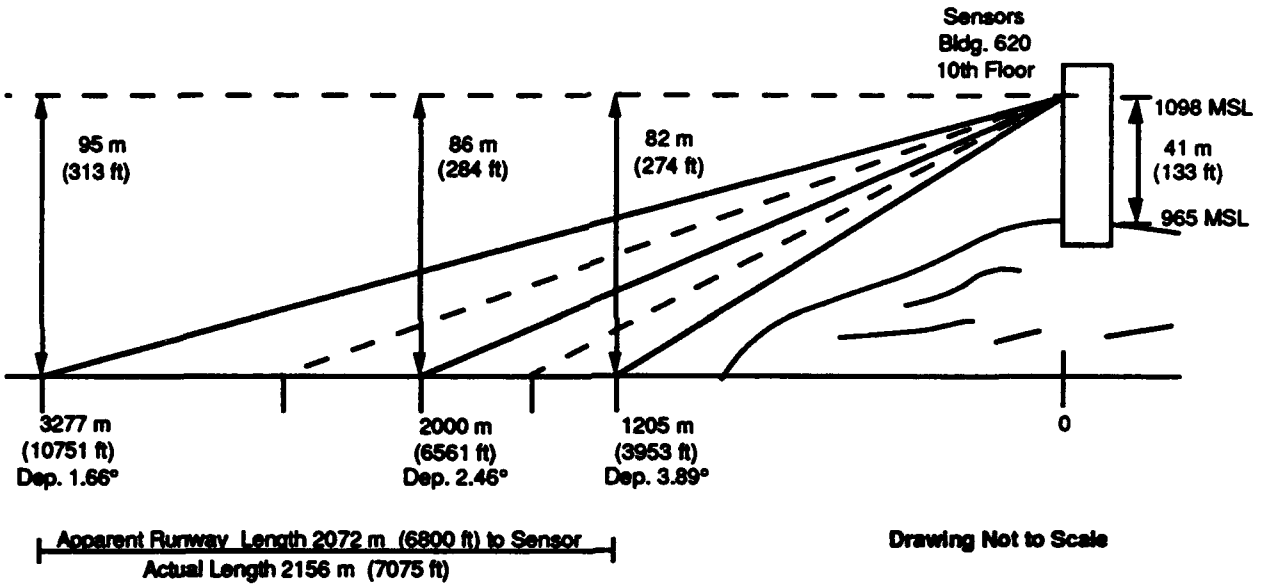

Figure 15. Elevation drawing of test area.

Efforts to define the scene included acquiring detailed information on the scene geometry and identifying elements of the scene to be quantified in terms of the sensor representation.

4.1.1 SCENE GEOMETRY

A detailed analysis of the scene was conducted in preparation for interpreting the sensor data as a function of the terrain represented. A blue scale 28" x 40" map of the area was obtained from the Air Force. The first level of effort was to identify what area(s) would be included in the scan or field of vision of the sensor(s). It was assumed that for all sensors the down-range center of this area would be a line between the sensor location at the tower of Building 620 and a point which fell

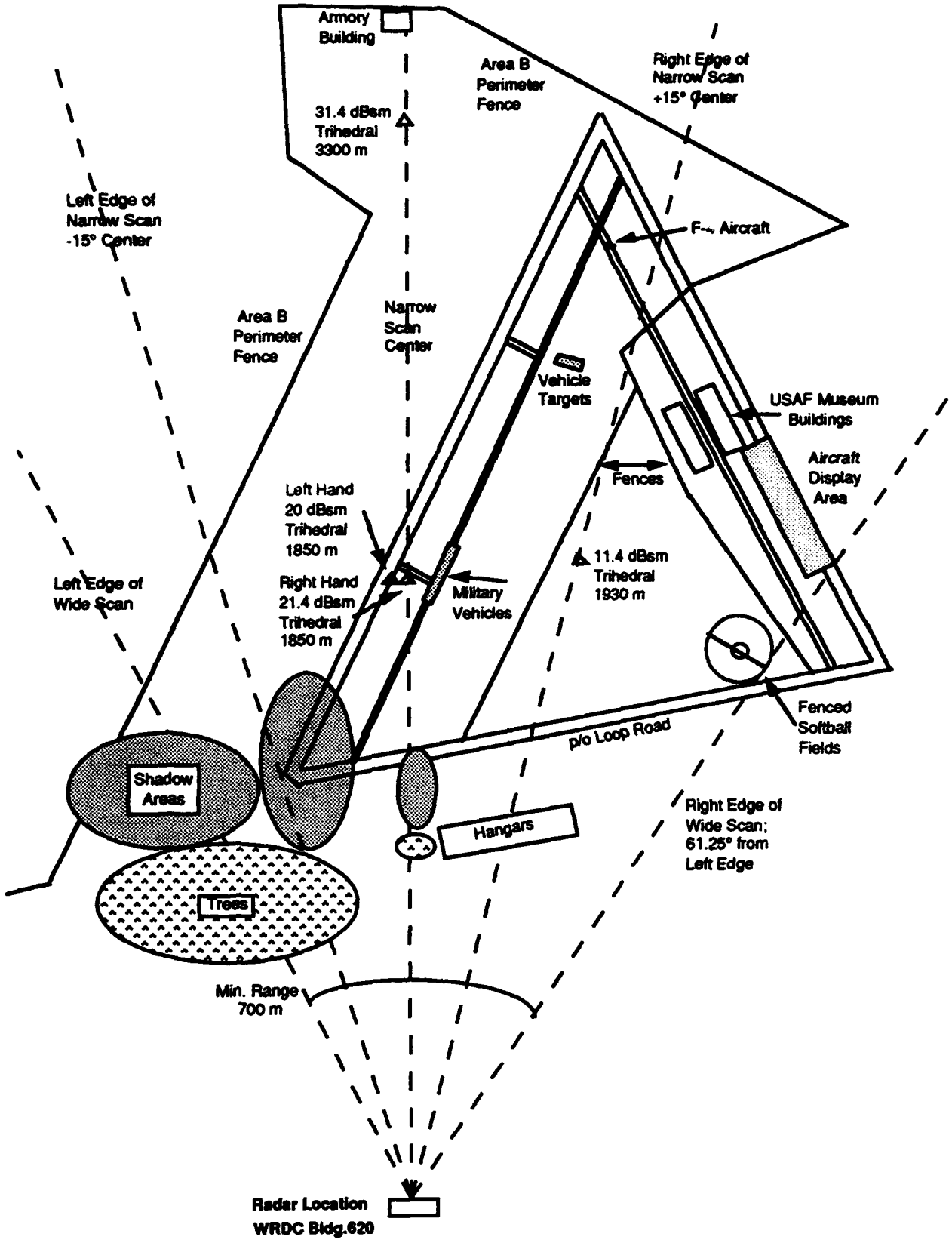

Figure 16. Top view drawing of test area.

approximately halfway between the taxiway and the runway at a distance of approximately 1,825 meters from the tower. Some of the notable scene elements, as seen in the images, are included in Table 15.

Table 15. Scene elements

Object	Description
Sensor	located in lower right corner of map, Building 620 tower
Runway	width 46 meters, length 2,156 meters; distance from sensor ranged from 1,200 to 3,300 meters; range from 1,200 to 1,650 meters was shadowed by trees
Taxiway	width 23 meters, length 1,951 meters; joined to runway at five cross points
Fences	located on both right and left sides of scene
Housing	located on left of scene
USAF Museum	located on right side of scene
Softball fields (fenced)	located on lower right side of scene
Military Vehicles	parked or randomly moving on taxiway
Loop Road	located in between sensors and runway area
Weather trailers	parked on right side of taxiway
Corner reflectors	one always placed at 1,825 meters from sensor, sensor centerline in azimuth; others at various locations in scene depending on test setup

Corner reflectors were placed in the scene to serve multiple purposes in the data acquisition and data analysis tasks. For most of the data collection, there were at least two corner reflectors. Those two corner reflectors were placed in direct line with the sensor center line of sight; one was always at 1,825 meters, and the second one was placed at either 2,425 or 2,925 meters. The corner reflector(s) were used initially to set the alignment of the sensor so that there would be consistency in pointing from one run to the next. The magnitude of the reflector power was used to verify the accuracy of the radar transfer function calibration method. For each data set, the exact data resolution cell containing the peak value in the known area of the corner reflector(s) was used to define offsets to account for minor pointing inconsistencies. The corner reflectors were further used to assess range and azimuth resolution as well as to calculate attenuation.

It should be noted from Figure 16 that one geometric constraint created by the sensor location relative to the runway was that the sensor center beam was not aligned with the runway centerline. Looking down the centerline of the sensor, that line crosses the runway center at a distance of approximately 2,000 meters from the sensor and makes an angle of approximately 16° with the runway centerline. The synthetic vision implementation of the sensor(s) would create a scene where the sensor centerline would run very close to being parallel and directly in line with the runway centerline.

Calculations were made to evaluate the error involved with equating ground range and slant range in processing the data. The sensor is located at approximately 1,098 meters above mean sea level (MSL). At a ground range of 2,000 m from the sensor, the runway is located at approximately 1,012 meters above MSL. Using the ground range instead of slant range at this geometry, the analyst would have a 0.09% error. From one end of the runway to the other, the error varied from 0.04% error (far end) to 0.23% error (near end). Due to this small degree of error in defining range and in order to simplify the calculations, it was decided that slant range would be equated to ground range.

4.1.2 MMW RADAR PROCESSING PATCH MAPPING

4.1.2.1 Data Resolution

In making the original decision regarding the resolution of the data collected, it was determined that the size of the data resolution cells would be of higher resolution than the sensor resolution. A standard scene would represent a total of 30° in azimuth and either 3,379.2 or 3,840 meters in range depending on the sensor. This quantity of data is represented as 300 azimuth steps by 512 range steps. A map of a set of data resolution cells is shown is Figure 17 with a single sensor resolution cell superimposed to illustrate the concept of higher data resolution than sensor resolution. The drawing on the left indicates the data resolution cell size. On the right, the sensor cell with range 15 meters and azimuth 0.4 degrees is seen in comparison with a group of data resolution cells.

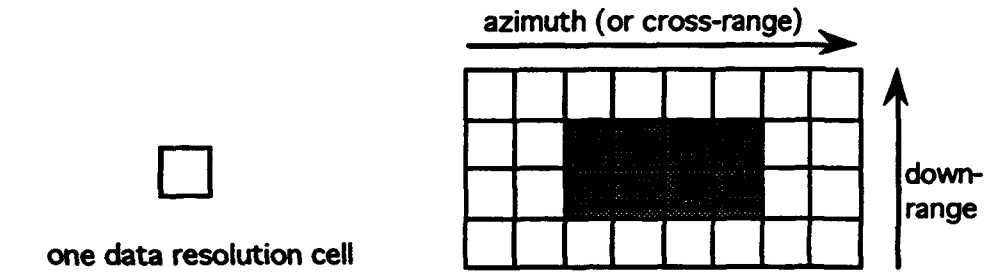

Figure 17. Data and sensor resolution cell comparison.

As a consequence of using this method of defining data resolution cells, each data cell represents overlapping sensor data. As the sensor steps 0.1 degree in azimuth, the returned power would be repeated, or overlapping, in 6 of the 8 data resolution cells, as illustrated in Figure 18.

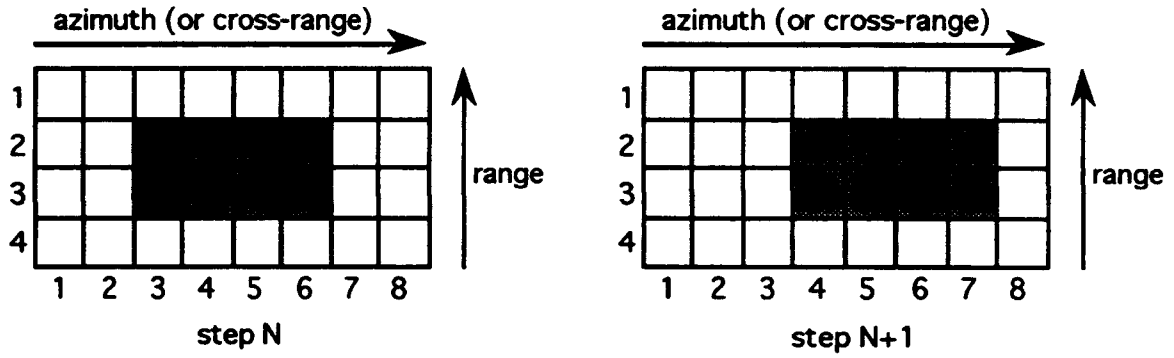

Figure 18. Sequential azimuth stepping in terms of data resolution.

4.1.2.2 Patch Definition

For any single surface type in the scene, i.e., grass or pavement, there was a high degree of variability within even a relatively small cluster of azimuth and range resolution cells. In order to more accurately represent the return from a surface at a given range and reduce the effects of the variability, we defined the return from that location as an average of the values from a group of neighboring cells, referred to as a patch. A patch is defined to be a cluster of range and azimuth data resolution cells. The patches selected in each scene represent different classes of scene characteristics, namely runway, taxiway, and grass, in addition to background targets such as corner reflectors, trees, buildings, aircraft and fences. These patches were chosen with great care to represent only the environment of interest. In the case of a target such as a corner reflector, a square patch was defined. In representing the value from such a patch, the peak value was used rather than an average.

Because the sensor was not looking straight down the runway, compensation had to be made in identifying cells to be included in runway (or taxiway) patches, so as to avoid cells that might include the edge. A procedure was defined for calculating the size of patches. The drawing , Figure 19 identifies the values identified in the first three steps.

1. Calculate the angle of the sensor line of sight to the runway as a function of range.

2. Calculate the effective width of the runway.

3. Calculate the reduction in the width of the runway due to the cells extending over the edge.

4. Given that the data resolution beamwidth is 0.1°, calculate the data resolution chord width, $r\theta$, approximated for small angles.

5. Calculate the effective width of the runway in data resolution cells.

6. Reduce the effective width in cells by 2 cells on each side to compensate for pointing errors and sensor beamwidth overlap.

7. Select the number of data resolution cells in depth so as to keep the total patch area approximately equal for the different ranges.

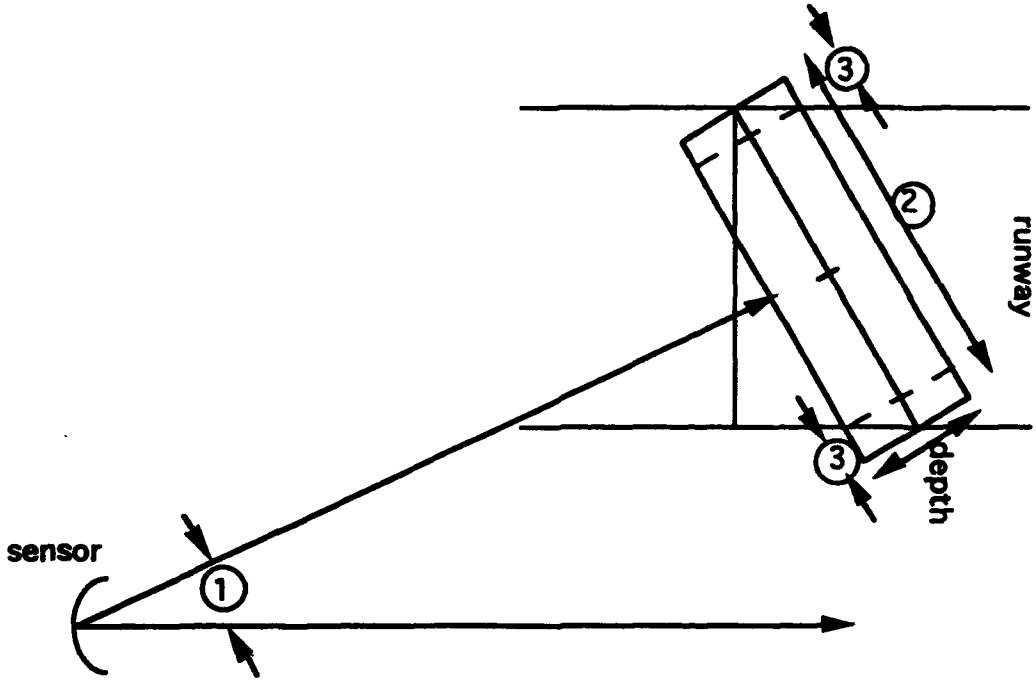

Figure 19. Runway geometry considerations for patch size calculations.

In addition to the single target patches, another type of patch which requires a different analysis approach is the profile. A profile patch starts at some distance to one side of the runway and ends beyond the other side of the runway. Rather than simply averaging all the power values within the profile, this type of patch is analyzed independently as a function of azimuth so that the sharpness of the runway edge profile can be analyzed. The cells in adjacent ranges were averaged and then analyzed independently in azimuth in order to reduce the inconsistencies in return when looking at a single range. The typical range extent of such a profile patch included 6 to 8 data resolution cells in range. A concept drawing of such a patch is shown in Figure 20.

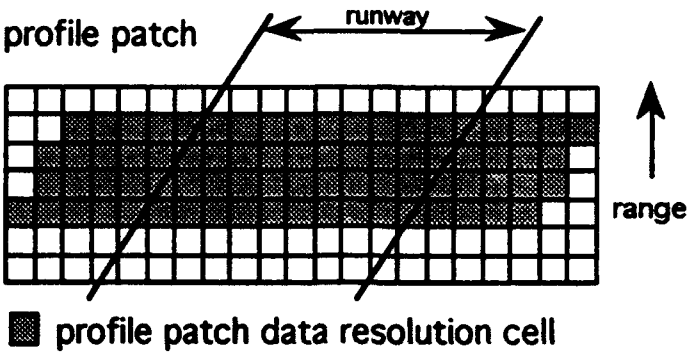

Figure 20. Profile patch representation.

A concept drawing of the field of patches is shown in Figure 21. Runway and grass patches were chosen in pairs at approximately 100 meter intervals along the runway. Locations of other objects in the scene dictated where those patches were sited.

4.1.2.3 Patch Specification

The reference points for areas of interest in the scene were identified by the map x- and y-coordinates. The sensor was identified by a single point. Clutter (grass), and targets (runway, corner reflector, fence), and profile patches crossing the runway were defined by the four corners of each patch. These data were collected manually using a clear grid overlay on the map to identify the coordinates. A whole unit grid on the map was a 1.5 inch square, representing a physical square of 182.8 meters on a side. An accuracy of approximately 1.8 meters was obtained by using map coordinates in defining the coordinates to two decimal places, . The coordinates for each patch were stored in patch definition files (extension .DEF) which were later read in during data processing (see Section 7.2.3).

For sensors with wide azimuth beamwidths, runway and taxiway patches at long distances were not valid because a single radar resolution cell included the edges of the runway (or taxiway) and therefore biased the received power values. Profile patches were defined individually by sensor in order to account for the range averaging requirement (see Section 4.1.2.2). In addition, different patch definition files were required when the location of corner reflectors was changed. A sample file is included in Appendix B; the general format of a single patch definition is:

Patch Num: 5
Patch type: runway
Vertex 1: 8.37,4.92
Vertex 2: 8.53,4.94
Vertex 3: 8.50,5.12
Vertex 4: 8.35,5.10

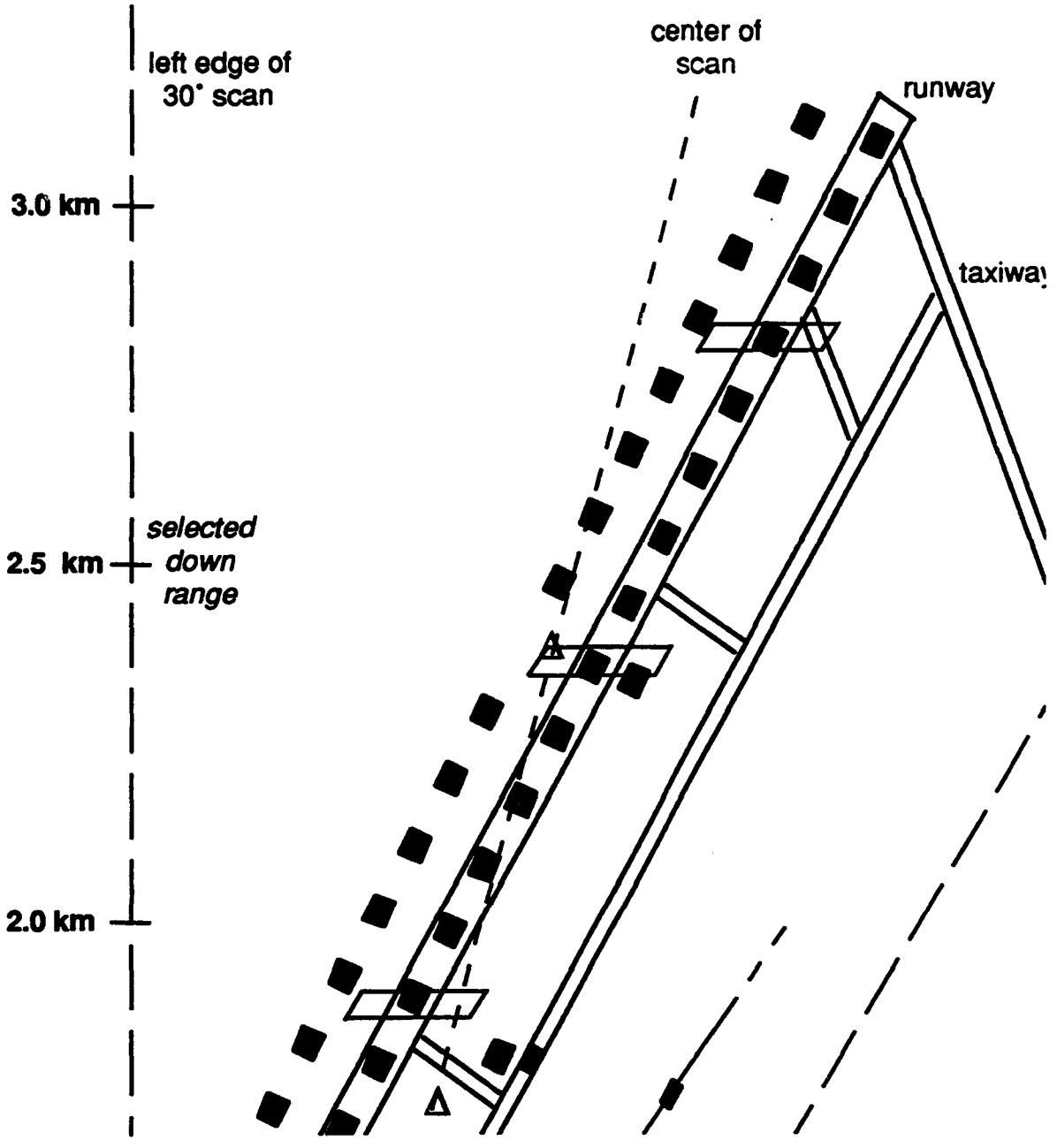

Figure 21. Concept drawing of field of patches.

The Patch Num is assigned ordinally and simply names the patch in the file. The patch types used were runway, long grass, taxiway, corner, fence, and profile. The vertices are the coordinates of the patch in terms of the map scale. In addition to the single patch definitions, these files were used to list pairs of patches for contrast calculations. The patch pairs are identified by the "Patch Num" value shown above.

4.1.3 IR PATCH DEFINITION

In the case of the IR data, three cross-runway patches at different ranges, similar to the profile patches defined in Section 4.1.2.2 and illustrated in Figure 22, were studied. The Figure shows a typical IR image with overlays to delineate features of the image data reduction process. Note that warmer areas are lighter and colder areas are darker in the video image. Patches and linear profiles were defined in the image at three locations along the runway. The mean and standard deviations were computed for the patches, and the radiance was extracted from the profile samples and plotted. The mean and standard deviation values were used to compute contrast and signal-variability ratio (SVR) at three distances from the sensor. The plotted profile was used to derive values for the sharpness of the runway image.

In terms of the individual pixels making up these patches, the angular separation of individual pixels is 0.06 degrees in both vertical and horizontal orientations. At a range of 2,500 m, this corresponds to a projected separation of approximately 2.6 meters. Details which are much smaller than this size will not be resolved. The runway that was imaged was 46 meters wide and was oriented at an angle of approximately 30 degrees with the line of sight in the horizontal plane. The line of sight to the runway was depressed approximately 2 degrees. At a sensor depression angle of 2 degrees, the runway projected image was 53 meters horizontally across the screen and 3.2 meters vertically on the screen. The runway was, therefore, not highly resolved on the screen in the direction perpendicular to the projected runway image.

4.2 METEOROLOGICAL DATA COLLECTION

Meteorological data was collected by E-OIR, Inc., simultaneously with the sensor measurements.[40] The measurements were performed at a location near the center of the imaged scene in order to characterize the average weather conditions at measurement time. An analysis of the relative effect of various measured meteorological parameters on the MMW and IR sensor performance was also produced.

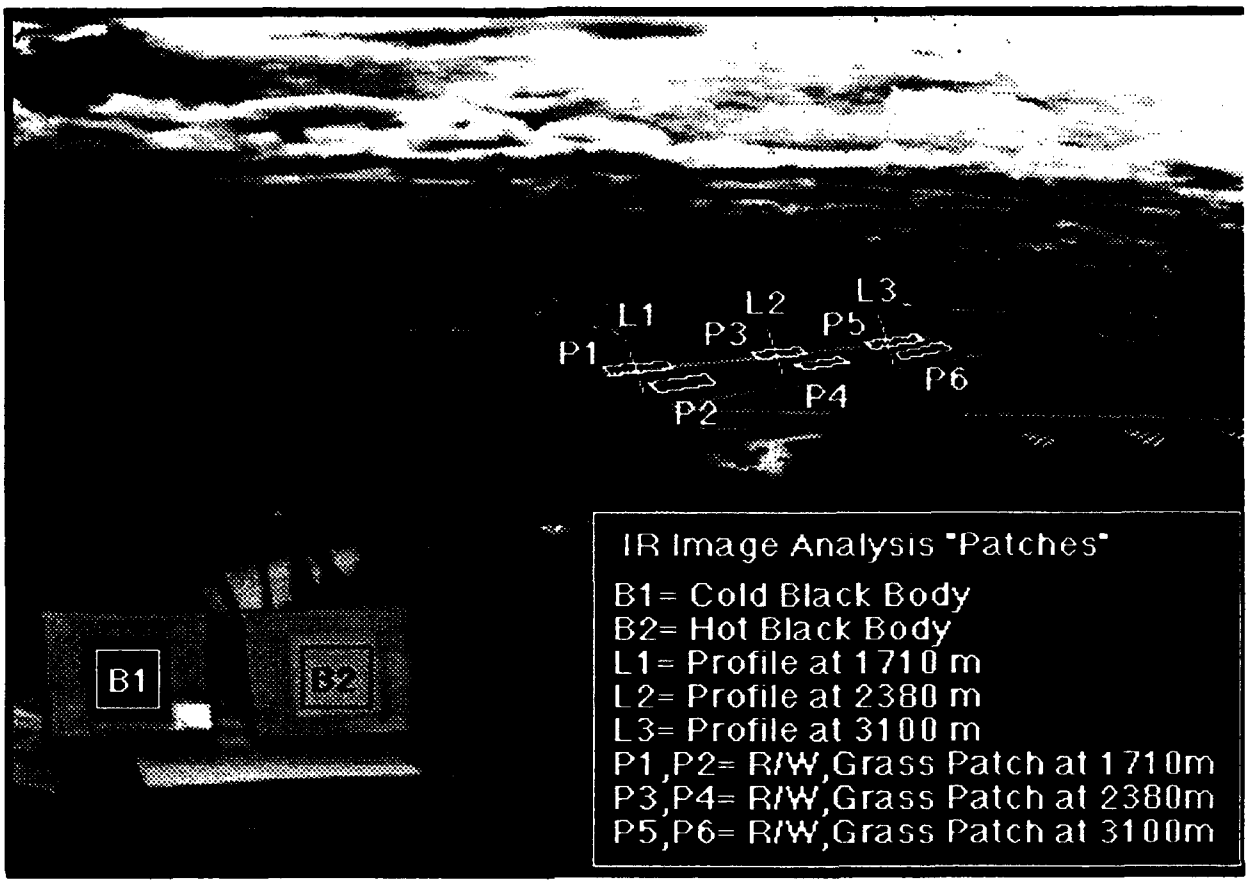

Figure 22. IR image with profile patches overlaid.

4.2.1 DATA SPECIFICATION

It was first necessary to determine what features of the sensors' response are most important to the runway and scene detection process in order to properly specify those meteorological variables which were to be of most importance to the analysis of the sensor data. The primary sensor/scene parameter which is utilized to determine runway detection and identification, as well as to produce clear images, is the contrast between the runway surface and the adjacent clutter areas. A secondary parameter or scene feature which is utilized by the pilot in recognizing and differentiating the runway areas is the grouping and connection of image elements into 'runway' and 'clutter' areas.

The contrast which exists between adjacent runway and clutter surface elements is determined by the relative amounts of incident radiation scattered back to the sensor from each surface element. The surface scattering from these patches will be controlled by the dielectric and thermodynamic

properties of the surface, the angle between the surface patch and the incident sensor, and the surface roughness of the patch. This surface scattering will then be modified by the passage of the sensing radiation through the atmosphere between the sensor and the surface patch.

4.2.1.1 Inherent Contrast

The baseline measure of the inherent contrast of a runway scene is the ratio of the power returned by a dry, level patch of runway to the power returned from a dry, level patch of adjacent clutter. Measurements performed by GTRI at 95 GHz indicate differences on the order of 15 to 20 dB between the returns from dry grass and from dry asphalt for grazing angles of about 5 degrees.[29]

The main effect of varying the incident viewing angle of the sensor on the runway or clutter patch occurs as the sensor scans out to large distances and consequently views the scene at smaller depression angles. This reduction in depression angle and decrease in backscatter occurs for both the runway surface and the adjacent clutter cells. The study cited above indicated that an increase in range, and corresponding decrease in grazing angle, lead to a slight increase in the contrast between the asphalt and the grassy clutter cells on the runway edges for vertical transmit / vertical receive (VV) polarizations. The results from VV polarized returns are summarized in Figures 23 and 24. The cited research shows the normalized VV backscatter from the grassy patches remains relatively constant dropping from -20 dB to -23 dB, as the depression angle varies from 7 to 2 degrees. The normalized backscatter from the asphalt decreases a larger amount dropping from -32 dB to -42 dB, over these depression angles. The difference in the VV returns from the grass and the runway would seem to vary from 12 dB at 7 degrees to a higher value of 19 dB at 2 degrees.

The horizontal polarized transmit/horizontal polarized receive (HH) backscatter, presented in Figure 25, shows slightly different behavior. In this case, the grass backscatter varied from -22 to -25 dB, and the asphalt backscatter varied from -41 to -43 dB. In this case, the normalized backscatter difference between the grass and the asphalt showed very little variation, changing from 19 dB at 7 degrees to 18 dB at 2 degrees.

In general, the study found normalized backscatter differences from 10 to 30 dB between the grassy areas and the runway areas of asphalt and concrete. The backscatter difference generally increased as the depression angle decreased. It would be expected that the backscatter from the relatively smoother asphalt and concrete surfaces would decrease faster than the backscatter from the rougher grass and dirt surfaces as depression angles became closer to grazing angles.

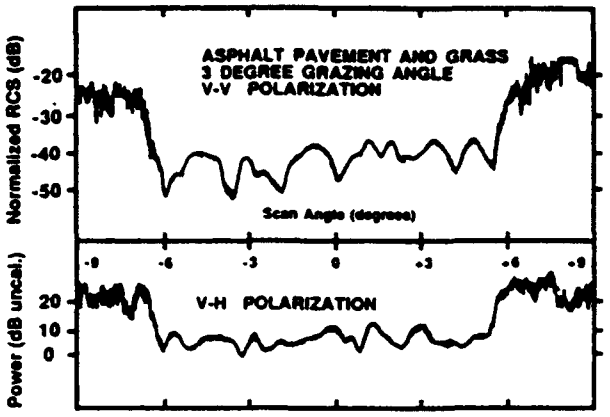

Figure 23. RCS scan of pavement and grass.

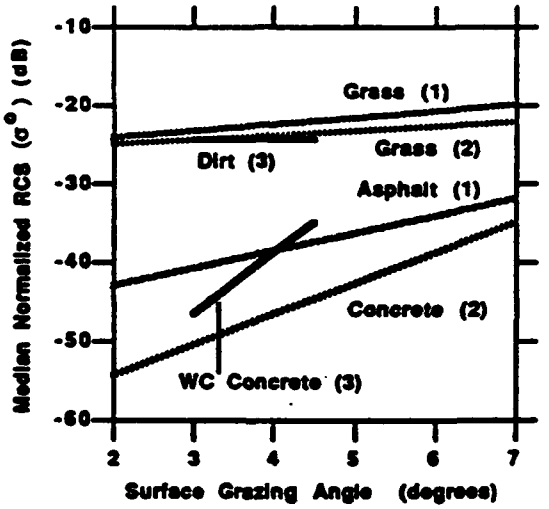

Figure 24. Median RCS for several surfaces with VV polarization.

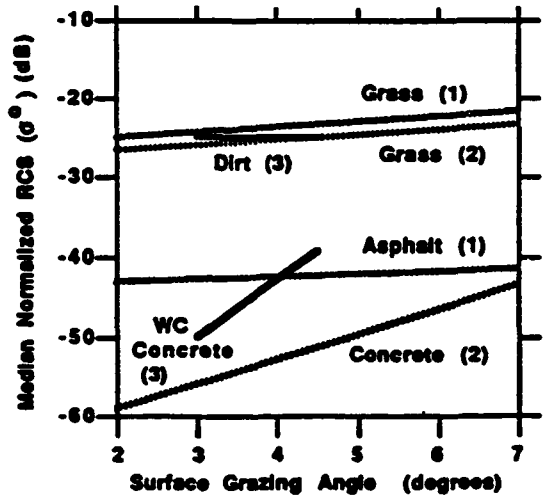

Figure 25. Median RCS for several surfaces with HH polarization.

4.2.1.2 Expected Effect of Surface Water on Inherent Contrast

The effect of accumulated water on the runway and border surfaces at 35 and 95 GHz will be have two major contributions. First, the film of water on the surface will tend to act as an absorber at the MMW frequencies. A secondary effect of the surface water will be the tendency of the water film to fill in small irregularities in the surface profile of the clutter, thus resulting in a generally smoother surface. This smoother surface should act as a more specular reflector and present a reduced backscatter power to the sensor. Thus, it is expected that the returned power from both the runway and the border clutter areas will decrease with wetting from precipitation.

The effect of this reduction in backscatter on the contrast between the clutter and the runway will depend upon which areas are most affected by the wetting. On initial theoretical considerations, it would seem as though the runway might show a greater reduction in RCS with wetting, as it should afford a greater horizontal area for the collection of pooled water and the water pools could more easily level the irregularities in the pavement. This would serve to increase the contrast between the pavement and the adjacent grassy areas.

The effect of surface water on IR contrast will be to equalize the apparent temperatures in the scene through two mechanisms. Primarily, the physical temperature differences are decreased due to the cooling or warming effect of the thermal mass of the water. As a secondary effect, emissivity differences are eliminated, since the emitting surfaces are all liquid water.

4.2.1.3 Expected Effects of Surface Snow on Inherent Contrast

Limited measurements of snow at 35 and 95 GHz indicate that snow covered areas should produce larger MMW backscatter than grassy areas.[20] [27] If the runways have been plowed and the surfaces are clear of snow and ice, a large contrast should appear between the snow covered fields and the runways. It is also expected that the snowfields will evidence more speckle than the clear runway surfaces. As the runways are plowed, piles of accumulated snow to the sides of the runway may also provide high return edges to the runway image.

It is expected, however, that the average contrast will be reduced if the runway surfaces remain covered with snow and ice. In the unplowed scene, the small layer of snow on the runway surface will produce backscatter as similar to that from the thicker layers on the surrounding grass edges. Only very dry or very thin snow layers will exhibit significant differences due to the underlying surfaces.

Surface snow affects the IR scene in a manner similar to that of rain. The surface temperature differences are eliminated due to the insulating effects of snow covering scene elements, and the emissivity of the scene elements are uniform over the extent of snow cover.

4.2.1.4 Atmospheric Effects on Inherent Contrast

The effect of the propagation of the sensor's radiation through the intervening atmosphere will modify the apparent contrast between the runway and the adjacent clutter areas. Two different atmospheric phenomena will affect the contrast. These phenomena are attenuation, due to both the atmospheric gases and the suspended and precipitating particles, and atmospheric backscatter of MMW radiation primarily from precipitation particles. The atmospheric effects on the passage of IR radiation along the path from the scene to the sensor include attenuation but do not include backscattered radiation, since the IR sensor is a passive system. A similar result is brought about, however, by radiation emitted by atmospheric constituents along the path.

Atmospheric attenuation, whether caused by molecular absorption or scattering, will tend to reduce both the radiation incident on the runway or grass cell under study and the backscattered radiation received by the sensor. If the backscatter from the runway and the grass areas are both of sufficient strength that the atmospheric attenuation will not bring either below the noise level of the receiver, the atmospheric attenuation will have no effect on the contrast between the two areas. The attenuation will cause a similar decrease in the level of both received powers in log space but no overall decrease in power ratios. If, however, one or both of the backscattered powers are sufficiently close to the receiver noise floor, the additional reduction caused by atmospheric attenuation may cause the signal to bottom out at this floor. The contrast perceived by the sensor will then be limited by the noise floor rather than the true inherent contrast between the two areas.

The effects caused by radiation backscattered from rain, snow, and suspended fog particles will tend to decrease the contrast perceived between the runway and the clutter cells. The backscattered power normally received from an area of the runway should be lower than the amount of power received from an equivalent area of adjacent terrain. If backscatter due to raindrops is also present in the volume being sensed by the MMW radar, the rain backscatter should essentially add to the power backscattered by either surface area, as all scatterers involved are relatively independent. While the difference in power between the two areas remains the same, the background against which this difference is judged, the terrain, has an increased intensity. The contrast, therefore, will tend towards a smaller, negative value; that is, the contrast will tend towards zero. This contrast degradation will be especially noticeable on a logarithmic

scale, as an addition of the same increment, in linear power space, to the low return from the runway surface will produce a greater logarithmic increase than the addition of the same amount of power to the higher power return from the terrain.

The magnitude of the IR path radiance is coupled to the amount of absorption by particulate and molecular components of the atmosphere through a form of Kirchoffs Law. This means that the energy radiated by a segment along the path must balance the energy absorbed within that segment at all wavelengths. If there is no absorption, then there is no path radiation at a given wavelength. Conversely, as the path length is made longer so that the amount of absorption grows more significant, the amount of path radiance grows accordingly. The path radiance acts as a constant additive signal over the entire IR image and also contributes to the overall noise level in the image data. Attenuation of IR radiation causes the signal levels and differences to be reduced in all areas of the image, thereby lowering the contrast.

4.2.1.4.1 RAIN EFFECTS

The most important weather parameters in terms of potential impact on the radar observations are the precipitation parameters. The rainfall rate and raindrop size distributions will both produce significant effects on the MMW sensor performance due to both absorption and scattering of the incident millimeter wave radiation by raindrops.

The raindrop sizes are much greater than the wavelengths used by the IR sensor, so Mie scattering theory is not required to compute the attenuation of IR radiation in rainy conditions. In the large drop size regime, the extinction efficiency is approximately equal to 2.0, and the extinction contributed by individual drops is twice their cross sectional area. The drop size distribution in rain may be adequately approximated with the applicable empirical raindrop size distribution models discussed below in connection with MMW scattering computations. IR extinction by raindrops was computed from the measured raindrop size distributions when measured data were available. Measured rain rate was used with an empirical drop size model when measured drop sizes were not available.

A common and well-accepted model which relates attenuation to rain expresses the attenuation as an exponential function of rain rate, as is shown below.[41]

$$k = aR^b \tag{8}$$

where: k is attenuation coefficient (dB/km)
R is rain rate (mm/hr)
a and b are empirical coefficients.

The empirical coefficients, 'a' and 'b', were calculated using Mie scattering theory by Olsen using four of the most widely used models of raindrop size distributions. These calculations were performed at -10° C, 0° C, and 20° C and at several frequencies between 1 and 1,000 GHz. Results of these calculations at 35 and 95 GHz are reproduced below in Table 16. In this table, the two-letter abbreviations refer to the four empirical raindrop size distributions as follows:

LP-l is the Laws and Parson distribution in light rains,
LP-h is the Laws and Parson distribution in heavy rains,
MP is the Marshall-Palmer distribution,
JT is the "Thunderstorm" distribution presented by Joss, et al., and
JD is the "Drizzle" distribution presented by Joss, et al.

Approximate attenuation values at 35 and 95 GHz for the tabulated values of 'a' and 'b', a Marshall-Palmer raindrop size distribution, and an ambient air temperature of 10° C are shown in Table 17. These calculations predict that attenuation of greater than 3 dB/km will be produced by rainfall rates greater than about 10 mm/hr at 35 GHz and by rainfall rates greater than 3 mm/hr at 95 GHz.

Table 16. Parameter Values for Exponential Attenuation Expression

case	temperature	LP-l	LP-h	MP	JT	JD
'a' values						
35 GHz	-10°	0.236	0.346	0.275	0.376	0.197
	0°	0.232	0.345	0.268	0.372	0.180
	20°	0.235	0.337	0.269	0.360	0.167
95 GHz	-10°	1.020	0.946	1.350	0.877	1.110
	0°	1.050	0.956	1.420	0.909	1.180
	20°	1.060	0.948	1.460	0.936	1.240
'b' values						
35 GHz	-10°	1.021	0.910	1.002	0.784	1.016
	0°	1.022	0.907	1.007	0.783	1.053
	20°	1.009	0.904	0.999	0.782	1.107
95 GHz	-10°	0.757	0.776	0.753	0.657	0.943
	0°	0.749	0.775	0.742	0.650	0.941
	20°	0.745	0.775	0.733	0.642	0.936

Table 17. Modeled Attenuation as a Function of Rain rate

Rain rate (mm/hr)	Attenuation (dB/km) 35 GHz	95 GHz
0.254	0.07	0.53
2.54	0.7	2.9
12.7	3.4	9.4
50.8	14	26
152.4	41	58

An additional important effect of the rain on the millimeter wave sensor performance is the backscatter return from the rain itself. This backscatter has been measured by GTRI and BRL.[46][18] Approximate values of this backscatter were calculated from the empirical exponential relationship $\eta = cR^d$, where η represents the rain backscatter, R represents the rainfall rate, and the parameters 'c' and 'd' are empirical coefficients determined from data recorded during that investigation. It should be noted that these backscatter coefficients, 'c' and 'd', differ from the attenuation coefficients, 'a' and 'b', presented earlier. A table of several backscatter values calculated using formulae of this form, for both the GTRI and the BRL data sets, is presented below in Table 18.

Table 18. Backscatter from Rain

Frequency	Rain Rate (mm/hr)	Linear Polarization from BRL	Linear Polarization from GTRI	Circular Polarization from GTRI
35 GHz	1	2.21×10^{-5}	1.3×10^{-6}	2.6×10^{-8}
	10	2.48×10^{-4}	6.2×10^{-5}	3.4×10^{-6}
	50	1.34×10^{-3}	9.8×10^{-4}	8.3×10^{-5}
		$\eta = 2.21 \times 10^{-5} R^{1.05}$ (from BRL)		
95 GHz	1	8.89×10^{-5}	1.5×10^{-5}	2.2×10^{-6}
	10	3.30×10^{-4}	1.9×10^{-4}	2.8×10^{-5}
	50	8.27×10^{-4}	1.1×10^{-3}	1.7×10^{-4}
		$\eta = 8.89 \times 10^{-5} R^{0.57}$ (from BRL)		

The measurements can be seen to differ by a significant amount. A closer look at the scatter which existed in the individual measurements which make up the data sets shows that the representations are in statistical agreement with one another. The first major point one should infer from these data is that, although the cross-section for a single square meter is relatively small, for pulse lengths and beamwidths which encompass hundreds or thousands of cubic meters of volume, the backscattered radar return from rainfall can be considerable at higher rainfall rates. A second point to be recognized from the data is the significant reduction in radar backscatter seen with circular polarization as compared to linear polarization. The values for circular polarization were generally 10 to 15 dB lower in the GTRI data sets and about 20 dB lower in the BRL data sets.

The perceived rainfall rate may have a distinct dependence on integration time for rapidly evolving precipitation events such as thunderstorms and squall lines.[2] The choice of integration interval should be chosen such that it reflects the dimensions of the sensor resolution cell volume. Given the sensor pulse width, the sensor antenna pattern, and the ranges over which measurements were conducted, the ranges of backscatter which would be expected for various rainfall rates may be estimated based on the radar resolution cell volume. Indirectly from this volume, some general expectations on the variability of the rainfall rate can be calculated, and appropriate sampling intervals may be defined.

4.2.1.4.2 CLEAR AIR, FOG AND HAZE EFFECTS

Suspended fog and haze particles produce attenuation effects on the perceived runway visibility. This attenuation generally has a smaller effect than the attenuation and backscatter due to rain, but it is still significant and warrants close and careful observation. Fog and haze droplets will

affect the MMW sensor performances through absorption and scattering of the MMW energy by the droplets. The sizes of the drops in fog and haze are small enough, compared to the wavelengths of the incident radiation, to allow treatment of these particles as scatterers in the Rayleigh regime. This simplifies the scattering and absorption calculations for these particles.

The attenuation of IR radiation by fog and haze particles is generally significant whenever optical visibility is reduced by the fog or haze. The sizes of the aerosol particles involved are of the same order of magnitude as the wavelengths used by the IR sensor, so the drop size distribution is crucial to understanding the effect of fog or haze on IR radiation. Measured droplet size data must be available, and Mie scattering theory must be used to compute the attenuation of IR radiation by fog or haze particles. GTRI implemented an IR attenuation model based on droplet scattering for two example fog droplet size distributions, as described in Section 3.2.2. Additionally, the effects of molecular scattering, especially by water vapor, are also non-negligible at the IR sensor wavelengths. Modeling of molecular effects for the IR tower test data would be a complex effort and was therefore beyond the scope of IR analysis on this contract.

Humidity and air temperature affect the millimeter wave attenuation to an order of magnitude less than the condensed precipitation effects. These water vapor and oxygen absorption effects are still somewhat significant and may be estimated using several generally accepted models based on O^2 and H^2O absorption lines and the water vapor continuum absorption.

One of the most widely referenced models for clear air absorption at millimeter and near millimeter wave frequencies is the MPM-N model of the National Telecommunications and Information Administration (NTIA) of the U. S. Department of Commerce.[35] This model gives predicted attenuation values of 0.03 to 0.35 dB/km at 35 GHz and 0.04 to 2 dB/km at 95 GHz for relative humidities ranging from 0% to 100% (P = 101.3 kPa, T = 25° C). This model is capable of adding rain and fog events on top of the oxygen and water vapor absorption effects to predict attenuation due to rain in a humid atmosphere. Example calculations are presented in Table 19.

Table 19. Calculated Attenuation From MPM-1

Frequency (GHz)	ATTENUATION (dB/km) Dry Air +	Water Vapor +	Haze, Fog Cloud +	Rain =	TOTAL
Case Number 1 (Clear Air, 0% Relative Humidity)					
35	0.03	0.00	0.00	0.00	0.03
95	0.03	0.00	0.00	0.00	0.03
Case Number 2 (100% Relative Humidity)					
35	0.03	0.13	0.00	0.00	0.16
95	0.03	0.74	0.00	0.00	0.77
Case Number 3 (Light to Medium Fog, 0.01 g/m^3)					
35	0.03	0.13	0.07	0.00	0.23
95	0.03	0.74	0.41	0.00	1.18
Case Number 4 (Heavy Fog, 1 g/m^3)					
35	0.03	0.13	0.71	0.00	0.87
95	0.03	0.74	4.08	0.00	4.86

Accurate measurements of both precipitation and suspended particle size distributions are important in determining both the scattering and absorption of the IR radiation. The nature of the effects of the particles followed the effects shown for radar sources. The major difference between the two radiation regimes comes from the difference in wavelength between the IR and the MMW radiation. The IR wavelengths are much shorter, on the order of 10^{-6} m compared to 10^{-3} m for MMW radar. The IR radiation is therefore scattered significantly by the smaller fog and haze particles which tend to have a lesser influence on the MMW radiation. The scattering and absorption at IR wavelengths by rain, fog, haze, humidity, and clear air conditions are treated in the LOWTRAN and FASCODE computer models.[4]

4.2.1.5 Soil Temperature

Soil surface and runway surface temperatures are important for the interpretation of the IR measurements. The actual temperature of the surfaces is less important for MMW applications than the determination of frozen versus unfrozen surfaces. It has been shown in previous studies, that the liquid water content of the surface layer of snow, as well as the melt/freeze history of that surface, is very important in determining the MMW backscatter characteristics of the snow.[27] The backscatter generally decreases with increasing liquid water content, due to increased absorption by the water. Metamorphic snow, which has undergone at least one

melt/freeze cycle, has been shown to produce considerably more backscatter than fresh fallen snow.

The IR image contrast is mainly driven by runway and background temperature differences. A temperature sensor attached to the runway surface is adequate to provide the temperature of the radiating surface of the runway, but it is much more difficult to determine the actual temperature of the radiating elements of the grass background. Since portions of the blades of grass at differing temperatures are contributing to the image, any single temperature probe position would not be sufficient to characterize the radiant temperature. The soil temperature as measured by a probe at the soil surface was utilized to give some rough idea of the temperature of the radiation source in the grass background.

4.2.1.6 Radiation Flux Measurements

The IR measurements use direct and indirect solar radiation as an illuminator of the measured scene and as a source of heating and cooling of scene component elements. The two major IR parameters which must be measured are the direct and indirect solar radiation and the long wave re-radiation from the earth. This IR loading may also have an indirect effect on the MMW measurements through its influence on the metamorphic processes occurring within the snowpack.

4.2.1.7 Wind Measurements

Wind speed and direction influenced the measurements directly through a number of means. Winds could cause the bending of grasses and trees, thereby influencing the clutter backscatter properties. Strong winds may also pick up dust and sand. The suspended dust and sand particles may then influence the propagation of the sensor's signals. Indirectly, wind speed and direction measurements may enter into the 'active volume' and sampling interval calculations.

4.2.1.8 Hourly Surface Observations

Precipitation, wind, temperature, and humidity histories are important in determination of the state of frozen/metamorphic surfaces. These variables also aid in the determination of the presence or absence of water on the ground in the form of standing pools of water or in the form of a film which wets the ground clutter. Experimental observations as well as theoretical considerations lead to the expectation that thin water films, as well as pools of standing water, will tend to decrease the MMW RCS of the clutter through absorption of the RF radiation as well as by providing a smoother surface which will provide less backscattered radiation. It was also

suggested that adequate measurements be made of snow depth and snow liquid water content to allow these parameters to be included in the parameterization of runway visibility.

4.2.2 METEOROLOGICAL DATA PROCESSING

4.2.2.1 Overview of Meteorological Parameters Measured

The suite of instruments deployed in the field to measure the meteorology for these tests was chosen by the subcontractor responsible for the actual weather measurements, E-OIR, Inc. The choices they made were based on the availability of instrumentation, the requirements of the sensor test plan, and the results of the meteorological variable analysis. Therefore, while there were parameters which would have been helpful that were not measured, a great majority of the important meteorological parameters were monitored. A summary of the variables which were recorded and the frequency at which measurements were made is presented in Table 20. A summary of the operating characteristics of all the instrumentation, their exact locations within the experimental range, the data recording process, and the data verification and reduction procedures employed by E-OIR, Inc. are included in the E-OIR final report.[40] This information is summarized below.

Meteorological ground truth was collected using the Yellow Meteorological Measurement and Collection package (YMAC), an OPTEC Long Path-length Visibility (LPV) transmissometer, a NASA rapid response Rain Rate System (NRRS), a PMS Forward Scattering Spectrometer Probe (FSSP), and a PMS Ground Based Precipitation Probe (GBPP). The YMAC collected a wide variety of basic meteorological data over two different measurement intervals, one minute and ten minutes. The data collected by YMAC and the interval at which the data were collected are summarized in Table 20. The one minute data items from the YMAC data set were collected every minute and stored for later retrieval. The ten minute data items from the YMAC data set were collected at a ten second sampling rate and averaged over a ten minute interval, and these ten minute averages were stored for later retrieval. Thermistors were placed on the runway surface to monitor these temperatures beginning in Phase 4 of the project, starting on March 2, 1992. Data from these sensors were collected at a one minute interval.

The OPTEC LPV transmissometer collected data at an effective sample rate of 1.25 kHz. These samples were averaged to produce one minute averages of visibility. The FSSP collected fog particle size spectra over two different ranges, 0.5 to 8 μm and 2 to 47 μm, over alternating one minute sampling intervals. The effective rate at which a specific fog particle size range was collected was therefore every two minutes. The GBPP collected rain droplet data over a single size range, 0.2 to 12.4 mm, at one minute intervals. The raw counts from the size bins of the

PMS probes and the LPV one minute average data were saved for later retrieval. These data, and data from an HSS Forward Scatter visibility instrument, are discussed in greater detail in Section 4.2.2.4.

The NRRS collected rain weight values at one second intervals. E-OIR recorded both the one second raw weight values and a ten second running average of calculated rain rate for later retrieval. While these ten second running averages were useful in the initial verification of data received from E-OIR, GTRI applied a different set of averaging algorithms to the one second rain weights to produce 10, 30, and 60 second average rain rates for use in interpreting the MMW radar and IR data sets.

As an aid in determining the meteorological conditions which led up to the instrumented test periods, copies were requested of the hourly surface reports made by the WPAFB observer. These observations were used to gain a general feeling for the overall weather situation at the test site and as a check against the conventional meteorological parameters measured by E-OIR. These reports would also aid in the determination of snow depth and condition had such situations been important during the test.

Table 20. Meteorological Parameters Monitored

Parameter	Measurement Interval
YMAC Data Set	
Air Temperature	10 minutes
Dew Point	10 minutes
Solar Irradiance	10 minutes
Terrestrial Radiance (2)	10 minutes
Barometric Pressure	10 minutes
Temperature from Absolute Humidity Sensor	10 minutes
Soil Temperature - Short Grass	10 minutes
Soil Temperature - Long Grass	10 minutes
Rain Amount (Tipping Bucket)	1 minute
Wind Speed	1 minute
Wind Direction	1 minute
HSS Visibility (Forward Scattering Probe)	1 minute
Absolute Humidity	1 minute
Runway Thermistor Data (after 1 March 1992)	1 minute
Non-YMAC Data	
Long Path Optical Visibility	1 minute
Fog Droplet Size Distributions	1 minute
Rain Drop Size Distributions	1 minute
Rapid Response Rain Rate Sensor Data	1 second

4.2.2.2 Rain Instrumentation

Three instruments were used to measure rainfall parameters during the course of the experiment. These instruments were a conventional tipping bucket rain gauge, the NASA rapid response Rain Rate Sensor (NRRS), and the Ground Based Precipitation Probe (GBPP). Each of these instruments collects rain data in a different way and, therefore, each instrument has different uses and different strengths and weaknesses. In this section, the three instruments are described and compared. Justifications for the preferred use of one instrument in favor of another is also presented. Finally, the unique data products available from the NRRS and the GBPP are described.

The Weathertronics model 6021-A tipping bucket rain gauge was used in this experiment. The resolution of this device is 0.01 inch of rainfall. That is, the gauge records every 0.01 inch of accumulated rainfall. A strength of the tipping bucket is its ability to continuously record rain rates. The major disadvantages of the tipping bucket gauge are the necessity of the device to accumulate 0.01 inch of rainfall before an output is produced. In very low rain rate situations tips become very infrequent and therefore the temporal resolution of the tipping bucket may be much greater than the sensor measurement run. A second disadvantage of the device, again related to the necessity of recording 0.01 inch, occurs during periods of relatively high rainfall. The tipping bucket will act as a low pass filter on the rain data. Relatively short periods of extremely intense rainfall may be averaged in with longer periods of less intense rainfall, resulting in an overall mean rain rate which may not be representative of the time the sensors were surveying the scene.

NASA developed the NRRS to address a second deficiency, the under representation of intense precipitation episodes, inherent in the measurement of rain rate with conventional tipping bucket gauges. The NRRS allows the calculation of rain rate by using a sensitive load cell to weigh accumulated rain captured by the instrument once a second. The resolution of the load cell and associated electronics in the NRRS is 0.01 pounds (17.6 g). The equivalent rainfall rate resolution this weight resolution represents depends on the sampling time used to collect the data. At the maximum sampling rate of 1 Hz, this weight change represents a rain rate resolution increment of 17.6 mm/hr. At 0.1 Hz, or a ten second sampling rate, the same weight resolution translates into a rain rate resolution of 1.76 mm/hr. A thirty second sampling rate leads to a rain rate resolution of 0.59 mm/hr.

When the NRRS is first turned on, it enters a 'rain search mode'. If the instrument senses an increase in the load cell weight of more than 18 grams over any single one hour interval, it enters into a data acquisition mode. During the data acquisition mode, the weight of the load cell is sampled every second, and the result is saved to disk. After 20 minutes of operation, the data file is closed, and the instrument returns to the rain search mode. If it is still raining, the device will again wait until the load cell weight has increased by 18 grams before opening a new data file and acquiring additional data. During periods of prolonged rain, this may lead to significant gaps in the rainfall rate record.

Raindrop size spectra were measured using a Particle Measurement Systems (PMS) Ground Based Precipitation Probe (GBPP). The GBPP is capable of measuring particles with diameters ranging from 0.2 to 12.4 mm. The GBPP sorts detected raindrops into 62 size bins with mean diameters separated by approximately 0.2 mm. These raw drop counts may be used to calculate

number concentration densities of the drop size spectra, that is, the number density of drops contained within a specific size interval. These number concentration densities may then be further processed, using size specific terminal velocities, to obtain estimates of the prevailing rainfall rate. The same number concentrations may be used, by applying scattering theory, to obtain estimates of attenuation and backscatter due to the rain.

4.2.2.3 Fog Instrumentation

Fog and haze droplet parameterization were obtained through measurements performed by a PMS (Particle Measuring Systems) FSSP-100 (Forward Scatter Spectrometer Probe) instrument. This instrument is capable of measurements of fog and haze droplet size spectra over four overlapping size intervals, each of which is divided into 15 linear size intervals. These ranges and intervals, in terms of droplet diameters, are enumerated in Table 21.

Table 21. FSSP-100 Drop Size Ranges

Range Setting	Size Range (μm)	Size Interval (μm)
0	2 - 47	3
1	2 - 32	2
2	1 - 16	1
3	0.5 - 8	0.5

The optimum range settings used for the Synthetic Vision Tower Tests were determined so as to provide adequate information for interpretation of both the MMW and the IR data. Of secondary importance, for this particular test, was a desire to adequately describe the fogs and hazes to provide feedback for various MMW and IR modeling efforts. With these objectives in mind, two range settings were chosen for recording during the tests. The size intervals measured were range '0', covering droplet diameters of 2 to 47 μm, and range '3', covering droplet diameters of 0.5 to 8 μm.

An appropriate investigation into the performance of the FSSP instruments and the general practice of fog and haze measurement techniques has been performed by the Air Force Geophysical Laboratory (AFGL). AFGL conducted over 90 hours of fog and haze measurements at Otis Air National Guard Base on Cape Cod in Massachusetts.[34] Both the measured characteristics of the fogs and the performance of the FSSP instruments were examined in this work.

During the AFGL tests, the FSSP was operated in a manner such that the instrument was sequentially stepped through the four measurement ranges. Spectra were obtained over 10 second intervals for the three smaller droplet ranges and over a 20 second interval for the largest droplet range. The possibility of operating the EO/IR FSSP in such a sequentially stepped manner should be investigated to allow more thorough coverage of the fog and haze droplet distributions.

The AFGL tests were performed using two separate simultaneously operated FSSPs. The instruments were mounted at 5 and 30 meter heights. The comparison of the fog and haze spectra measured at these two heights reveals major differences in both the composition and effects of the droplets with height. The major differences are delineated as follows in Kunkel's paper.[34]

"1. higher extinction coefficients and liquid water contents, derived from the drop-size spectra, at the 30 m level by a factor of two or three over those measured at the 5 m level.
2. generally, higher mean fog drop sizes (droplets > 2.5 μm) at the 5 m level because of a substantial increase in the number of small fog droplets at the 30 m level.
3. higher concentrations of haze particles at the 5 m level than at the 30 m level, as illustrated in Figure 4. (not reproduced here)
4. higher concentrations and more pronounced peak in droplet spectra between 5 and 10 μm at the 30 m level. This, in combination with 3), indicates a growth of haze particles into small fog droplets as they ascend to the higher levels.
5. lower concentrations in the 10-20 μm range at the 5 m level resulting in a relatively flat distribution in the 10-30 μm range as compared with a sloping distribution in the same range at the 30 m level ..."

The results of the AFGL report should highlight two issues in the fog and haze droplet measurements. Adequate measurement of the droplet size distributions can be achieved by stepping through the gain settings, or at least by taking measurements at both the highest and lowest gain settings, so as to provide complete spectral coverage. A second issue raised by the results of this reports was the optimum placement of the FSSP instrument to provide a representative sample of the droplet spectra. The best arrangement would have been to obtain an additional FSSP instrument and measure the fog parameters at two different levels, ideally at the sensor elevation and at ground level. Unfortunately, the tests were limited to the use of a single FSSP. The placement of the single sensor then defined the single point at which the fog/haze spectra would be valid. In an effort to adequately sample ground fogs, but also to attempt to characterize the fog spectra at heights more representative of the path between the sensor and the scene, the FSSP was raised as high as practical while remaining in the vicinity of the

meteorological sensors suite. This action placed the FSSP atop the operators shelter at a height of about 4.57 m above the ground.[40]

The Kunkel paper also contains some study results relating to both mean terminal velocity of the fog droplets and the optical extinction coefficient. For the Synthetic Vision meteorological analyses, only the optical extinction coefficient results are of interest.

Liquid water content, obtainable from the fog/haze droplet distributions, can be related to an extinction coefficient 'b' or visibility 'V'. These two terms are related as

$$V = - (\ln(e)/b) \tag{9}$$

where 'e' is the threshold of contrast and is assumed equal to 0.02 for meteorological applications and 0.05 for operational applications with the FAA. For a known drop-size distribution

$$b = \pi * \Sigma (Q_{ext} n_i r_i^2) \tag{10}$$

where Q_{ext} is the normalized extinction cross section.

4.2.2.4 Optical Visibility

Optical visibility was measured with both the HSS VF-500 forward scatter visibility sensor and the OPTEC Long Path Visibility (LPV) transmissometer.[40] The HSS instrument was used to measure the runway visual range (RVR) and the OPTEC LPV was used to measure the slant visual range from the sensor location to an area centrally located in the sensor field of view. The LPV is capable of visibility measurement at four wavelengths (550, 750, 800 and 900 nm) in the visible band. The operating frequency of the HSS instrument has not been declared, but it is assumed to also operate in the visible light region. These instruments provided information for use in determining the category of reduced visibility events against which to evaluate the IR and MMW sensor performance. They also provided a check on the measurements of the fog and haze droplets, as optical visibility could be computed from the drop size distributions.

SECTION 5
MMW PERFORMANCE MODELING

5.1 MODEL DEFINITION

5.1.1 MMW SCENE IMAGE PREDICTION MODEL DESCRIPTION

Georgia Tech Research Institute (GTRI) radar modeling software was used to predict real beam MMW sensor images of the Wright Patterson Airfield scene. Figure 26 shows the basic steps in modeling MMW radar sensor images and the computer program associated with each step.

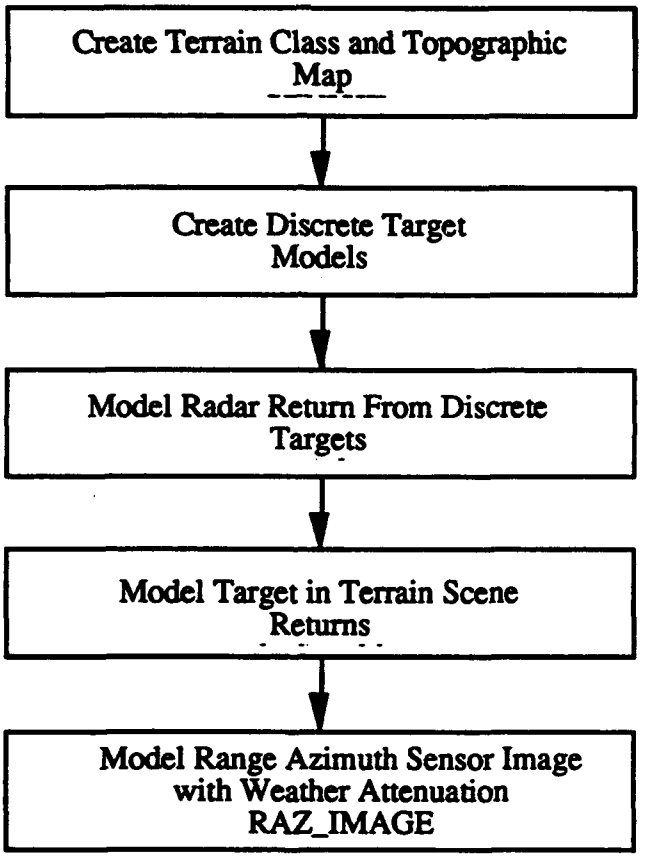

Figure 26. Flowchart of MMW scene image prediction.

5.1.1.1 Terrain and Target Geometry Models - GTVISIT and MAX

MMW scene image prediction begins with describing the input terrain and discrete target features. GTSPECS requires an input terrain data base specified by a terrain class file, a terrain topographic file, and a terrain classification information file. The terrain class file specifies an x, y grid of terrain class numbers that correspond to the different terrain types in the scene described by parameters in the terrain classification information file. The terrain topographic file

specifies an xy grid of terrain elevations. The terrain elevation points in the topographic file correspond to the terrain class numbers in the class file. Therefore, the number of grid points in the topographic file and the class file must be the same.

For the Wright Patterson airfield scene, the terrain class map and topographic map were created with the GTVISIT program.[25] The class map was created by dividing the scene into polygonal blocks of the same terrain. A sample terrain setting is shown in Figure 27a. The accompanying input terrain class map is shown in Figure 27b. Each block of terrain in the scene was assigned a terrain class number. In Figure 27b, the class numbers are indicated with a leading C.

The topographic map describes the terrain surface height profile. A mean height and standard deviation of height was specified for each terrain type in the class map, and the terrain heights for each class were distributed based on the mean height and standard deviation of height for the class.

The terrain classification information files were created by the user. For each terrain class in the scene, the following parameters must be specified:

σ_h - rms surface roughness of the terrain type,

γ - surface reflectivity parameter of the terrain type, and

b - Weibull slope parameter of the terrain type.

The surface reflectivity parameter of the terrain type, γ was derived from published measurement data terrain clutter from various types of terrain. The rms surface roughness of various terrain types and the Weibull slope parameter were also taken from published data.

Discrete target models were created with MAX, a graphical geometric data base editor.[42] For target in terrain images, the target model must be built with flat plate target primitives. Different material types on a target surface were modeled by grouping scatterers of the same material type together and assigning a material number. Figure 28 shows the MAX model of the aircraft bunker used in the Wright Patterson Scene. The aircraft bunker surface was modeled as metal, and the windows were modeled as glass.

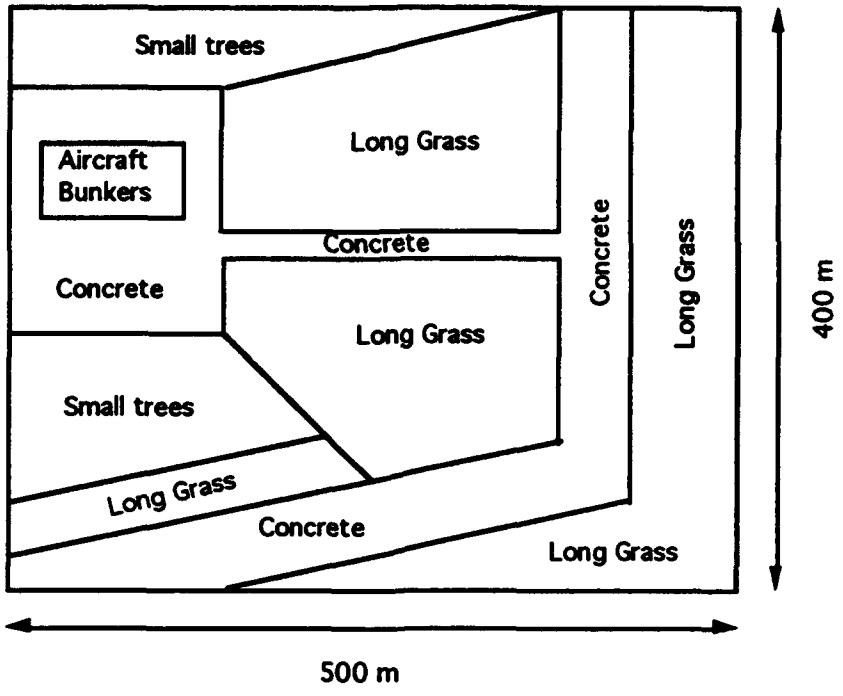

Figure 27a. Example terrain area map.

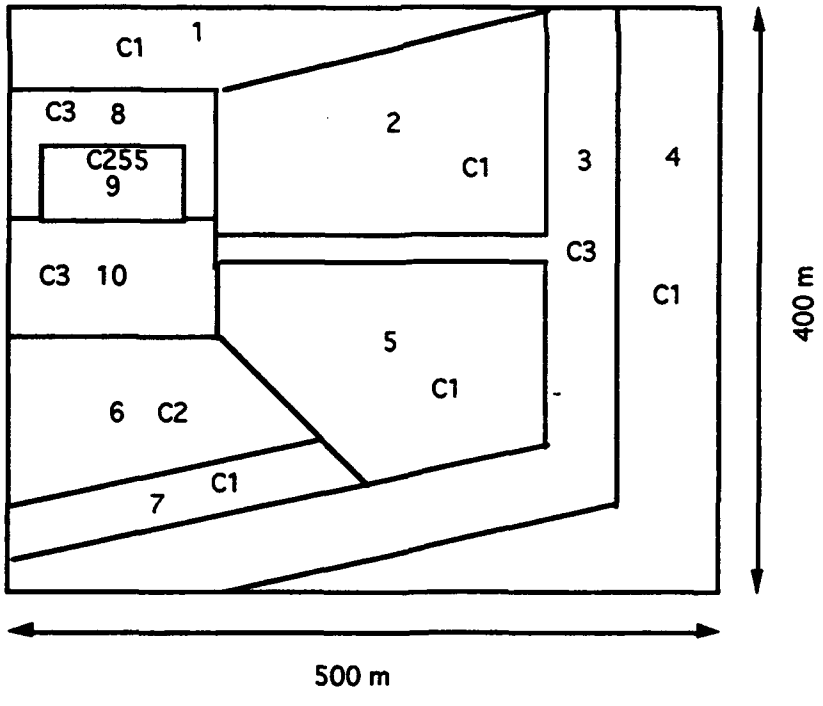

Figure 27b. Example terrain area polygon class map.

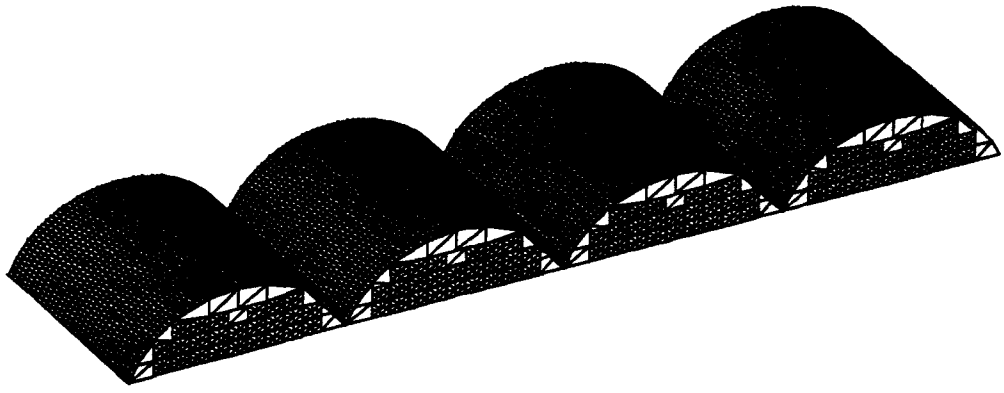

Figure 28. MAX model of aircraft bunker at Wright Patterson airfield scene.

5.1.1.2 MMW Radar Models

TRACK was used to predict the RCS of each flat plate in a MAX discrete target model.[21] Physical Optics (PO) techniques were used to compute the radar return from the flat plates in the discrete target model. The Method of Equivalent Currents (MEC) was used to predict the edge diffraction from discontinuities on a target body.

The RCS models in TRACK include the effects of diffuse scatter from rough target surfaces. PO theory assumes that the scatterers are perfectly smooth. At MMW radar frequencies, the specular scattered return from a realistic target surface is less than the specular scattered return from a smooth surface. The diffuse scatter from a target surface at MMW frequencies is greater than the PO prediction for a smooth surface. In TRACK, a rough surface is modeled as a distributed surface with heights defined by an rms surface roughness and an rms surface height.[10] The PO integral for scattering from the surface is evaluated with an approximation developed by Barton for low angle radar tracking.[7] The rms surface roughness determines the amount the rough surface reduces the RCS in magnitude from that of a completely smooth surface. The rms surface slope determines the broadening of the main lobe of the scattering pattern as compared with the main lobe of the scattering pattern of a smooth surface.

GTSPECS computes the scene terrain clutter and performs shadowing calculations for target on terrain shadowing and terrain on terrain shadowing. In GTSPECS, the Barton land clutter model is used to compute the clutter reflectivity, χ [6]

$$\chi = \sigma^o F_c^4 \tag{11}$$

where σ^o is the mean RCS per unit area of illuminated surface, and F_c is the two way pattern propagation factor for radar, clutter, and path geometry. Published data for σ^o agree with a constant gamma model

$$\sigma^o = \gamma \sin \psi \tag{12}$$

where γ is a reflectivity parameter associated with the terrain type, and ψ is the grazing angle of the incident radiation. Usually, γ values for different terrain types are given in decibels. In the above equation, γ is an absolute value. γ_{dB} and γ_{abs} are related by

$$\gamma_{abs} = 10^{\frac{\gamma_{dB}}{10}} \tag{13}$$

$F_c \approx 1$ for grazing angles above a few degrees. For lower grazing angles, Barton discusses some approximations for F_c. For most scenarios in GTSPECS, the grazing angle, ψ, will always be large enough that $F_c \approx 1$, so the reflectivity per unit area will be equal to σ^o.

The value for σ^o calculated by Barton's model is the mean RCS per unit area for a terrain area of a class type that has certain scattering properties associated with it. In a scene, each terrain area includes a large number of clutter cells. The mean value for the RCS of a clutter cell in a terrain area is given by

$$\sigma^{ccm} = \sigma^o A_{ccm} \tag{14}$$

where A_{ccm} is the average area of a clutter cell in the terrain area. The area of a clutter cell is given in square meters, so σ^{ccm} will be in square meters.

The Weibull distribution is used to model the spatial statistics of terrain clutter return. The probability density function, $W(\sigma / \sigma_m)$, for the RCS ratio σ / σ_m is given by [16]

$$W(\sigma / \sigma_m) = (\ln 2)\, b \left(\frac{\sigma}{\sigma_m}\right)^{b-1} \exp\left[-(\ln 2) \left(\frac{\sigma}{\sigma_m}\right)^b \right], \tag{15}$$

where: σ is proportional to RCS or power,
σ_m is the median value of σ, and
b is the Weibull slope parameter.

The slope parameter "b" varies between 0.1 and 1 and specifies the "width" of the distribution. A low value of b specifies a wide distribution corresponding to a wide dynamic range for clutter returns. A high value of "b" specifies a narrower distribution. A Weibull distribution with the slope parameter b = 1 is equivalent to a Rayleigh Distribution. At grazing angles above 5 degrees, the spatial statistics of terrain clutter returns tend to obey Rayleigh statistics.[16]

GTSPECS uses the terrain data base and discrete target data base for discrete shadowing calculations throughout the entire scene. Depth buffering techniques with two passes through the scene data base (terrain and discrete) are used to check for areas within the scene that are blocked by another area. The shadowing calculations result in dark sections within the scene that are caused by a section (terrain or discrete) in the scene of higher elevation blocking another section in the scene of lower elevation from the radar. In the Wright Patterson scene, the trees on the hill cast a shadow on the airfield.

GTSPECS outputs the cross section of all visible facets in the data base as seen from an isotropic source. RAZ_IMAGE forms an angle/range radar image of one elevation swath of the scene. A distribution in both the elevation plane and the azimuth plane is used to weight the returns when summing into a radar cell to simulate an antenna pattern. Figure 29 shows a flowchart of the RAZ_IMAGE program.

Scene predictions were planned for both clear and inclement weather; however, unforeseen software problems with the large data bases necessary for modeling the scene prevented clear and inclement weather image predictions. A literature search of existing models for MMW propagation through fog and haze was conducted, so that a global attenuation factor for the scene could be modeled. The models identified are discussed in Section 5.1.2, and the criterion for model selection is discussed in Section 5.1.3. A scene prediction for the Honeywell radar in clear weather is presented in Section 5.2

5.1.2 LITERATURE SEARCH

A survey of the technical literature on Millimeter Wave (MMW) radar propagation modeling through haze, fog, non precipitating clouds, and rain was conducted in August 1991. A paper, in the October 1990 IEEE Antennas and Propagation Magazine compared five different cloud models and was used as the starting point for the literature survey on fog and clouds.[26] Additional references were obtained from the Georgia Tech Library Online Search System. Recent course notes from a propagation course taught at the Ohio State University in 1986 and a Georgia Tech Final Report, "Millimeter Wave Clutter Reflectivity and Attenuation Handbook,"

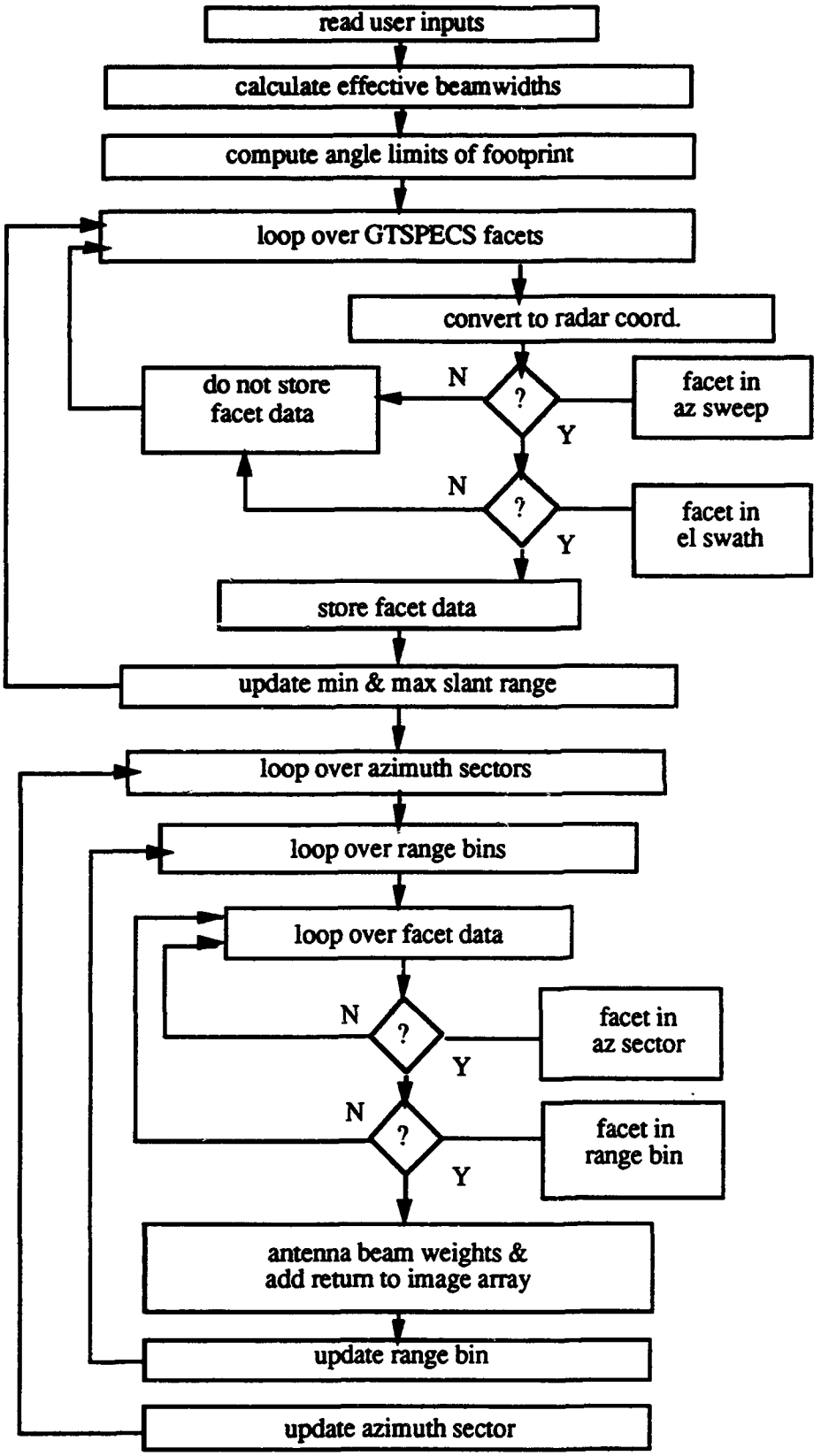

Figure 29. Flowchart of RAZ_IMAGE program.

were also consulted. (11) This section summarizes the propagation models for fog. haze, and clouds identified as appropriate for the scope of the synthetic vision modeling task.

Haze, fog, and non-precipitating clouds are assumed to be composed of spherical water droplets with diameters less than 100 μm to keep them suspended in the air. Fog and Clouds are composed of larger drops than aerosol haze and cause higher levels of attenuation at MMW frequencies. Advection fog forms when warm moist air moves across a cooler surface, and radiation fog forms when the ground becomes cold at night and cools the adjacent air mass until it becomes supersaturated. The suspended water droplets (SWDs) in an advection fog are larger than those in a radiation fog. Therefore, an advection fog causes more attenuation. To support a significant (0.001 g/m^3) water droplet concentration, the air mass must be saturated or slightly supersaturated. For fog and cloud conditions, the relative humidity is in the range 100% to 101%. In terms of water droplet concentration,

- Light fog, w = 0.001 to 0.01 g/m^3
- Moderate fog, w = 0.01 to 0.1 g/m^3
- Heavy fog, w = 0.1 to 1.0 g/m^3.

In non-precipitating clouds "w" usually ranges from 0.1 to 1.0 g/m^3. Thus, for propagation calculations, a non-precipitating cloud is similar to a heavy fog. In rain clouds (precipitating), "w" can often exceed 2 g/m^3.

Mie scattering theory is the basis for fog/cloud attenuation models. At MMW frequencies, the water droplet size in fogs and clouds is small compared to the wavelength. Therefore, the Rayleigh small sphere approximation is used to simplify the Mie scattering computations. Liebe et al. compared simultaneous Rayleigh and full series Mie attenuation calculations for the case of w = 1 g/m^3, T = 20° C, and a drop size distribution with r_o = 6 μm and all r ≤ 50 μm. The results are shown in Table 22.[36] For frequencies less than 300 GHz, the percent error of the Rayleigh approximation is zero.

5.1.2.1 Gunn and East Model

The Gunn and East model is the only theoretical model that has not been modified to accommodate empirical data. This model uses Mie scattering theory for spherical particles in a nonabsorbent medium. In haze and fog, the water droplets are usually between 1 and 100 μm. Therefore, because the particle sizes are small compared to the incident signal wavelength, the

Rayleigh approximation for small spheres is used to calculate the total absorption cross-section, Q_t of a spherical particle of water. Q_t, accounts for the scattered energy from the particle and the energy dissipated as heat. Since water is a lossy dielectric and the particle sizes are small compared to the incident signal wavelength, most of the lost energy is dissipated as heat. The absorption cross section, Q_t, is approximated by

$$Q_t = \frac{\pi^2 D^3}{\lambda} \text{Im}\left[-\frac{\varepsilon - 1}{\varepsilon + 2} \right] \text{m}^2 \qquad (16)$$

where: D is the water particle diameter in meters,
λ is the wavelength in meters, and
ε is the complex relative dielectric constant of water.

Table 22. Percent error of Rayleigh approximation in attenuation calculations

Frequency (GHz)	α (Mie) (dB/km per g/m^3)	α (Rayleigh) (dB/km per g/m^3)	$\frac{\alpha_R}{\alpha_M} - 1$ (percent)
300	15	15	0
400	20.5	20.3	-1
500	26	25.	-4
800	41	38.0	-7
1000	50	43.0	-14

Because the complex relative dielectric constant of water is dependent on temperature and frequency, the expression for Q_t is both temperature and frequency dependent. The attenuation, α (dB/km), is derived by summing the individual particle absorption cross sections over a cubic meter and using practical units.

$$\alpha = 0.4343 \left[\frac{6\pi}{\lambda \rho_d} \right] \text{Im}\left[-\frac{\varepsilon - 1}{\varepsilon + 2} \right] \rho_1 \qquad (17)$$

where: ρ_d is the density of water (g/cm^3), and

ρ_1 is the liquid water content of the cloud (g/m^3).

Note that ε, the relative dielectric constant of water, and ρ_d, the liquid water content of the cloud, are dependent on temperature. The attenuation is dependent on the cloud temperature, frequency, the liquid water content of the cloud, and path length through each cloud section of

constant liquid water content. Since the Rayleigh small sphere approximation is used to derive the attenuation, the model is useful for frequencies less than 300 GHz. The main limitation of the model is that cloud temperature and cloud liquid water densities are not standard reported meteorological parameters.[26]

5.1.2.2 Liebe Layton Model - Millimeter Wave Propagation Model (MPM)

Liebe, Manabe, and Hufford start with a complex refractivity model to describe the interaction between radio waves and suspended particles in the atmosphere. Complex refractivity, N is given in parts per million (ppm) by [35] [36]

$$N = N_o + N'(f) - j\, N''(f) \text{ ppm} \tag{18}$$

where: f is the frequency in GHz,

N_o is the nondispersive refractivity,

$N'(f)$ is the refractivity spectra of the complex refractivity as a function of frequency in parts per million (ppm), and

$N''(f)$ is the loss spectra of the complex refractivity as a function of frequency in parts per million (ppm).

The plane wave propagation factor and reduction to practical units are used to derive propagation terms: the power attenuation, α, the phase change, β, and the propagation delay, τ. The plane wave propagation factor is given by

$$\exp\left[-2\pi j f L\left(1 + n\,10^{-6}\right)/c\right] \tag{19}$$

where:

L is the length of the path, and c is the speed of light in a vacuum. In terms of complex refractivity, the power attenuation in dB/km is

$$\alpha = 0.1820\, f\, N''(f) \quad (\text{dB/km}) \tag{20}$$

The phase change, β, and propagation delay, τ, are given by

$$\beta = 1.2008\, f\left[N_o + N'(f)\right] \ (\text{deg/km}) \tag{21}$$

and

$$\tau = 3.3356 \left[N_o + N'(f) \right] \ (\text{ps/km}) \tag{22}$$

The Rayleigh approximation for small spheres is applied to express the complex refractivity as

$$N = w \left(\frac{3}{2} m_{w,i} \right) \left(\frac{\varepsilon - 1}{\varepsilon + 2} \right) \text{(ppm)} \tag{23}$$

where: w = the mass content of water per unit of air volume in g / m^3

$m_{w,i}$ = are the specific weights for water or ice in g / cm^3

$m_w = 1 \ g / cm^3 \quad m_i = 0.916 \ g / cm^3$

and

ε = the complex permittivity of liquid water or ice given by

$$\varepsilon = \varepsilon'(f) - j\varepsilon''(f) \tag{24}$$

Liebe et al. verified that the Rayleigh approximation to Mie's forward scattering function is valid for frequencies up to 300 GHz when the drop diameters are limited to less than 100 μm.[36] It also should be noted that propagation effects by suspended ice crystals (SIC) are negligible. Ice clouds occur as cirrus at altitudes greater than 8 km, and their mass content of water is small, $w < 0.001 \ g / m^3$. The signal depolarization caused by suspended ice crystals is significant and should not be ignored if they are in the propagation path. The Rayleigh approximation given by Equation (23) is rationalized to describe the nondispersive refractivity, N_o, the refractivity spectra, $N'(f)$, and the loss spectra, $N''(f)$

$$N_o = w \frac{3}{2} \left[1 - \frac{3}{(\varepsilon_o + 2)} \right] \tag{25a}$$

$$N'(f) = w \frac{9}{2} \left[\frac{1}{(\varepsilon_o + 2)} - \frac{y}{\varepsilon''(y^2 + 1)} \right] \tag{25b}$$

$$N''(f) = w \frac{9}{2} \left[\varepsilon''(y^2 + 1) \right]^{-1} \tag{25c}$$

where $y = \dfrac{(\varepsilon' + 2)}{\varepsilon''}$

The permittivity of liquid water for the frequency range extending from 0 to 1000 GHz is given by a double Debye formulation which accounts for a primary and secondary relaxation frequency.[36]

$$\varepsilon = (\varepsilon_o - \varepsilon_1)\left[1 + \frac{f}{f_p}\right] + \left[\frac{(\varepsilon_1 - \varepsilon_2)}{1 + j(f/f_s)}\right] + \varepsilon_2 . \tag{26}$$

The real part, $\varepsilon'(f)$, and the imaginary part, $\varepsilon''(f)$, of the complex permittivity are given by

$$\varepsilon'(f) = \frac{(\varepsilon_o - \varepsilon_1)}{\left[1 + \left(\frac{f}{f_p}\right)^2\right]} + \frac{(\varepsilon_1 - \varepsilon_2)}{\left[1 + \left(\frac{f}{f_s}\right)^2\right]} + \varepsilon_2 \tag{27a}$$

and

$$\varepsilon''(f) = \frac{(\varepsilon_o - \varepsilon_1)(f/f_p)}{\left[1 + \left(\frac{f}{f_p}\right)^2\right]} + \frac{(\varepsilon_1 - \varepsilon_2)(f/f_s)}{\left[1 + \left(\frac{f}{f_s}\right)^2\right]} \tag{27b}$$

The permittivity constants are given by

$$\varepsilon_o(T) = 77.66 + 103.3(\theta - 1) \tag{28a}$$

$$\varepsilon_1 = 5.48 \text{ and } \varepsilon_2 = 3.51 \tag{28b}$$

where θ is the relative inverse temperature variable given by

$$\theta = \frac{300}{[T(^\circ C) + 273.15]} \tag{29}$$

The principal and secondary relaxation frequencies are

$$f_p(T) = 20.09 - 142.4(\theta - 1) + 294(\theta - 1)^2 \text{ GHz} \tag{30a}$$

and

$$f_s(T) = 590 - 1500(\theta - 1)\ \text{GHz} \tag{30b}$$

The Liebe model has been implemented in the FORTRAN code Millimeter Wave Propagation Model (MPM) to run on an IBM or IBM compatible computer. MPM model predictions have been validated with measured data of fog events in Japan and in Huntsville, Alabama.[36] [38]

5.1.2.3 Staelin/Goldstein Model

Like the Gunn and East Model and MPM models, the Staelin/Goldstein model uses the Rayleigh approximation to Mie Scattering theory to derive an attenuation coefficient.[26] Goldstein used empirical data for the refractive index of water at 18° C and provided a correction factor to account for the temperature and frequency dependence. Staelin used Goldstein's data to derive an equation for the cloud attenuation coefficient

$$\alpha = \frac{w\ 10^{0.0122\,(291 - T)^{-6}}}{\lambda^2}\ \text{cm}^{-1} \tag{31}$$

where: w is the liquid water density of the cloud in g / m^3, T is the temperature in °K, and λ is the wavelength in cm. The correction factors for the temperature and frequency dependence limit the model to frequencies ranging from 10 to 37.5 GHz. In this frequency range, water droplet diameters in fog and cloud conditions satisfy the Rayleigh criterion. Slobin and Flock rationalized the equation to arrive at attenuation in dB/km.

$$\alpha = \frac{4.343\ w\ 10^{0.0122\,(291 - T)^{-6}}\ 1.16}{\lambda^2}\ \text{dB/km} \tag{32}$$

Slobin added the 1.16 factor to the Staelin/Goldstein model to make the model a better approximation to the Gunn and East Model.

Model Inputs include liquid water density of the cloud, cloud temperature, frequency, and frequency range (10 - 37.5 GHz).

This model does not require knowledge of the temperature dependence dielectric constant of water.

5.1.2.4 Slobin Model

Slobin used the Staelin model with meteorological data from 15 Weather Service stations throughout the US to characterize 12 different cloud models ranging from clear air to heavy cloud conditions.[50] Radiosonde measurements were made to determine Cloud liquid water content and cloud base and top heights. The cloud temperature was inferred from surface temperature by assuming a lapse rate of 6.5° K / km. Cloud attenuations and noise temperatures for 12 cases are presented in tabular form in Reference [50], and cumulative probability distributions are also given. This model relies heavily on empirical data and inferred liquid water densities and cloud temperatures and would be most useful for U.S. geographical locations with climates similar to one of the locations tabulated in the report.

5.1.2.5 Altshuler Model

5.1.2.5.1 FOG

One limitation of the Gunn and East model, the Liebe model, and the Staelin/Goldstein model is that measurements of vertical liquid water and vapor profiles are difficult. In 1984, Altshuler computed fog attenuation using the Rayleigh model and indices of refraction that were tabulated by Rozenberg.[5] He then performed a regression analysis of the computed attenuations as a function of wavelength and temperature. An almost perfect fit to the computed attenuation data was obtained with a four-term regression on wavelength and temperature for wavelengths in the range 3 mm < λ < 3 cm and temperatures in the range -8° C to 25° C. The expression for attenuation is given by

$$A = -1.347 + 0.0372\,\lambda + \frac{18.0}{\lambda} - 0.022T \qquad (33)$$

where A is the attenuation in dB/km/g/m^3, λ is the wavelength in mm, and T is the temperature in °C.

The total path attenuation is easily computed by multiplying the normalized attenuation by the fog density in g/m^3 and extent in km.

Fog density data is not a common meteorological parameter found on weather data sheets. Altshuler presents an empirical formula derived by Elridge for fog density in terms of visibility, when it is not possible to get measured fog density data[24]

$$w = \left(\frac{0.024}{V} \right)^{1.54} \qquad (34)$$

where w is the fog density in g/m^3, and V is the fog visibility in km.

For dense haze or special type fogs, where there is an abundance of very small drop sizes, the coefficient 0.024 should be replaced by 0.017. Altshuler states that this formula is appropriate for fogs in which the drop diameters are between 0.3 and 10 μm. For dense haze or other special types of fogs that are characterized by a lot of very small drops, the coefficient 0.024 in Equation (34) should be replaced by 0.017. The predicted visibility has been documented to be slightly low for advection or heavy fog where the SWD drop diameters can be as high as 100 μm.[44] This equation is useful for estimating the fog density used in the Gunn and East model, the MPM model and the Staelin/Goldstein model, when measured data are not available.

5.1.2.5.2 CLOUD COVER

Altshuler and Marr analyzed 341 sets of measured 15 and 35 GHz attenuation data for cloud cover in the Boston area to empirically derive a formula for estimating cloud attenuation as a function of angle, humidity, and frequency.[4] In the measurements, the sun was used as the source, and extinction was measured at 29 elevation angles between 1° and 20° during sunrise and sunset. The zenith attenuations were inferred from the extinction measurements. 210 data sets were measured under complete cloud cover conditions, and 131 data sets were measured under conditions of partial cloud cover. 58 data sets were designated clear sky conditions. The measured results have been compared with theoretical results.[3] The surface temperature, pressure, and dew point temperature were recorded at the start and completion of each set of data and then averaged.

The data were used to study separately the dependence of attenuation on angle, humidity, and frequency. They found that 80% of the cloud attenuation data and over 90% of the mixed cloud attenuation data were proportional to the distance through the atmosphere. They concluded that the attenuation at any angle could be estimated from the zenith attenuation. The effective height, h_e,of the absorbing layer is a function of the vertical distributions of oxygen and water vapor. Since the water vapor is related to the surface absolute humidity, ρ, the effective height should be related to the surface absolute humidity. So in a previous study a regression of effective height, h_e, as a function of surface absolute humidity was performed.[3] The regression line is:

$$h_e = 6.35 - 0.302\ \rho\ . \qquad (35)$$

The correlation coefficient, r, is 0.668 which is due to the variability of the humidity aloft in the air.

A zenith attenuation for uniform cloud was extrapolated from each set of uniform cloud cover data to examine the dependence of attenuation on humidity. They were plotted as a function of absolute humidity, and regression lines of the form

$$A = a_d + a_w \rho \tag{36}$$

were derived. In Equation (36), a_d is the dry term coefficient corresponding to the oxygen attenuation, and a_w is the wet term coefficient which corresponds to the water vapor and liquid water attenuation. A similar regression analysis was performed for uniform mixed cloud conditions. For complete cloud cover

$$A_{15\,GHz} = 0.051 + 0.0047\ \rho \tag{37a}$$

$$A_{35\,GHz} = 0.182 + 0.0161\ \rho \tag{37b}$$

For uniform mixed cloud conditions

$$A_{15\,GHz} = 0.048 + 0.0036\ \rho \tag{38a}$$

$$A_{35\,GHz} = 0.176 + 0.0115\ \rho \tag{38b}$$

A similar analysis was reported by Altshuler in for clear air [3]

$$A_{15\,GHz} = 0.048 + 0.0035\ \rho \tag{39a}$$

$$A_{35\,GHz} = 0.177 + 0.0093\ \rho \tag{39b}$$

A statistical analysis was done on all 210 sets of cloud data including cases which were designated nonuniform. It was found that the dry and wet term regression coefficients did not differ significantly from those values obtained for uniform cloud and uniform mixed cloud conditions. The correlation coefficients, r, were significantly lower, indicating that the regression line fit was not as good for the nonuniform cases.

Altshuler and Marr also assume that the cloud particulates are small in diameter and apply the Rayleigh approximation. They use Rozenberg 's tabulated data for the index of refraction of water and assumed a temperature of 10 °C to calculate the normalized attenuation in dB/km per g/m^3 at 13 wavelengths from 3 mm to 2 cm in the window regions of the millimeter wave spectrum.[47] Attenuation was found to have the following dependence on wavelength:

$$A = -1.20 + 0.0371\ \lambda + \frac{19.96}{\lambda_{mm}^{1.15}} \tag{40}$$

The wavelength dependence was fit to the absolute humidity equations to obtain the zenith attenuation, A_z, in dB.

$$A_z(\lambda, \rho) = \left(-0.0242 + 0.00075\,\lambda + \frac{0.403}{\lambda_{mm}^{1.15}}\right)(11.3 + \rho) \tag{41}$$

It was noted that Equation (41) produces attenuations that are slightly low compared to the measured values at 15 GHz. The equation is a better fit at the shorter wavelengths.

Equation (41) is multiplied the distance through the absorbing atmosphere, D(θ), to include the path geometry. For high elevation angles, the flat earth approximation may be used, and D(θ) is proportional to the cosecant of the elevation angle. At low elevation angles, the curvature of the earth must be included in D(θ).

$$D(\theta) = [(a_e + h_e)^2 - a_e^2 \cos^2\theta]^{1/2} - a_e \sin\theta \tag{42}$$

where θ is the elevation angle, a_e is the effective earth radius, and h_e is the effective height of the absorbing layer. The effective earth radius, a_e, is a function of the refractivity profile of the atmosphere. A common radar approximation

$$a_e = 4/3\ a \tag{43}$$

where a is the earth radius yields

$$a_e = 8497 \text{ km} \tag{44}$$

The effective height of the absorbing layer, h_e, is given by Equation (35). In summary

$$A(\theta, \lambda, \rho) = \left(-0.0242 + 0.00075\,\lambda + \frac{0.403}{\lambda_{mm}^{1.15}}\right)(11.3 + \rho)\,D(\theta) \tag{45}$$

where:

$$D(\theta) = \csc\theta, \qquad \theta > 8^\circ$$

$$D(\theta) = [(a_e + h_e)^2 - a_e^2 \cos^2\theta]^{1/2} - a_e \sin\theta \qquad \theta \leq 8^\circ \tag{46}$$

Altshuler and Marr estimate that for higher humidities the mixed cloud attenuations are approximately 85 percent of the attenuation for full cloud cover at 35 and 15 GHz,

$$A(\theta, \lambda, \rho) \text{ mixed cloud} = 0.85\, A(\theta, \lambda, \rho) \text{cloud}. \quad (47)$$

Since the model is derived from long slant path measurements taken in the Boston area, the Altshuler/Marr model is most appropriate for similar climates and scenario geometries. Also, this model predicts the total path attenuation in dB. Equation (45) would need to be divided by the distance through the absorbing layer to obtain the specific attenuation in dB/km.

5.1.2.6 PCTRAN/LOWTRAN

One of the major upgrades in PCTRAN 7 was the extension of the wavelength region to include microwave and millimeter wave frequencies. LOWTRAN computes complete path attenuation, given the propagation scenario geometry and meteorological conditions. The user can define atmospheric profiles by:

1. Defining desired atmospheric layers. The user must specify liquid water content and aerosol or cloud extinction and absorption coefficients as a function of wavelength. Users can also define their own aerosol or cloud scattering phase function. Defining an atmospheric profile requires knowledge of the atmospheric parameters.

2. Using a generic model atmosphere that comes with the PCTRAN model. Model atmospheres contain a 34 layer atmosphere with 1 km thick layers from 0 -25 km altitude, 5 km thick layers from 25 - 50 km and the two layers going to 70 and 100 km. Six generic model atmospheres dependent on geographical location and season come with LOWTRAN7. For Wright Patterson, the mid latitude Summer and Winter models would be used.

The LOWTRAN model outputs total path transmittance. The attenuation in dB/km would have to be computed from the total path transmittance to obtain data that would be compatible with the GTSPECS multispectral image model. The sources for the PCTRAN model are not available in the open literature, and the learning curve for using the PCTRAN model is higher than that for using MPM or other models for which equations are available.

5.1.3 MODEL SELECTION

Table 23 summarizes the strengths and weaknesses of the fog/cloud attenuation models identified in the literature survey. Figure 30 shows a comparison of the MPM model, the Gunn and East model, the Staelin model and the Altshuler model, attenuation predictions as a function of fog

density for November weather conditions at 35 GHz. Figure 31 shows a comparison of the MPM model, the Gunn and East model, and the Altshuler model as a function of fog density for November weather conditions at 94 GHz. At both 35 and 94 GHz, the MPM model predicts a worst case estimate of fog attenuation. Because the MPM model is an available program that is

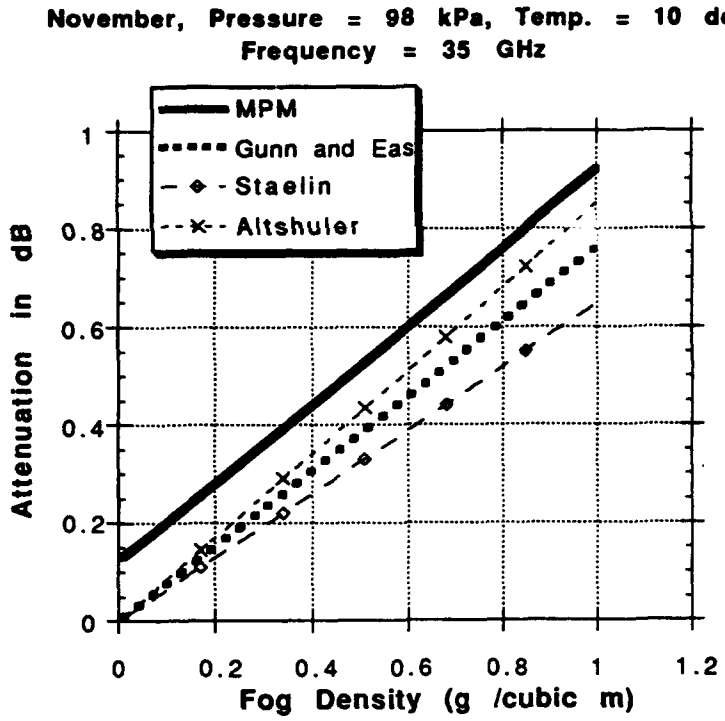

Figure 30. Comparison of fog attenuation models at 35 GHz.

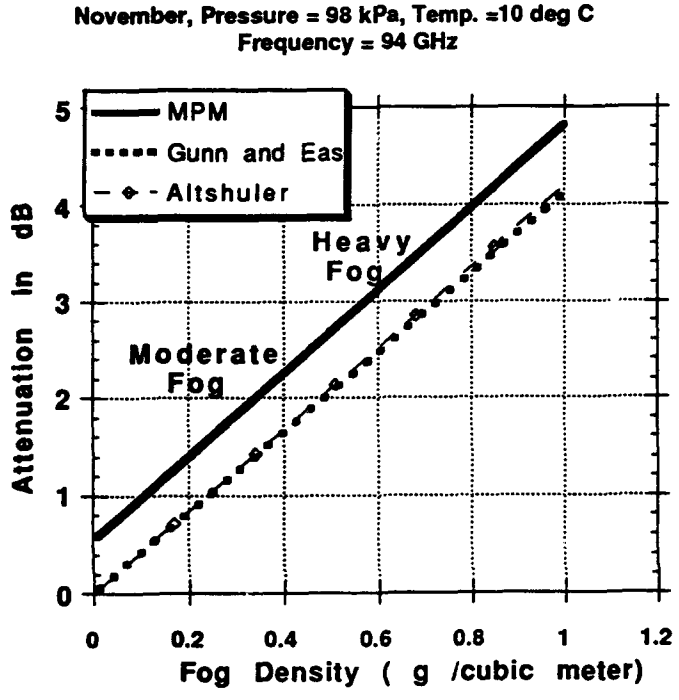

Figure 31. Comparison of fog attenuation models at 94 GHz.

well documented in the open literature and provides a worst case estimate of fog attenuation, it is identified as the most promising empirical model for fog attenuation.

Table 23. Summary table of Empirical fog/cloud attenuation models

MODEL	STRENGTHS	WEAKNESSES
Gunn and East	Theoretical Broad frequency range	Inputs not standard meteorological parameters
Millimeter Wave Propagation Model (MPM)	Selected Existing computer program Well documented (in open literature) Broad frequency range	Empirical data for complex permittivity of water
Staelin and Slobin	Not really considered	Narrow frequency range Empirical data for complex permittivity of water
Altshuler	Innovative empirical analysis Broad frequency range Not as dependent on accurate weather data	Empirically derived from measured data sets
PCTRAN	Broad frequency range Existing computer program	Sources not in open literature

5.2 MODEL IMPLEMENTATION

5.2.1 SCENE GENERATION AND MODELED DATA GENERATION

The GTRI MMW modeling programs, MAX/TRACK, GTVISIT, G87, GTSPECS, and RAZ_IMAGE discussed in Section 5.1.1, were used to predict a clear air real beam radar image of the Wright Patterson airfield scene. The image prediction is for the Honeywell 35 GHz circular polarization synthetic vision sensor. A map of the scene, a site visit, and photographs were used with the GTVISIT program to create the polygon class map and the topographic file. Figure 32 shows a sketch of the modeled class map and the terrain types included in the scene. Table 24 shows the mean height and standard deviation of height for each terrain class used to generate the topographic information. The facet heights in a given terrain area are modeled with a distribution. The standard deviation of height is the rms roughness of the terrain type.

The spacing between grid points in the terrain class and topographic files is 2 meters. The 3,500 meter by 2,500 meter scene area is represented by a 1,750 facet by 1,250 facet grid, and each facet has an area of 4 square meters.

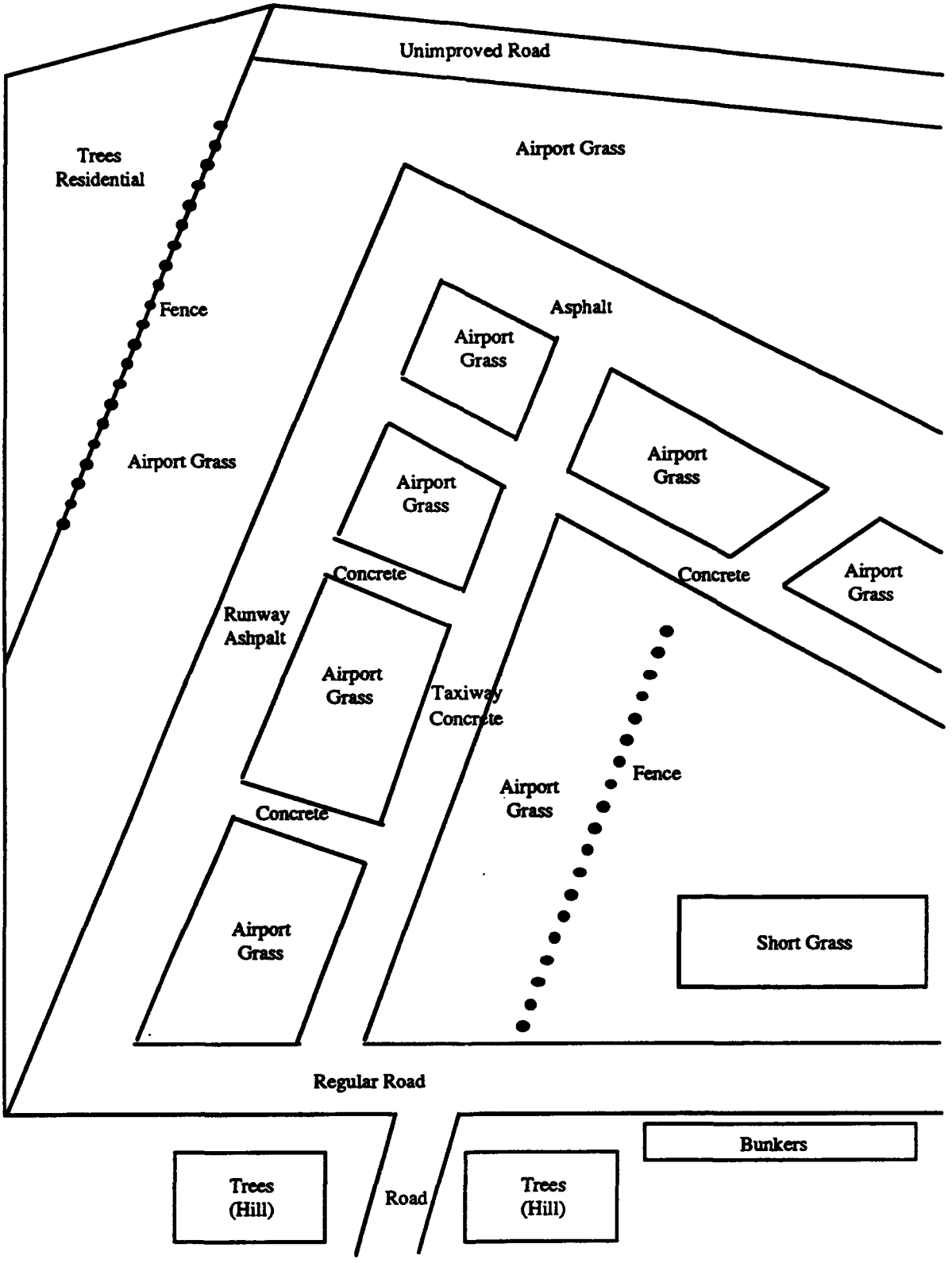

Figure 32. Sketch of modeled Wright Patterson airfield scene.

Table 24. Elevation data used to generate topographic file for Wright Patterson airfield scene

TERRAIN TYPE	MEAN HEIGHT (m)	σ_0 (m)
Airport grass	0.25	0.05
Short grass	0.07	0.01
Trees (hill)	15	3
Trees (residential)	12	3
Runway asphalt	0.01	0.005
Taxiway concrete	0.01	0.01
Regular road	0.01	0.00
Unimproved road	0.01	0.01

Table 25 shows the terrain reflectivity and Weibull slope parameter used by GTSPECS to compute the return clutter value for each terrain type in the scene. The terrain reflectivity is derived from published clutter data in References [11-12], [15-17], [24], [37] and [53]. The Weibull slope parameter determines the width of the distribution for clutter returns and is also taken from published literature.

Table 25. Reflectivity and Weibull slope parameter for Wright Patterson scene

TERRAIN TYPE	MEAN REFLECTIVITY (dBm)	WEIBULL SLOPE PARAMETER
Airport grass	-11.0	0.7
Short grass	-13.7	0.85
Trees (hill)	-7.9	0.5
Trees (residential)	-7.9	0.5
Runway asphalt	-30	1.0
Taxiway concrete	-19	0.9
Regular road	-32.6	1.2
Unimproved road	-24.0	0.8

Aircraft bunkers and a line of fence posts were included in the scene model. Figure 28 shows the MAX target model of the aircraft bunkers. Each bunker was modeled with width = 22.9 m, length = 22.9 m, and height = 7.2 m. The bunker dimensions were estimated from the scene map and pictures. Each fence post was modeled with a circular cylinder.

Table 26 shows the radar parameters the RAZ_IMAGE program used in predicting the scene image. A global clear air path attenuation of 0.05 dB/km was included in the range azimuth cell return power computations. The radar resolution was modeled as equal to the range bin sample spacing of 7.5 meters. An unresolved memory allocation problem in RAZ_IMAGE prevented the range bin and the range bin sampling interval to be modeled. Therefore, the modeled return in each range/azimuth cell is expected to be approximately 3 dB low. This error should not adversely effect the predicted contrast in return between the runway and the surrounding grass and the taxiway and the surrounding grass.

Table 26. Radar parameters for Wright Patterson airfield image prediction

Parameter	Value
Frequency	35 GHz
Azimuth beamwidth	0.9 degrees
Elevation beamwidth	5.5 degrees
Antenna gain	33 dBi
Azimuth sweep angle	±15 degrees
Azimuth step angle	0.1 degrees
Transmitter power	795 watts
Range resolution	7.5m
Range sampling interval	7.5 m
truncation point	-13 dB

5.2.2 CONCLUSIONS FROM THE MMW SENSOR PERFORMANCE MODELING EFFORT

Image modeling tools were used to predict a clear air MMW radar sensor image of the Wright Patterson airfield scene. Contrast ratios between the runway return and surrounding terrain return and between the taxiway return and surrounding terrain return were computed from the predicted image and compared with actual measured contrast ratios for the Honeywell 35 GHz synthetic vision sensor. The effects of fog can be included in the image prediction model by including a global attenuation factor which can be precomputed using the millimeter wave propagation empirical model or Mie scattering theory.

SECTION 6
ON-SITE DATA COLLECTION

6.1 DATA COLLECTION PROCESS

6.1.1 COLLECTION SCHEDULE

Eight sensor tower tests were supported at Wright-Patterson AFB between August 1991 and August 1992, as shown in the tower test schedule Figure 33. During a one to two week "baseline test" period, the sensor was installed, calibrated, and prepared for an extended test period. GTRI installed and made operational the data collection system and other test support equipment. The sensor manufacturer's field teams were assisted with installation of their sensor system in the 10th floor tower laboratory. Once the sensor system was made operational, it was connected to the USAF data collection system, and the configuration parameters and test procedures were optimized. A series of specialized tests was then conducted to establish a performance baseline for the sensor. These tests measured the sensor's ability to image the runway and bordering grass areas of the test scene in clear weather conditions. Also measured were range and angular resolution, transmitter power, receiver sensitivity, and maximum detection range.

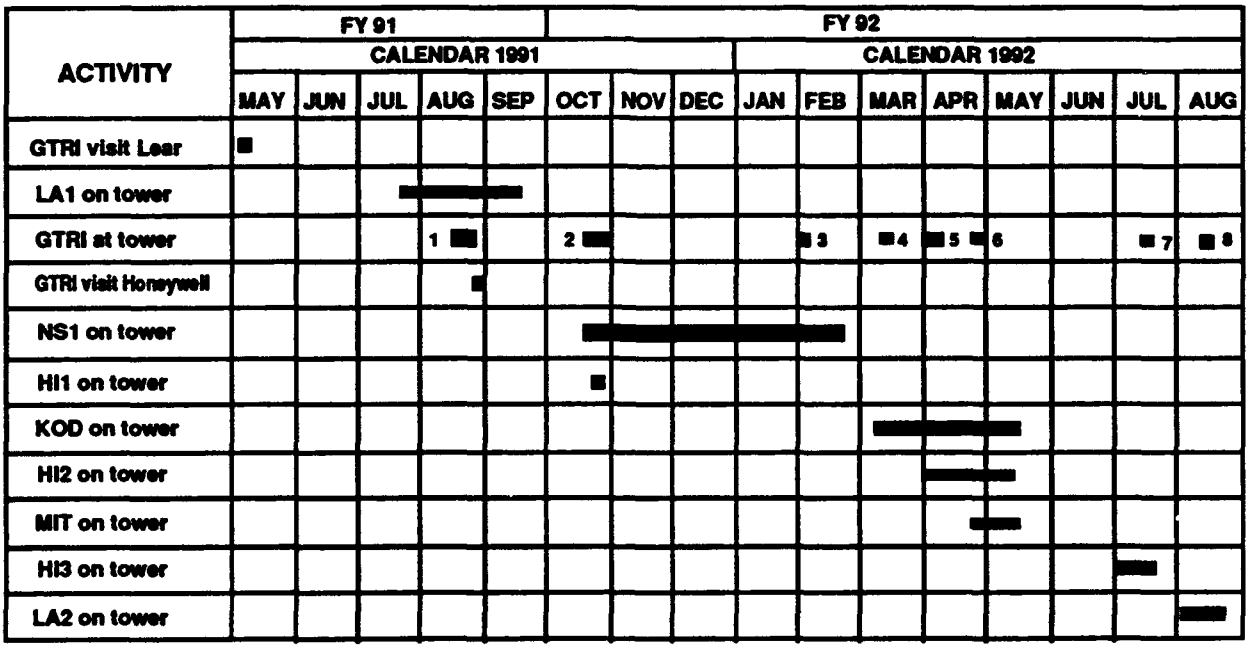

Figure 33. Tower test schedule.

6.1.2 COLLECTION PROCEDURES

After the baseline test period, the sensor and support equipment were left in a state of readiness, so that test measurements could be conducted whenever adverse weather conditions occurred. In the case of the NS1 sensor, this extended test period lasted through four months of winter. The USAF tower test director utilized weekly and daily weather predictions to initiate tower test activity. Operator training, refined test procedures, and an automated data collection system were key elements to the success of this approach. Data quality could be monitored daily from images generated with the quick-look image processing software.

6.2 DATA ACQUISITION SYSTEM

6.2.1 DAS EQUIPMENT

A sensor data collection system developed during this project gives the USAF a continued capability for supporting MMW radar and IR imaging sensor tests at the WPAFB tower test facility. Figure 34 is a block diagram of the data collection system, shown connected to a MMW radar and Kodak IR camera. The radar sensor consists of an antenna, receiver/transmitter (R/T) unit, and radar processor. Analog baseband video data from the radar processor are digitized by the LeCroy data acquisition unit and then transferred to the computer over the IEEE-488 control bus. An RF signal generator is connected to the radar R/T unit during the occasional calibration process. There is additional support equipment for signal monitoring that is not shown in the diagram. The radar antenna and R/T unit together are mechanically scanned in azimuth by the Klinger motorized X-Y table. The 80486 computer interfaces with the Klinger table controller over the IEEE-488 bus to position the table under software control. The Kodak IR camera is mounted on a separate fixed tripod (not shown) and connected through a remote electronics unit (REU). A video "frame grabber" board in the computer acquires individual frames of the monochrome RS-170 television video from the Kodak REU under software command. A television monitor connected to the video output of the frame grabber board can display either captured IR camera images or processed radar sensor images.

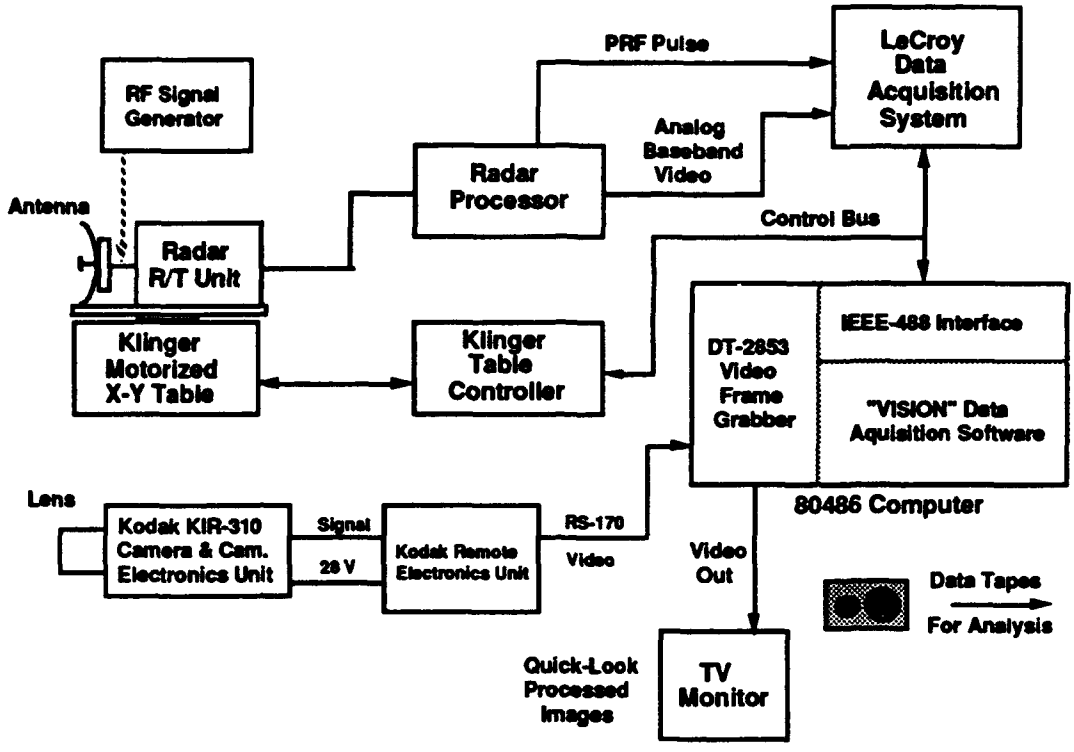

Figure 34. Data collection system diagram.

The data acquisition process is controlled by the VISION software running on the host 80486 computer. On the computer monitor (not shown), the operator is presented multiple-choice command menus to conduct a data collection mission. The command options include changing operating parameters, acquiring new sensor data, collecting calibration data, or quick-look data analysis. MMW radar data collection is performed by stepping the Klinger table in small increments while the radar video is digitized over multiple range bins at each step. A MMW radar azimuth scan pattern is typically completed in three to five minutes. Quick-look imaging of the radar data frame takes another five to ten minutes. IR camera data collection and display are virtually instantaneous. Subsequent frames of IR sensor data can be collected as frequently as every five seconds. Data collection can be alternated between the MMW radar sensor and the IR sensor without exiting the data collection program. Operating parameters may be reconfigured from menu selection to accommodate changes in scan width or sensor resolution. A record of the current configuration and time stamp are automatically saved to computer disk along with the sensor data.

6.2.2 TEST SENSOR INSTALLATIONS

The MMW radar and IR test sensors were installed on the 10th floor laboratory of the WPAFB building 620 tower facility overlooking an inactive runway complex to the west. The MMW and IR test sensor specifications are given in Section 3.1.1. The sensor systems were connected to the DAS for data collection and antenna scanning control. The 95 GHz Norden TALONS radar antenna, Figure 35a, was designed for slow scanning in azimuth under servo loop control, so GTRI configured the DAS to develop synchro voltages to step scan the antenna under computer control. The entire TALONS radar pod, shown in Figure 35b, was mounted on a machine table to permit manual azimuth and elevation angle adjustments. The 30° azimuth scan sector was centered between the runway and parallel taxiway at a range of 2,000 m, as shown in Figure 35c. The data acquisition system (DAS), as configured for Norden 95 GHz radar sensor data collection, is shown in Figure 35d. Data collection operations could be performed by a single operator.

The remaining five different MMW radar test configurations utilized a Klinger Scientific precision elevation-over-azimuth motorized table to perform antenna scanning. As shown in Figure 36a, the Honeywell 35 GHz radar antenna assembly was mounted on the Klinger table, and radiated through a wall opening. The plexiglass window was removed during sensor data collection to prevent any MMW or IR signal attenuation. The data acquisition equipment, Figure 36b, was configured for alternating data collection between the MMW radar and IR sensors operated simultaneously. Figure 36c shows the 30° azimuth field of view that was step-scanned by the MMW radar antennas on the Klinger stepper table under computer control. The runway centerline was offset approximately 20° from the radar scan sector center at 2 km range, but this angle offset had little effect on the usefulness of the sensor data. Figure 36d depicts the asphalt runway from a more realistic end view without the angle offset.

The Kodak 3-5 micron IR sensors, and later the Mitsubishi 3-5 micron IR sensor, were mounted on a sturdy tripod as shown in Figure 37a. Primarily, the IR sensors were operated from the tower laboratory viewing the same measurement scene as the MMW radar sensors, as shown in Figure 37c. Two IR blackbody targets, one cooler than the equivalent scene temperatures and one warmer, were placed in front of the IR sensors within the field of view. A second sensor location was tried from an instrumentation van located on the runway (Figure 37b) to address the possibility of collecting IR sensor data in very low visibility fog. Figure 37d shows the IR measurement scene from the van in clear weather with the same 34° field of view as the IR sensor.

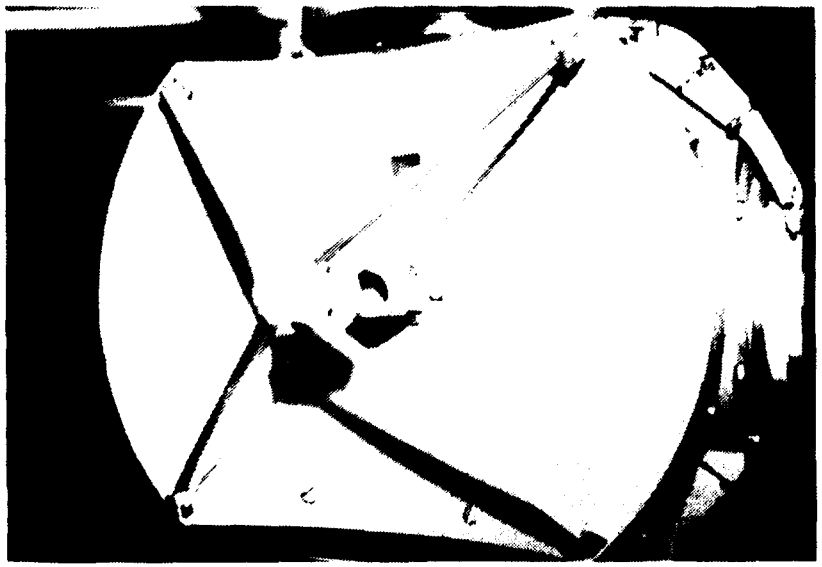

Figure 35a. 95 GHz Norden radar antenna.

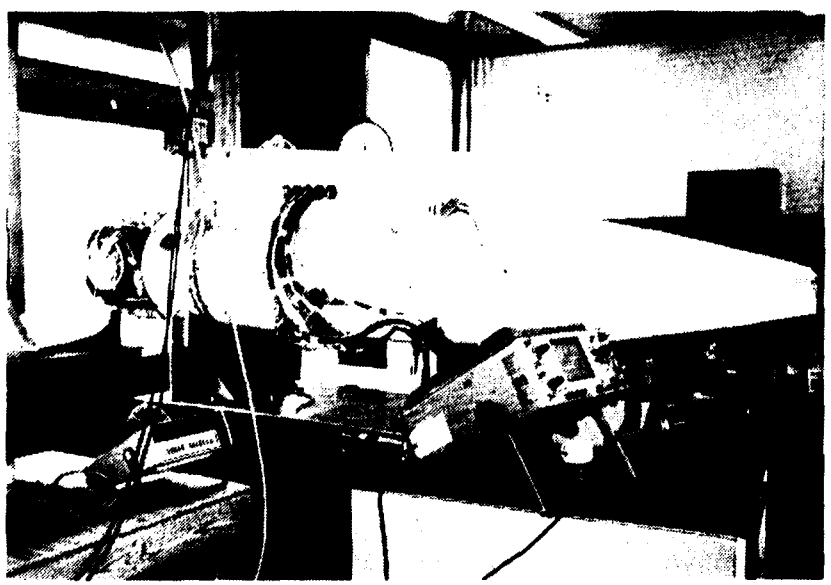

Figure 35b. 95 GHz Norden TALONS radar pod.

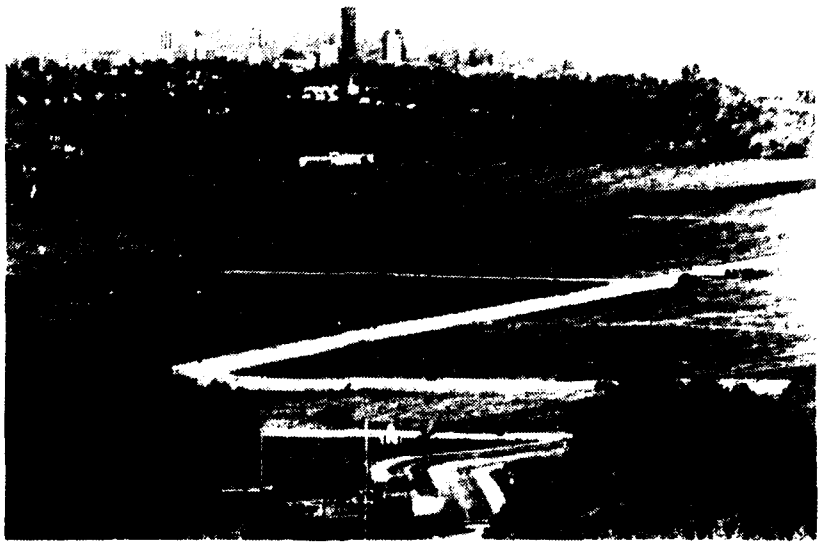

Figure 35c. View of runway (dark) and taxiway (light) from tower.

Figure 35d. Data acquisition system in tower laboratory.

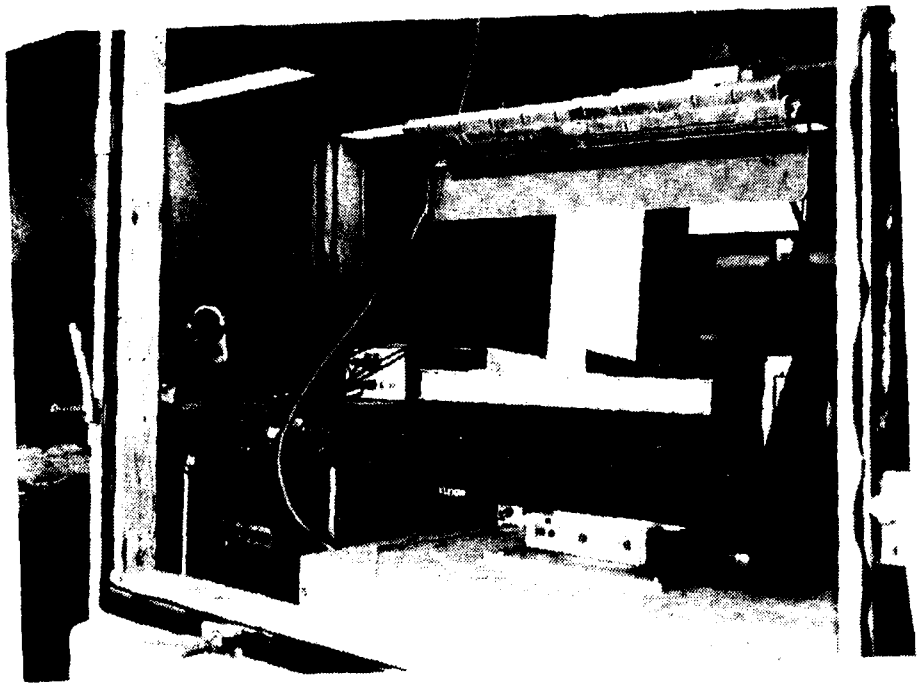

Figure 36a. 35 GHz Honeywell radar mounted on motorized table.

Figure 36b. Data acquisition system and Air Force operator.

Figure 36c. Wide angle view of measurement scene from tower.

Figure 36d. Asphalt runway as viewed without angle offset.

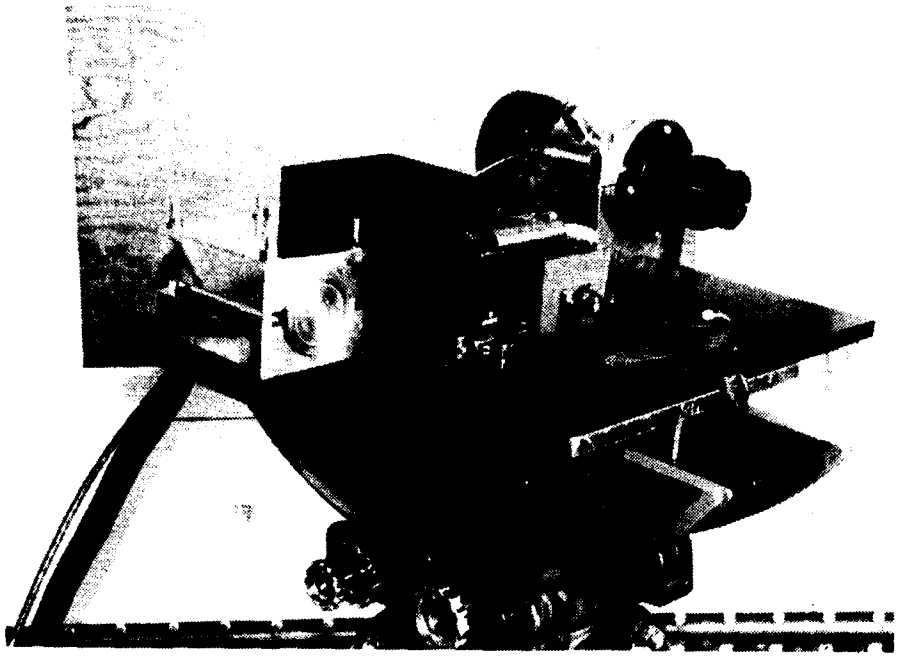

Figure 37a. 3-5 μm Kodak IR camera assembly on tripod.

Figure 37c. IR measurement scene from tower with blackbody targets.

Figure 37b. Instrumentation van located on runway for IR measurements.

Figure 37d. IR measurement scene from van on runway.

6.2.3 IR DATA COLLECTION

Specific test procedures were developed and provided to system operators to increase the chance of acquiring usable IR sensor data. The IR image data quality can be deficient in several ways. If the image data are valid but can not be calibrated due to saturated image data for the calibration blackbody sources, then sharpness measurements and signal-variability-ratio values can still be derived from the image data. Contrast values could still be computed using the raw digitized video levels in the image, but they would be inconsistent with other contrast values derived from absolute scene radiance. If the image of the runway and surrounding background are saturated at either high or low levels then the data are not usable at all.

The image is saturated if the image data values are outside of the usable range of the camera sensor which results in clipping the output video signal. The image is also saturated if the video level produced at the camera system output is not within the range of voltage levels that the 8-bit A/D converter on the Data Translation DT-2853 frame grabber board can digitize.

The camera system video output signal was observed using a Tektronix video waveform monitor, so that the absence of clipping of the video output by the camera system could be verified before saving the image data. If the video output signal showed evidence of clipping, then the camera gain and offset were adjusted to eliminate the saturation of the video signal and retain as much signal amplitude as possible. If the radiance of the scene was high enough, the sensor elements could saturate regardless of the gain and offset control settings. This level of scene radiance was observed on several occasions near sunset when the sun was aligned so that the specular reflection of sunlight off the runway produced bright solar glints in the image. This mode of saturation of the camera sensor occurs when the electron wells in the individual photodiodes in the focal plane array completely fill with photoelectrons. The only remedy for this mode of sensor saturation is to reduce the sensor integration time or to reduce the radiation incident on the sensor by reducing the lens aperture or with the use of filters. Neither of these options were available for the camera systems used in these measurements, so saturated pixel values in the solar glints must be interpreted as a lower bound for the true radiance data.

A test procedure for detecting of A/D converter saturation was provided in the measurement procedures to check the video data for acceptable voltage levels for digitization in the frame grabber. The test consisted of freezing a test image in the frame grabber memory and displaying the digitized image. Voltages which were too high would produce digital pixel values of 255 and voltages too low would digitize to the value 0. The DAS software was provided with options to

highlight values in the displayed image which were too high or too low, so that the operator could easily determine that the data values were within the usable range or correct the levels by an adjustment of camera gain and offset before storing the captured image data.

The calibration of the image data is based on the digitized values for the two blackbody sources at known temperatures. In principle, the sensor signal output is linearly related to the scene radiance imaged on the sensor. A linear calibration of the captured image data is derived from the digitized blackbody images. The known temperatures of the blackbodies and the camera sensor spectral response are used to derive the radiance of the two blackbody sources to provide known radiance values for the two-point linear calibration of the image data. The measurement procedures directed the operators to adjust the temperature settings for the blackbody sources so that the runway and background video levels were within the bounds set by the levels in the blackbody images.

6.3 DAS SOFTWARE

The data acquisition software was developed to provide automated control of the government furnished LeCroy CAMAC crate, Klinger positioning table, DDC Syncro, and Data Translation Frame Grabber board in collecting radar and IR camera scene data. In addition, software was developed to provide a quick-look analysis for verification and validation of the collected radar data. This software was written in Microsoft C Version 5.0 for use on an IBM PC compatible platform which was also part of the Government furnished equipment (GFE). It was designed to be menu-oriented and user-friendly in order to allow a rotating team of operators working from a procedures manual to collect and verify scene data under a variety of weather conditions. The synthetic vision executable program, SV.EXE, serves as a main menu shell for providing access to the individual software components for data collection and quick-look analysis. A block diagram showing the primary modules of the synthetic vision shell program is shown in Figure 38. The data collection software modules consist of the VISION, GRAB, and TAPE stand-alone programs as well as the operating system commands issued from SV for removing collected data files from the computer hard disk. The VISION and GRAB executables were developed by GTRI and can be called as stand-alone programs from the disk operating system (DOS) or from within the SV main menu program. The TAPE standalone program was developed by Colorado Memory Systems for controlling their tape drive unit and can be executed via menu selection from within SV. The quick-look analysis software components are the REFORM and QLOOK stand-alone programs which were developed by GTRI. In addition, the SV program provides a menu selection for automatically generating images from the radar data files contained on the hard disk without prompting for operator input. The software

modules for both data collection and quick-look analysis are discussed in greater detail in the following subsections.

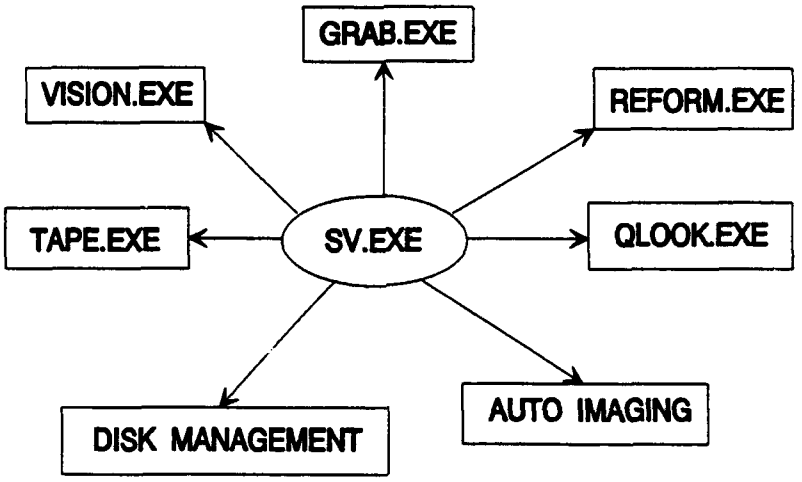

Figure 38. SV.EXE main menu shell program.

6.3.1 DATA COLLECTION

The data collection software was developed for automated control of the DAS hardware in collecting radar and IR camera scene data. Chronologically, the quick-look analysis software was developed first on the project. Experience gained during manual data collection with an early prototype of the Honeywell sensor proved the need for a computer-controlled data collection system. Positioning the sensor's antenna by manually operating the Klinger precision X-Y table was both tedious and time-consuming. The manual data collection runs were requiring as much as thirty minutes for scanning a thirty degree azimuth swath. The inability to rapidly acquire a radar image was unacceptable because weather conditions over the test runway area could change appreciably during the data collection run. The data acquisition system developed by GTRI did not yield real-time acquisition rates, but it did shorten the data collection run time to an acceptable average of approximately five minutes. In addition, to eliminating the tedium of collecting a radar scene, the data acquisition software enabled collection of a much larger number of radar images. The data acquisition software allowed the operator to collect both scene and calibration data with all of the millimeter wave sensors and the IR camera. The software also provided the operator with a means of saving the configuration of the DAS hardware used in radar data collection using a system of configuration hard disk files. In addition to the DAS configuration files, the software provided automated data file management

for the IR camera data. Preprinted operator's data log sheets were provided with entry fields for radar data run numbers.

A major part of the data acquisition software development effort involved the creation of the program VISION. This program whose top level design diagram is found in Figure 39 was designed to provide a menu-oriented operator interface for DAS configuration file management, selection of the LeCroy CAMAC digitizing crate parameters and the Antenna Positioner parameters, automated radar scene and calibration data collection, and radar range line plotting. The program was originally designed to be a stand-alone program called from the DOS prompt but was later included as a menu selection from within the SV main menu shell program. The DAS configuration files contain the CAMAC and Antenna Positioner parameters used during data collection and are stored by the operator on the PC hard disk with the file name extension .CFG. These files are generally named by the operator using a convention which corresponds with the sensor under test. For example, the Honeywell sensor might have a configuration file of "HONEY.CFG" associated with it. These configuration files provided an automated way of documenting the DAS setup used to collect scene data with the sensor as well as a means of quickly reloading the correct setup parameters at the start of a data collection run.

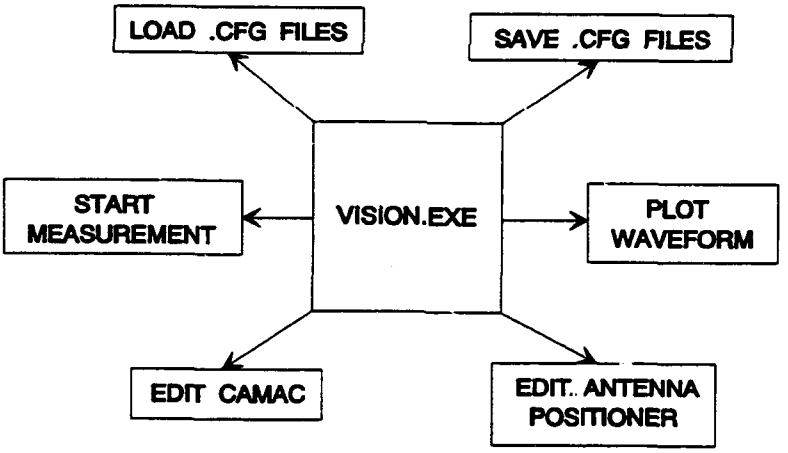

Figure 39. VISION.EXE block diagram.

The VISION submenu for selecting the LeCroy CAMAC parameters is shown in Figure 40. The Digitizer Module Type refers to the type of plug-in digitizer module used in the crate for sampling the baseband receiver output signal of the sensor under test. The Digitizer Slot number refers to the slot in the crate where the digitizer module is installed, for example, the module which provided for communication between the CAMAC crate and the PC controller was installed in Slot 0. The software allowed the operator to select one of three different

digitizers (TR8828C, TR6840, and TR6810). The amount of memory available for sample storage is dependent on the digitizer. The CAMAC digitizers could be externally clocked in order to allow for a wider range of sampling rates. In the sensor configurations tested on the tower, the external clock was provided by another CAMAC plug-in module, the 8501. The 8501 Slot refers to the CAMAC slot where the 8501 Clock Module is installed. The Samples per PRF determines the number of samples collected by the digitizer for each range line collected by the sensor under test. For the Lear Astronics sensor, the number of Samples per PRF refers to the number of samples passed to the FFT during data reformatting for generation of the radar range lines. The number of Pulses Integrated establishes the number of the range lines collected from the sensor for noncoherent averaging during data reformatting. The total number of samples collected by the data acquisition system per azimuth scan line is equal to the Samples per PRF times the number of Pulses Integrated.

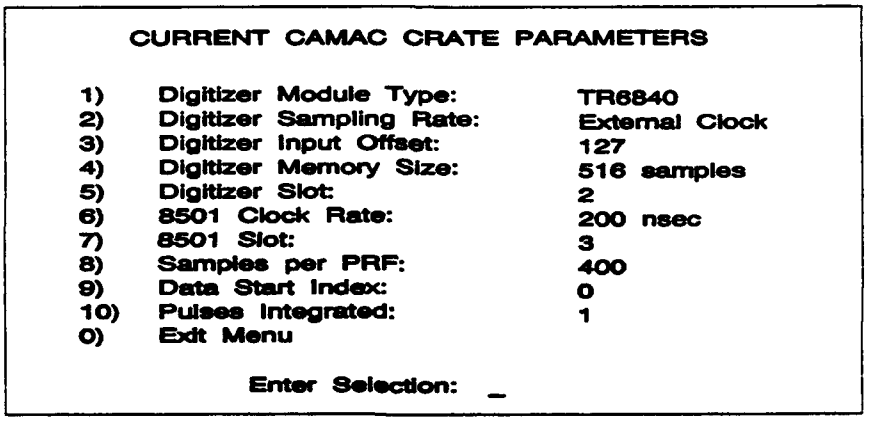

Figure 40. CAMAC Crate parameter selection menu

The VISION submenu for editing the Antenna Positioner is shown in Figure 41. The Left Edge of Scan refers to the reading on the front panel of the Antenna Positioner when the antenna of the sensor under test was boresighted at the left edge of the runway scene. The Antenna Positioner for Honeywell and Lear Astronics sensors was the government furnished Klinger X-Y Precision Table, and a DDC Synchro/Resolver was used to control the antenna of the Norden sensor. The total azimuth scan width is equal to the Azimuth Step Size times the Number of Azimuth Positions. The Inclinometer Elevation Angle provides the operator with the ability of recording the elevation angle where the azimuth cut was taken; however, during tower testing, elevation angle repeatability was provided by boresighting the sensors on a calibration reflector on the runway rather than inclinometer measurements. Also, the software allowed the operator

to record the azimuth and elevation position of calibration reference targets in the scene, but this feature was not used during tower measurements.

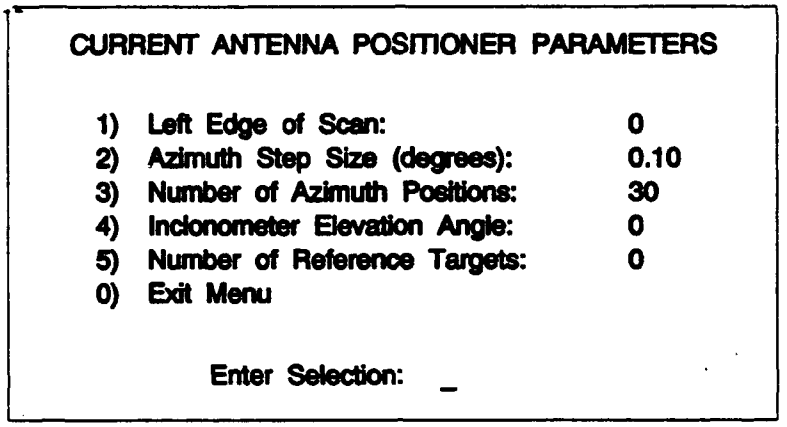

Figure 41. Antenna positioner parameter setup menu.

To begin data collection, the operator loads a measurement configuration .CFG file containing the desired CAMAC and antenna positioner parameters. The operator can modify any or all of these parameters and then save them to a new .CFG file. Once the desired DAS parameters are selected, the operator chooses Start Measurement from the VISION main menu to begin data collection. The software prompts the operator to enter whether the data run is for collecting calibration data or scanning the runway scene. If runway scene data are being collected, the operator is required to enter the sensor type (Lear Astronics, Norden or Honeywell) used for the data run. Next, the software prompts the operator to enter a file name which will contain the samples collected from the sensor. This data file is stored automatically on the computer's hard disk during data collection with the file name extension .UNF. Also, the software prompts the operator to enter the number of seconds of delay between positioning the antenna and collecting the data with the digitizer. This feature was added on the tower because the abrupt movement of the PC controlled positioning table caused vibration of the antenna which produced an image that which was smeared in azimuth. In general, a one second delay between positioning the antenna and triggering the digitizer for collecting the received radar signal was sufficient to minimize smearing the data without significantly increasing the data collection run time. Once the operator enters the time delay, the PC controller assumes control of the DAS hardware for scanning the runway scene. The PC host moves the sensor antenna to the left edge of the scene and scans the runway from left to right in azimuth. Once the data collection run is complete, the computer returns the antenna to the left edge of the scene. After data collection, the operator may plot a collected range line from the .UNF data file for analysis.

To collect a radar calibration data run, the operator injects a signal from a calibrated power source into the front end of the sensor under test. The output signal of the power source is passed through an attenuator before being injected into the radar receiver. The attenuator provides precise control of the signal power level being injected into the radar receiver. A receiver transfer curve for the sensor under test can be formed by setting the attenuator at various levels and digitizing the receiver output signal with the CAMAC crate. Each attenuator setting corresponds to a power level on the transfer curve. The transfer curve relates the output values of the A/D converter to the corresponding received power levels of the sensor under test. At the start of the calibration data run, the software prompts the operator for entering the number of attenuator settings used in the calibration run. Also, the software prompts the operator to enter the start attenuation setting and the step size between attenuator settings. During the calibration data run, the operator is prompted by the software to set the input attenuator and hit RETURN on the PC keyboard to collect samples with the CAMAC digitizer. The calibration data are stored in a .UNF data file on the PC's hard disk under a file name entered by the operator. These calibration data, at least one run per sensor, are used later during data preprocessing.

Calibration and scene image data are collected from the IR camera using the program GRAB. A block diagram of the GRAB executable is shown in Figure 42. The Video Frame Pass Through/Capture Mode selected from the GRAB main menu is used to collect video data using the Data Translation DT2853 Frame Grabber board. The Pass Through/Capture Mode begins by prompting the operator to enter a kernel name and starting value for the video files collected during data capture. The first video frame captured by the Data Translation board will be stored on the PC's hard disk under a file name created by appending the kernel name with the starting value. The video data file name will have an extension of .IMG, for example "FRAME1.IMG." Each subsequent video frame captured will have the same kernel name with an incremented value appended to it, for example, "FRAME2.IMG" and "FRAME3.IMG." Once a video frame was collected, the operator could review the stored image by selecting Display Captured Video File from the GRAB main menu. Also, the operator could easily evaluate the pixel values contained in the image of a captured video file by calling the stand-alone executable FINDCR.EXE from within the GRAB program. The FINDCR program was also written in Microsoft C and developed by GTRI. The program displays the captured image using the frame grabber board with a small box superimposed on the screen. Simultaneously, the pixel values of the image contained in the box are displayed on the monitor of the PC. By moving the box on the screen with the arrow keys on the PC keyboard, the operator can examine the captured image in real time.

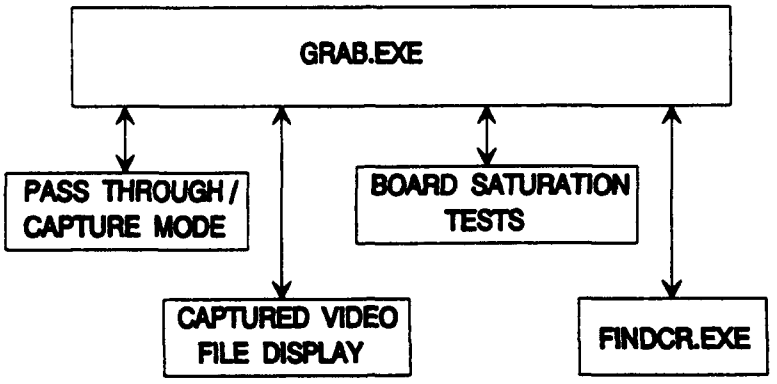

Figure 42. GRAB.EXE software block diagram.

Calibration of IR camera data is provided with each image of the runway collected with the GRAB program by placing calibrated hot bodies in the field of view directly in front of the camera. During tower testing, a two-point bracketing calibration scheme was used by using two blackbodies. One calibration target was set at a temperature slightly hotter than the runway scene, and the other target was slightly colder than the runway scene. Another set of calibrations performed on-site were the Video Board Saturation Tests. The DT2853 Video Board used on the tower contained an eight bit digitizer which provided image pixel values between 0 and 255. In the saturation test mode, the operator entered hot and cold pixel saturation values for determining which pixels in the image exceeded the upper and lower pixel value limits. During the hot saturation test, pixels which were higher in value than the entered hot saturation value were turned to white (255) while the pixels lower than the hot value set to black (0). The cold saturation test caused values higher than the cold saturation value to be set to white (255), and the lower pixels were set to black (0). By examining the binary (black/white) images created by these tests, the operator could determine if the runway scene was within the dynamic range of the video frame grabber board.

Data file archiving is provided in the synthetic vision data collection system using the Colorado Memory Systems Jumbo tape drive unit. Stand-alone program TAPE.EXE can be called via menu selection from within the SV shell program to operate the tape drive. The program is provided by Colorado Memory Systems for computer control of the tape drive unit. The software allows the operator backup and restore data files from/to the PC's hard disk using QIC-40 format cartridge tapes. In addition, the program provides for data file compression which allows for more tape storage capacity. A complete description of the software can be found in the installation manual from Colorado Memory Systems. Tape storage was a useful media for transporting data files collected on the tower to GTRI for reduction and analysis.

6.3.2 QUICK-LOOK ANALYSIS

The requirement for an on-site method of verifying the collected radar image was identified at the outset of the project. Data verification for the IR camera is provided as part of the data collection process itself, since the operator can visually inspect the quality of the captured image in real time on the TV display. Without the availability of quick-look image analysis in the field, the quality of the radar data would not have been established until after the data were sent to GTRI for reduction. This would have allowed a number of data collection runs performed under the desired weather conditions to produce invalid data due to incorrect DAS setup or hardware malfunction. Therefore, a reasonably fast, on-site radar image generation capability was developed using the government furnished Data Translation Frame Grabber board. Stand-alone programs REFORM.EXE and QLOOK.EXE were developed to produce an image of the collected radar data on the TV screen in under five minutes. As discussed in the previous sections, both the REFORM and QLOOK programs could be executed from within the synthetic vision main menu shell program SV. The quick-look image generation process involved two steps. First, the REFORM software was called upon to read the .UNF files generated by the VISION data acquisition software and create a standard format input file to the QLOOK program. Next, the QLOOK program is called to load the radar image into the DT2853 board for display on the TV screen.

The REFORM program whose block diagram is shown in Figure 43, was designed for both quick-look imaging and data preprocessing which are described later in Section 7.2.1. For quick-look imaging, the program reads the .UNF radar data files and generates a .QLK output file for input into the QLOOK program. The .QLK output file is a standardized file which contains the azimuth range lines of the radar image in a B-scope format with the output range values in each range line truncated to eight bits (0-255) for display using the frame grabber board. A real, radix-2 fast Fourier transform (FFT) was used to generate range lines from the linear frequency modulated continuous wave (linear FMCW) sensor used by Lear Astronics. This FFT was obtained from Version 1.0 of the 387FFT digital signal processing software package which is commercially available from MicroWay, Inc. The REFORM program also provides the operator with the option of decimating the range samples by an integer number to produce range lines which are shorter in total length. The maximum image height which can be displayed on the TV screen with QLOOK is 512 range values (pixels). The operator can also specify a start range which is the first range value of each range line written into the output .QLK file. This allows the operator to shift the front edge of the radar image out in range to remove the transmit pulse produced by the pulsed sensors. In addition, the image quality can be improved by performing

noncoherent averaging of the collected pulses at each azimuth position using REFORM. Finally, REFORM can produce an output file whose range values are in either Linear or Logarithmic magnitude formats.

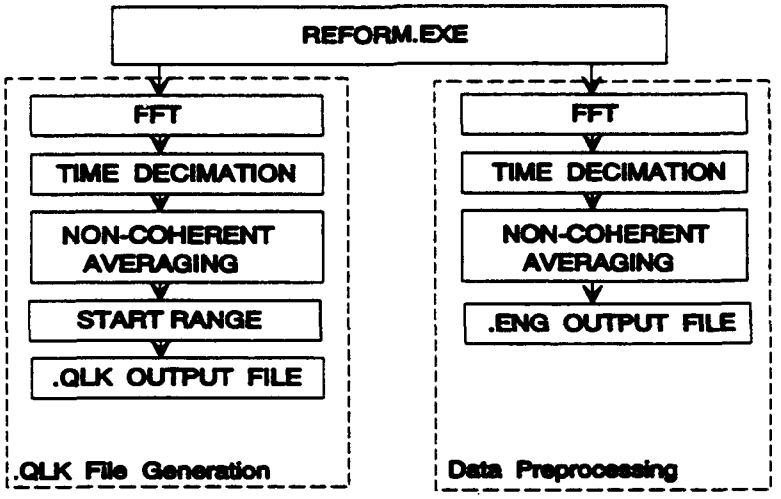

Figure 43. REFORM software block diagram.

The QLOOK program uses subroutines provided by Data Translation's DTIRIS software library to load pixel values stored in the .QLK input file into the DT2853 Frame Grabber board for image display on the TV screen. The operator is prompted to enter the format of the output image to be displayed, either B-scope or C-scope. The C-scope, or perspective view, display is generated from the input B-scope format data of the .QLK file using the geometry of the tower - runway scene and equations for slant range-to-elevation angle conversion documented in a technical memorandum by Dr. Mark Richards at GTRI. Once the output image format is selected, the operator may enter gain and offset values for modifying the pixel values of the displayed output image. These parameters allow the operator to adjust the brightness of the image displayed on the TV screen. Once the image is displayed, the operator can select to save the image to a file on the computer hard disk. The image hard disk files have the extension .IMG and are saved to disk using a software function provided by the DTIRIS subroutine library. The image files can be redisplayed on the TV screen using the IRIS tutor software provided by Data Translation.

SECTION 7
DATA PROCESSING

7.1 SENSOR PERFORMANCE DATA BASE

A concept drawing of the synthetic vision data base process is provided in Figure 44. As illustrated in this drawing, the purpose of the data base is to conduct queries yielding correlated information from all of the data sources. The first source of data, as discussed in Section 4.1.1, was a map of the vicinity as illuminated by the sensors and was used to extract scene geometry characteristics. The three sources of sensor data were the actual radar received power, the simulated radar received power, and the infrared radiance. The final source of data was from the meteorological sensors and included visibility metrics, rain rates, humidity, wind speed and direction, irradiance, ground temperature, dew point, barometric pressure, and thermistor values, as well as observations. The initial block receiving data from the multiple sources, "Time and/or Scene Coordinate Correlation," consisted of a number of processing elements, in some cases chained processing, employed to perform calculation-intensive operations on the data before inserting the final processed data into the data base. The software chosen for the data base implementation was Borland Paradox — a relational PC data base software package available via site license at Georgia Tech. This section describes in detail the theory behind the approach to gathering the required information as well as the processing required.

7.1.1 DATA BASE DEVELOPMENT

The term "data base" is used to describe an organized collection of related information stored in tables. The tables can be used to define relationships among the various items of information. The synthetic vision data base was the mechanism which joined data from the meteorological and sensor measurements and where "what if?" types of questions were asked and resolved. The data base provided query capabilities between time-related meteorological data and MMW radar and IR sensor dat. Each type of data could also be analyzed independently.

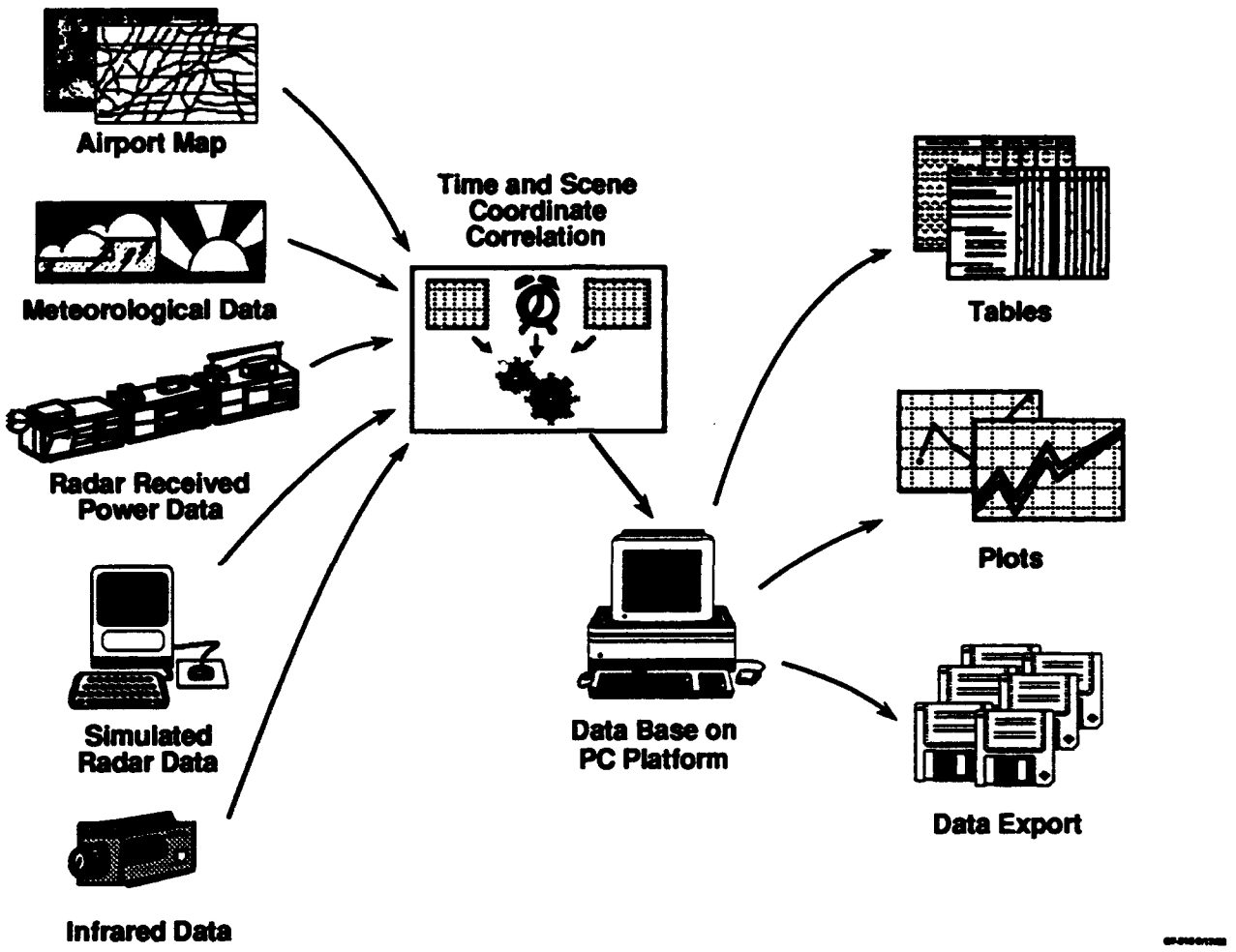

Figure 44. Synthetic vision data base process.

7.1.2 DATA INPUT

The contents of the data base can best be described by looking at the categories of information stored for the MMW radar sensors, IR images, and meteorological sensors as shown in Tables 27, 28, and 29. These summary tables address general categories of information which in the actual data base may be implemented with multiple tables. For instance, rain rates were collected with both tipping bucket and NASA rain gauges. The tipping bucket gauge collected data ever minute, while the NASA rain gauge reported data every second. As a consequence of this different collection rate, the data were stored in separate tables.

Table 27. MMW Radar Sensor Variables

MMW Radar Sensor Data	Description
run name	assigned during data collection
date	day-month-year
time	hours-minutes-seconds
range	meters from sensor
azimuth	degrees from sensor centerline
surface characteristic	runway, grass, corner reflector, profile, etc.
received power	measured in dBm
variability (received power)	standard deviation within a patch
radar cross section (σ)	calculated from received power using radar equation (dBsm)
normalized radar cross section (σ^0)	calculated from received power and radar cell area ($dBsm/m^2$)
contrast	defined as $(power_{runway} - power_{grass})/power_{grass}$
attenuation	calculated from rain rates and corner reflector power values (dB/km)
volumetric backscatter (σ^v)	calculated from received power and radar cell volume ($dBsm/m^3$)
sharpness	calculated in 1/degrees, companion value to contrast, indicates rate of change from grass surface to runway surface power return

Table 28. IR sensor Variables

Infrared Data	Description
run name	assigned during data collection
date	day-month-year
time	hours-minutes-seconds
range	meters from sensor
sharpness	10% to 90% slope (degrees)
runway radiance	measured in W/m^2 steradians
runway radiance variability	standard deviation
grass radiance	measured in W/m^2 steradians
grass radiance variability	standard deviation
contrast	defined as $(radiance_{runway} - radiance_{grass})/radiance_{grass}$
noise (calculated)	$\sqrt{\frac{\text{runway variability}^2 + \text{grass variability}^2}{2}}$ (W/m^2 steradians)
SVR	runway radiance to noise ratio

Table 29. Meteorological Variables

Meteorological Data	Description/Units
date	day-month-year
time	hours-minutes-seconds
runway visual range	km
long path visibility	km
rain rate	mm/hr
humidity	%
wind speed	km/hr
irradiance (solar and terrestrial)	W/m^2
air temperature	°C
ground temperature(s)	°C
dew point	°C
barometric pressure	millibars
averaged rain rates	mm/hr
drop size distributions	$\#/m^3$/size interval
equation of state humidity	g/m^3
# concentration (PMS probes)	$\#/m^3$
liquid water content (PMS probes)	g/m^3
visibility(PMS probes)	km
rainfall rate (GBPP probe)	mm/hr
observed conditions	from operator

7.1.3 OUTPUT PRODUCTS

In general terms, the potential output from the data base can be envisioned as any combination of information gleaned from the tables above. That information can be from a single table of data such as meteorological trends over a period of time or from multiple tables such as sensor contrast performance as function of a meteorological variation. In the case of multiple table data, the information is correlated based on matching date and time values. A list of the outputs most frequently obtained and the table source(s) are listed in Table 30.

Table 30. Outputs from data BASE

Output	Data Table Source
air, runway, and ground temperatures as a function of time	meteorological
thermistor temperatures as a function of time	meteorological
tipping bucket and NASA rain rates as a function of time	meteorological
long path visibility and runway visual range as a function of time	meteorological
raindrop concentration as a function of size at a given time	meteorological
contrast or received power as a function of range for a given run	MMW sensor
received power as a function of cross-range at a given downrange value (profile patch)	MMW sensor
normalized radar cross-section as a function of range for multiple MMW sensors	MMW sensor
attenuation as a function of rain rate	MMW sensor and meteorological
volumetric backscatter as a function of rain rate	MMW sensor and meteorological
received power as a function of cross-range at a given downrange value for varying rain rates and/or observed weather conditions	MMW sensor and meteorological
contrast or received power as a function of visibility at a given range	MMW sensor and meteorological
number of MMW sensor data runs matching specified meteorological conditions (observed or measured)	MMW sensor and meteorological
contrast or SVR as a function of range for a given run	IR sensor
contrast or SVR as a function of time at a given range	IR sensor
contrast or SVR as a function of cross-range at a given downrange value	IR sensor

Table 30 (Continued). Outputs from data BASE

contrast or SVR as a function of cross-range at a given down-range value for varying rain rates and/or observed weather conditions	IR sensor and meteorological
contrast or SVR as a function of runway and background temperature differences	IR sensor and meteorological
contrast or SVR as a function of visibility at a given range	IR sensor and meteorological
number of IR sensor data runs matching specified meteorological conditions (observed or measured)	IR sensor and meteorological

7.2 MMW RADAR SENSOR DATA

7.2.1 DATA PREPROCESSING

Data preprocessing was conducted at GTRI in Atlanta upon receipt of the collected .UNF data files from the tower at WPAFB. The purpose of data preprocessing is to generate a standard format input file for the data reduction software which contains the received power of every range sample contained in the collected data file. This received power "map" of the runway scene is produced by calibrating the range samples in the scene .UNF data file with the calibration data collected with the sensor under test. In addition, preprocessing involved correction of a data collection problem encountered with triggering the CAMAC crate digitizer. This intermittent hardware triggering problem caused the desired zero range sample collected for some of the range lines to be offset in the data stream read from the digitizer memory. Therefore, data preprocessing for the pulsed sensor types involved three software steps. First, a program called SKEW developed at GTRI was used to correct the hardware triggering problem. De-skewing was not required for the Lear Astronics sensor type. Second, the REFORM program was used to generate a B-scope format data file from the collected data with range samples in floating point precision. Finally, a program called RTCCAL developed at GTRI was used to generate the received power map from the floating point range samples using the calibration data collected from the sensor under test.

The SKEW program was written to ensure that the desired zero range sample was the first sample in the range lines generated by the pulsed sensors. The trigger signal used to start data collection with the CAMAC digitizers was derived from the transmitter pre-trigger signals of the Norden and Honeywell radars. This configuration allowed the digitizers to collect several samples prior to the firing of the sensor's transmitter. Although blanking was used to protect the sensor's receiver, internal leakage of the transmit pulse into the sensor's receiver caused a white

band to form at the edge of the image generated by the radar; however, when the intermittent triggering error would occur, the range line would be offset by several samples including the white saturated pixels which marked the transmit pulse. The SKEW program took advantage of this effect when searching for the transmit pulse within a window at the front edge of each range line within the input .UNF data file. The program would then offset the entire range line by the number of samples necessary to align the leading edge of each transmit pulse. The program then writes the de-skewed data out to a new .UNF file with a "D" appended to the original file name. For example, if the original file is named "NS1R01.UNF," then the output file is named "NS1R01D.UNF." De-skewing of the Lear Astronics sensor was not required, since the FFT output from a linear FMCW signal places the zero range sample in the DC range bin by definition.

The REFORM program, whose block diagram was shown earlier in Figure 43, is called to read the corrected .UNF data files and generate an output file containing range lines with floating point precision values for processing by the RTCCAL software module. As before with quick-look imaging, the real radix-2 FFT from the MicroWay software package was used to generate range lines from the Lear Astronics linear FMCW sensor. Also, the operator is allowed to decimate the range samples and noncoherently average the range lines collected at each azimuth position. The output floating point precision range samples are written in B-scope format to an output file with the extension .ENG.

The program RTCCAL is called to apply the sensor's calibration data to the .ENG data file to produce a file containing a "map" of the received power at each range sample collected by the sensor. The program begins by prompting the operator to enter the .ENG file name containing the runway range samples and the .UNF file name containing the collected calibration data. Next, the operator is prompted to enter the power level in dBm produced by the millimeter wave source at the front end of the receiver during calibration. The RTCCAL program then equates a power level with the A/D converter value measured at each attenuation setting in the .UNF file. These calibration settings identify discrete points on the sensor's receiver transfer curve (RTC) which relates received power to A/D converter output. The RTCCAL takes each floating value in the input .ENG file and linearly interpolates the sensor's receiver transfer curve to assign a received power level to each range sample in the runway scene. The resulting received power map in B-scope format floating point precision is written to an output file with the extension .RTC. These .RTC files are later used during data reduction for runway/grass feature extraction and sensor analysis.

7.2.2 VISUALIZATION TOOLS

A number of different tools evolved during the data analysis process using the RTC files. These tools, which are more fully described in the subsections that follow, include production images of the scene, down-range power and contrast plots, cross-range power plots, 3-D plots of regions of interest in the scene, and cloud plots of received power as a function of range.

7.2.2.1 Production Images

The requirement for producing runway images from radar data consisting of floating point precision range samples was identified during the early stages of data reduction. Originally, this capability was envisioned to serve as a form of quick-look analysis for the .RTC files generated for data reduction and feature extraction. Imaging radar data files generated by computer model from the Modeling and Analysis Laboratory at GTRI was later added as an additional requirement.

The program IMAGE was developed at GTRI to produce TV images from data files containing floating precision range samples. This program creates a production quality image of the data in either B-scope or C-scope formats from .ENG or .RTC input data files. The operator is required to select a gain and offset applied to the floating point numbers to bring their values within the limits of 0 and 255. This is necessary to display the samples as pixel values which are limited to eight bit precision. The gain and offset is usually chosen to maximize the brightness and contrast of the displayed image. Also, the program calculates an eight level gray scale legend with text to show how a range of the input floating values translate into shades of gray in the image. In the case of a .RTC input file, these values correspond to received power levels in dBm. Finally, the program generates the image with the bordered gray scale along the right side of the TV screen using the DT2853 Frame Grabber board and the subroutines provided in the DTIRIS software package. The operator is allowed to save the displayed production image to an .IMG file using DTIRIS subroutine.

One example of a production image is provided in Figure 45. This particular image is from a clear weather run for the Honeywell 2 configuration. The run name is HI2R11, and the data were collected on 14 April 1992 beginning at 14:36. Additional images are provided in Appendix C.

7.2.2.2 Down-range Power and Contrast Plots

The simplest display format of power data for each run is a plot of received power from runway and grass patches as a function of range from the sensor (see Figure 46). A corresponding plot of contrast between grass and runway as a function of range for the same data set is shown in Figure 47. As verification of data quality, every run of data collected during the Synthetic Vision program, as well as modeled data, was reviewed in these two formats.

7.2.2.3 Cross-range Power Profiles

As defined in Section 4.1.2.2 and illustrated in Figure 20, cross-range patches were defined for use in the analysis of areas which included both grass and runway. The power profile observed across such a patch is shown in Figure 48.

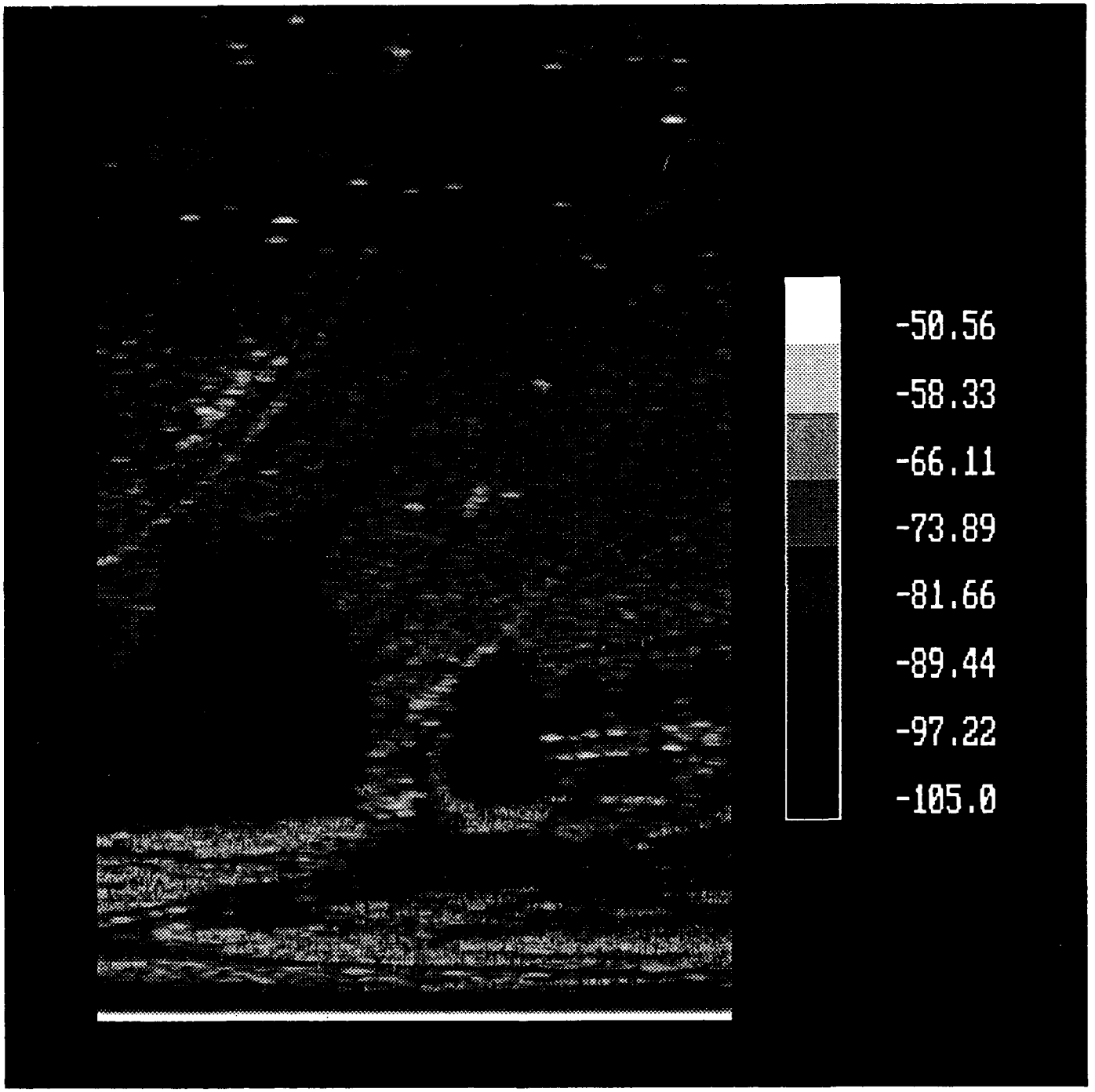

Figure 45. Production image of Honeywell 2 clear weather run.

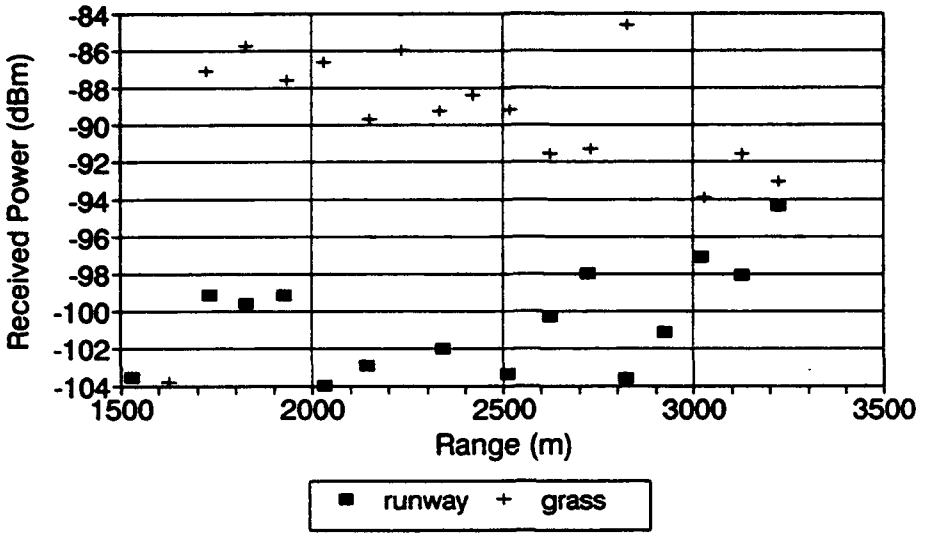

Figure 46. Sample plot of received power as a function of range.

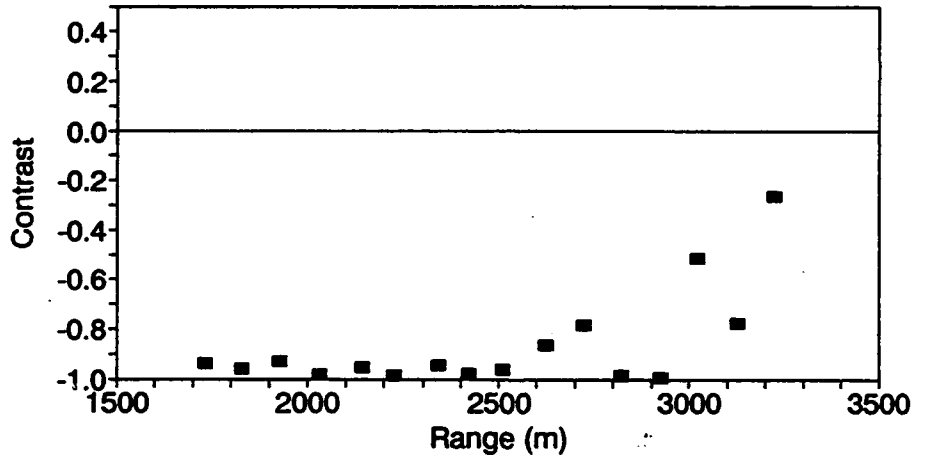

Figure 47. Sample plot of contrast as a function of range.

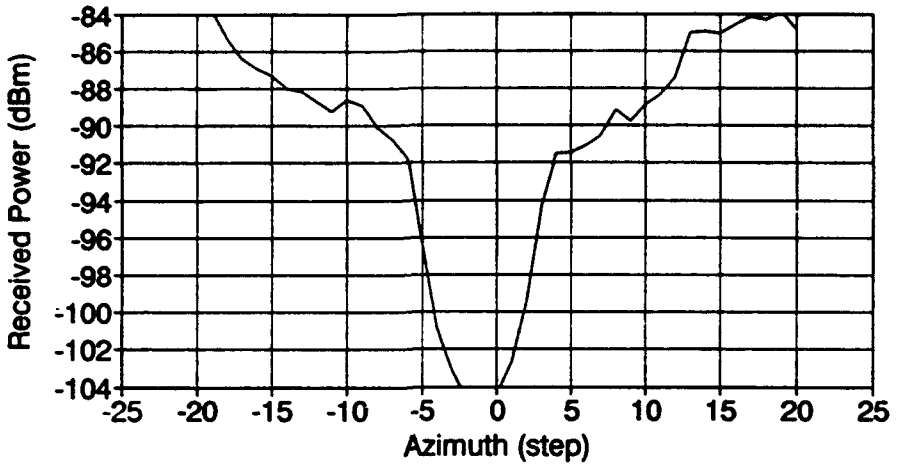

Figure 48. Sample plot of cross-range power at 2.5 km down-range.

7.2.2.4 3-D Plots

The 3-D plots were created using Data Analysis Plotting Software developed by J. M. Baden at GTRI. For use with the synthetic vision data, a subset of the 300 azimuth by 512 range cells of received power data was defined and written to a file. The plotting software used this information to create 3-D plots such as the examples shown in Figure 49 and 50. The analyst had the option of plotting the simple received power values or values which were smoothed in azimuth using a weighted smoothing procedure. This weighted smoothing (or averaging) procedure was implemented by calculating a value for each point which gave a weight of 1 to values on the right and left and a value of 4 to the center point. Figure 49 shows a region of 60 azimuth cells by 40 downrange cells at 1.8 km containing a corner reflector. Figure 50 is a region of the same size which includes the runway at 2.0 km. The runway region was manually added to Figure 50 to indicate the runway location. Both of these images represent smoothed data.

7.2.2.5 Cloud Plots

Initial observations of the data indicated that there was a high degree of variability for regions with similar surfaces at similar ranges. The "cloud plot" tool further confirmed this observation. The plot in Figure 51 shows received power for a clear weather data run as a function of range for two regions: the runway (represented by the + symbol) and the adjacent grass area (represented by the rectangle symbol). In this particular plot, there appears to be some target, such as a vehicle, on the runway at about 2,950 m. The band at the bottom of the plot represents

the noise floor for the system. The data clearly follow the theoretical range trends and substantiate the high degree of variability observed generally.

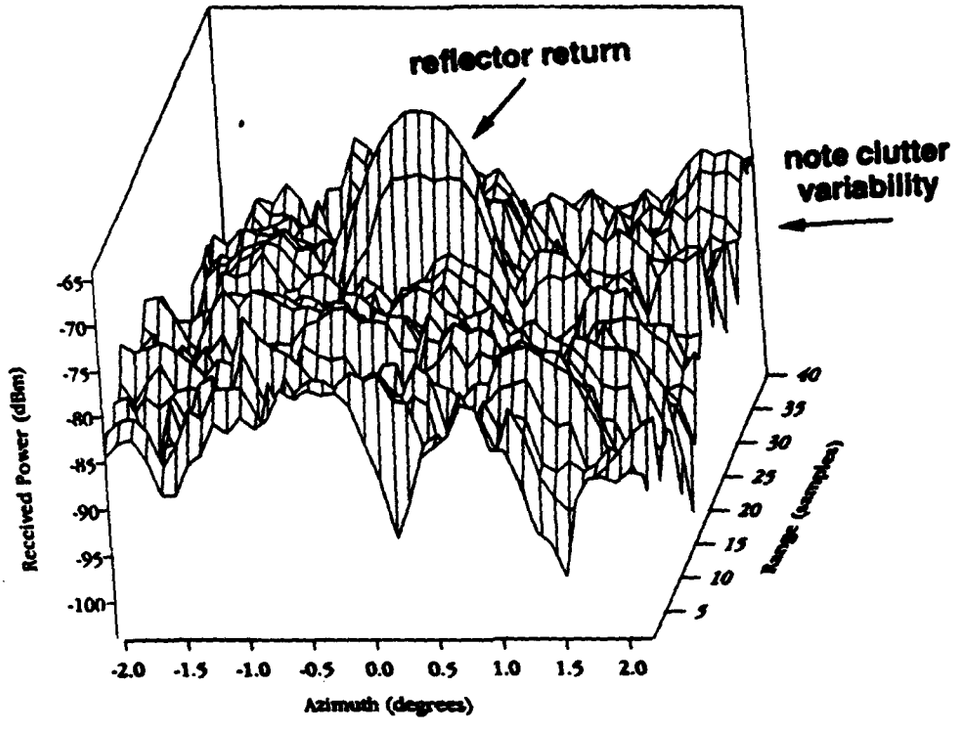

Figure 49. 3-D plot of corner reflector region.

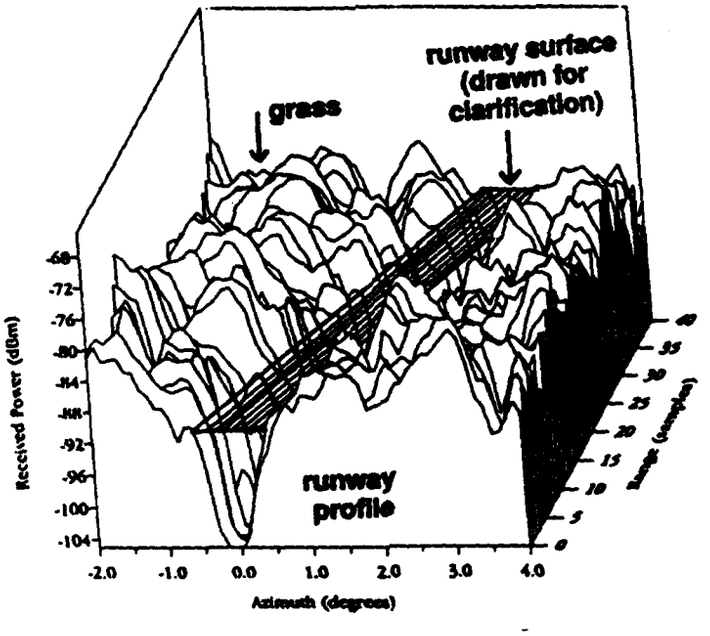

Figure 50. 3-D plot of runway and vicinity.

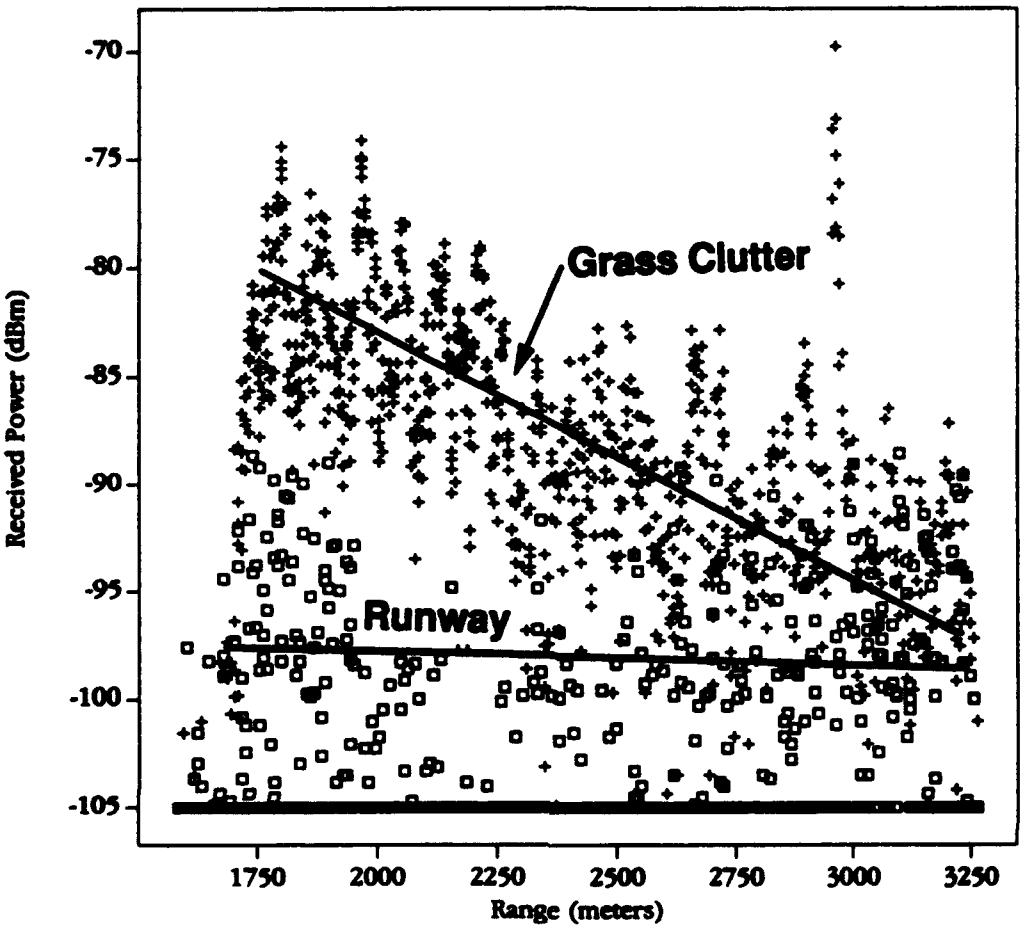

Figure 51. Cloud plot of received power from runway and grass regions.

7.2.3 DATA REDUCTION

Once the patches were defined from the map (see Section 4.1.2) and the MMW radar sensor data were preprocessed (see Section 7.2.1), the data from these two sources were merged to extract representative values for the features of interest. The procedure, entitled DATA_RED, was implemented using Borland C code and provided values for received power, contrast, radar cross section (σ), normalized radar cross section (σ^0), and volumetric backscatter (σ^v). A summary of the steps follows.

1. As described in the method of test, a minimum of one corner reflector was placed in the scene along the centerline of the sensor beam. Patches were defined for the corner reflector(s) based on the information regarding the location. After reviewing several data files, range and azimuth locations for each corner reflector were defined as the reference values. The first step in processing each RTC file is to look at the power values from a 20x20 block of data resolution cells around the

known vicinity of the corner reflector and identify the range and azimuth location of the peak. Using these values, calculate the range and azimuth offsets by taking

observed value - reference value

for range and azimuth. These offsets are then stored and used to register the scene to account for small pointing inconsistencies occurring in the data collection.

2. The header values for the received power files which were created as a part of the preprocessing are shown in Table 31 on the left. The run name points to information, stored in the DATA_RED code, on sensor parameters shown in the table on the right. Specifically, the first 3 characters in the run name define the sensor and the configuration. For instance, runs HI2R012 and HI3R006 point to sensor parameters for the Honeywell Configurations 2 and 3, respectively. Run NS1R77D points to sensor parameters for the Norden Configuration 1.

Table 31. RTC Header Data and Sensor Correlation

data file name
HEADER PARAMETERS
sensor name
date and time
start azimuth (degrees)
azimuth increment (degrees)
scan width (azimuth cuts)
range increment
sample rate
PRF samples
azimuth time increment

SENSOR PARAMETERS
azimuth beamwidth
elevation beamwidth
transmit pulse
wavelength
peak power
gain
radar losses
propagation losses (clear weather)
runway resize factor

3. The map coordinates and patch type names for the patches are read in. For the case of sensors with a wide azimuth beamwidth, the runway patches are constricted in cross-runway width to minimize errors from the beam overlapping into the area beside the runway. A module within the code, RESIZE.C, conditionally handles this requirement.

4. The map coordinates read in above are then converted into a list of data resolution cells. (see Appendix D for definition of this procedure.) These data resolution cell identities are then registered to the scene by adding the range and azimuth offsets identified in step 1.

5. Using the list of data resolution cells, read in the power values (dBm) for each patch.

6. For each patch, calculate the median range, azimuth, and event time as well as the approximate ground area, single radar cell area, and single radar cell volume. (The equations used in the area and volume calculations are provided in Appendix A.)

7. For non-profile patches, de-log the power values and calculate a representative value for each patch. For runway, taxiway, and grass patches, this value is the mean. For the corner reflector and fence patches, use the peak value. Calculate additional statistics for each patch: minimum, maximum, standard deviation, absolute deviation, and variance. Calculate radar cross section, normalized radar cross section, and volumetric radar cross section. Selected values from these calculations are then written to the DATABASE.TXT and RCS.TXT files for incorporation in the data base. It should be noted here that, for the sake of consistency in data processing, clear weather attenuation values were used in calculating the initial radar cross section values. These values were later adjusted for those data sets not occurring during clear weather. (The equations used for these adjustments are provided in Appendix A.) These adjustments were done within the data base.

8. For profile patches, de-log the power values and average in range for each azimuth stripe. Calculate smoothed values for the profile using both a linear 3-point moving average and a weighted moving average. The algorithm for the weighted average was similar to the linear moving average, except that the center value is given four times the weight of the values on either side. These values are then written to the PROFILE.TXT file for incorporation in the data base.

9. For each contrast pair defined in the patch definition file, calculate the contrast values and store in the DATABASE.TXT file.

In addition to the features extracted during the procedure described above, an additional procedure was used to calculate sharpness using a MATLAB routine. Sharpness was chosen to serve as a figure of merit in comparing the performance of different sensors in terms of how clearly the edge of the runway could be seen, i.e., the more rapidly the received power changes from the grass mean level to the runway mean level, the sharper the image is. Sharpness is measured in degrees^{-1} according to the following procedure and is illustrated in Figure 52.

1. Given a cross-range plot of a profile patch, select 6 points which clearly define three lines. Line (a)(b) is the grass to the left side of the runway, line (c)(d) is the runway, and line (e)(f) is the grass to the right side of the runway.

2. Calculate the absolute value of the angular change, in degrees, represented by lines (b)(c) and (d)(e). Note that in Figure 52, each azimuth cut represents an azimuth step of 0.1°.

3. Take the average of these slopes on the left and right side.

4. Define the sharpness to be 1/average slope.

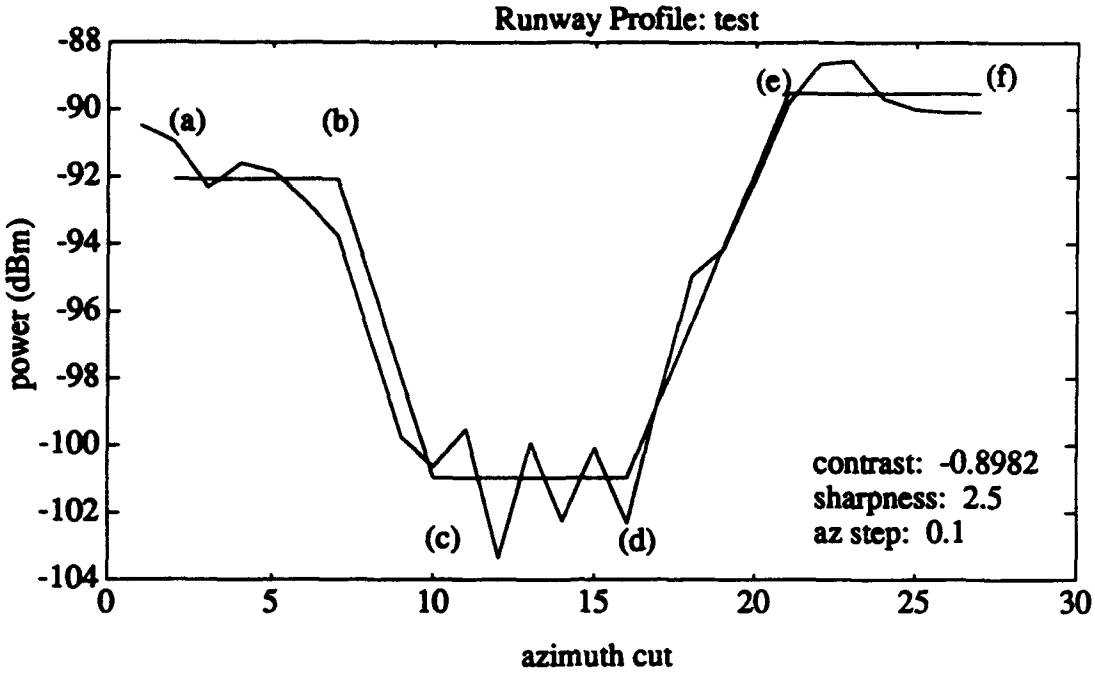

Figure 52. Illustration of sharpness concept and calculation.

7.3 IR SENSOR DATA

7.3.1 DATA REDUCTION

The infrared images were collected by capturing the image from the RS-170 video output of the camera. The images were digitized and captured with an 8-bit A/D converter on a Data Translation DT-2853 frame grabber board mounted in an IBM compatible PC with an 80486 processor. The digitized images were saved to disk files by calls to Data Translation software driver procedures for further data reduction and processing. Each pixel in the image was stored as an 8-bit byte in the binary image file. The images were stored in a top to bottom sequence of lines and from left to right by column location of pixels. The binary image data are preceded by a 512-byte header which contains information in a format specific to Data Translation software which was not utilized in this analysis effort.

The reduction of data stored in the captured images was conducted in stages, resulting in computed values of the desired measures of image quality. The products of the data reduction were contrast, sharpness, and signal-to-variability ratio for the desired elements of the scene. These products were evaluated at three selected points along the runway with nominal camera to runway ranges of 1,710 m, 2,380 m, and 3,300 m. Image analysis software was used to select regions in the image and to compute and report for each defined region the mean digital pixel

value and the variance of the pixel levels within the region. The defined regions for relatively large area blackbody sources were rectangular boxes lying within the constant temperature zones of the sources. For regions on the runway and in the nearby background, line segments were used, since the narrowness of the projected image of the runway made it very difficult to select polygonal regions lying entirely within the runway image.

The mean pixel level values for the regions defined within the two blackbody sources were then used to determine the slope and intercept for a linear relation between digitized pixel level and scene radiance. Radiance values used for the linear calibration fit were computed for the two blackbody sources from their known temperatures. The blackbody effective radiance was computed by integrating Planck's equation combined with the camera spectral response over the response band of the IR camera.

The calibration parameters were used to convert the mean and standard deviation for each region in all of the analyzed images into effective scene radiance values in the units ($W/m^2/str$). These mean and standard deviation radiance values were entered into a Quattro Pro spread sheet which was used to compute the image quality measures, contrast, and SVR for each measurement point. The data base of measured and computed values stored in the spread sheet file was imported into a Paradox data base along with the weather data base for analysis. The spread sheet was used to generate summary printouts and was the form in which the data base of image quality measurements was stored.

Contrast is determined from the relation

$$C = \frac{B_{runway} - B_{background}}{B_{background}} \tag{48}$$

B(runway) and B(background) are the measures of brightness of the runway and background areas extracted from the image video data. Since the IR camera is operated in the manual gain control mode, it is appropriate to calibrate the image brightness in terms of absolute radiance units, so the brightness measure used in the determination of contrast will be the absolute in-band radiance in units of watts per meter squared per steradian. The contrast measure determined when brightness is equated with absolute in-band scene radiance will differ from that determined directly from the RS-170 video level. This difference in contrast value which results from defining brightness as calibrated radiance is due to the DC bias in the level of the IR camera video signal which produces a zero or "black" video level at some nonzero absolute radiance level which is determined by the camera "offset" setting. If RS-170 signal levels were used to determine the contrast, then slight adjustments of the offset could result in large differences in

contrast by changing the B(background) in the denominator of the equation while not affecting the numerator.

Signal to variability ratio is computed from

$$SVR = \frac{B_{runway} - B_{background}}{Variability} \tag{49}$$

where B(runway) and B(background) are as defined above. Variability is the noise level in the signal and would be derived from the variance of the signal within the background area. Both the numerator and denominator in the expression for SVR are differential measures, so the effect of an offset in the video level is eliminated. The SVR derived from the expression above is consequently independent of calibration of the brightness measure. It is possible to specify a threshold level of SVR which would represent the required magnitude of SVR for detection of the runway. In general, the precise value of this threshold level depends on many variables related to the image display system, geometric parameters related to the size and shape of the object to be detected, and characteristics of the human vision system. A value somewhere in the range from 0.1 to 0.5 appears to be a reasonable threshold interval which should cover a variety of "nominal" observation conditions.

Sharpness in the infrared images was determined from plots of the brightness measure along linear profiles which crossed the runway image at right angles to the projected runway image. The linear segment profiles were defined and extracted with the image analysis software mentioned above. Sharpness values were determined directly from the plots as the angular interval taken for the image video level to transition from the background level to the runway level from the 10% to the 90% level. This measure is also unaffected by the calibration of the image data. The sharpness was determined at both the right and left edges of the runway at the three selected locations along the runway for most of the images where the runway could be detected. The narrowness of the projected runway image made the determination of sharpness difficult, since the runway was only a few pixels wide as viewed from the tower with the 32 degree field of view Kodak camera.

7.3.2 DATA ANALYSIS

The diurnal variation of image quality in the baseline measurements was investigated by plotting the image quality measures against a variety of other parameters. The effects of low visibility conditions were derived from plots of contrast or SVR as the dependent variable and various weather parameters as the independent variable.

Particle size data for fog and haze size ranges were available as part of the weather measurements for some of the low-visibility tests. These size distributions were used with a computer program to calculate Mie scattering parameters for the fog droplets.

Raindrop size distributions were available for a few of the IR images as well. A relation between rain rate and drop size distributions was proposed by Marshall and Palmer in 1948 and modified more recently by Joss and Waldvogel.[Joss and Waldvogel, 1969] The relationship was used to generate size distributions and compute extinction coefficients for the rain rate values determined with the NASA rain rate sensor.

7.4 METEOROLOGICAL DATA PROCESSING

During the course of the tower tests, meteorological measurement data would first be recorded on site by E-OIR, Inc. After some post-processing, these data would then be shipped to GTRI for evaluation and inclusion in the sensor test data base. GTRI aided in the meteorological data processing through the application of a number of post-processing routines applied to data supplied by E-OIR Inc. These post-processing routines included data conditioning algorithms as well as procedures used to incorporate the meteorological data into a common data base with the sensor data sets.

During the course of the project, Georgia Tech performed data integrity checks on the received data. As a result of these checks and observations by project personnel from other organizations, GTRI performed a number of specialized examinations using portions of the data sets. These included examinations of the results from the two different measures of optical visibility, an examination of the relative humidity measurements, examinations of the rain and fog drop size distributions, and calculations of MMW and IR attenuation factors and rain rates from the PMS particle probes data.

7.4.1 DATA PREPROCESSING

Raw data output stored at 1 and 10 minute intervals from the meteorological instrumentation were preprocessed by E-OIR, Inc. before it was sent to GTRI for further analysis and incorporation into the sensor data base. The data received by GTRI was typically in the form of a set of QUATTRO spread sheet files. This format enabled easy analysis and further data processing at GTRI. All data elements were converted to engineering units before incorporation into the spread sheet files. Several raw data elements were also kept with the files. These raw data elements were the one second readings from the NRRS and the raw particle counts from the

two PMS particle probes. These raw data items were later subjected to further processing at GTRI before being incorporated into the final data base.

7.4.2 DATA SELECTION

Each meteorological data set was examined, upon arrival at GTRI, for general consistency and completeness, and any discrepancies present were noted. If sufficient discrepancies had existed in any of the data sets, they were to be discarded. In general, the data received from E-OIR was found to be of high quality, and all data sets were included in the sensor test data base.

7.4.3 DATA REDUCTION

Some processing was required to put the meteorological data received from E-OIR into a format amenable to use with the sensor data base program. This processing consisted of three steps. In the first step, meteorological parameters unrelated to a particular sensor technology, such as sky irradiance for MMW radars, and any duplicate parameters were removed. The second step integrated the 1-second samples from the NASA rapid response rain rate sensor (NRRS) to reduce variance and to eliminate false negative rain rates. Integration periods of 10, 30, and 60 seconds were computed. The third processing procedure converted the tipping bucket rain rate data from one minute samples into a sliding window ten minute average rain rate. The fourth and final meteorological data preprocessing step combined one minute and 10 minute sampled data from the two data collection trailers, data from a long path length visibility measurement, and data collected from the NRRS for input to the sensor performance data base.

7.4.4 DATA QUALITY INVESTIGATIONS

During the course of the tower test program, several investigations were undertaken to determine the utility and validity of certain meteorological data products. Two of these investigations concerned the correlation of the two different visibility measurement methods and the measurements of absolute humidity by the OPHIR brand humidity sensor.

7.4.4.1 HSS and LPV Visibility

The visibility values calculated from the HSS sensor data and the long path visibility (LPV) transmissometer were compared after it became apparent that these two instruments often gave different readings for the optical visibility. The HSS sensor was located on the runway's edge and measured optical visibility by examining the amount of optical energy scattered out of a relatively short optical path. The LPV sensor consisted of two parts: a transmitter collocated with the MMW and IR sensors on the 10th floor of building 620 overlooking the runway test

area and a receiver located with the remainder of the meteorological instrumentation near the runway.

Eleven test runs were examined in the study. The LPV sensor yielded higher visibility in five instances, and the HSS sensor yielded higher visibility on five instances. In the eleventh case examined, the LPV visibility was initially lower than the HSS measurement, the readings coincided about halfway through the test run, and the LPV visibility exceeded the HSS visibility by the conclusion of the test. It was concluded that the major factor influencing the different calculated visibility was the location of the equipment. The HSS sensor was located completely at ground level adjacent to the meteorological equipment. The LPV sensor, on the other hand, sampled the entire path from the MMW and IR sensor location to the runway, a distance of 1.79 kilometers. In the case of ground fogs, it was entirely possible for the HSS sensor to yield a smaller value for visibility than the LPV sensor which indicated the visibility integrated over the entire 1.79 kilometer path. Smaller LPV visibility could also be indicative of levels of reduced visibility due to fog or precipitation which lay at heights above the HSS sensor location. The LPV values of visibility were considered to be of greater value in characterizing sensor performance, as the path over which this sensor operated was more characteristic of the path over which the MMW and IR sensors operated.

7.4.4.2 OPHIR Sensor and Equivalent Humidity

The meteorological officer at WPAFB first noticed discrepancies between the absolute humidity measured from the 'OPHIR' sensor and the absolute humidity obtained from independent measurements of air temperature, dew point, and barometric pressure. Five test cases were examined to discover if the cause for this discrepancy could be discovered. In all these cases, the OPHIR sensor produced absolute humidity values that were greater than those calculated from the independently measured parameters using the equation of state. The differences between the two values for the absolute humidity generally differed by five to ten percent. During the course of this investigation, it was determined that the OPHIR temperature readings were generally a degree lower than the temperatures recorded by the independent temperature probe.

A sensitivity analysis was conducted to discover which variable in the equation of state would produce the most change in calculated absolute humidity, given small changes in measured values. Three variables were examined: temperature, dew point, and barometric pressure. The variable which exerted the greatest influence was, not surprising, the dew point. In the range of temperatures, dew points, and pressures encountered during this test, a change in the measured dew point of a single degree could change the calculated absolute humidity nearly ten percent.

The calculation of absolute humidity was found to be much less sensitive to the measured value of temperature or pressure.

The OPHIR instrument was designed to measure humidity fluctuations, and the instrument's accuracy had been shown, in studies, to deteriorate as the air approached saturation. One obvious advantage of the OPHIR values are that they are a better measure of the fluctuations in the absolute humidity. Changes in the absolute humidity which occur on times scales of a minute or two and are apparent in the OPHIR data do not appear in the equation of state humidity values. As it was not possible to determine the exact cause of the measured discrepancies and it was desired to have the greatest data resolution possible, use of the OPHIR data was continued with the caveat that the data may get less accurate as atmospheric saturation is approached.

7.4.5 Droplet Size Investigations

The data produced from the two particle measurement probes were examined separately from the other data. Both data sets were first processed to convert the data from raw counts to the more useful form of numbers of drops per cubic meter per millimeter size class interval, also known as 'number concentration'. Several useful rain and fog parameters, including attenuation, backscatter, and rain rate, may then be derived using these new values. The shape of the fog droplet size distribution curves were compared to modeled distribution curves and to those reported from other investigations.

7.4.5.1 GBPP Rain Drop Size Distribution

The ground based precipitation probe (GBPP) data sets provided by E-OIR consisted of computer spreadsheet files in two parts. The first part of the data files contains multiple lines of data representing the number of particles detected within each droplet size bin per second. Each line of the file includes a time mark, plus characters denoting the instrument type and operating range. The second part of the GBPP data files contained various data elements that were used by E-OIR to calculate particle number concentrations and integrated visibility.

The integrated visibility results, in files delivered by E-OIR prior to 18 March 1992, calculated from these numbers did not seem to be of the correct order of magnitude. Attempts by GTRI to calculate normalized drop size distributions, optical visibilities, MMW attenuations, and MMW backscatter values on the basis of these numbers also yielded values which did not seem to be consistent with previous investigations or independent measurements taken during the tower tests. These inconsistencies have been traced to several causes. The two areas where these

errors were found were in the calculation of the sampled volume used for each size interval and in the calculation of the terminal velocity of particles contained in different size bins.

The conversion of the raw number of detections determined in each size channel to normalized number concentrations which may be compared with results from other investigations and used to calculate derived quantities may be described as follows. The number concentration, NC, for each size channel, n, may be defined for each sampling interval as

$$NC_n = N(D_n) / SV_n \tag{50}$$

where: NC is the number concentration in number per cubic meter within size channel n,
D_n is the mean diameter of the drops detected in size channel n in μm,
$N(D_n)$ is the number of particles detected in channel n, and
SV_n is the sampled volume for channel n during the sampling interval in m^3.

The calculations can be seen to depend heavily on the determination of SV_n. This sampled volume may be defined as

$$SV_n = SA_n \times TAS_n \times TS\ 10^{-4} \tag{51}$$

where: SV_n is the sample volume in m^3,
SA_n is the sample area for size channel n in cm^2,
TAS_n is the mean terminal air speed for particles in size channel n in ms^{-1},
TS is the sampling period in seconds, and
10^{-4} is a conversion factor to return a result in m^3.

Values for SA_n were initially calculated from instrument parameters and algorithms from PMS documentation provided by E-OIR. The documentation was not explicit on which, of several, algorithms were to be used for GBPP data. A relation was determined from this documentation and discussions with E-OIR and PMS to calculate the sample areas. This is the relation used by E-OIR in their final report. Discussions with PMS, however, led to a simpler result. Records had been kept at PMS detailing the sample areas for each instrument sold. These values of sample area were provided and could simply be substituted into the equations for each size bin.

The E-OIR calculations provided prior to March of 1992 also neglected the dependence of terminal velocity on the mean size of the particle. Terminal velocity was simply estimated at 9.8 ms^{-1} for all size bins. While the terminal velocity of the larger particles certainly approach this value, smaller particles fall at significantly lower speeds. An empirical relation, proposed by

Gunn and Kinzer was used to calculate terminal velocities appropriate for each size channel.[Gunn 1949] This relation, which yields terminal velocities in units of meters per second, is given as

$$TAS_n = 9.65 \times 10.3 \exp(-0.6\, D_n) \tag{52}$$

Both GTRI and E-OIR calculations determined the mean diameter of particles detected within each size channel using the following equation.

$$D_n = RES \times n \times SC_n \tag{53}$$

where: RES is the probe resolution in μm per probe element (200 μm for GBPP), n is the size channel number (1, 2, 3, ..., 62), and SC_n is a size correction factor dependent on the channel number.

The number concentrations produced using the above equations represent the number concentration in the ambient atmosphere of drops detected within each size channel. To produce spectra of number concentration which may be compared to results produced in other investigations, we divided each channel's number concentration by a factor of 0.2 to convert the result to particles per cubic meter per millimeter size interval.

The equations given above were applied to the data files supplied by E-OIR to provide number concentration values for use in producing drop size distributions, MMW attenuation values, and MMW backscatter values. Examinations of these derived quantities are presented in the next few subsections.

7.4.5.1.1 Drop Size Distribution Parameters

The drop size distributions (DSDs) gathered by the Ground Based Precipitation Probe (GBPP) were first plotted as number concentration versus mean diameter. The number concentration values were plotted as the dependent variable on a logarithmic scales. A linear regression analysis was then performed on the middle portions of these distributions in order to estimate the No and Λ parameters of a simple exponential drop size distribution, represented as $N(d) = N_0 \exp(-\Lambda d)$. The results of this analysis were inconclusive but did correlate well with published examples of curve fitting to drop size distributions from natural rain. One problem with this simple distribution fit is the wide range of values for N_0 and Λ that are found in measured distributions.

7.4.5.1.2 Estimations of MMW Attenuation

One use of the raindrop size distributions is in estimating the radar attenuation due to the rainfall. Several cases have been studied using Mie scattering theory along with the calculated number concentrations to estimate the radar attenuation. Reasonable agreement between the rain DSD derived and the directly measured MMW radar attenuations were found.

The largest differences found between the GBPP derived and measured attenuations occurred during periods when the rain rate was rapidly changing. The measured attenuation was caused by all the rain contained in the radar beam during the measurement interval, but the calculated attenuation was determined based on a spot measurement of the drop size distribution. The presence of a few highly attenuating areas in the radar beam, not coincident with the GBPP sensor, would lead to a higher value of measured attenuation. The calculated values of attenuation are of value in those situations where no direct measurement of attenuation was possible, as long as the limitations of the GBPP measurements are kept in mind.

7.4.5.1.3 Estimation of Rainfall Rate

The GBPP drop size distributions may also be used to produce estimates of the rainfall rate. As the rainfall rate is more influenced by larger particles, well within the range of the GBPP sensor, it was expected that the GBPP derived and the directly measured rain rate from the NRRS device would be reasonably correlated. These rain rates were also calculated as a check on the correct operation and calibration of the GBPP sensor data.

Results from the data sets taken on 14, 18, and 21 April indicate that the calculation of rain rate from DSDs was able to provide a reasonable estimate of the rainfall rate. The best agreement between the two rain rates occurs at the lower rates. As the rain rate increases, the differences between the two measurements also increases. This error may be due to slight misregistrations in the time tags between the NRRS data and the GBPP data.

7.4.5.2 FSSP Fog Drop Size Distributions

The Forward Scatter Spectrometer Probe (FSSP) data were first converted from raw counts of particles within each size bin to a calculated number concentration using a procedure similar to that described in Section 7.4.5.1. Again, the basic formula is

$$NC_n = N(D_n) / SV_n \quad (54)$$

where $SV_n = SA \times TAS \times TS \times 10^{-4}$.

In the processing for the FSSP, the velocity of the particle through the sensor is not the terminal air speed of particles of that diameter; the velocity is that of the sampled air as provided by an aspirator. The sample area of each size channel is a nominal sample area defined for the instrument reduced by a series of factors which compensate for particles which pass to near to the edges of the sample area, coincident particles, and instrument dead time. The only difference between the GTRI and E-OIR processing of the FSSP raw particle count data was a difference in the total sample areas used. Again, discussions with PMS indicated that the proper total sample area for the FSSP fielded should have been 0.615 mm^2, rather than 0.496 mm^2 as assumed in the E-OIR calculations.

7.4.5.2.1 FSSP Drop Size Distribution Parameters

The number concentrations derived from the FSSP data have units of number of particles per cubic meter per micron size interval. Again, these number concentration distributions may be plotted as a function of mean particle diameter on log scales to determine the values of N_0 and Λ for an exponential drop size distribution. These parameters were compared with results found in other investigations. These number concentrations were used to estimate two important atmospheric parameters: suspended liquid water content (SLWC) from fog particles and optical visibility.

7.4.5.2.2 Liquid Water Content Calculations

The calculation of the SLWC is relatively straightforward. The volume occupied by all the drops measured is estimated by multiplying the number of drops found in each size bin by the volume occupied by a drop having the mean diameter of drops in that size bin. The total volumes calculated for each size bin are summed and multiplied by the density of liquid water to yield a measure of SLWC in grams per cubic meter. That is

$$LWC_n = (4/3)\,\pi\,(D_n / 2)^3\, NC_n\, \rho \quad (55)$$

where: LWC_n is the liquid water content of drops detected in channel n,
D_n is the mean diameter of drops detected in size channel n,
NC_n is the number concentration in number per cubic meter in channel n, and
ρ is the density of the water in the drops.

The total liquid water content measured by the probe is then the sum over all size channels of the quantity computed above. This figure may then be used to estimate MMW attenuation due to fog.

7.4.5.2.3 Optical Visibility Calculations

The FSSP sensor number concentrations were also used to calculate the optical visibility. This simple calculation makes several assumptions, such as no shadowing of particles by others and an effective optical scattering cross section which is twice the geometric cross section due diffraction effects. The equation used to calculate optical visibility is

$$V = \ln (1/0.02)[(\pi/2) \times \Sigma (NC_n D_n^2)]^{-1} \quad (56)$$

This calculation assumes that the particles scatter optically, i.e., the scattering cross section of the particles is twice the area of a circle of a diameter the same as the water drop. It also assumes that the limit of visibility occurs at a visual threshold of a 0.02 contrast value. If the FAA limit of visual threshold of 0.05 contrast is used, the values must be reduced by a factor of 0.77. The calculated optical visibilities showed reasonable agreement with the measurements made by the LPV and HSS sensors.

7.5 DATA CORRELATION

The processes for creating the values which are inserted into the data base have been fully defined. For the synthetic vision application, data were imported into Paradox tables from Quattro spread sheets (meteorological and IR data) and from ASCII text files created during the Borland C processing (MMW radar data). Within the data base, some computations were done using the imported data. In general though, the main purpose of the data base was to provide a vehicle for conducting queries which related the different data sets. The results of the queries could be exported in the form of printed tables and plots, Quattro files, and ASCII files.

7.5.1 CORRELATION METHOD

As noted earlier, the key fields used for correlating sensor and meteorological data were the date and time (hours, minutes, and seconds) fields. Paradox provides the user the capability to record and store frequently used queries in script files. These script files are stored in ASCII format and can be modified from within Paradox or by using any editor. Approximately seventy script files were created during the synthetic vision data analysis. The user can also define individualized graph and report formats to display the results of queries. The following script is a simple example which queries the "SENSOR" table and the "METDATA" table for a list of the sensor

run names where there is no matching meteorological data set for the MMW radar sensor data. The first line, which begins with a ";" is a comment. After the query is executed, the script calls up a previously defined report format and sends the results to the screen.

```
;SCRIPT NAME is NOMATCH
ClearAll Esc {Ask} {sensor} Tab Tab Tab Example "a" Tab Example "b" Tab Example
"c" Tab Tab Tab Tab Tab Tab Tab Check Menu {Ask} {metdata} Tab Example "a" Tab
Example "b" Tab Example "c" Do_It! Menu {Tools} {Rename} {Table} {Answer}
{temp1} {Replace} Menu Esc ClearAll Esc {Ask} {sensor} Tab Tab Tab Tab Tab Tab
Tab Tab Tab Tab Tab Tab Check Do_It! Menu {Tools} {Rename} {Table} {Answer}
{temp2} {Replace} Menu {Modify} {Restructure} {Temp2} Down "Runname" Tab
"a8" Do_It! Menu {Ask} {temp2} Tab Tab "changeto " Example "a" Left Example "a"
UpImage ClearImage Do_It! ClearAll {Ask} {temp1} "set" Tab Example "run" Menu
{Ask} {temp2} Tab "no " Example "run" Tab Check Do_It! Menu {Report} {Output}
{Answer} {R} {Screen} Menu {Scripts} {End-Record}
```

Since the meteorological data were stored in two main tables, METDATA and NASARAIN, a similar query was done to identify missing NASA rain data. While the script looks fairly cryptic in recorded form as shown above, the procedure for creating and storing such a script from within the Paradox application is far more straightforward and obvious to the user, leaving little or no margin for error.

The following query captures returned power as a function of range from the runway for two runs and then returned power from the grass for the same runs. These two temporary answer tables are then restructured and joined, and the information is plotted using a predefined plot form called "Hpower." The labeling for the plot is changed before the plot is sent to the printer.

```
;SCRIPT NAME is HPOWER
Esc {Ask} {sensor} Tab "H" Tab "0" Tab "10/24/91" Tab "12" Tab ">0" Tab Tab Check
Tab Tab Check "AS runway" Tab "runway" Do_It! Menu {Tools} {Rename} {Table}
{answer} {power} Menu {Modify} {Restructure} {power} Down Right Right Tab
"Grass" Tab "n" Do_It! Menu {Ask} {sensor} Backspace Backspace Backspace
Backspace Backspace Backspace "longgrass" Left Backspace Backspace Backspace
Backspace Backspace Backspace "grass" Do_It! Menu {Modify} {Restructure}
{answer} Down Ins Tab "runway" Tab "n" Do_It! Menu {Tools} {More} {Add}
{answer} {power} Menu {Modify} {Sort} {power} {Same} Do_It! Right Menu {Image}
{Graph} {Load} {Hpower} Right Menu {Image} {Graph} {Modify} Menu {Overall}
{Titles} Tab Tab Backspace Backspace Backspace Backspace Backspace Backspace
Backspace Backspace Backspace Backspace Backspace Backspace Backspace "10/24/91
Runs 6 and 7 Clear Weather" Do_It! Menu {Image} {Graph} {ViewGraph} {Printer}
Menu {Scripts} {End-Record}
```

The user could take this same query and change the bold-faced print to display the same information for a different run or set of runs.

The next example queries the sensor table for data from the Norden sensor for the returned power from the near and far corners correlated to the tipping bucket rain rates measured at the same times.

```
;SCRIPT NAME is RAIN_COR
ClearAll {Ask} {sensor} Tab "N" Tab "0" Tab Example "a" Tab Example "b" Tab
Example "c" Tab Tab "<" "2000" Tab Tab Check "AS Corner 1" Tab Tab "corner"
Tab Check Menu {Ask} {metdata} Tab Example "a" Tab Example "b" Tab Example
"c" Tab Tab Tab Tab Tab Tab Check ">.1" Do_It! Menu {Modify} {Restructure}
{answer} Down Down Tab Tab Tab "Corner 1" Tab Tab "Corner 2" Tab "n" Do_It!
Menu {Tools} {Rename} {Table} {answer} {rain_cor} {Replace} UpImage UpImage
Left Left Left Backspace "2" Left Left Backspace Backspace Backspace Backspace
Backspace ">2000" Do_It! Menu {Modify} {Restructure} {answer} Down Down Right
Right Tab "Corner 1" Tab "n" Tab "Corner 2" Tab Do_It! Menu {Tools} {More}
{Add} {answer} {rain_cor} Right Right Menu {Modify} {Sort} {Rain_cor} {Same}
Down "1" Do_It! Tab Rotate Menu {Image} {Graph} {Load} {Npowrain} Right Menu
{Image} {Graph} {ViewGraph} {Screen} Esc Menu {Scripts} {End-Record}
```

7.5.2 DATA REPORT GENERATION

Samples of the results from some of the possible data base queries are provided in Table 32 and Figures 53 through 66.

Table 32. Sample Table of Runs, Met and NASA Data, and Visibilities

Record #	Run	Observed	Date	Hour	Min	Met	NASA	RVR (ft)	LPV (ft)
1	NS1R11D	clear	10/26/91	10	27	Y	N	92200	110471
2	NS1R12D	clear	10/26/91	11	8	Y	N	31005	54786
3	NS1R14D	clear	10/26/91	11	34	Y	N	79842	102230
4	NS1R16D	fog	10/28/91	9	41	Y	N	29130	24160
5	NS1R18D	fog	10/28/91	10	5	Y	N	25449	26021
6	NS1R75D	fog	11/22/91	8	8	Y	N	23457	30630

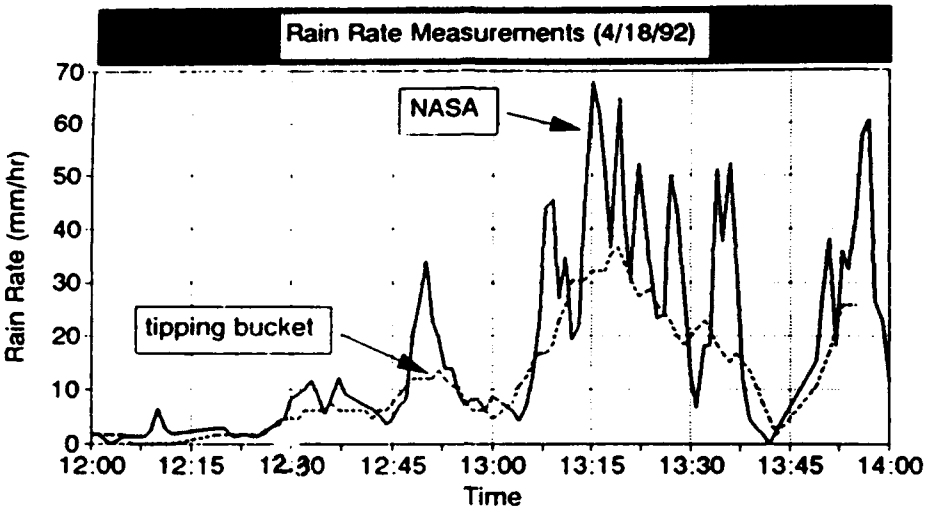

Figure 53. NASA and tipping bucket rain rates as a function of time.

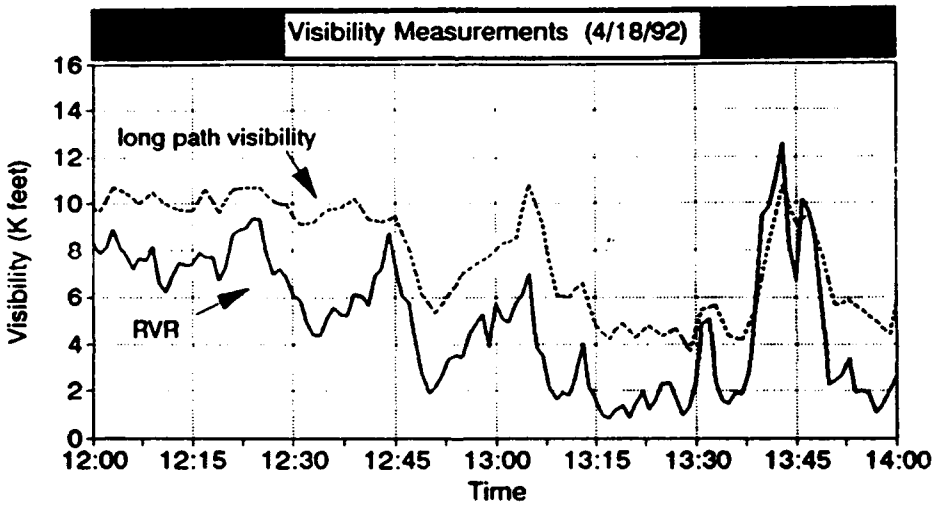

Figure 54. Long path and runway visual range visibility measurements as a function of time.

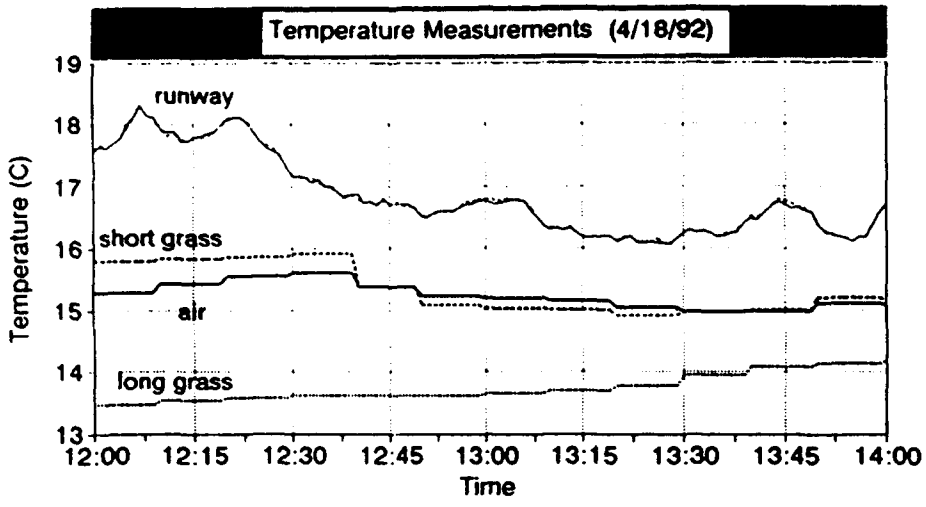

Figure 55. Multiple temperature measurements as a function of time.

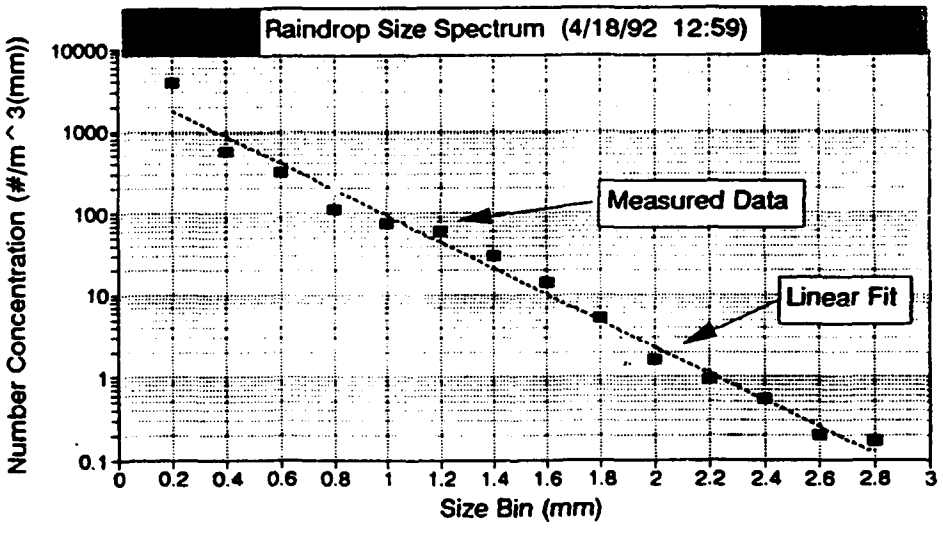

Figure 56. Raindrop size spectrum (concentration as a function of size bin).

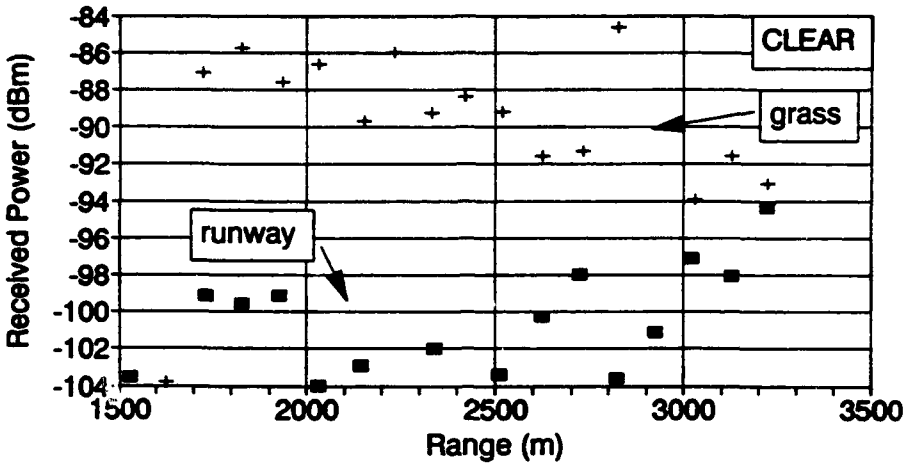

Figure 57. Received power as a function of range for grass and runway patches.

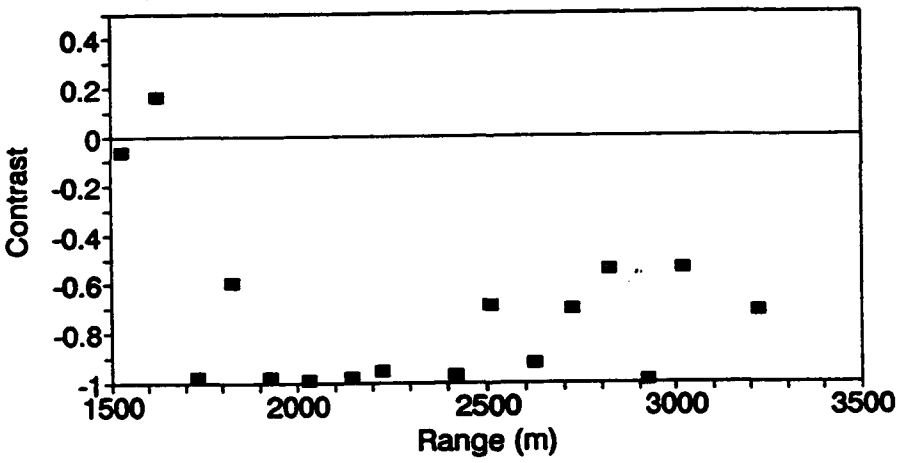

Figure 58. Contrast as a function of range for a single run.

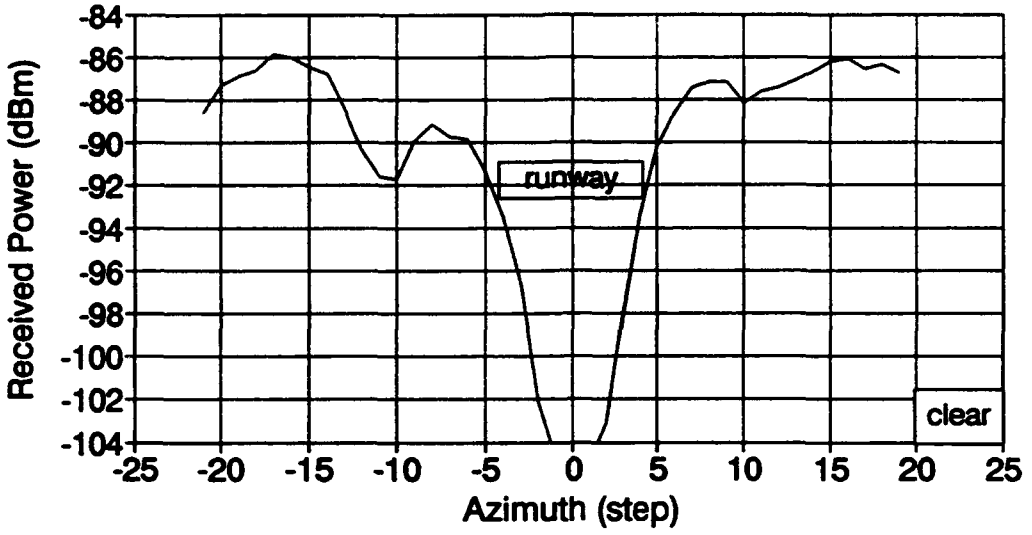

Figure 59. Received power as a function of cross-range for a single run at 2.5 km.

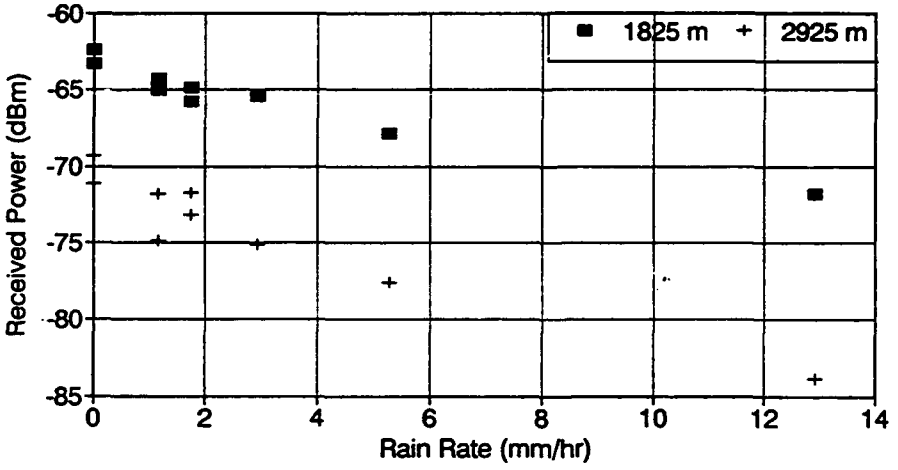

Figure 60. Received power from corner reflectors as a function of tipping bucket rain rate.

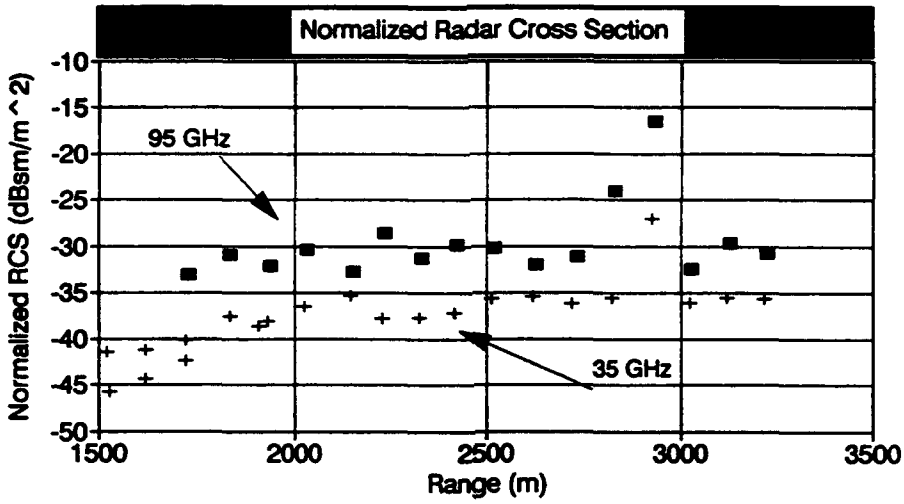

Figure 61. Normalized radar cross section as a function of range for two radar frequencies.

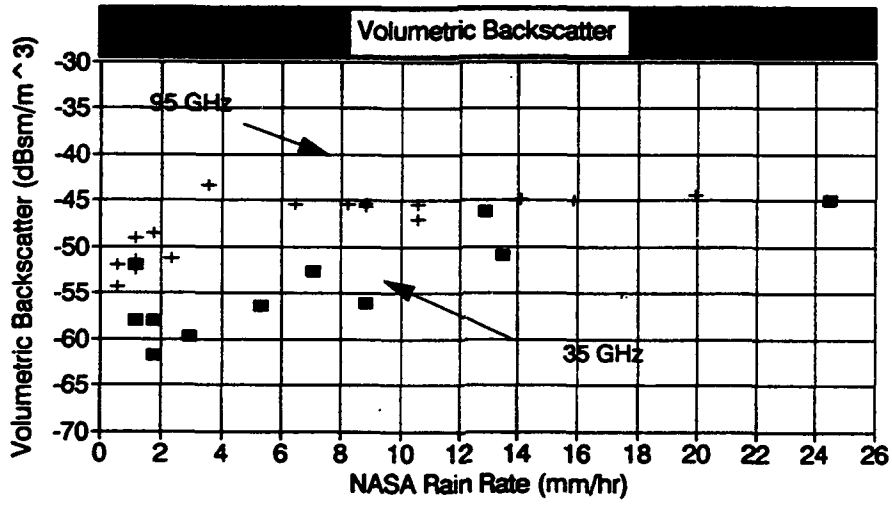

Figure 62. Volumetric backscatter as a function of NASA rain rate for two frequencies.

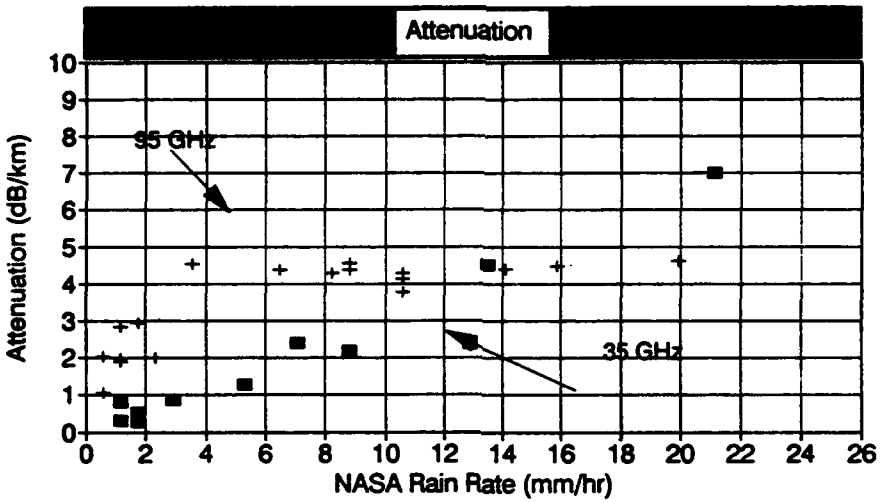

Figure 63. Attenuation as a function of NASA rain rate for two frequencies.

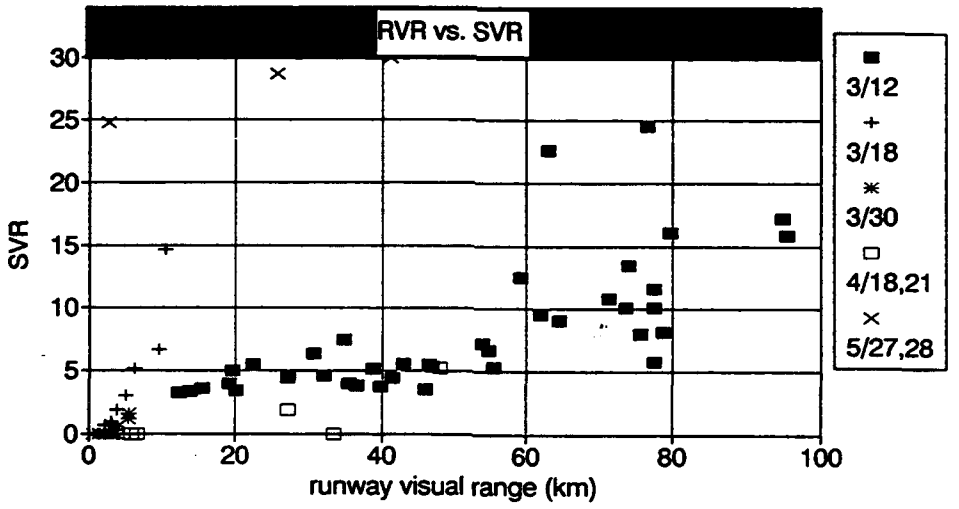

Figure 64. SVR at a single range in the IR data as a function of runway visual range.

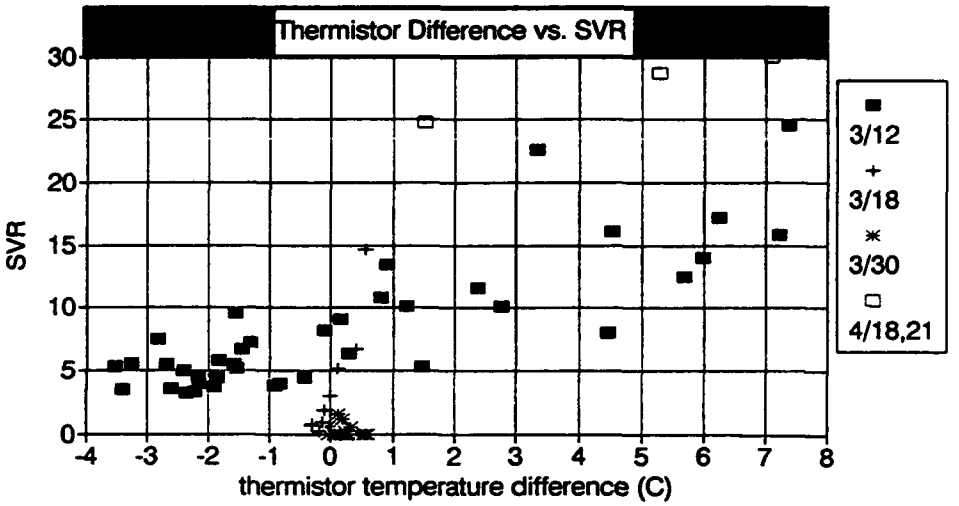

Figure 65. Signal to variability ratio at a single range in the IR data as a function of mean thermistor temperature.

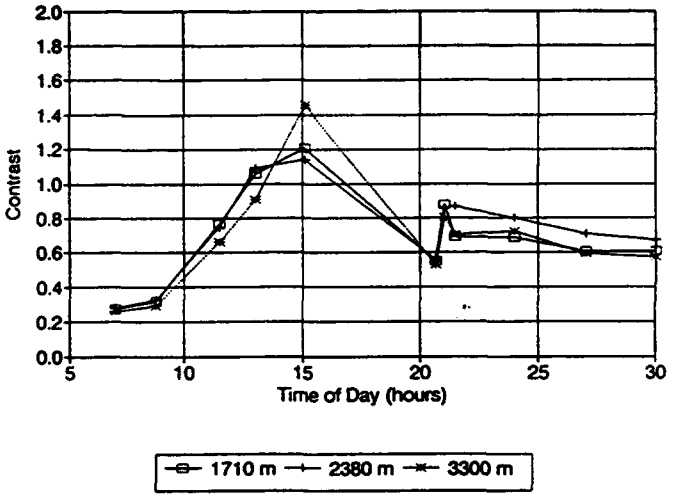

Figure 66. IR contrast at three ranges as a function of time during a diurnal.

SECTION 8
EXPERIMENTAL RESULTS

8.1 MMW RADAR RESULTS

Sufficient MMW sensor data from the Honeywell 35 GHz and Norden 95 GHz radars were collected during the tower tests to report sensor performance results for a variety of weather conditions. Of these two MMW sensors, only the Honeywell 35 GHz radar was designed specifically to perform the runway imaging mission. The Norden 95 GHz radar was less optimum for high-resolution runway scene imaging, but it provided valuable test data on the adverse weather performance of a 95 GHz radar sensor. Since both of these radars were calibrated, valuable phenomenology data were also collected at the two MMW frequencies. Performance results for the Lear Astronics 94 GHz radar sensor also tested at the tower are documented in a separate report[Hudson, Sept.1992]

Results for the Honeywell 35 GHz and Norden 95 GHz radar sensors are summarized in Figure 67 for the three primary performance categories of contrast, signal-to-variability ratio (SVR), and sharpness. 35 GHz and 95 GHz performance categories are graphed side-by-side for the six weather conditions of clear, medium snow, light fog, very light rain, light rain, and medium rain. These performance values are for runway and grass at 2 km range. The heights of the bars, or relative performance factors, have been normalized to the maximum value measured by these two sensors. No sharpness values could be extracted from the 95 GHz data for the higher rain rates.

The relative performance advantage of this 35 GHz sensor over the 95 GHz sensor in clear weather is due to the design parameters of these particular radars and not due to any fundamental limitations of the 95 GHz frequency band for runway imaging. The degradation in performance with increasing precipitation for each MMW sensor, relative to its own clear weather performance, does reflect the greater impact of precipitation at 95 GHz.

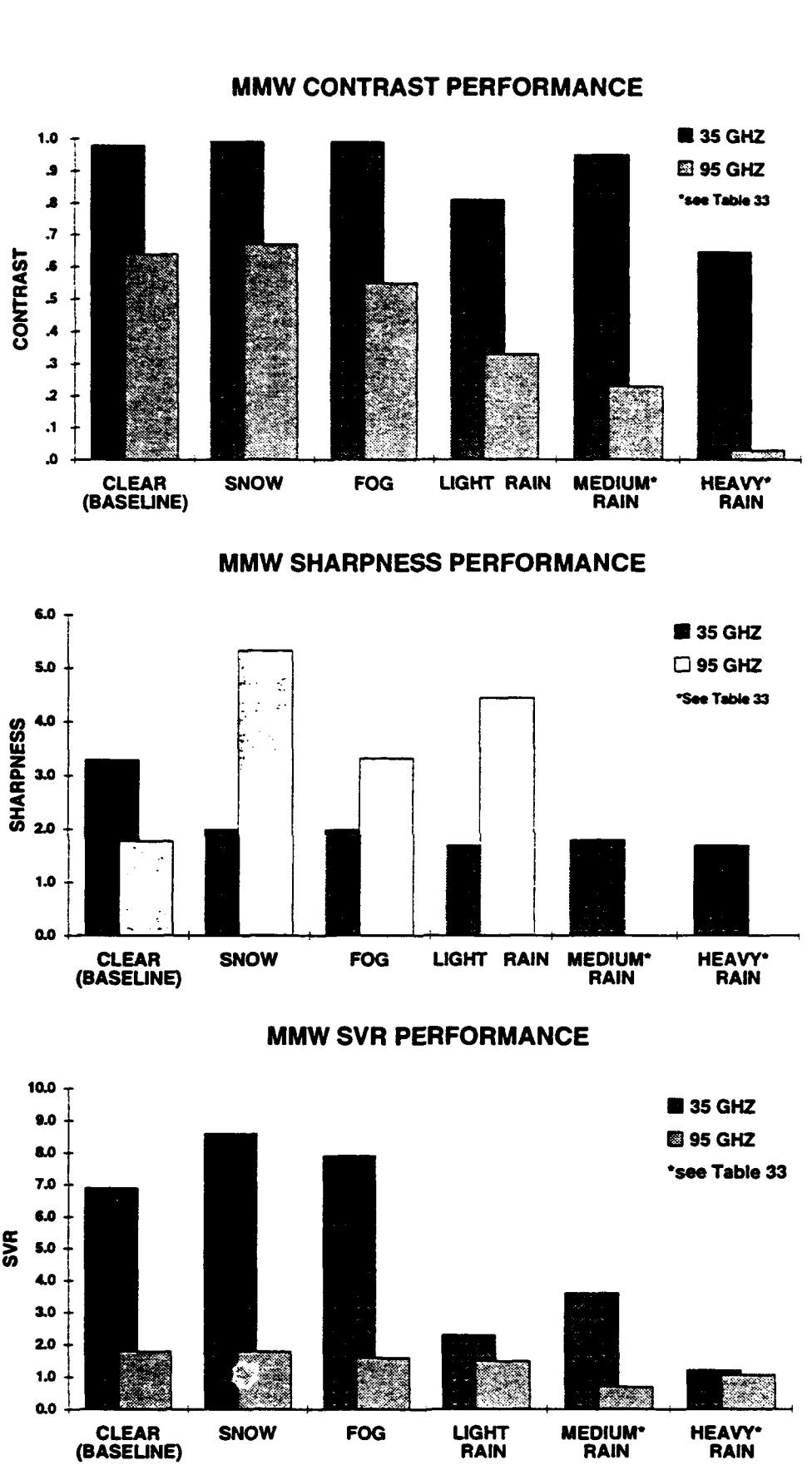

Figure 67. MMW sensor performance at 2 km.

The numeric values for the MMW performance parameters plotted above are listed in Table 33. Contrast is probably the performance criteria that contributes most to runway detection by a MMW synthetic vision sensor. Fortunately, contrast for the 35 GHz radar was high and remained acceptably high (> -0.6) in a rain of 12.9 mm/hr. Contrast for the 95 GHz sensor was acceptable in clear weather but declined more at higher rain rates. SVR at 35 GHz was acceptably high (> 5) in clear, snow, and fog, but it dropped dramatically in rain. This would indicate that, although the 35 GHz radar image became "noisy" in rain, the contrast remained acceptable. SVR for the 95 GHz radar was lower, even in clear weather, suggesting that this particular 95 GHz radar was more "noisy" than the 35 GHz radar. 95 GHz SVR also declined in rain conditions, but less so than the 35 GHz radar values. The sharpness values are more difficult to relate to sensor band and meteorological condition, but the 95 GHz radar had higher sharpness. The inconsistencies in reported sharpness suggest that the method used to measure sharpness does not provide a reliable performance criteria.

Table 33. MMW Performance Summary at 2 KM Range

Meteorological Condition	Freq (GHz)	Contrast	SVR	Sharpness (deg^{-1})
Clear (Baseline)	35	high (-0.98)	high (6.9)	high (3.3)
	95	high (-0.64)	medium (1.8)	medium (1.78)
Snow	35	high (-0.99)	high (8.6)	medium (2.0)
	95	medium (-0.67)	medium (1.8)	high (5.33)
Fog	35	high (-0.99)	high (7.9)	medium (2.0)
	95	medium (-0.55)	medium (1.6)	high (3.33)
Rain (1.2 mm/hr)	35	high (-0.81)	medium (2.3)	medium (1.7)
	95	low (-0.33)	medium (1.5)	high (4.44)
Rain (5.3 mm/hr)	35	high (-0.95)	medium (3.62)	medium (1.8)
Rain (8.8 mm/hr)	95	low (-0.23)	low (0.7)	not measurable
Rain (12.9 mm/hr)	35	medium (-0.65)	low (1.22)	medium (1.7)
Rain (20.0 mm/hr)	95	low (-0.03)	low (1.08)	not measurable

8.1.1 TEST DATA MATRIX

The tower test data matrix for the Honeywell 35 GHz (HI2) and Norden 95 GHz (NS1) radar sensors is presented in Figure 68a, grouped by observed weather conditions, and in Figure 68b, sorted by long path visibility (LPV) in feet. Although there were several runs with weather conditions of fog, the visibility was usually greater than 1,700 feet (520 m). Conditions of low-visibility fog did not occur at the tower during the sensor test periods. Note that the numbers of measurement runs listed are those that were processed by GTRI from among a larger set that were collected. Table 34 presents a more detailed MMW data matrix for all six sensor configurations tested. The total numbers of runs collected and processed for each sensor configuration are shown, along with the numbers of processed runs sorted by meteorological conditions.

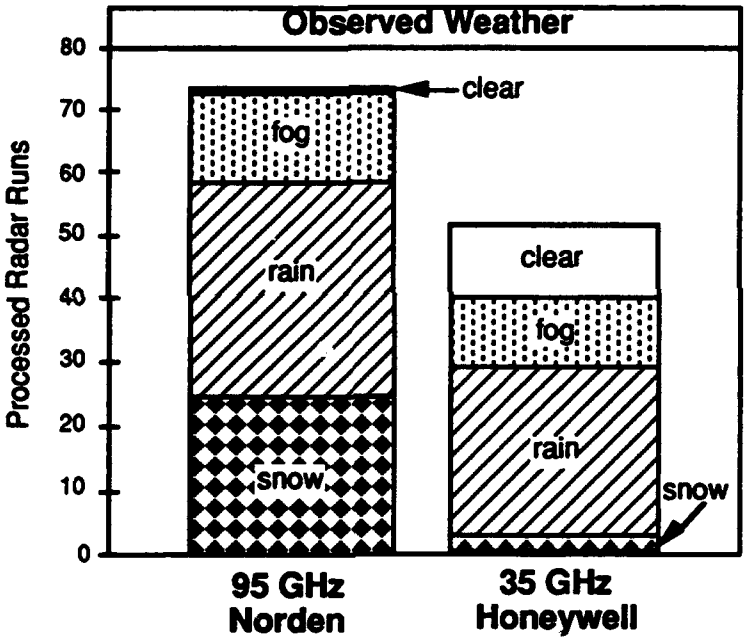

Figure 68a. MMW test data matrix sorted by observed weather.

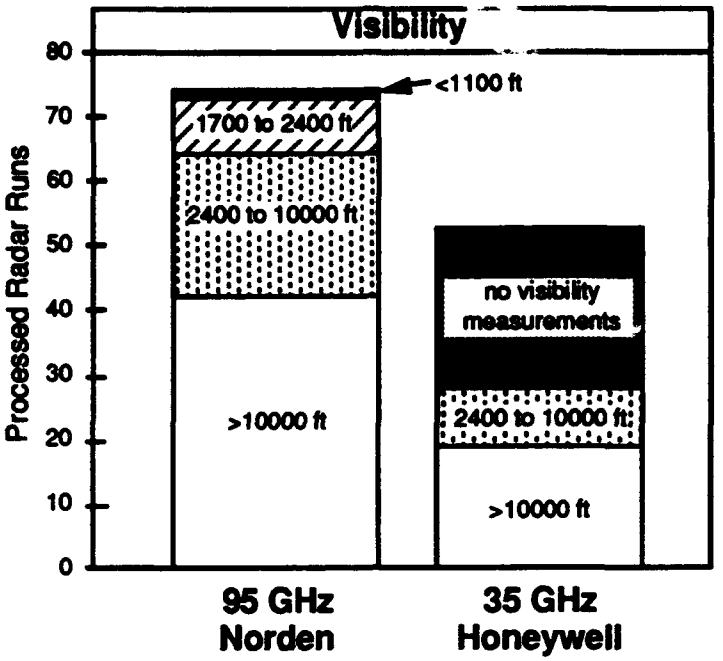

Figure 68b. MMW test data matrix sorted by long-path visibility.

Table 34. MMW Radar Sensor Data Matarix

MMW Sensor Description	Measurements Performed	Total Runs		Number of Runs Processed (by Meteorological Conditions)				
		Collected	Processed	Clear	Snow	Fog	Rain	F&R
Lear development system	sample runs	3	3	3	0	0	0	0
Lear flight system	acceptance test	6	3	3	0	0	0	0
Norden TALONS	full matrix	165	76	4	25	14	33	0
Honeywell development system	sample runs	11	6	6	0	0	0	0
Honeywell flight system	full matrix	46	35	5	3	3	20	4
Honeywell spare unit	sample runs	25	13	2	0	9	2	0

8.1.2 BASELINE PERFORMANCE

Analysis of the MMW sensors in clear weather established a performance baseline against which the effects of weather could be determined. Baseline measurements also allow comparisons of perceived image quality to the operating parameters of these particular radar sensors. Figure 69 shows how the radar resolution cell sizes at 2 km range compare with the width of the runway at the tower test scene. The radar resolution cell dimensions, downrange and cross-range, are defined by the range and azimuth resolution of the radar sensor, respectively. The fine grid overlay represents the sampling resolution of the data acquisition system (DAS), which in every case exceeded the sensor resolution. DAS oversampling gave a constant data set resolution independent of the MMW sensor under test and provided additional sample points for averaging.

Downrange profiles of equivalent received power are a good method of rating a MMW radar sensor's ability to discriminate the runway from the bordering grass areas. As described in Section 4.1.2, a series of patch areas were defined along the runway and grass for data processing purposes. A downrange power profile plot presents the equivalent received power values from the patches spaced along the grass and runway between 1,700 m and 3,300 m range. Figure 70a is a downrange power profile for the 35 GHz radar, and Figure 70b is the same profile for the Norden 95 GHz radar sensor. Curves have been fit to the points from the grass patches (plus signs) and the runway patches (solid squares). The difference in received power between the grass patches and the runway patches provided by the radar sensor is converted by the signal processor into image contrast. This power difference decreases with range and in weather, reducing the resulting image contrast and the detectability of the runway.

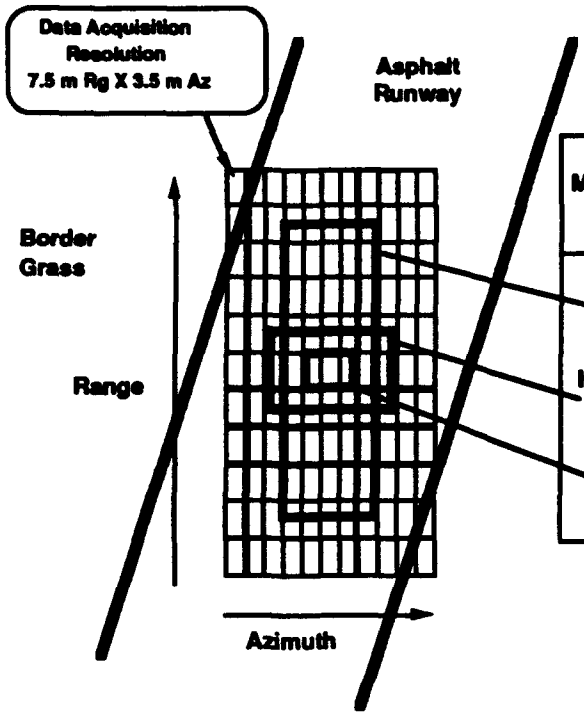

MMW Radar Sensor	Pulsewidth / Antenna Azimuth	Resolution Range / Cross	Sharp-ness
Norden 95 GHz	400 ns / 0.7°	60 m / 24 m	1.8
Honeywell 35 GHz	120 ns / 0.8°	18 m / 28 m	3.3
Lear 94 GHz	FMCW / 0.35°	6.6 m / 12 m	2.5

Figure 69. MMW sensor resolution of runway at 2 km range.

Received power from the grass patches declines with increasing range, as predicted by the radar range equation. Received power from the runway patches increases with range for the 35 GHz sensor; this does not appear to correlate with the range equation. The RCS of the runway pavement is so small that the received power from runway backscatter at 2 km range is near or below the radar receiver's thermal noise power level. Instead of measuring the runway RCS, the runway patch power values may simply be indicating the receiver noise power "floor." At ranges beyond 2,500 m, the radar antenna has insufficient azimuth resolution to completely isolate the runway returns from the bordering grass area returns. The resulting "contamination" of the runway patch returns from the adjacent grass clutter areas causes the received power values from the runway patches to increase with range. A SV-aided pilot will detect a runway at long range from a polygon area within the SV image, rather than from individual dark pixels. The clutter contamination effect on runway patches shown in these power profile plots is representative of the azimuth resolution limitations in an operational SV radar sensor.

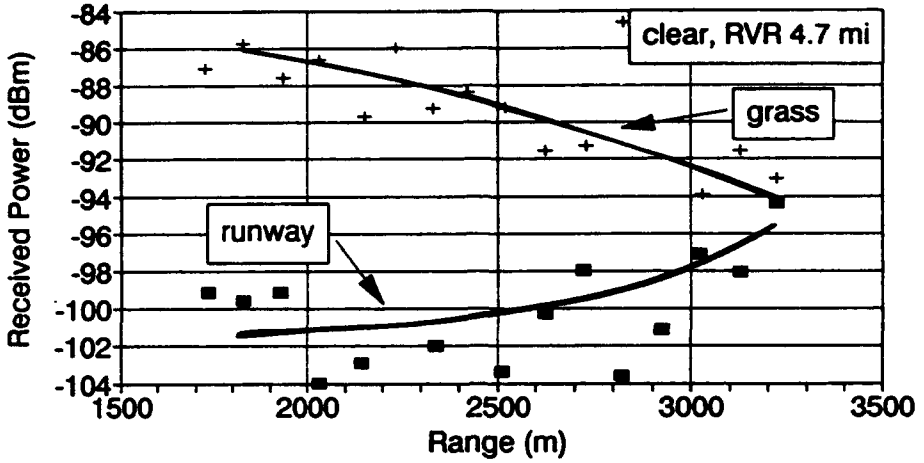

Figure 70a. 35 GHz downrange power profile.

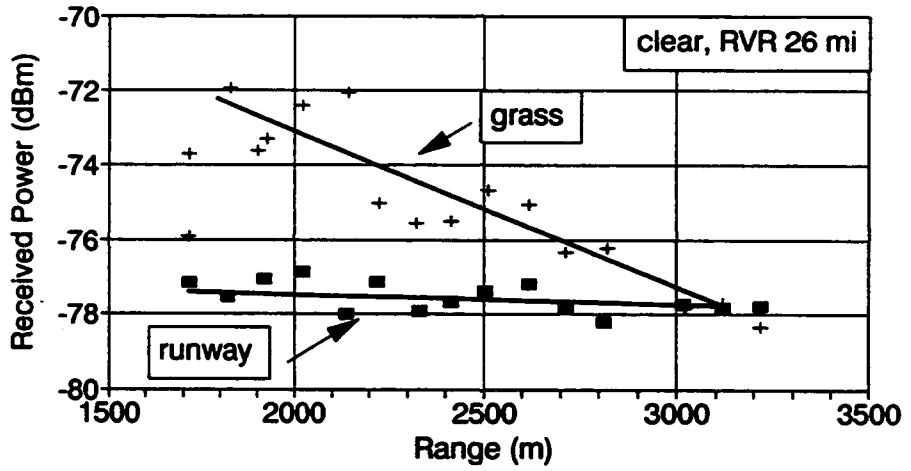

Figure 70b. 95 GHz downrange power profile.

Received power values were converted into contrast during MMW data analysis, as described in Section 7.2 and Appendix A. Contrast is the runway value minus the grass value, divided by the grass value. Since the grass return power value was nearly always greater than the runway value, the resulting contrast was a negative number ranging from -1.0 (ideal) to 0 (none). Clear weather contrast over range is plotted in Figure 71 for the Honeywell 35 GHz and Norden 95 GHz radar sensors. A supplementary vertical axis is shown on the right, so that received power differences can be related to contrast values. A difference of 3 dB is a contrast of -0.5, 6 dB is a contrast of -0.75, 10 dB equals a contrast of -0.9, and 20 dB gives a contrast of -0.99. A contrast of -0.6 (about 4 dB) was established as a reference point for minimum detectable contrast, or MMW extinction. This is not an absolute limit; but it is merely a reference contrast value established for comparative analysis. Enhanced signal processing can improve on this reference contrast value.

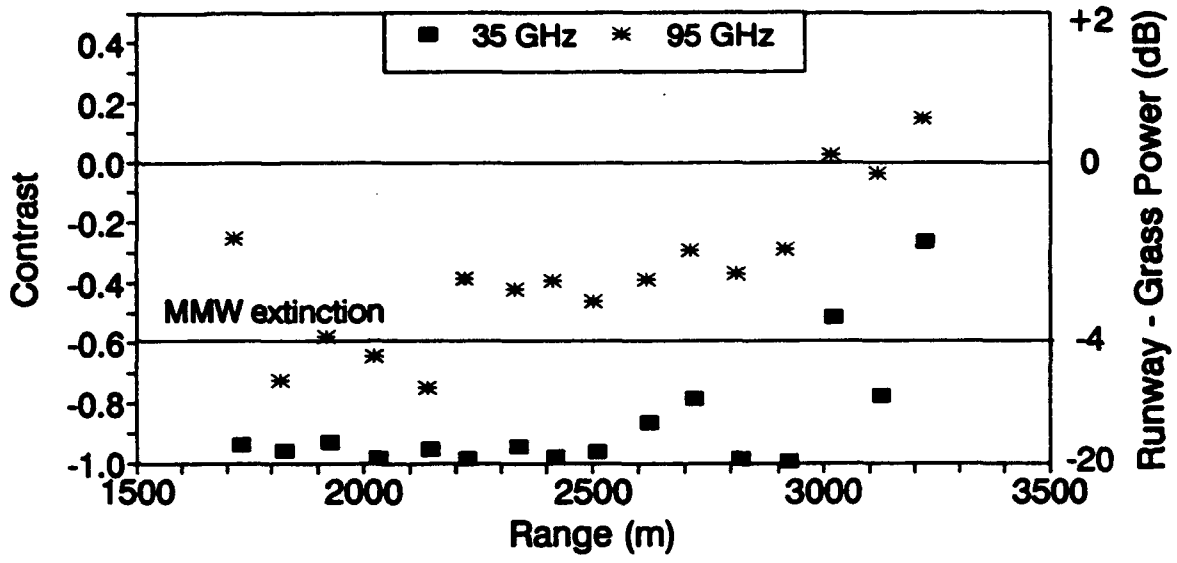

Figure 71. 35 GHz and 95 GHz contrast in clear weather.

Cross-runway profile plots were developed from the data points within three profile patches, as described in Section 4.1.2. Cross-runway patches were about 40 data resolution cells in azimuth (4°) and 7 data resolution cells in range (53 m). The seven range values were averaged for each azimuth and plotted by azimuth step. Figures 72a and 72b are cross-runway profile plots at 2.5 km for the Honeywell 35 GHz and Norden 95 GHz radar sensors, respectively. The actual runway width at that range is drawn for reference as a rectangular box. The profiles reveal that, for the 35 GHz sensor, only three azimuth samples in the middle of the runway have received power values equal to the post-integration noise floor of -104 dBm. The remaining points across the runway width have some contamination from the higher-RCS grass clutter. The transition between the dark runway and the brighter grass areas in the resulting image is not immediate and has some finite azimuth width. That transition is expressed in analysis as the sharpness criteria.

Figures 73a and 73b are B-scope images in clear weather from the Honeywell 35 GHz and Norden 95 GHz radars, respectively. The runway and taxiway are visible over a much greater range in the 35 GHz image. The rolloff in contrast of the 95 GHz image with increasing range is due in part to the narrow elevation beamwidth of the Norden antenna.

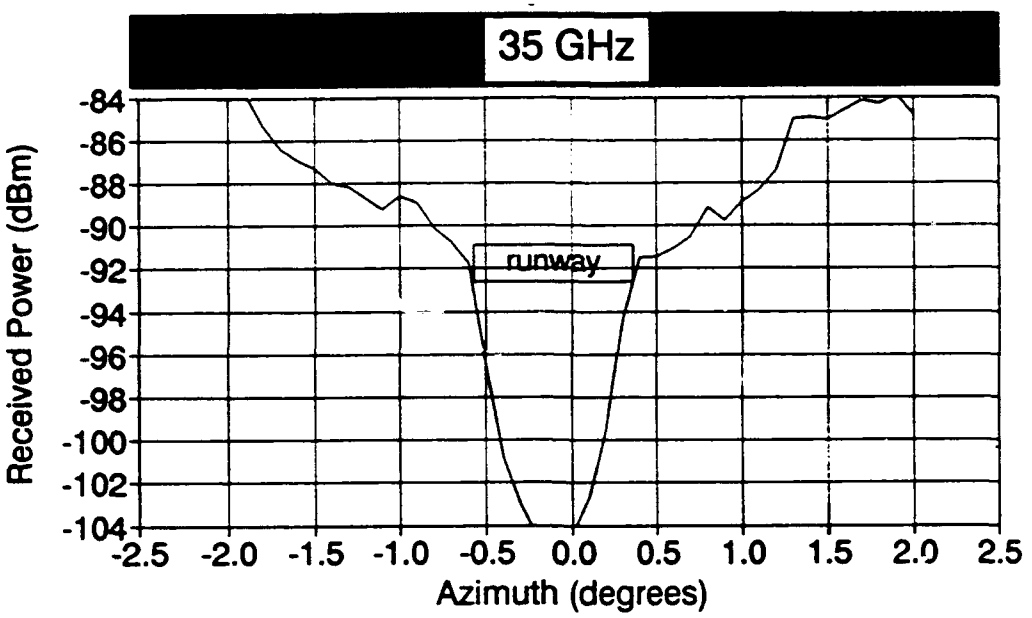

Figure 72a. 35 GHz cross-range profile at 2 km in clear weather.

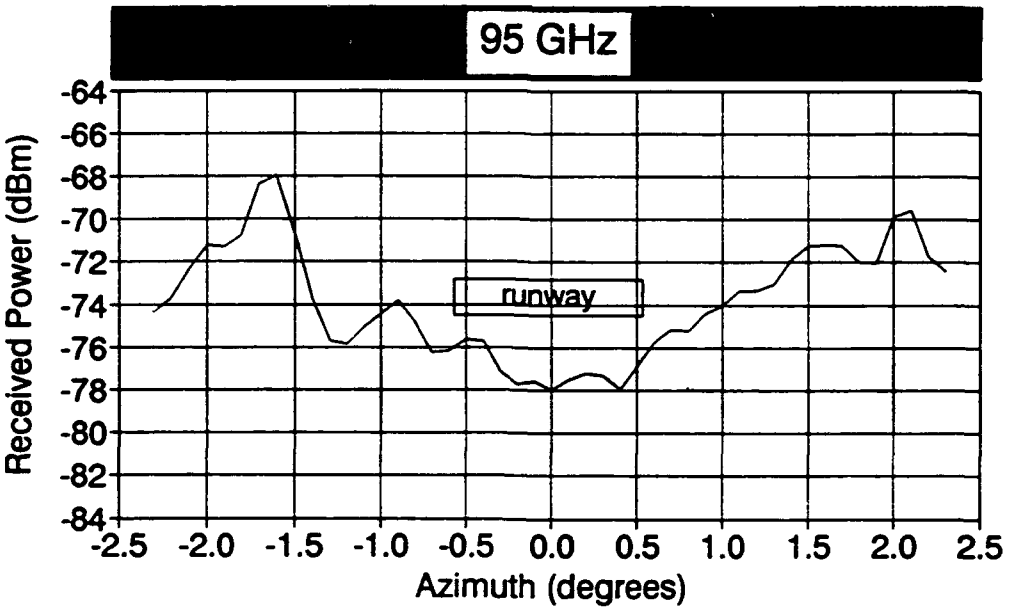

Figure 72b. 95 GHz cross-range profile at 2 km in clear weather.

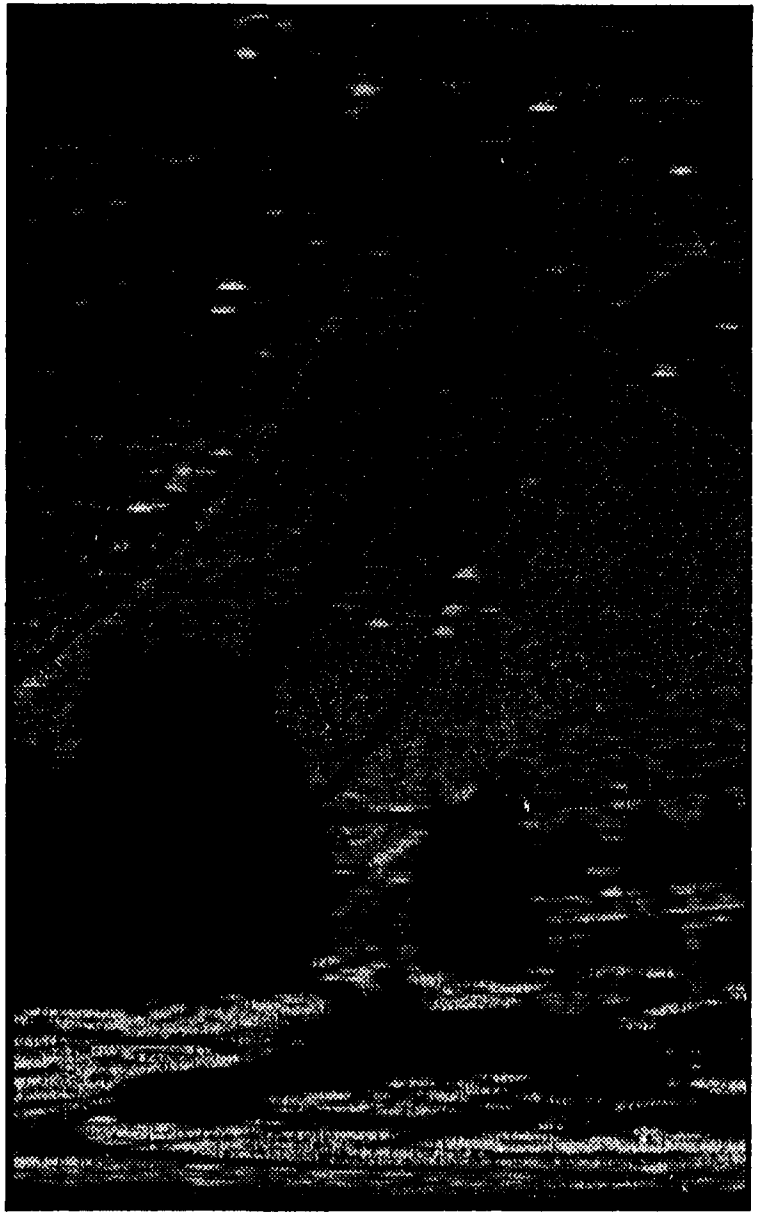

Figure 73a. 35 GHz B-scope image in clear weather.

Figure 73b. 95 GHz B-scope image in clear weather.

8.1.3 PERFORMANCE IN FOG, SNOW, AND RAIN

Performance of the Honeywell 35 GHz and Norden 95 GHz radar sensors in fog, snow, and rain is presented here using the performance curves introduced in the previous section. Figures 74a through 74f present a sequence of downrange received power profiles for the 35 GHz sensor in clear, fog, snow, and rain of three different rates. Figures 75a through 75f present a similar sequence of downrange power profiles for the 95 GHz sensor. Precipitation increases the received power from both the grass and runway patches, due to volumetric backscatter from the airborne water. Atmospheric attenuation from precipitation increases the downward slope of the received power from grass patches, as the path length, hence the cumulative attenuation, increases with range. These two effects of precipitation collapse the grass and runway power profiles together, with a corresponding reduction of image contrast.

The loss of contrast in rain is shown for the 35 GHz radar sensor in Figure 76. For a MMW extinction contrast of -0.6, the MMW extinction ranges are indicated on the horizontal axis for three rain rates measured. The large dispersion in the contrast values plotted for 12.9 mm/hr is due to the irregularities present in rainfall at higher rates. For the 95 GHz radar sensor, the extinction range was less than 1,700 m for comparable rain rates. MMW extinction ranges for different weather conditions are summarized in Table 35.

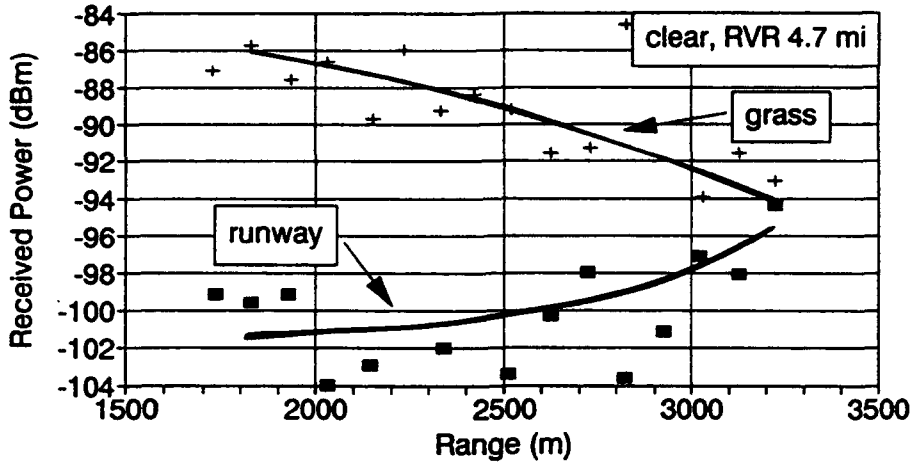

(a)

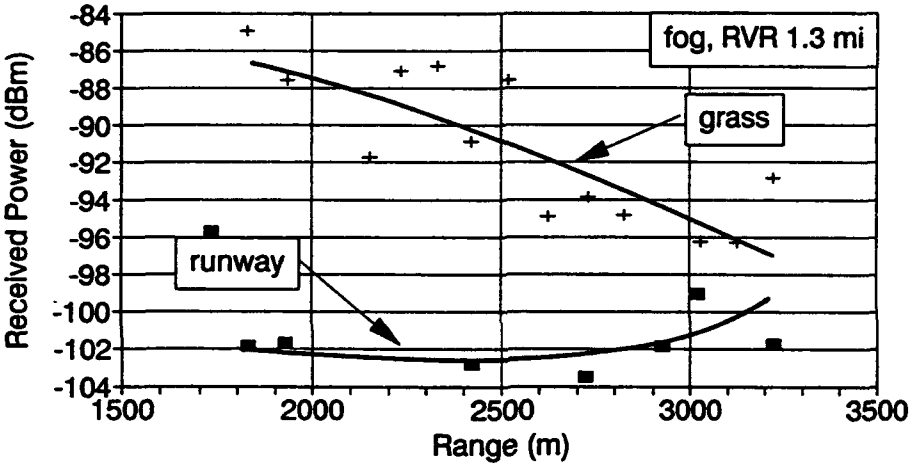

(b)

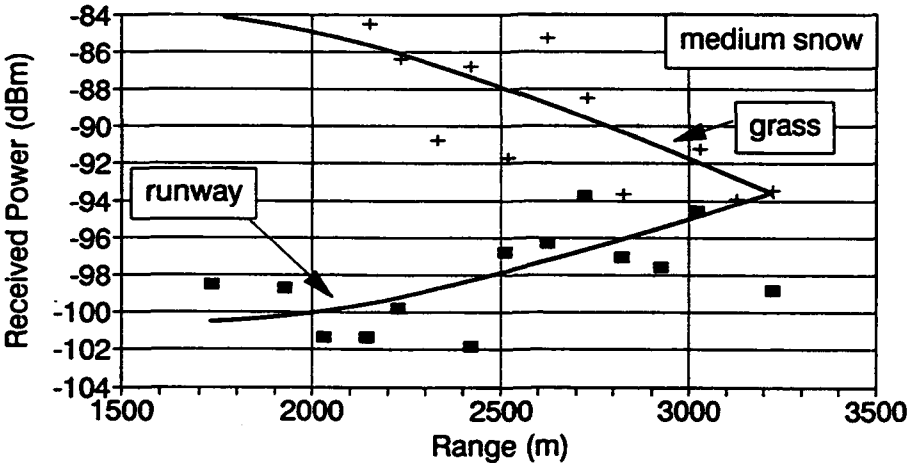

(c)

Figure 74 a-c. 35 GHz downrange power profiles in clear weather, fog and snow.

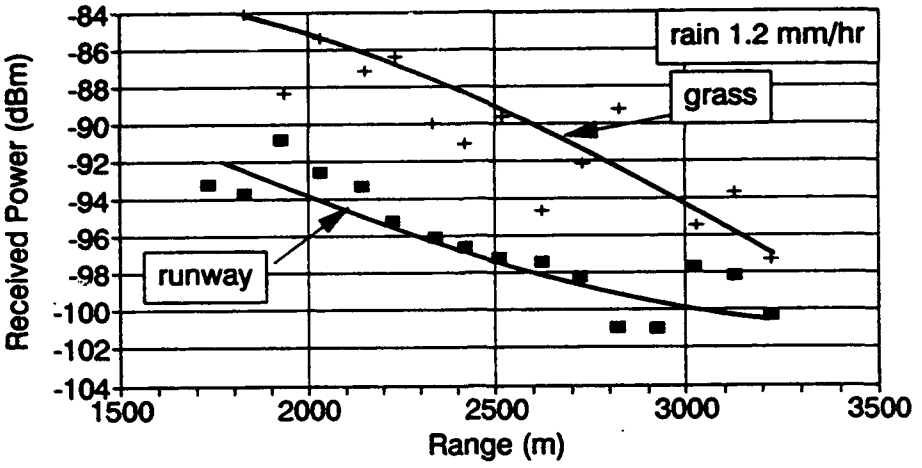

(d)

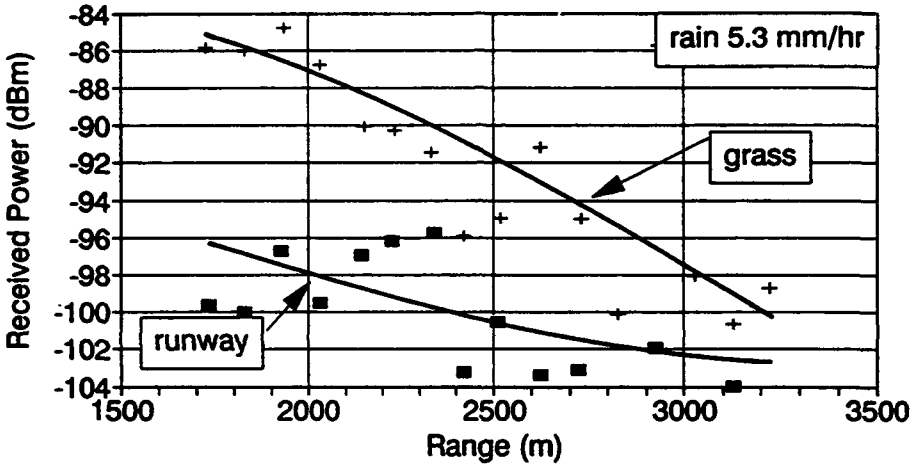

(e)

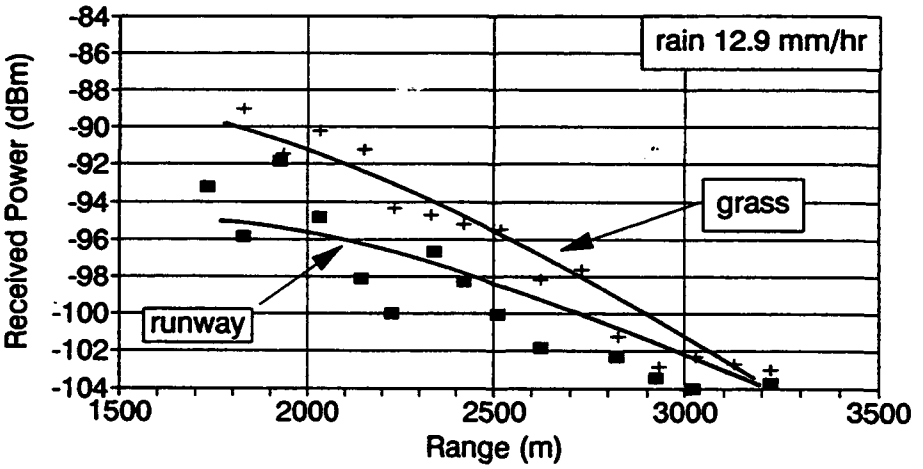

(f)

Figure 74 d-f. 35 GHz downrange power profiles at varying rain rates.

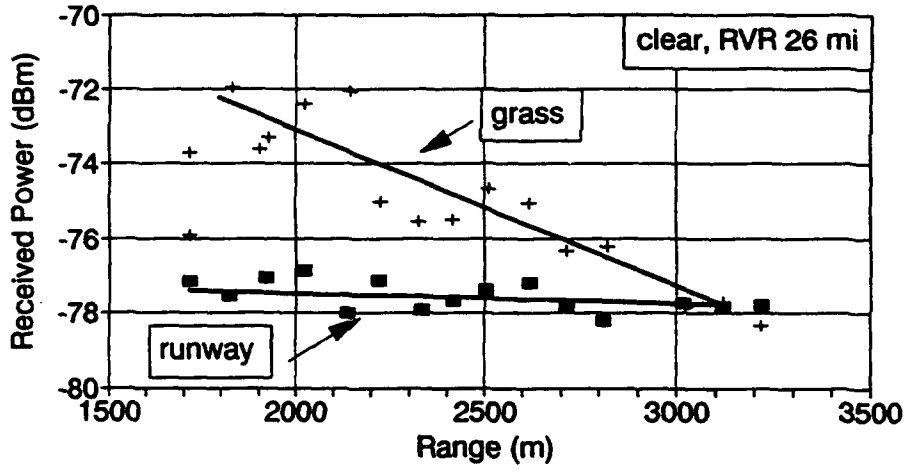

(a)

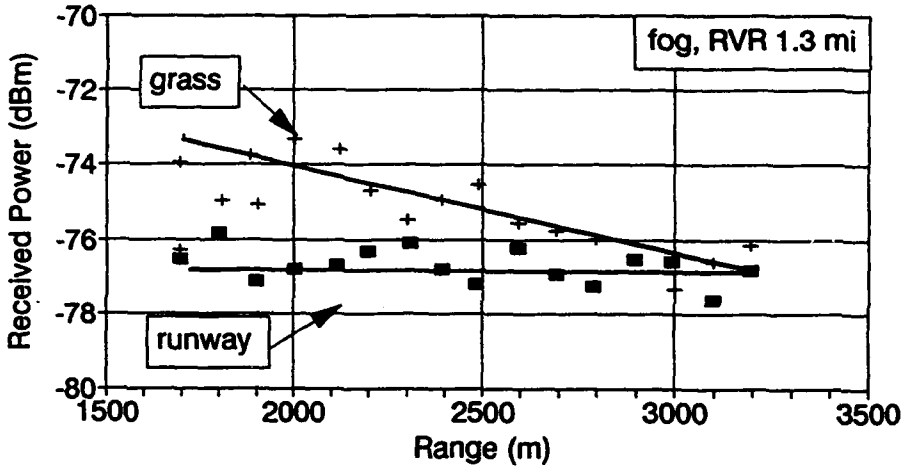

(b)

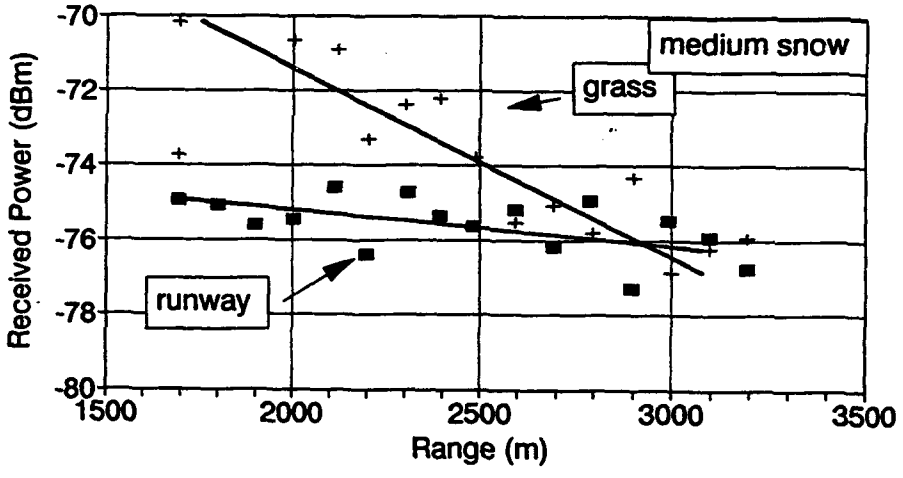

(c)

Figure 75 a-c. 95 GHz downrange power profiles in clear weather, fog and snow.

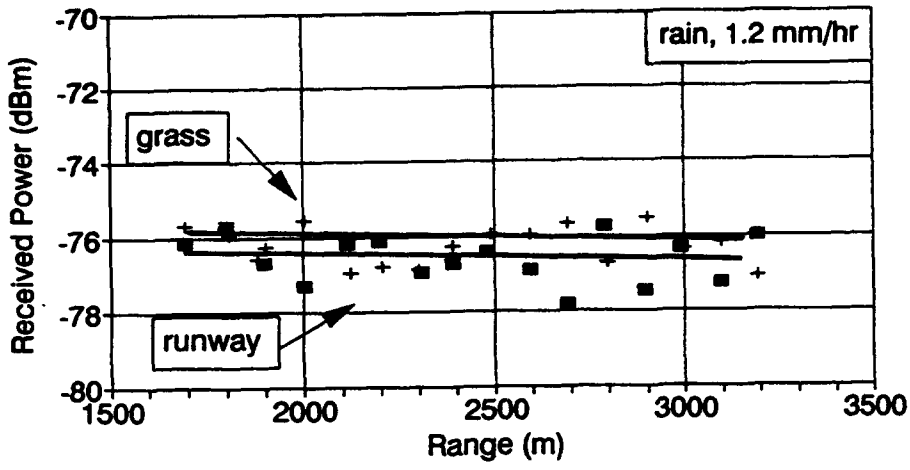

(d)

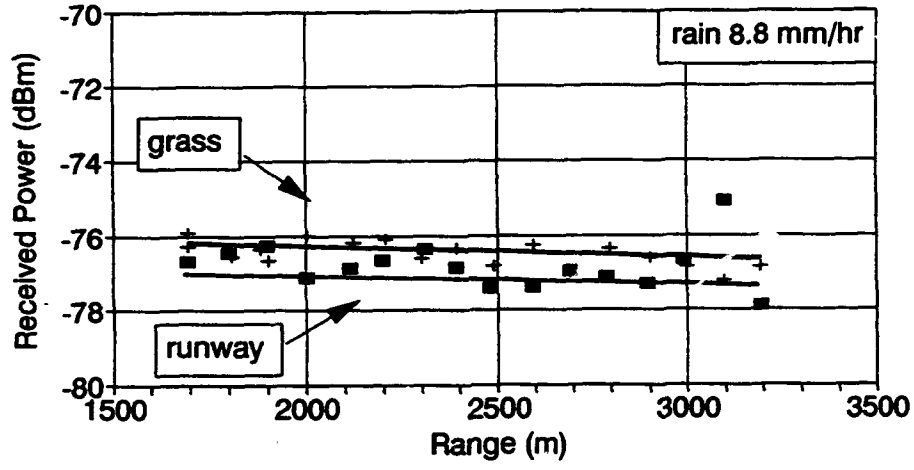

(e)

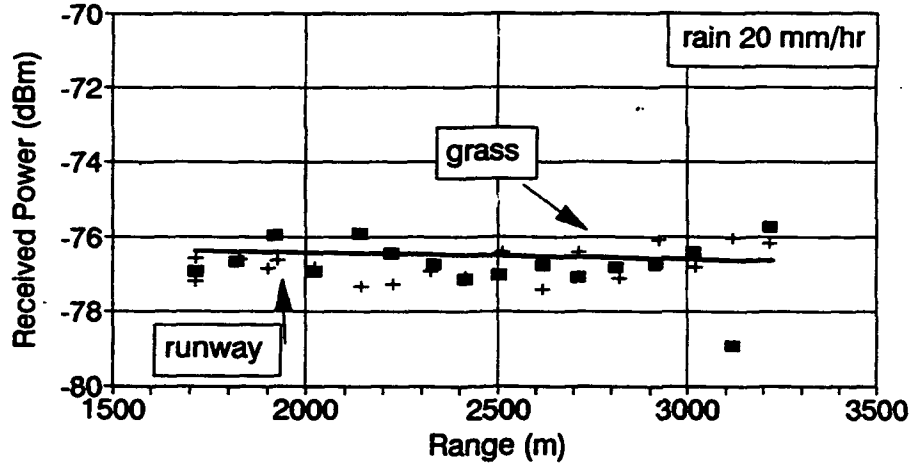

(f)

Figure 75 d-f. 95 GHz downrange power profiles at ing rain rates.

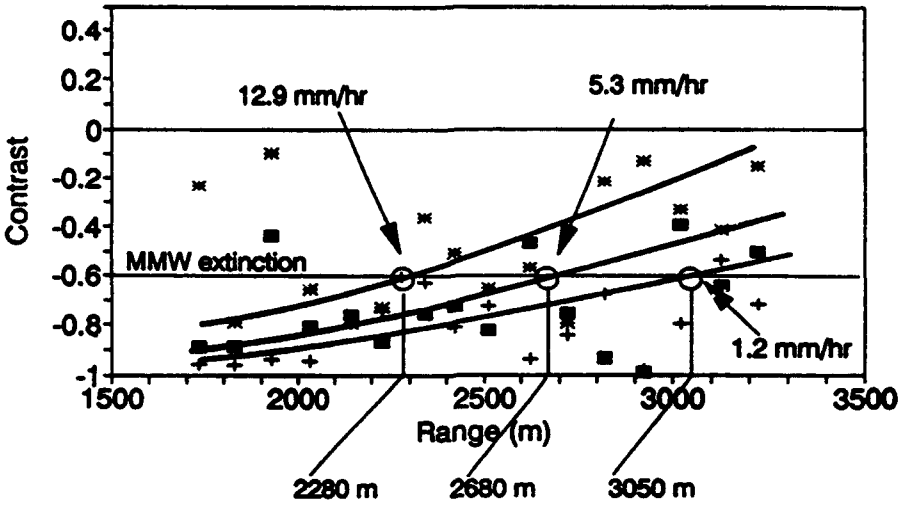

Figure 76. Loss of contrast in rain for the 35 GHz radar.

Table 35. MMW Extinction Ranges

Radar Sensor	MMW Extinction Range (meters) (< .6 contrast)					
	Clear	Snow	Fog	Very Light Rain	Light Rain	Medium Rain
Honeywell 35 GHz	3100	3100	3200	3000	3000	2400
Norden 95 GHz	2100	2150		<1700	<1700	<1700

Cross-range profiles can reveal the same loss of contrast in precipitation. Figures 77a through 77f present a sequence of 35 GHz cross-range profiles at 2 km in weather. The 95 GHz profiles in weather are included in Appendix E.

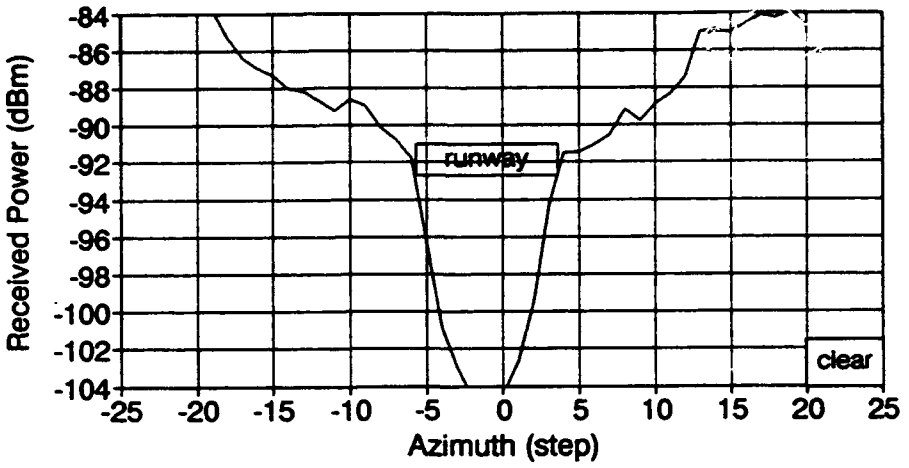

(a)

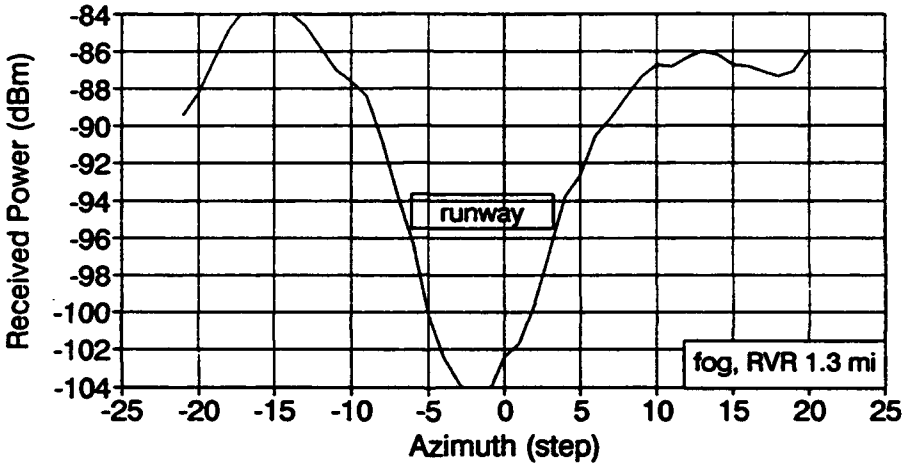

(b)

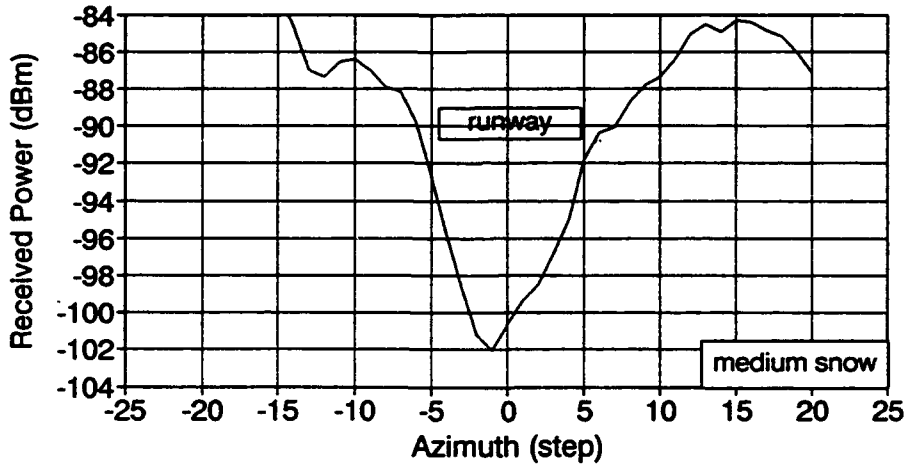

(c)

Figure 77a-c. 35 GHz cross-range profiles in clear weather, fog and rain.

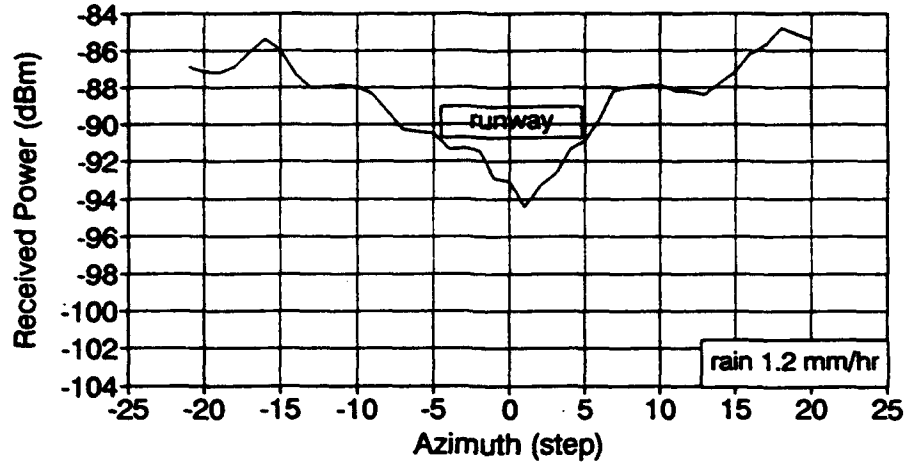

(d)

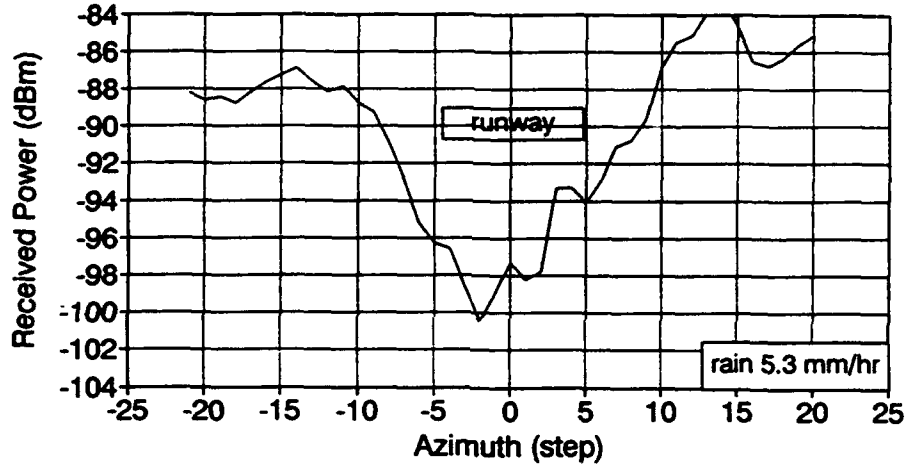

(e)

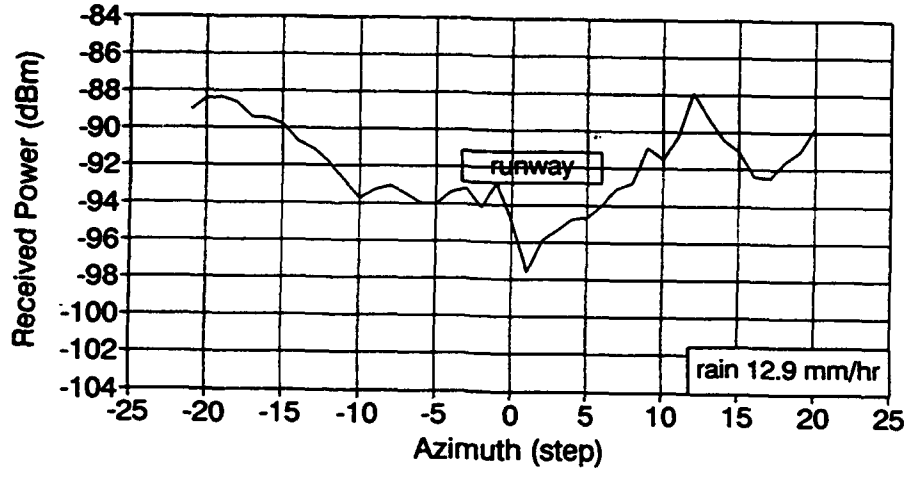

(f)

Figure 77d-f. 35 GHz cross-range profiles at varying rain rates.

8.1.4 PHENOMENOLOGY

The radar phenomenology criteria developed from the MMW tower test data are normalized RCS, attenuation, and volumetric backscatter, as described in Section 3.1.2. Figure 78 compares the normalized RCS values of the grass measured at 2 km range for four different radar configurations tested. The grass RCS is greater at 35 GHz and 95 GHz for linear transmit/receive polarization than for circular polarization, indicating the grass clutter is predominantly a single bounce scatterer. RCS is 10 dB higher at 95 GHz than at 35 GHz for linear polarization in the summer. RCS is greater at both frequencies in summer months over winter months, due to the higher moisture content of the grass.

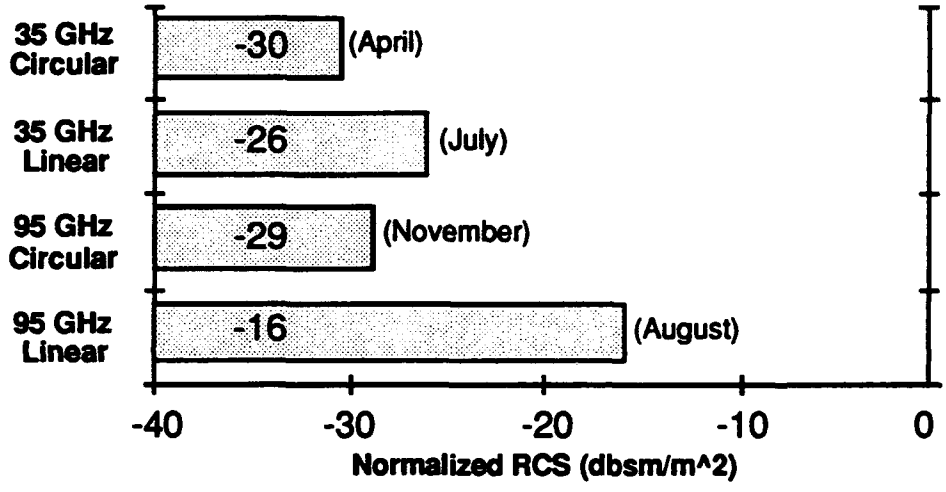

Figure 78. Measured normalized RCS for grass clutter at tower.

Figure 79 compares the measured atmospheric attenuation at 35 GHz and 95 GHz for rain rates from 1 to 22 mm/hr. Signal-to-noise ratio limitations of the 95 GHz sensor prevented attenuation measurements above 5 dB/km (8 mm/hr), so the curve was extended using rain attenuation values calculated using the drop size distribution model described in Section 8.1.5.

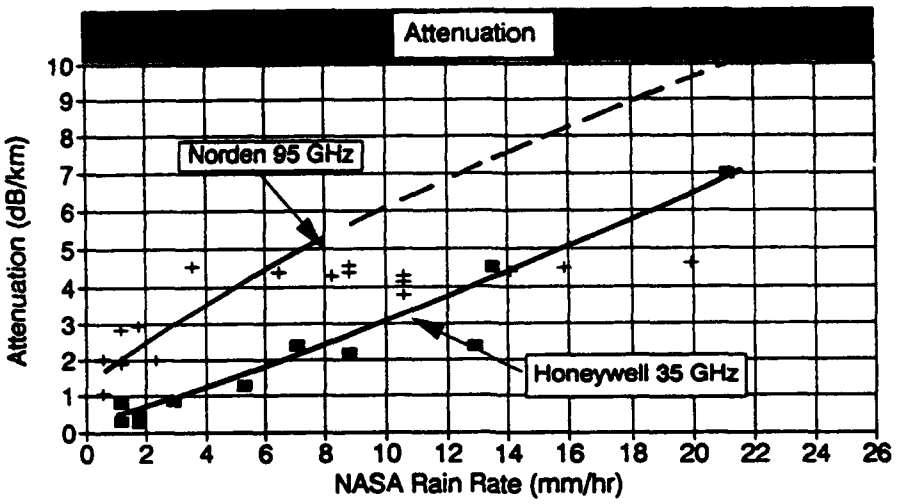

Figure 79. Measured atmospheric attenuation at 35 GHz and 95 GHz for rain.

Figure 80 compares the normalized volumetric backscatter (volumetric RCS) in rain at 35 GHz and 95 GHz. Signal-to-noise ratio limitations of the 95 GHz sensor prevented volumetric backscatter measurements for rain rates above 8 mm/hr, so the curve was extended using data from previous MMW measurements.

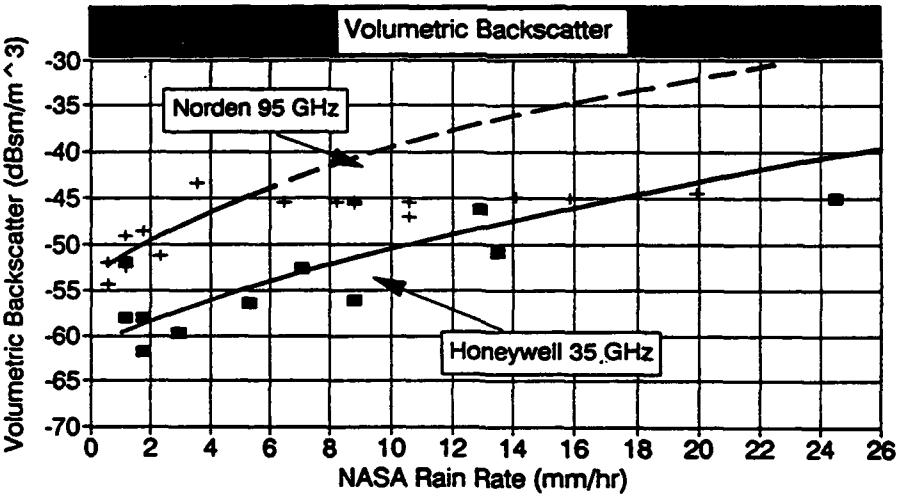

Figure 80. Measured volumetric backscatter at 35 GHz and 95 GHz for rain.

8.1.5 CALCULATED VERSUS MEASURED ATTENUATION

The data set allowed the comparison of rain rates measured with a NRRS rapid response rain gauge and attenuation measured by MMW radars with corresponding quantities calculated from

measured precipitation size spectra. These attenuations have been compared with results found in previous investigations as well as those expected from various modeled rain distributions.

Radar attenuation at 35 and 95 GHz was determined by comparing returns from a trihedral corner reflector during clear weather and rain. Rain rates were calculated at 30 second intervals using the NRRS. Thirteen events were measured at 35 GHz, and eighteen events were measured at 95 GHz. Rain rates were measured from 0.59 to 38.15 mm/hr for the 95 GHz data and from 0.59 to 19.95 mm/hr for the 35 GHz data.

The use of a PMS GBPP-100 rain probe allowed the independent calculation of rain rate and MMW attenuation. Rain rate was calculated using an empirical fit to measured size dependent terminal velocities.[1] Attenuation was calculated using size dependent Mie scattering coefficients and temperature dependent indices of refraction.[2,3] The GBPP-100 data set was slightly smaller than the NRRS data set. A total of eleven 35 GHz and ten 95 GHz runs were analyzed in this manner.

Measured and calculated rain rates and attenuations for the 35 GHz data set agreed within the bounds of expected errors. Plots comparing the measured and calculated rain rates and attenuations are presented in Figures 81 and 82. The comparison of measured and calculated rain rates from the 35 GHz data set presented in Figure 81 show good agreement when rain rates are low and generally less agreement as rain rates increase. It would be expected that the correlation between these two independent measures of rain rate decrease with rain rate, as the rain rate becomes highly variable as intensity increases. A small misregistration in time between the time tags for the two data sets and the small difference in the two sensors locations could both lead to discrepancies between the measurements. The correlation between the two attenuation values is comparable to that found for the rain rates.

The correlation between the measured and calculated rain rates and attenuations for the 95 GHz data set is presented in Figures 83 and 84. There does not appear to be any reasonable correlation between the measured and calculated 95 GHz rain rates. Later analysis indicated that the poor correlation may have been due to a time or date tag difference between the NRRS and the GBPP-100 data sets for the day involved. The attenuations, compared in Figure 84 show the same poor correlation.

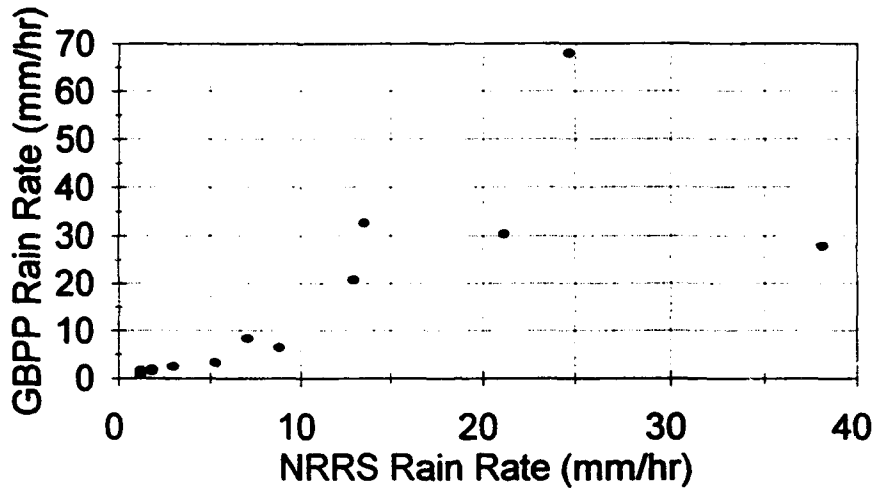

Figure 81. 35 GHz Rain Rate Comparison (Calculated vs. NRRS Rate).

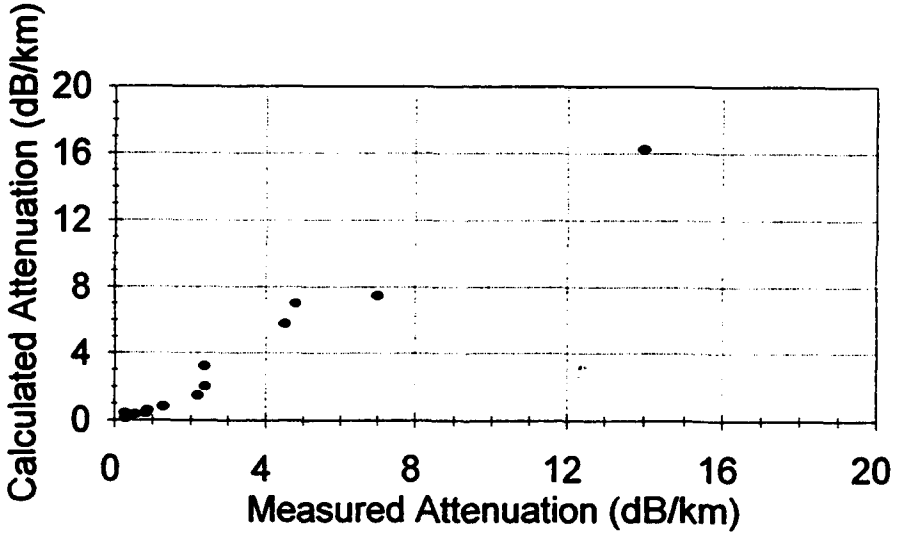

Figure 82. 35 GHz Attenuation Comparison (GBPP-Calculated vs. Measured).

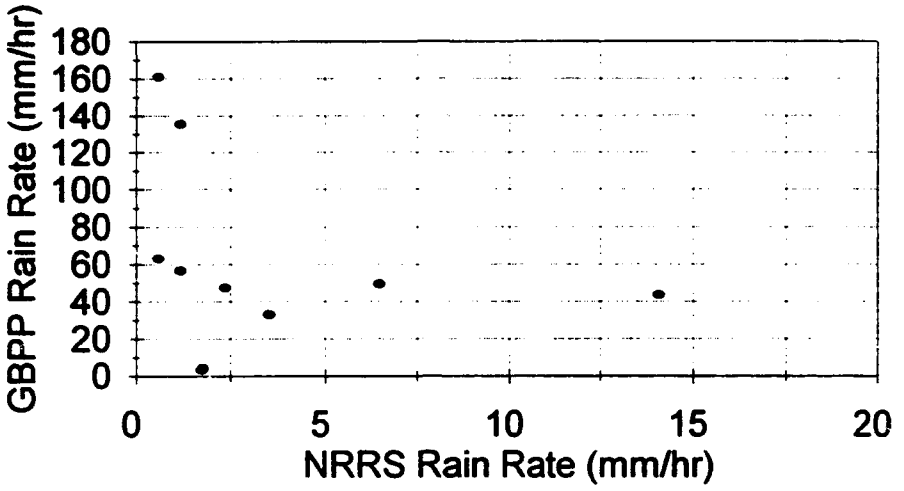

Figure 83. 95 GHz Rain Rate Comparison (Calculated vs. NRRS Rate).

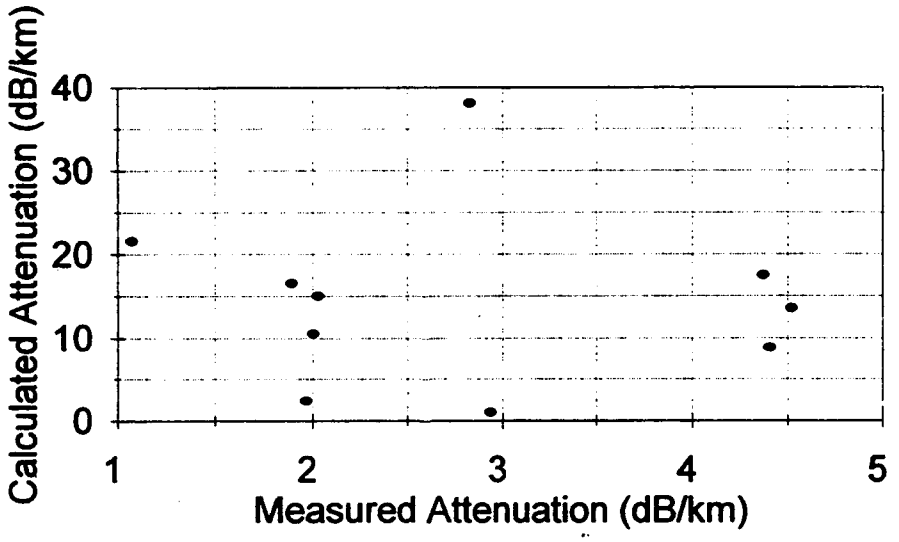

Figure 84. 95 GHz Attenuation Comparison (GBPP-Calculated vs. Measured).

The measured and calculated data showed the same general dependence of attenuation on rain rate, for both the 35 and the 95 GHz data sets, as is illustrated in Figure 85 and 86. Both the measured and the calculated 35 GHz attenuations follow the same dependence on rain rate. The fact that both the calculated and measured dependence of 95 GHz attenuation on rain rate are of a similar form, although the two data sets lie on different portions of the scale, supports the idea that the poor correlation between the two variables was due to a time misregistration of one of variables.

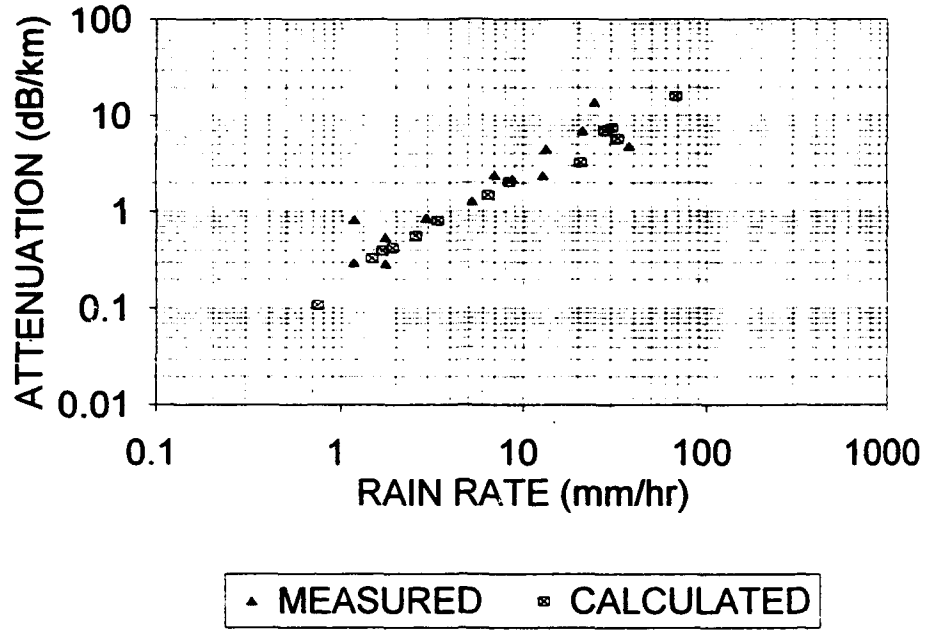

Figure 85. Comparison of measured and calculated attenuation rates from the 35 GHz data set.

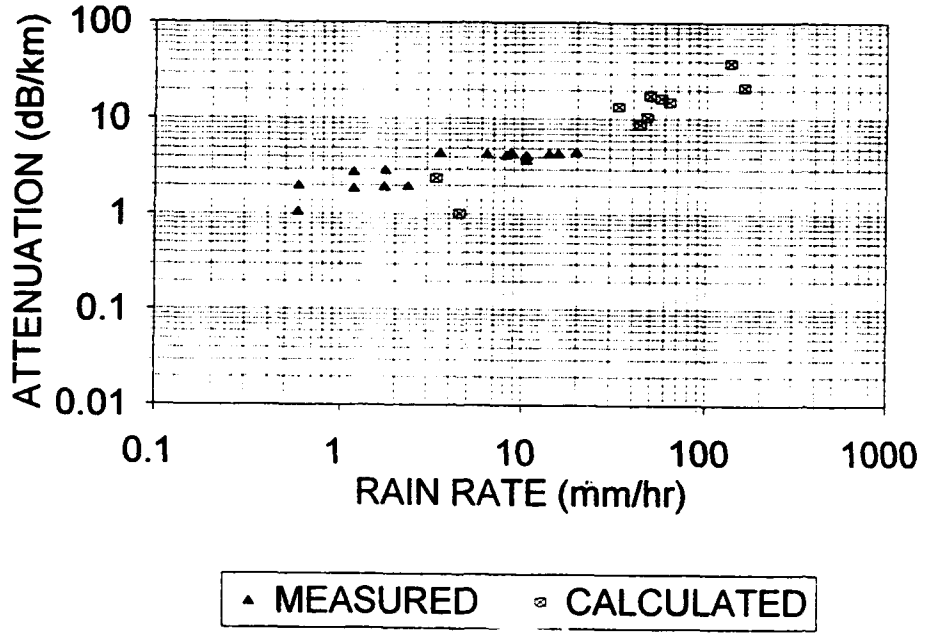

Figure 86. Comparison of measured and calculated attenuation rates from the 95 GHz data set.

This dependence was compared to previously computed coefficients of the well-known relation, $A = aR^b$.[4] In this relation, 'A' represents the attenuation, in dB/km, 'R' represents the rain rate, in mm/hr, and 'a' and 'b' are usually empirically determined coefficients. Reasonable agreement with these models and good correlation between measured and calculated values encourage the

use of the rain probes in estimating rain rate and attenuation values. The values determined for the coefficients 'a' and 'b' for these measurements, for previous measurements, and those appropriate for a Marshall-Palmer raindrop distribution are compared in Table 36.

Table 36. Comparison of Attentuation and Rain Rate Coefficients

	Coefficients			
	'a'		'b'	
Source	35 GHz	95 GHz	35 GHz	95 GHz
Synthetic Vision Project	0.257	1.52	0.978	0.521
GTRI - 1975 [18]	0.273	1.6	0.985	0.64
Marshall-Palmer Model [39]	0.269	1.46	0.999	0.733

8.2 COMPARISON WITH MMW PERFORMANCE MODEL

The MMW imaging radar performance model developed for the WPAFB tower test scenario was exercised for clear weather conditions using parameters of the Honeywell 35 GHz radar sensor (HI2). A model data file equivalent to one antenna sweep was generated in RTC format compatible with the MMW performance analysis software. The modeled radar data were analytically processed in the same manner as a run collected with the 35 GHz radar sensor. Comparisons of measured versus modeled sensor data for this example 35 GHz radar sensor in baseline (clear weather) conditions serves to validate the performance modeling technique.

8.2.1 COMPARISON OF IMAGING

Figure 87 presents a Honeywell 35 GHz radar sensor B-scope image of the WPAFB test scene from measured data (Figure 87a) with an image from the modeled 35 GHz radar data (Figure 87b). As in the other B-scope images presented, the frame dimensions are 30° azimuth horizontal by 3,800 m vertical, and brightness is proportional to the logarithm of received power. The images show that the scene geometry was accurately modeled, with exception of the radar "shadowed" areas in the foreground. The runways, taxiways, fences, and two calibration reflector targets are properly oriented in the image. The "urban clutter" area outside the fence to the upper left is too dense in the modeled image. The grass clutter areas within the fence have the correct relative brightness, but the grass clutter "speckle" caused by large amplitude variability in the measured image is absent in the modeled image. This image texture difference

is attributed to the modeled variability parameter and a Gaussian smoothing algorithm employed. These parameters can be adjusted to better match the measured clutter variability.

8.2.2 COMPARISON OF GRAPHS

Additional graphs were developed from the modeled 35 GHz radar data using the tools available from the sensor performance data base. Example results from clear weather measurements with the Honeywell 35 GHz radar sensor were plotted on the same charts as performance values from the modeled data for comparison of modeled versus measured data. The performance curves are a down range received power profile (Figure 88), a runway-to-grass contrast curve (Figure 89), and a cross-runway received power profile (Figure 90). In Figure 88 the received power from processing patches between 1,700 m and 3,300 m for modeled grass (+) and measured grass (*) compare very closely, indicating a good selection of clutter RCS and radar parameters for the model. The modeled runway patches (dark boxes) have higher received power than the measured runway patches (open boxes), because the Gaussian smoothing of the modeled data increases "contamination" of the runway patches with power from adjacent grass areas. This contamination results in less runway/grass contrast (closer to zero) for the modeled data than measured data at all ranges, as shown in Figure 89. The effects of smoothing of modeled received power values are also noticeable in the example cross-runway profile, Figure 90. The modeled grass clutter power left and right of the runway are much smoother than the measured values, and modeled runway values are higher than the measured. The higher modeled runway values reduce the computed contrast, and narrow the apparent runway width in the B-scope image, Figure 87b. These effects can easily be eliminated from future model runs.

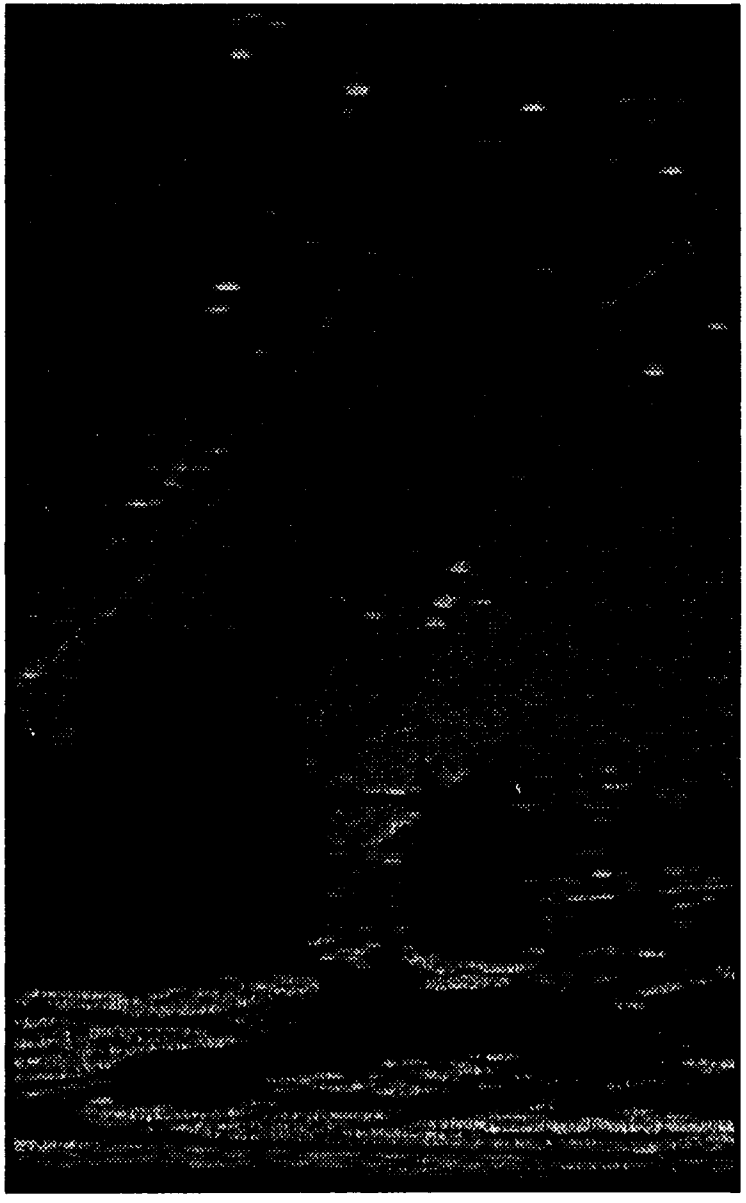

Figure 87a. Measured 35 GHz image in clear weather.

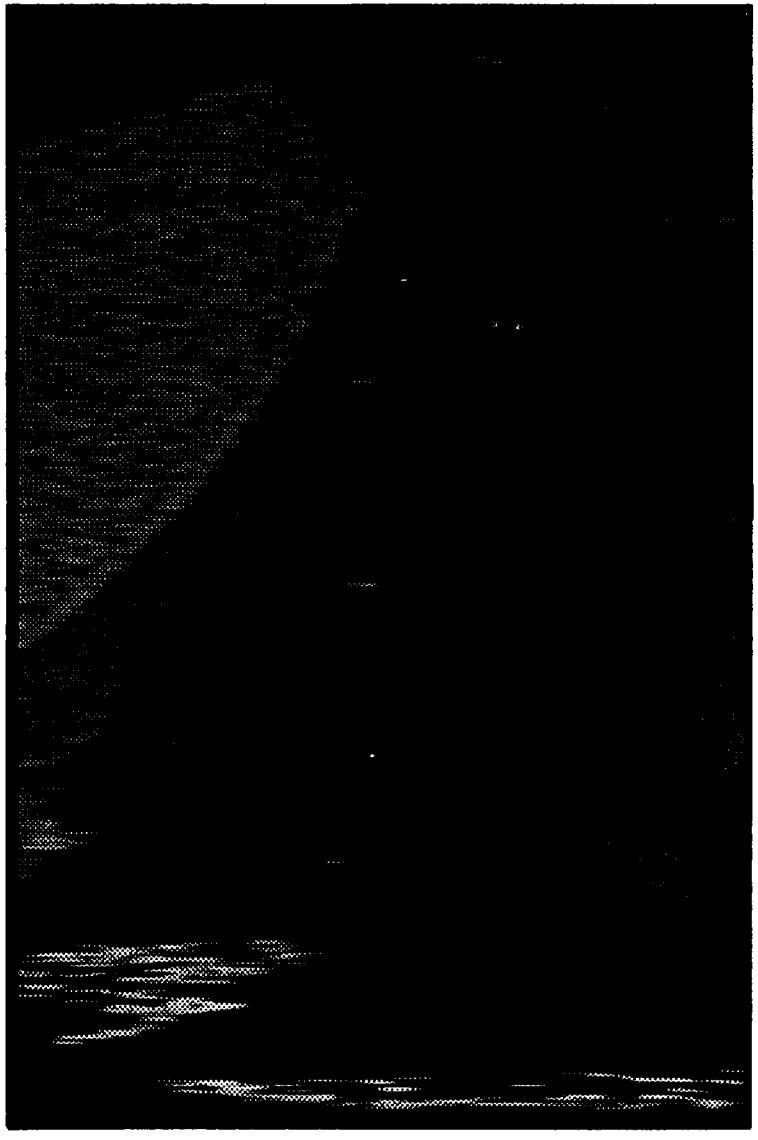

Figure 87b. Modeled 35 GHz image in clear weather.

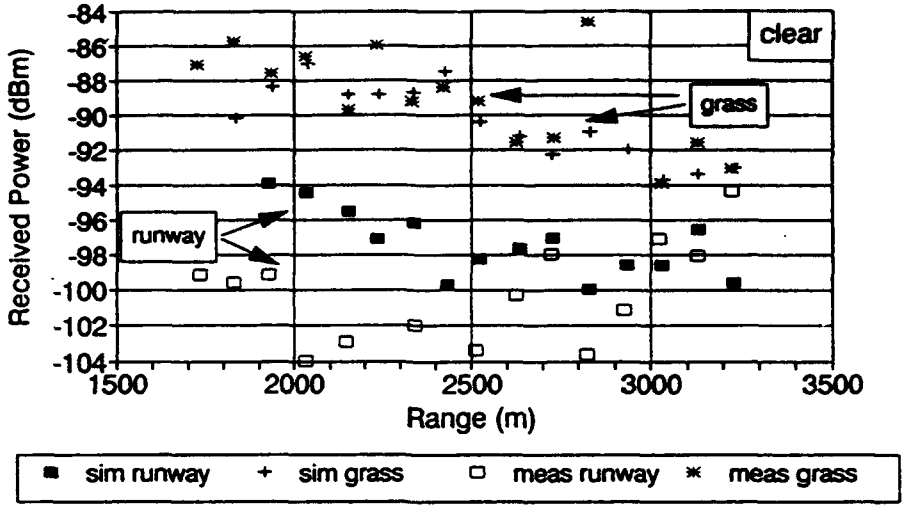

Figure 88. Comparison of measured and modeled down-range power for the 35 GHz system.

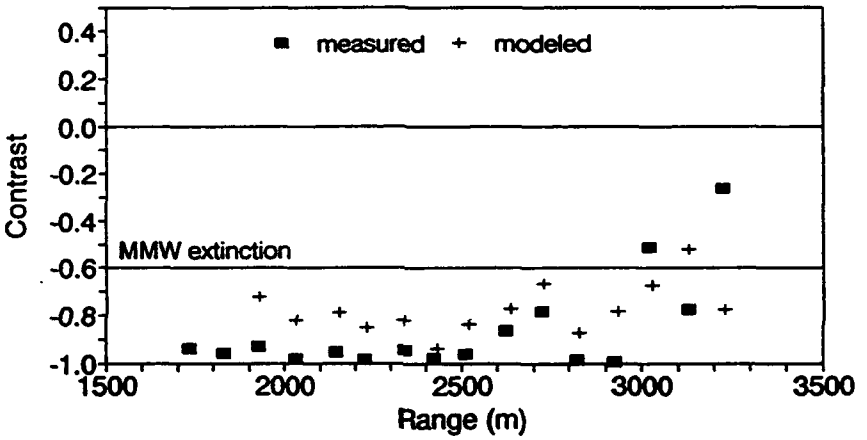

Figure 89. Comparison of measured and modeled contrast for the 35 GHz system.

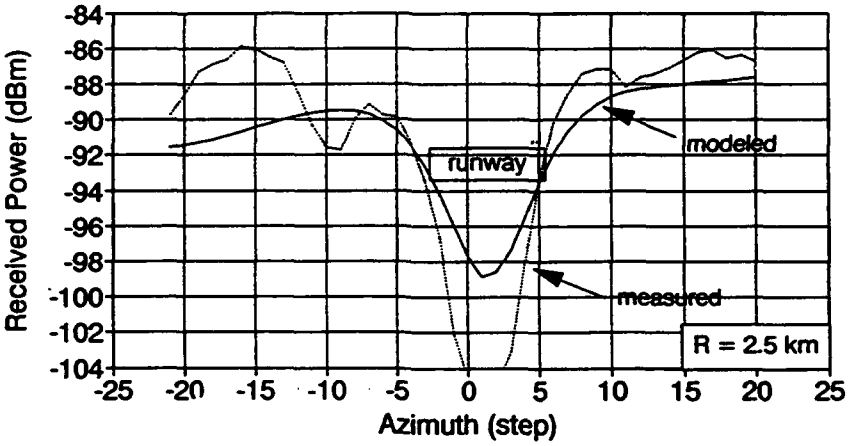

Figure 90. Comparison of 35 GHz measured and modeled cross-range power at 2.5 km.

8.3 IR RESULTS

8.3.1 TEST DATA MATRIX

Baseline data were collected with the Kodak IR camera system on two occasions. The images were collected over a 24 hour period with nominally clear weather for both collection periods. IR data in low visibility conditions were collected on four separate dates. The low visibility weather conditions were nominally identified as rain with accompanying fog. The visibility on those data collection periods ranged from less than a kilometer to nearly 28 kilometers. Tables 37 and 38 summarize the IR data collected and analyzed.

Table 37. IR Image Data Collected at WPAFB 03/31/92 Through 05/28/92

	Date Collected	Number of Images
Baseline Diurnal	03/12/92	41
Fog / Rain	03/18/92	9
Fog / Rain	03/30/92	16
Fog / Rain	04/18/92	7
Fog / Rain	04/21/92	8
Baseline Diurnal	05/27/92	33
Total Number of Images		114

Table 38. IR Image Data Analyzed

		Number Images Analyzed	Number with Runway Measurable
Baseline Diurnal	(03/13/92)	41	41
Fog/Rain	(03/18/92)	9	9
Fog/Rain	(03/30/92)	16	7
Fog/Rain	(04/18/92)	6	6
Fog/Rain	(04/21/92)	6	4
Baseline Diurnal	(05/27/92)	11	11
TOTALS		92	78
Total Number of Runway Radiance Measurements from Images			235

8.3.2 BASELINE PERFORMANCE

Since the source target contrast, determined largely by the temperature difference between runway and grass, depends on many variables including past weather history, the performance can not be portrayed simply in a single variable plot. For this reason, tabulated results for the conditions existing during the measurements are included in Appendix F, and included here are a number of plots relating performance to single parameters.

The diurnal plots below (Figures 91-94) show the baseline measured contrast and signal-variability-ratio (SVR) results as a function of time of day. The difference between the runway temperature and soil temperature is also plotted (Figures 95-96) against time of day to show the correlation of the image contrast values with the temperature difference which drives the contrast. The background temperature is measured at the soil level and not at the observed surface level which is not well defined in a grass surface. The main features of the driving temperature differences should be apparent even though the soil temperature differs somewhat from that of the apparent surface. The contrast and SVR are low during nighttime hours and reach a maximum in mid afternoon. The runway-background temperature difference shows the same basic behavior. The daily cycle of solar heating of the ground which reaches its maximum in early afternoon, and which is replaced at night by the cooling effects of radiation to the sky, is the source which drives the diurnal cycle seen clearly in the plots of both baseline data sets. An obvious peak in the contrast and SVR seen shortly before sunset, and which is not matched in the temperature difference plots, is from reflection of solar radiation from the runway surface. At that time of day, the sun is positioned so that the specular reflection from the runway is aligned with the line of sight of the IR camera situated in the tower, producing a strong solar glint. The difference in amplitudes of the contrast and SVR maximum on the plots of the data from 3/12/92 and the data from 5/27/92 corresponds to higher values of temperature difference. Higher temperatures in general characterize the data from 5/27/92, and the higher temperatures induce larger temperature differences as well. Crossover in the runway and background temperatures was not observed in images collected during the baseline diurnal measurements. The weather conditions required to produce thermal reversal of the runway and the grass background did not appear to exist on the dates 3/12 or 5/27. Thermal reversal was observed during measurements under low visibility conditions.

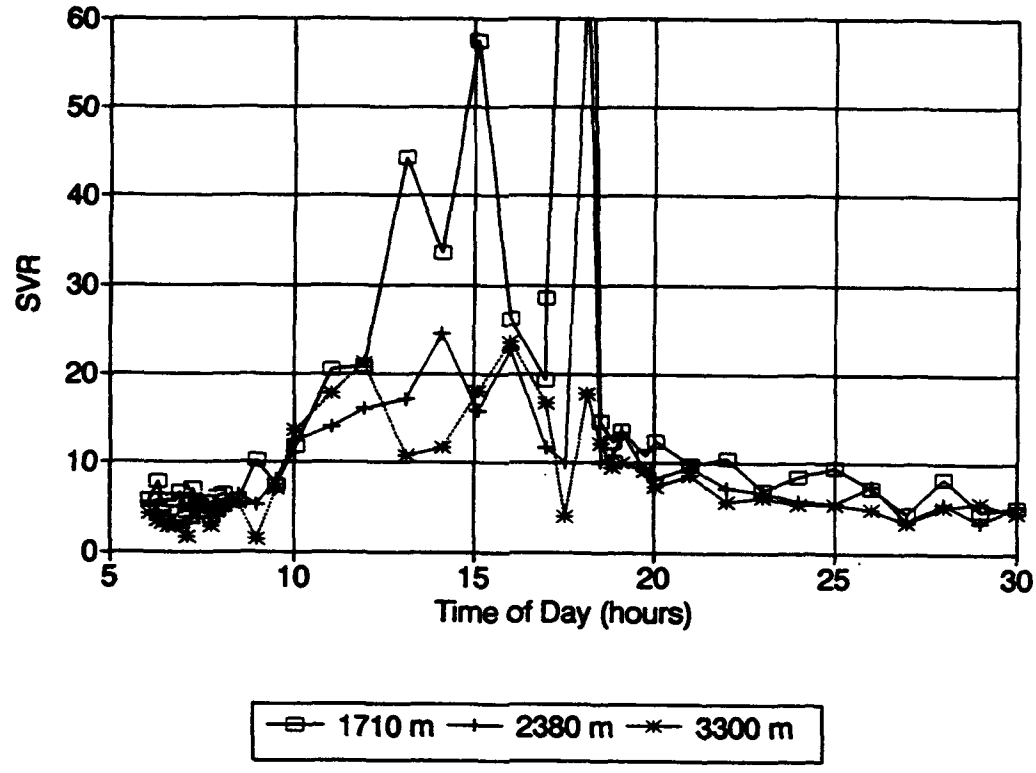

Figure 91. SVR plotted against time of day on 3/12/92 and 3/13/92.

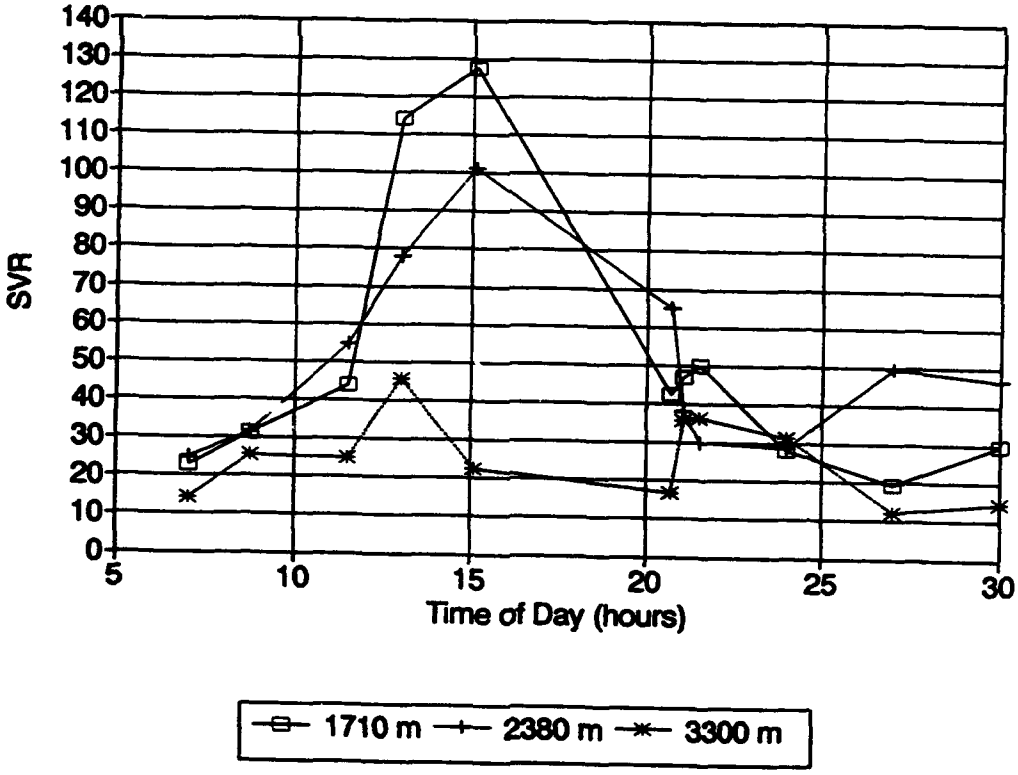

Figure 92. SVR plotted against time of day on 5/27/92 and 5/28/92.

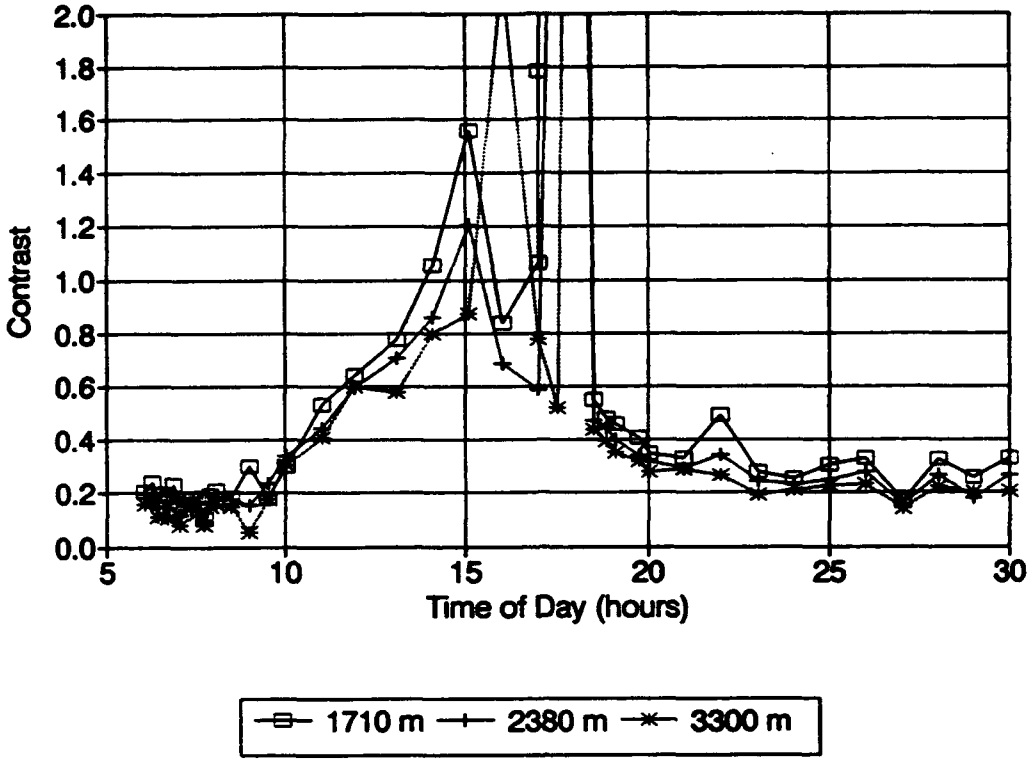

Figure 93. Contrast plotted against time of day on 3/12/92 and 3/13/92.

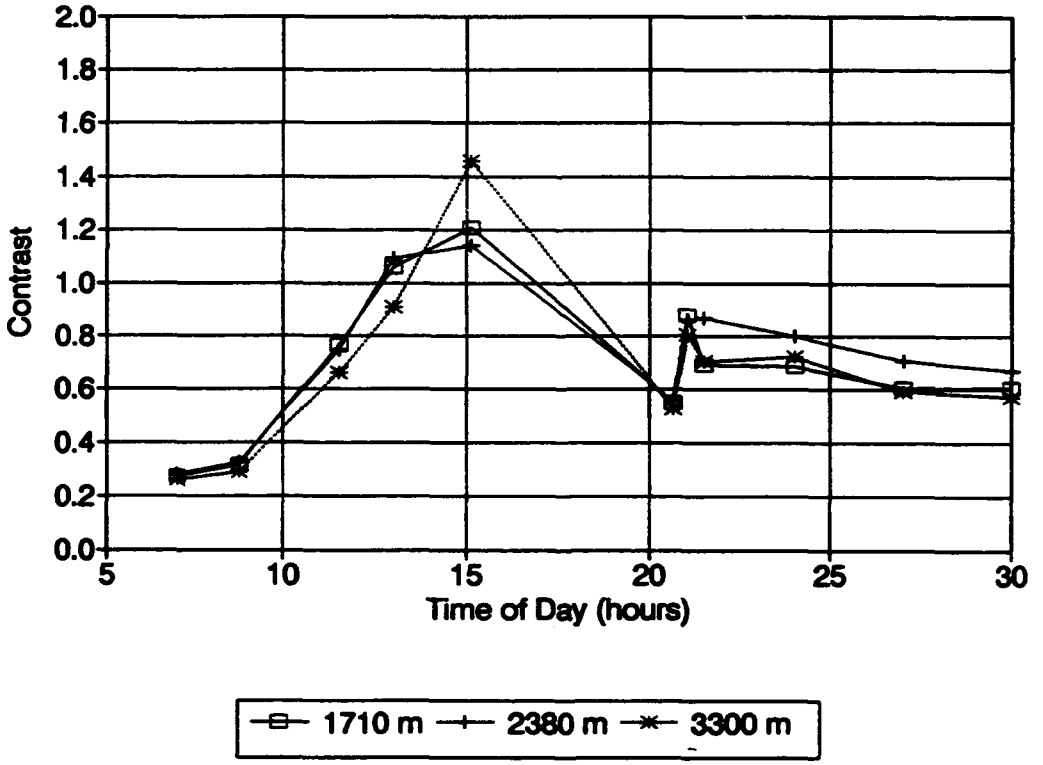

Figure 94. Contrast plotted against time of day on 5/27/92 and 5/28/92.

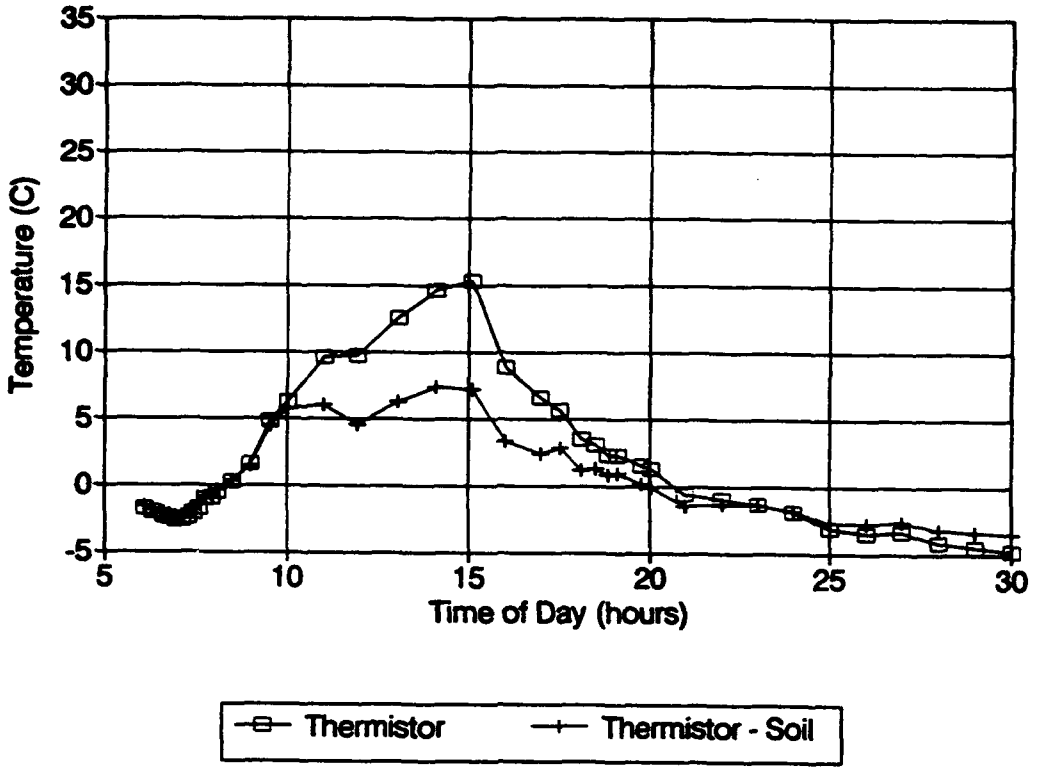

Figure 95. Runway temperature and difference with soil temperature vs time on 3/12/92 and 3/13/92.

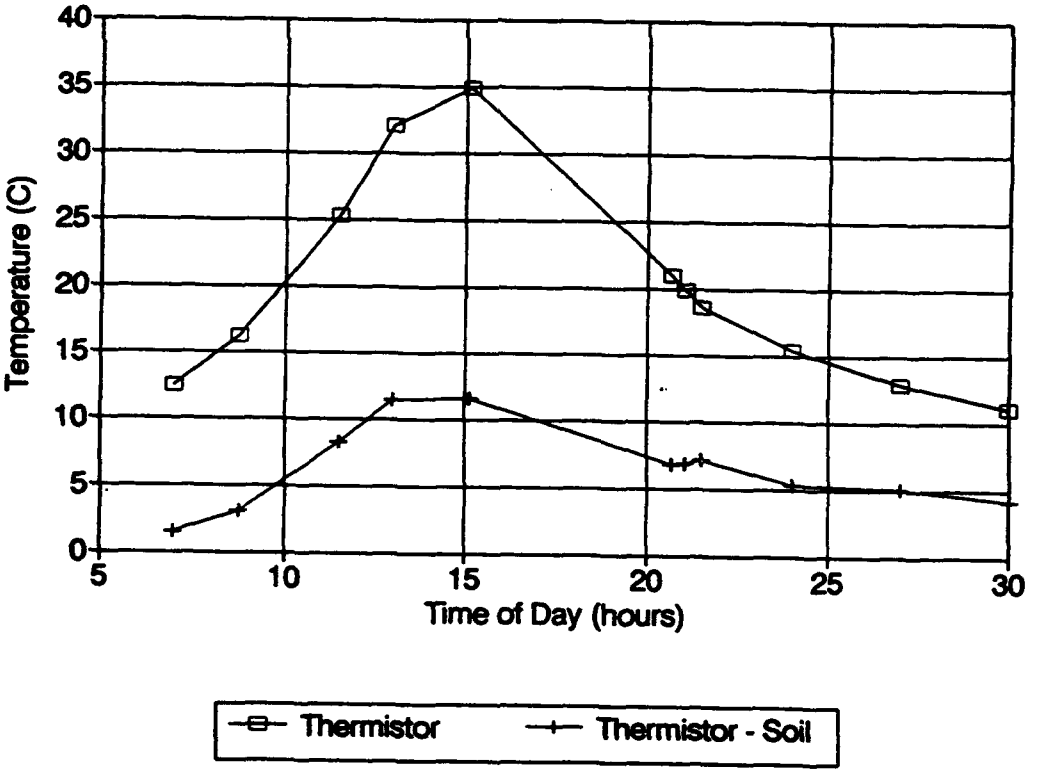

Figure 96. Runway temperature and difference with soil temperature on 5/27/92 and 5/28/92.

Sharpness measurements were possible for left and right sides for 140 runway profiles and resulted in angular transitions covering from 1 to 3 pixel spacings. The mean transition zone was 0.16 degrees which yields an average sharpness of 6.3 degrees^{-1}. No obvious systematic effects related to range, visibility, time of day, or other weather condition were apparent.

.8.3.3 Performance in Fog, Snow, and Rain

The results of IR measurements during the occurrence of low visibility conditions are summarized in Figures 97 through 102. SVR is used as the primary measure of image quality here in the interest of brevity and because some of the images could not be accurately calibrated and therefore did not permit consistent computation of contrast. The general level of the results can be seen in the plots of SVR against time of day. The values of SVR found in low visibility conditions are much lower than during baseline tests, principally because the temperature differences are much lower as shown in Figures 99 and 100. These SVR relationships are also apparent by inspection of the tabulated results in Appendix F. The plots relating SVR to visibility, Figures 101 and 102, indicate that IR obscuration and visibility have a complex relationship. Since the runway-background temperature difference was relatively constant during each of the low visibility measurement periods, any large changes in SVR should be ascribed to the changes in visibility which are taking place. Since the background area surface temperature was measured at the soil level, it is possible for variations in runway to background temperature differences to affect the image without being detected in the temperature plots.

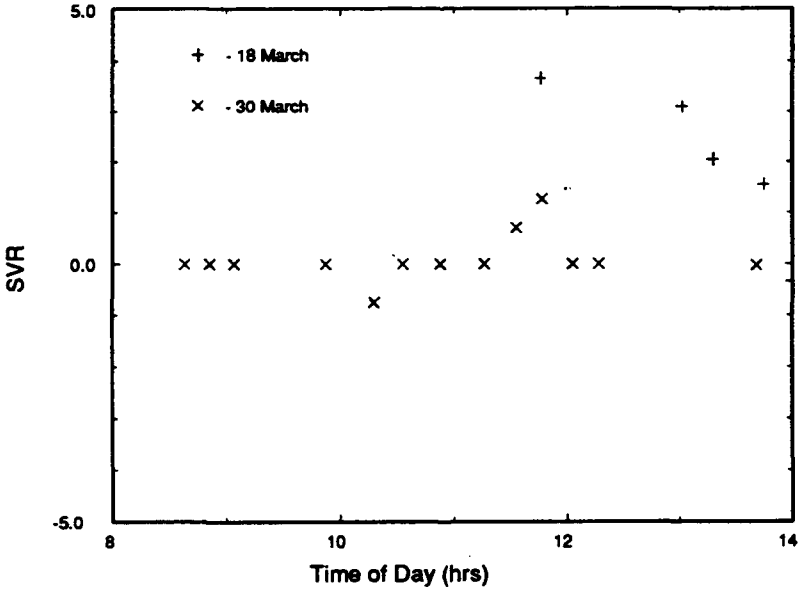

Figure 97. SVR against time of day on 3/18/92 (+), and 3/30/92 (X).

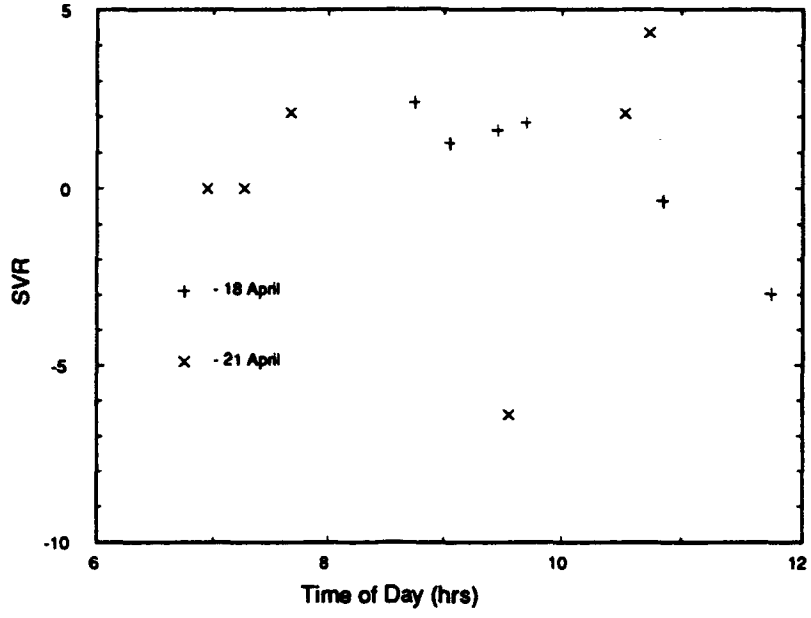

Figure 98. SVR against time of day on 4/18/92 (+), and 4/21/92 (X).

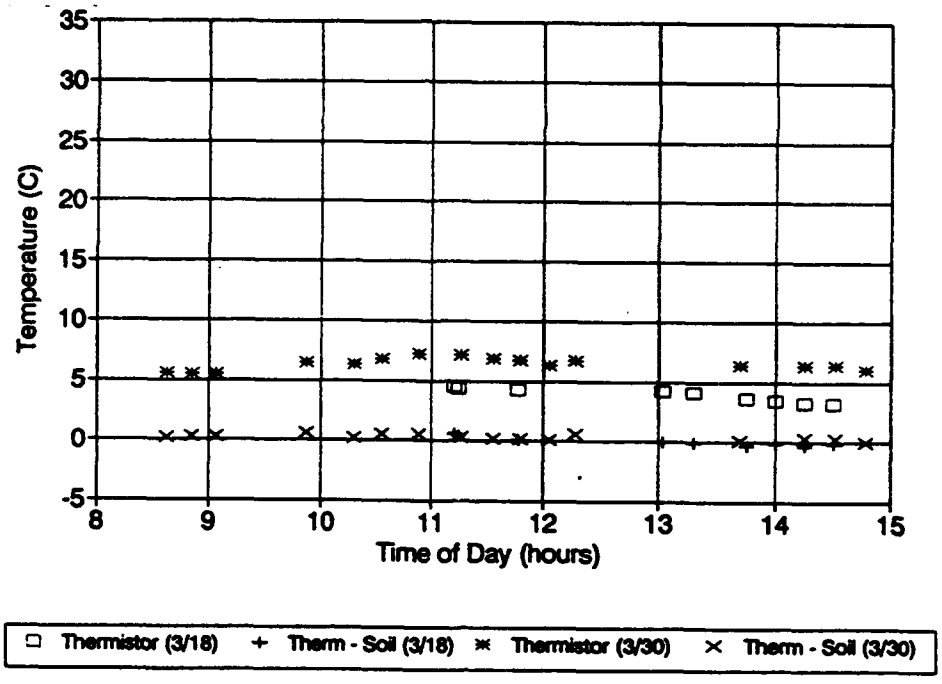

Figure 99. Runway temperature and difference with soil temperature on 3/18/92 (+), and 3/30/92 (X).

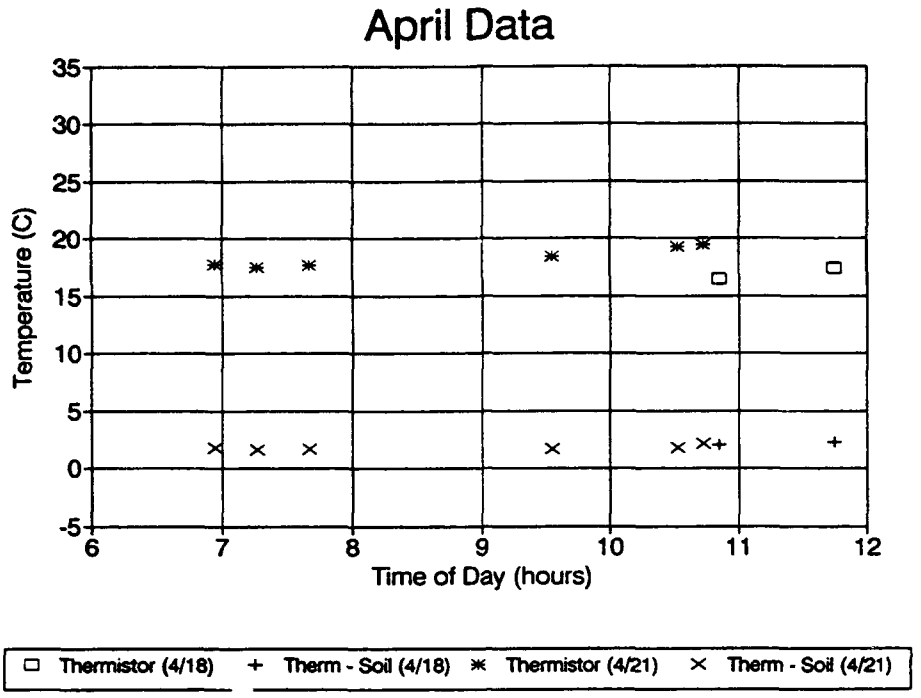

Figure 100. Runway temperature and difference with soil temperature on 4/18/92 (+), and 4/21/92 (X).

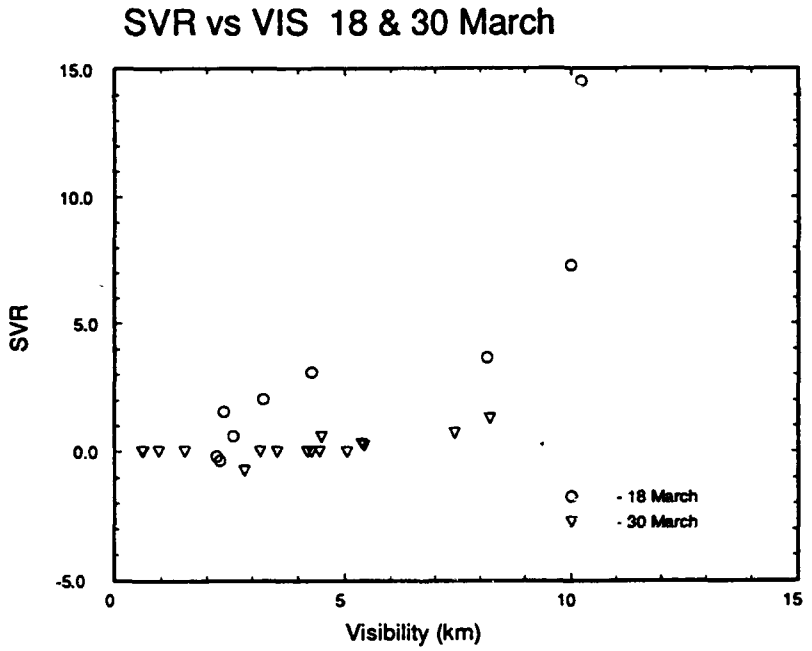

Figure 101. SVR against measured visibility on 3/18/92 (o), and 3/30/92 (Δ).

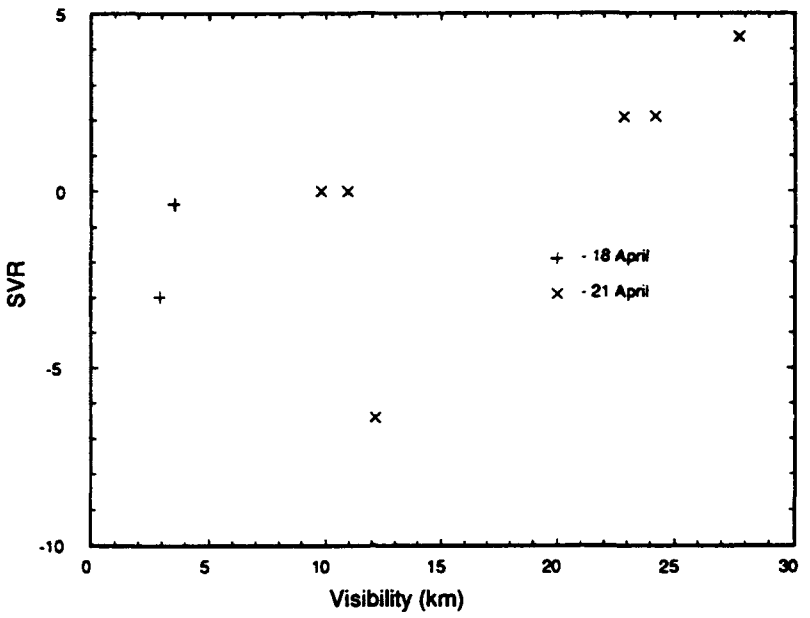

Figure 102. SVR against measured visibility on 4/18/92 (+), and 4/21/92 (X).

The fog drop size distributions yielded results which implied that the "fog" was very light and was composed of particles which are usually characterized as haze. Fog is generally identified with droplet diameters from 5 to 40 microns.[Dennis] The fogs represented in these measurements were composed of particles with sizes concentrated below 2 microns in drop diameter.

The extinction inferred from the measured visibility for the low visibility conditions was generally low enough to indicate some atmospheric obscuration but not always as great as expected. Visibility was not always low enough to indicate significant amounts of fog. Particle size distribution information was extracted from weather data and used to compute extinction coefficients in order to examine the relative contribution of fog and rain to extinction during these measurements. The FSSP data in the 0.5 to 8 micron size range were used to infer the amount of extinction caused by fog droplets. FSSP measurements were not available for all of the low-visibility measurements, so the results must be incomplete. Plots of size distribution data and the wavelength dependence of the computed extinction coefficient are shown in Figures 103 and 104 for one case. The extinction calculated from these size distributions was an insignificant fraction of the total extinction in all but a few cases.

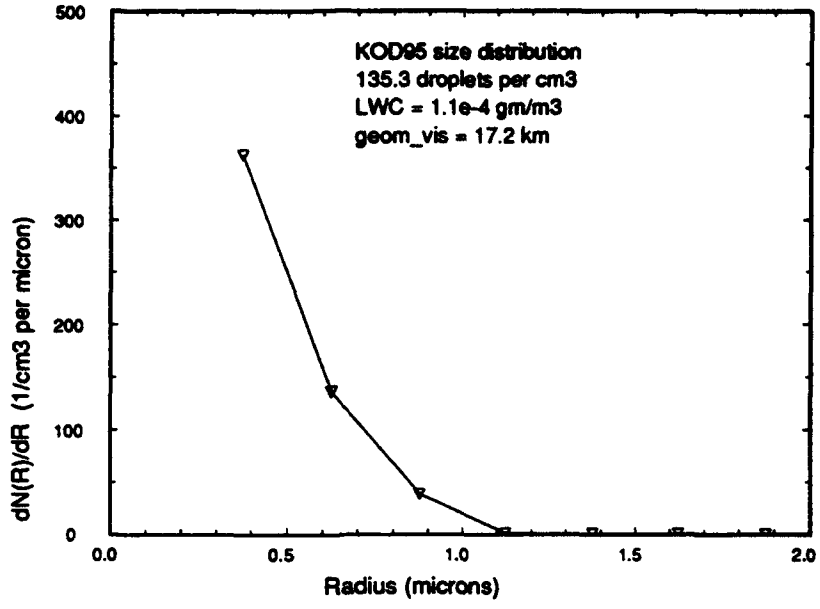

Figure 103. Particle size distribution measured on 4/18/92 at time of IR image kod95.

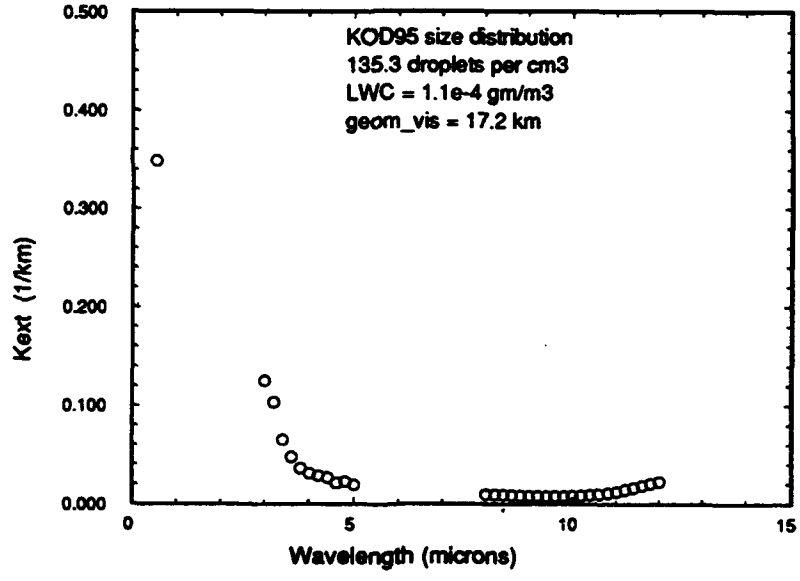

Figure 104. Extinction coefficient against wavelength computed for fog size distribution at the time of kod95.

Data from the GBPP instrument provided drop size distributions for a few measurements. These drop sizes were used to compute extinction coefficients for those measurements corresponding to the GBPP data times. For measurements at times not accompanied by GBPP data, the rain rate was used with Marshall and Palmer's relationship between rain rate and raindrop size distribution to compute extinction coefficients from the measured rain rates. The extinction was computed as

equal to the geometric cross section, 2*(drop cross sectional area), since the rain drops were so much larger than the wavelengths of the visible and IR bands considered. The results are plotted in Figure 105 in terms of the range required to block 98% of the radiation in passing through the rain. Corresponding values of the measured optical visibility and the results of extinction computations for the fog droplet size data are also shown. The y-axis which indicates range is nonlinear and is inverted with shorter ranges, corresponding to greater attenuation, at the top and greater ranges, or lower attenuation, at the bottom of the scale. Almost all of the limited number of data points generated from the fog size range of drop sizes are plotted at nearly zero attenuation or infinite range.

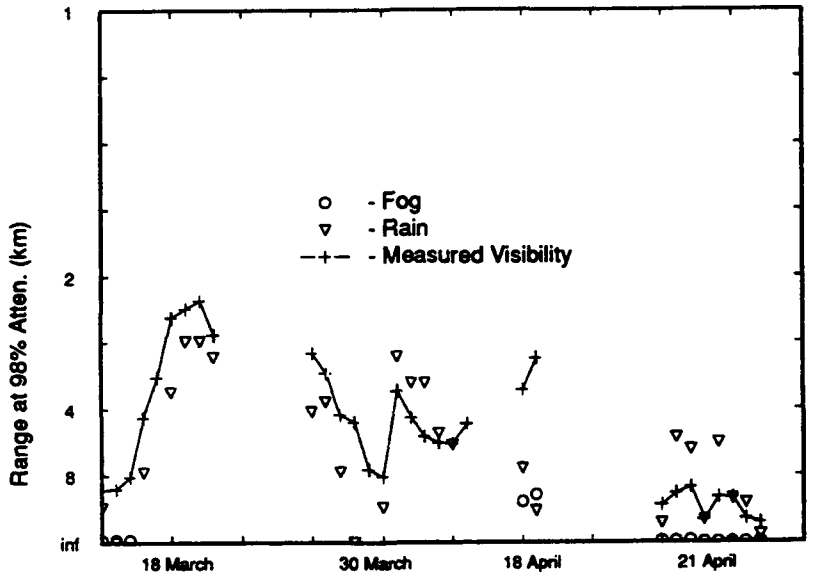

Figure 105. Plotted values of measured optical visibility with the range values for 98% attenuation calculated from rain and fog data during four low-visibility tests.

The results of the fog and rain extinction coefficient calculations shown above are included in the tabulated results referred to previously. It is clear from the plots shown above that the measured optical visibility agrees well with the ranges computed for the extinction by the raindrops and that the extinction due to fog particles is very small in all of the cases for which particle size data were available. The relatively large visibilities measured during these tests also indicates that the fog was in a range from light to none at all for the majority of the measurements.

SECTION 9
CONCLUSIONS

9.1 MMW RADAR

All six of the MMW sensors tested at the tower facility were capable of imaging the airport runway scene in clear weather conditions. There were significant differences in the MMW imaging sensors' angular resolution, runway-to-grass contrast, signal-to-noise ratio, and maximum runway detection range. As would be expected from antenna theory, the 95 GHz radar sensors have more than twice the angular resolution of the 35 GHz radars for the same 30 inch antenna aperture. The differences in MMW radar RCS between the runway pavement and bordering grass areas at the 2° to 3° incident angle are about 16 to 22 dB. Resolution limitations of the MMW sensors prevented them from fully converting this RCS difference into image contrast. The 95 GHz radar sensors tested lacked the performance to image the runway out to the end at 3,300 m range. The 35 GHz radars exhibited higher signal-to-noise ratio, and were able to image the runway to 3,300 m range.

Meteorological effects of fog, snow, and rain decreased the maximum runway detection range for the MMW sensors by varying degrees. The MMW detection range was not significantly reduced by the snowfall and fog conditions that occurred during the tests. More MMW tower test data are needed in fogs of less than one mile visibility to establish any performance limitations due to fog. Rainfall rates as low as 2 mm/hr reduced the MMW detection ranges, especially for 95 GHz. Runway detection by the 35 GHz radars was seriously degraded for rainfall rates greater than 20 mm/hr. As was predicted from MMW propagation theory, the dominant effect of rain on image quality at ranges of 2 to 4 km is signal attenuation. The 35 GHz radar sensor tested provided the best runway detection performance in clear and adverse weather conditions with adequate airport scene resolution.

9.2 IR

The contrast available in IR images collected during clear weather was observed to mirror the temporal variations in surface temperatures during the diurnal periods in which measurements were made, except at particular times of day when the sun was positioned to reflect from the runway surface into the camera field of view. The measured contrast was low during the night and reached maximum levels in mid afternoon, varying in a manner similar to the behavior of measured surface temperature differences. The solar reflection from the runway generated a

sharply peaked maximum in the late afternoon, corresponding to the time of alignment of the sun with the reflected line of sight from the tower. These observations prompt the conclusion that the ground surface temperature differences are the primary influence on IR image contrast collected in clear weather with a platinum silicide (PtSi) camera operating in the 3 to 5 micron band, and that reflections of illuminating radiation from the sun are only important when the solar alignment is near the specularly reflected line of sight.

The dependence of IR contrast on ground surface temperature differences implies the dominance of the IR radiation emitted by the scene components which is a function of surface temperature and the emissivity of surface materials. Reflection of sources of illumination are important only for the solar disk and only at times when the sun is properly positioned. The cyclic diurnal behavior is derived from solar heating of the ground which reaches its maximum in early afternoon, and which is replaced at night by the cooling effects of radiation from the ground to the cold sky. Other observers have reported cases of the grass background being warmer than the concrete runway at some times of day so that the computed contrast is a negative value. Crossover in the runway and background temperatures was not observed in IR images collected during the baseline diurnal measurements. Thermal reversal was observed during measurements under low visibility conditions.

Sharpness measured in cross-runway profiles showed transitions covering from one to three pixel spacing with no obvious systematic effects related to range, visibility, time of day, or other weather condition. The mean transition zone was observed to be 0.16 degrees wide.

Low visibility conditions of fog, snow, and rain imposed significant reductions in runway visibility. It was not possible to detect the runway in image data collected in rain or fog when the measured visibility was less than one mile.

The IR contrast is reduced in precipitation conditions, principally because the temperature differences are reduced. IR contrast was also affected to some degree by attenuation along the path through the atmosphere, but the relative importance of atmospheric attenuation was difficult to determine because of the small temperature differences observed.

The fog drop size distributions in those cases where measurements were available implied that the "fog" was very light and was composed of relatively small particles with diameters less than 5 micrometers. Fog is generally identified with droplet diameters from 5 to 40 microns.[Dennis]

The extinction inferred from the measured visibility for the low visibility conditions was generally lower than for clear weather, but the visibility was not always low enough to indicate

significant amounts of fog. The extinction calculated from rain and fog drop size distributions shows that the measured optical visibility is reduced primarily due to raindrop extinction and that the extinction due to fog particles is very small in all of the cases for which particle size data were available.

Definitive conclusions as to IR system performance in fog are not possible due to the lack of cases of thick fog which would generate significant obscuration of the runway. It can be supported, however, that the measured IR image data give no reason to believe that the performance estimates described above are not valid. There is no way to directly compare the IR system quantitatively with visible wavelength sensors, since comparison data in the visible band were not collected, but the PtSi IR sensor operating in the 3 to 5 micron IR band shows no obvious improvement over the visible band under the conditions encountered during these tests. This is in agreement with performance estimates based on drop size distributions representative of typical fog types. Those conditions were not sufficiently varied to provide a direct comparison for the moderate to heavy fog weather conditions of interest. The performance measurements on the PtSi IR system are consistent with the estimates described above.

REFERENCES

1. Air Force Geophysics Laboratory, "PC-TRAN 7 Personal Computer Version of the LOWTRAN 7 Atmospheric Model," Hanscom AFB, August 1990.

2. Ajayi, G. O. and E. B. C. Ofoche, "Some Tropical Rainfall Rate Characteristics at Ile-Ife for Microwave and Millimeter Wave Applications," *Journal of Climatology and Applied Meteorology*, vol. 23, pp 562-567, Apr. 1984.

3. Altshuler E. E. and R. A. Marr, "A Comparison of Experimental and Theoretical Values of Atmospheric Absorption at the Longer Millimeter Wavelengths," *IEEE Transactions on Antennas on Propagation*, Vol. AP-36, No. 10, October 1988, pp. 1471 - 1480.

4. Altshuler, E. E., and R. A. Marr, "Cloud Attenuation at Millimeter Wavelengths," *IEEE Transactions on Antennas on Propagation*, Vol. AP-37, No. 11, November 1989, pp. 1473 - 1479.

5. Altshuler, Edward E., "A Simple Expression for Estimating Attenuation by Fog at Millimeter Wavelengths," *IEEE Transactions on Antennas on Propagation*, Vol. AP-32, No. 7, July 1984, pp. 757 - 758.

6. Barton, D. K., "Land Clutter Models for Radar Design and Analysis," *Proceedings of the IEEE*, Vol. 73, No. 2, February 1985, pp. 198-204.

7. Barton, D. K., "Low Angle Radar Tracking," *Proceedings of the IEEE*, Vol. 62, No. 6, June 1974, pp. 687-704.

8. Barton, D. K., Modern Radar System Analysis, Artech House, Norwood, MA, 1988, p.11.

9. Barton, David K., Modern Radar System Analysis, Artech House, 1987.

10. Beckmann, P. and A. and Spizzichino, The Scattering of Electromagnetic Waves from Rough Surfaces, MacMillan, New York, 1963, pp. 70 - 97.

11. Belcher, C. L., E. S. Sjoberg, R. N. Trebits, N. C., Currie, and R. D. Hayes, "MMW Clutter Reflectivity and Attenuation Handbook," Final Technical Report on Contract DAAH01-84-D-A029 D. O. 0051, Georgia Institute of Technology, March 1987.

12. Billingsley, J. B. and J. F. Larrabee, "Multifrequency Measurements of Radar Ground Clutter at 42 Sites," Technical Report 916, Lincoln Laboratory, Massachusetts Institute of Technology, Lexington, Massachusetts, November 1991.

13. Bohren,Craig F. and Donald R. Huffman, Absorption and Scattering of Light by Small Particles, Wiley-Interscience, New York, 1983.

14. Chylek, P., "Extinction and Liquid Water Content of Fogs", *Journal of Atmospheric Sciences*, 35, 296-300, 1978.

15. Cosgriff, R. L., W. H. Peake, R. C. Taylor, Terrain Scattering Properties for Sensor System Design, (Terrain Handbook II), Engineering Experiment Station, College of Engineering, The Ohio State University, Columbus Ohio, May 1960.

16. Currie, N. C. (Editor), Radar Reflectivity Measurement: Techniques and Applications, Artech House Inc., Norwood, MA, 1987, pp. 233-235.

17. Currie, N. C. and C. E. Brown, (Editors), Principles and Applications of Millimeter Wave Radar, Artech House, Norwood Massachusetts, 1987, pp 75 - 394.

18. Currie, N. C., F. Dyer and R. D. Hayes, "Analysis of Radar Rain Return at Frequencies of 9.375, 35, 70, and 95 GHz," Eng. Exp. Sta., Georgia Inst. Tech., Atlanta, GA, Tech. Rept. 2, Feb. 1975.

19. Currie, N. C., MMW Clutter Characteristics, Chapter 5 in Principles and Applications of Millimeter-Wave Radar, Nicholas C. Currie and Charles E. Brown, editors, Artech House, 1987.

20. Currie, N.C., et.al., "Millimeter-Wave Measurements and Analysis of Snow-Covered Ground," IEEE Transactions on Geoscience and Remote Sensing, May 1988.

21. Davis, J. L., G. J. Bradley, R. B. Takes, J. H. Andrews, M. T. Tuley and P. A. Ryan, "TRACK 4.1 Radar Cross Section and Tracking Simulation User's Guide," Georgia Tech Research Institute, Georgia Institute of Technology, July, 1990.

22. Dennis, Richard, Handbook on Aerosols, U.S. Dept. of Energy, NTIS # TID-26608, January 1976, p. 3.

23. Eaves, J. L., and Edward K. Reedy, (Editors), Principles of Modern Radar, Van Nostrand Reinhold Company, New York, 1987, pp. 287 - 342.

24. Eldridge, R. G. "Haze and Fog Aerosol Distributions," *Journal of Atmospheric Sciences*, Vol. 23, September 1966, pp. 605 - 613.

25. Electro-Optics Laboratory, "GTVISIT User's Manual," Georgia Tech Research Institute, Georgia Institute of Technology, October 1991.

26. Gerace G. C. and E. K. Smith, "A Comparison of Cloud Models", *IEEE Antennas and Propagation Magazine*, October 1990, pp. 32 - 39.

27. Greneker, E.F., et. al., "Correlation Between the Radar Reflectivity of Snow and Measurable Snowpack Parameters," Final Report on Contract DAAH01-84-D-A029, D0 88, U.S. Army MICOM, Georgia Institute of Technology, Atlanta, Georgia, March 1987.

28. Gunn, R. and G. D. Kinzer, "The Terminal Velocity of Fall for Water Droplets in Stagnant Air," *Journal of Meteorology*, vol. 6, pp 243-248, Aug. 1949.

29. Hudson, B. H., and N. C. Currie, "Millimeter Wave Reflectivity of Paved Runway Surfaces" *IEEE Southcon '89 Conference Record*, Atlanta, GA, March, 1989, pp. 150-153.

30. Hudson, B. H., M. A. Richards, and J. L. Smart, "Image Sensor Test Support," Final Technical Report on Purchase Order No. A51771-1, Georgia Institute of Technology, March 1991.

31. Hudson, Brian H., GTRI, private communication with Sam Piper, 10 May 1991.

32. Joss, J. and A. Waldvogel, "Raindrop Size Distributions and Sampling Size Errors", *Journal of Atmospheric Sciences*, 26, 566-569, 1969.

33. Kneizys, F.X. et al , "Users Guide to LOWTRAN7", AFGL-TR-88-0177, (NTIS;AD A206773), 1988.

34. Kunkel, B. A., "Parameterization of Droplet Terminal velocity and Extinction Coefficient in Fog Models," *Journal of Climatology and Applied Meteorology*, vol. 23, pp 34-41, Jan. 1984.

35. Liebe, H. J. and D. H. Layton, "Millimeter-wave Properties of the Atmosphere: Laboratory Studies and Propagation Modeling," NTIA Report. 87-224, October 1987.

36. Liebe, H. J., T. Manabe, and G. A. Hufford, " Millimetre-Wave Attenuation and Delay Rates Due to Fog/Cloud Conditions," *IEEE Transactions on Antennas and Propagation*, Vol. AP-37, No.12, December 1989, pp. 1617 - 1621.

37. Long, M. W., Radar Reflectivity of Land and Sea, Lexington Books, Lexington, Massachusetts, 1975.

38. Manabe Takeshi, R. O. Debolt, and H. Liebe, " Moist-air Attenuation at 96 GHz Over a 21-km Line-of-Sight Path," *IEEE Transactions on Antennas and Propagation*, Vol. 37, No. 2, February 1989, pp. 262 - 266.

39. Marshall, J.S. and W. Palmer, "The Distribution of Raindrops with Size", *Journal of Meteorology*, 5, 165-166, 1948.

40. Nystrom, B. M., J. R. Cary and C. M. Shelton, "Synthetic Vision Program (SVP) Test Meteorological Data Quality Assessment Report," Final Report for period October 1991 - July 1992, E-OIR Measurements, Inc., Fredricksburg, VA., 1992.

41. Olsen, R. L., D. V. Rogers and D. B. Hodge, "The aR^b Relation in the Calculation of Rain Attenuation", *IEEE Trans. Antennas Propagation.*, vol. AP-26, no. 2, pp 319-329, Mar. 1978.

42. Peifer, J. W., R. B. Rakes, M. S. West, and J. H. Andrews, "MAX Geometrical Data Base User's Manual," Georgia Tech Research Institute, Georgia Institute of Technology, 1987.

43. Pinnick, R.G. et al. , "Verification of a Linear Relation Between IR Extinction, Absorption and Liquid Water Content of Fogs," *Journal of Atmospheric Sciences*, 36, 1577-1586, 1979.

44. Platt, C. M. R. " Transmission of Submillimeter Waves through Water Clouds and Fogs," *Journal of Atmospheric Sciences*, Vol. 27, May 1970, pp. 421 - 425.

45. Ray, Peter S., "Broadband Complex Refractive Indices of Ice and Water" *Applied Optics*, vol. 11, no. 8, pp 1836-1844, Aug. 1972

46. Richard, V. W., J. E. Kammerer and H. B. Wallace, "Rain Backscatter Measurements at Millimeter Wavelengths," *IEEE Trans. Geoscience and Remote Sensing*, vol. 26, no. 3, pp 244-252, May 1988.

47. Rozenberg, V. I. "Scattering and Attenuation of Electromagnetic Radiation by Atmospheric Particles," NASA TTF-771, Feb. 1974.

48. Sauvegeot, H., Radar Meteorology, Artech House, Boston, 1992.

49. Shettle, E.P, "Models of Aerosols, Clouds and Precipitation for Atmospheric Propagation Studies," 45th AGARD Symposium (Oct 9-13, 1989), Copenhagen, Denmark.

50. Slobin S., "Microwave Noise Temperature and Attenuation of Clouds: Statistics of These Effects at Various Sites in United State, Alaska, and Hawaii," *Radio Science*, Vol. 17, No. 6, Dec. 1982, pp. 1443 - 1454.

51. "Tower Test Plan for Evaluation of Imaging Sensors," Joint FAA/USAF Synthetic Vision Technology Demonstration (SVTD) Program, Controls Systems Development Branch, Flight Controls Division, Flight Dynamics Directorate, Wright Laboratory, May 1991.

52. Trebits, R. N., MMW Propagation Phenomena, Chapter 4 in Principles and Applications of Millimeter-Wave Radar, Nicholas C. Currie and Charles E. Brown, editors, Artech House, 1987.

53. Ulaby, F. T. and T. F. Haddock, "Millimeter -Wave Radar Scattering from Terrain: Data Handbook Version 2," Technical Report 026247 -3-T, The University of Michigan, Ann Arbor, Michigan, September, 1990.

54. Van de Hulst, H. C., Light Scattering by Small Particles. New York: Wiley, 1957.

APPENDIX A
PHENOMENOLOGY CALCULATION PROCEDURES

A number of different calculations were required in arriving at the phenomenology representations for the Synthetic Vision data set. A description of the procedures and equations used in these calculations is provided below.

Contrast

Contrast is defined as

$$\frac{\text{received power}_{\text{runway}} - \text{received power}_{\text{grass}}}{\text{received power}_{\text{grass}}}$$

These calculations required delogging the received power values before doing the calculation.

Radar Resolution Cell Area (pulse length limited)

The area A of the radar resolution cell is defined as follows. [Currie, p.54]:

$$A = \frac{2R}{\alpha}\frac{c\tau}{2}\tan\left(\frac{\phi_{az}}{2}\right)\sec(\theta) \qquad \text{(A-1)}$$

where R is the range in meters,
α is the beamshape factor ($\approx$1.38),
c is the speed of light in meters per second,
τ is the pulse length in seconds,
ϕ_{az} is the one-way azimuth beamwidth, and
θ is the depression angle.

Radar Resolution Cell Volume (beamwidth limited)

The airborne volume V of the radar resolution cell is defined as follows (assumes small azimuth and elevation beamwidths). [Currie, p.55]:

$$V = \frac{\pi}{4\alpha^2}\left[R^2\phi_{az}\phi_{el}\right]\frac{c\tau}{2} \qquad \text{(A-2)}$$

where R is the range in meters,
α is the beamshape factor ($\approx$1.38),
ϕ_{az} is the one-way azimuth beamwidth,
ϕ_{el} is the one-way elevation beamwidth,

c is the speed of light in meters per second, and
τ is the pulse length in seconds.

Since the sensor was pointed at the ground in the Synthetic Vision tower tests, a portion of the volume was not active as demonstrated in the drawing below (Figure A-1).

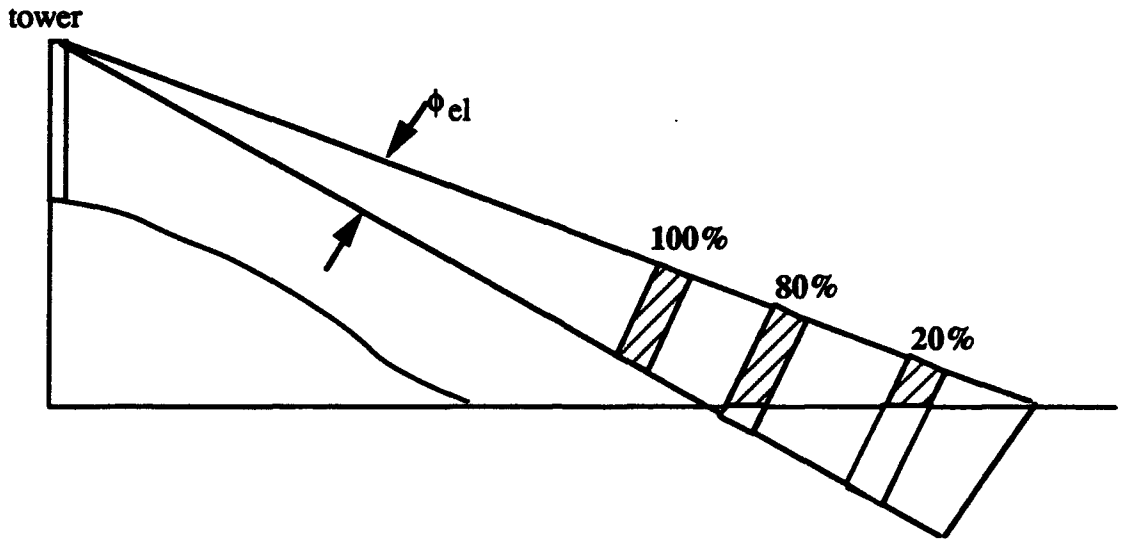

Figure A-1. Percentage active cell volume.

In order to compensate for this disparity in the percentage of active volume, a multiplier was calculated and applied for each sensor (dependent on elevation beamwidth) as a function of range. Calculations of these efficiency factors, or multipliers, began with the assumption that the sensor was always pointed downward with the center of the beam touching the ground at a range of 2 km. Based on the scene geometry, the depression angle was computed to be 2.46 degrees. It was assumed that at this range 50% of the volume was active. It was further assumed that the 25% and 75% efficiency points were at depression angles of 2.46 - .5*ϕ_{el} and 2.46 + .5*ϕ_{el} respectively. (Note: An efficiency factor of 25% corresponds to a multiplier of .25.). Table A-1 summarizes the depression angle and range values calculated.

TABLE A-1. DEPRESSION ANGLE AND RANGE CALCULATIONS

system	2-way ϕ_{el}	multiplier:	.75	.50	.25
95 GHz	.80	depression angle (°)	2.86	2.46	2.06
		range (m)	1721	2000	2387
35 GHz	3.89	depression angle (°)	4.41	2.46	0.52
		range (m)	1119	2000	9483

A sample of the multipliers used for the volumetric backscatter samples is provided in the table below. (Table A-2)

TABLE A-2. VOLUME MULTIPLIERS

sensor	approximate range (m)	multiplier
95 GHz	1500	.80
35 GHz	854	1.00
	1500	.70
	1800	.60
	2000	.50
	2500	.45
	3000	.40

Attenuation (α)

Three values of attenuation were studied using the received power values from the near and far corners and combination of the two values, for clear and rainy weather.

$$\frac{P_{\text{near corner clear}} - P_{\text{near corner rain}}}{2R} \qquad \text{(A-3)}$$

$$\frac{P_{\text{far corner clear}} - P_{\text{far corner rain}}}{2R} \qquad \text{(A-4)}$$

$$\frac{(P_{\text{near corner clear}} - P_{\text{far corner clear}}) - (P_{\text{near corner rain}} - (P_{\text{far corner rain}})}{2(R_{\text{far corner}} - R_{\text{near corner}})} \qquad \text{(A-5)}$$

The values used in the analysis for eight runs of the 35 GHz (HI2) data was an average obtained from the three methods defined above. For the remaining five cases, the antenna had been misaligned by approximately 15 degrees clockwise and the attenuation calculations were based on the peak values for a single bright target seen repeatedly in all of the data. In the case of the

95 GHz (NS1), since the near corner saturated the receiver most of the time, method 2 above was used to calculate the attenuation. Table A-3 indicates the particular data sets (by run name) used in the calculations. The runs with an asterisk (*) indicate those runs where the antenna had been misaligned.

TABLE A-3. ATTENUATION CALCULATION BASES

95 GHz				35 GHz			
clear (run name)	rain (run name)	rain rate (mm/hr)	attenuation (dB/km)	clear (run name)	rain (run name)	rain rate (mm/hr)	attenuation (dB/km)
NS1R77D	NS1R123D	.587	2.03	HI2R06*	HI2R09	1.174	.82
	NS1R115D	.587	1.07	HI2R11	HI2R30	1.174	.30
	NS1R122D	1.174	2.83	HI2R12	HI2R22	1.761	.54
	NS1R85D	1.174	1.97	HI2R13	HI2R33	1.761	.29
	NS1R114D	1.174	1.89	HI2R14	HI2R02	2.934	.87
	NS1R125D	1.761	2.94		HI2R23	5.282	1.29
	NS1R116D	2.347	2.00		HI2R24*	7.040	2.40
	NS1R112D	3.521	4.52		HI2R26*	8.800	2.20
	NS1R113D	6.456	4.37		HI2R31	12.911	2.37
	NS1R87D	8.216	4.29		HI2R25*	13.500	4.50
	NS1R90D	8.803	4.38		HI2R27	21.130	7.00
	NS1R94D	8.803	4.56		HI2R29*	24.650	14.00
	NS1R88D	10.564	3.79		HI2R28*	38.150	4.80
	NS1R89D	10.564	4.13				
	NS1R91D	10.564	4.28				
	NS1R121D	14.085	4.41				
	NS1R95D	15.845	4.47				
	NS1R93D	19.953	4.62				

Radar Cross Section (σ)

For a given power value, the radar cross section was obtained by using the radar equation. It should be restated that in the Synthetic Vision program patches, or groups of data resolution cells, were used to define the power received from a specific ground area. In the case of grass, runway, and taxiway patches, the power value used was an average of those cells comprising the patch. For corner reflector and fence patches, the values used were the peak values found within the group of data resolution cells. The radar equation follows.

$$\sigma = \frac{P_{rec}(4\pi)^3 R^4 L_{radar} L_{prop}}{P_{trans} G^2 \lambda^2} \qquad \text{(A-6)}$$

where P_{rec} is the received power in watts,
R is the range in meters,
L_{radar} is the radar loss,
L_{prop} is the propagation loss (assumed clear weather values for initial calculation),
P_{trans} is the transmitted power in watts,
G is the gain in watts, and
λ is the wavelength in meters.

In processing the Synthetic Vision data, the majority of the analysis dealt with simple values for received power, i.e., power as a function of range and meteorological conditions, contrast in power from runway and taxiway. The radar cross section values were initially processed using the propagation loss for clear weather. In processing the data further and using radar cross section values which were corrected for attenuation measured during rain, the following correction was applied.

$$\sigma = \sigma_{initial} + (\alpha_{rain} - \alpha_{clear})(2R) \qquad \text{(A-7)}$$

where $\sigma_{initial}$ is the value σ for assuming clear weather attenuation
α_{clear} is the clear weather atmospheric attenuation in dB/km,
α_{rain} is the calculated atmospheric attenuation in dB/km in rain, and
R is the range in km.

Normalized Radar Cross Section (σ^0)

The normalized radar cross section (in units of dBm^2/m^2) is defined to be the radar cross section per unit area. It is computed as

$$\sigma^0 = \frac{\sigma}{A} \tag{A-8}$$

where σ is the radar cross section, and
A is the radar cell area.

Volumetric Backscatter (σ^v)

Airborne volumetric backscatter (in units of dBm^2/m^3) is defined to be the radar cross section per unit volume. It is computed as

$$\sigma^v = \frac{\sigma}{V} \tag{A-9}$$

where σ is the radar cross section, and
V is the radar cell volume.

APPENDIX B
PATCH DEFINITION FILE

Patch Info: 10 June 1992 (hon2610.def)

Number of Patches: 47

Patch Num: 1
Patch Type: runway
Vertex 1: 8.41,4.49
Vertex 2: 8.57,4.57
Vertex 3: 8.55,4.76
Vertex 4: 8.39,4.68

Patch Num: 2
Patch Type: longgrass
Vertex 1: 8.37,4.92
Vertex 2: 8.53,4.94
Vertex 3: 8.50,5.12
Vertex 4: 8.35,5.10

Patch Num: 3
Patch Type: runway
Vertex 1: 8.95,4.77
Vertex 2: 9.11,4.84
Vertex 3: 9.10,5.03
Vertex 4: 8.93,4.95

Patch Num: 4
Patch Type: longgrass
Vertex 1: 8.99,4.44
Vertex 2: 9.17,4.44
Vertex 3: 9.17,4.62
Vertex 4: 8.99,4.62

Patch Num: 5
Patch Type: runway
Vertex 1: 9.44,5.02
Vertex 2: 9.64,5.12
Vertex 3: 9.62,5.30
Vertex 4: 9.42,5.20

Patch Num: 6
Patch Type: longgrass
Vertex 1: 9.51,4.71
Vertex 2: 9.65,4.71
Vertex 3: 9.65,4.89
Vertex 4: 9.49,4.91

Patch Num: 7
Patch Type: runway
Vertex 1: 9.95,5.28
Vertex 2: 10.15,5.39
Vertex 3: 10.14,5.55
Vertex 4: 9.94,5.46

Patch Num: 8
Patch Type: longgrass
Vertex 1: 10.00,4.98
Vertex 2: 10.14,4.98
Vertex 3: 10.14,5.16
Vertex 4: 10.00,5.16

```
Patch Num: 9
Patch Type: runway
Vertex 1: 10.45,5.53
Vertex 2: 10.64,5.61
Vertex 3: 10.63,5.81
Vertex 4: 10.46,5.73

Patch Num: 10
Patch Type: longgrass
Vertex 1: 10.54,5.21
Vertex 2: 10.71,5.22
Vertex 3: 10.70,5.38
Vertex 4: 10.52,5.37

Patch Num: 11
Patch Type: runway
Vertex 1: 10.96,5.80
Vertex 2: 11.12,5.87
Vertex 3: 11.11,6.03
Vertex 4: 10.97,5.98

Patch Num: 12
Patch Type: longgrass
Vertex 1: 11.07,5.48
Vertex 2: 11.23,5.49
Vertex 3: 11.22,5.64
Vertex 4: 11.06,5.63

Patch Num: 13
Patch Type: runway
Vertex 1: 11.49,6.07
Vertex 2: 11.67,6.16
Vertex 3: 11.68,6.28
Vertex 4: 11.49,6.21

Patch Num: 14
Patch Type: longgrass
Vertex 1: 11.57,5.78
Vertex 2: 11.77,5.80
Vertex 3: 11.75,5.93
Vertex 4: 11.55,5.91

Patch Num: 15
Patch Type: runway
Vertex 1: 12.04,6.34
Vertex 2: 12.24,6.42
Vertex 3: 12.31,6.58
Vertex 4: 12.09,6.50

Patch Num: 16
Patch Type: longgrass
Vertex 1: 12.17,6.03
Vertex 2: 12.33,6.05
Vertex 3: 12.31,6.20
Vertex 4: 12.15,6.18

Patch Num: 17
Patch Type: runway
Vertex 1: 12.51,6.58
Vertex 2: 12.69,6.68
```

Vertex 3: 12.67,6.81
Vertex 4: 12.49,6.72

Patch Num: 18
Patch Type: longgrass
Vertex 1: 12.60,6.29
Vertex 2: 12.80,6.32
Vertex 3: 12.78,6.45
Vertex 4: 12.58,6.42

Patch Num: 19
Patch Type: runway
Vertex 1: 13.02,6.88
Vertex 2: 13.22,6.96
Vertex 3: 13.18,7.07
Vertex 4: 13.00,7.00

Patch Num: 20
Patch Type: longgrass
Vertex 1: 13.10,6.54
Vertex 2: 13.30,6.59
Vertex 3: 13.27,6.71
Vertex 4: 13.06,6.68

Patch Num: 21
Patch Type: runway
Vertex 1: 13.50,7.10
Vertex 2: 13.69,7.19
Vertex 3: 13.67,7.30
Vertex 4: 13.47,7.22

Patch Num: 22
Patch Type: longgrass
Vertex 1: 13.39,7.43
Vertex 2: 13.58,7.50
Vertex 3: 13.55,7.61
Vertex 4: 13.35,7.57

Patch Num: 23
Patch Type: runway
Vertex 1: 13.95,7.30
Vertex 2: 14.12,7.39
Vertex 3: 14.12,7.51
Vertex 4: 13.93,7.45

Patch Num: 24
Patch Type: longgrass
Vertex 1: 14.03,7.05
Vertex 2: 14.23,7.11
Vertex 3: 14.21,7.22
Vertex 4: 14.00,7.18

Patch Num: 25
Patch Type: runway
Vertex 1: 14.50,7.60
Vertex 2: 14.70,7.70
Vertex 3: 14.68,7.82
Vertex 4: 14.48,7.72

Patch Num: 26

```
Patch Type: longgrass
Vertex 1: 14.57,7.31
Vertex 2: 14.80,7.35
Vertex 3: 14.78,7.46
Vertex 4: 14.54,7.42

Patch Num: 27
Patch Type: runway
Vertex 1: 14.96,7.82
Vertex 2: 15.18,7.92
Vertex 3: 15.15,8.06
Vertex 4: 14.95,7.95

Patch Num: 28
Patch Type: longgrass
Vertex 1: 15.03,7.55
Vertex 2: 15.27,7.60
Vertex 3: 15.26,7.70
Vertex 4: 15.02,7.66

Patch Num: 29
Patch Type: runway
Vertex 1: 15.49,8.08
Vertex 2: 15.66,8.18
Vertex 3: 15.64,8.31
Vertex 4: 15.45,8.23

Patch Num: 30
Patch Type: longgrass
Vertex 1: 15.58,7.77
Vertex 2: 15.77,7.81
Vertex 3: 15.76,7.97
Vertex 4: 15.55,7.92

Patch Num: 31
Patch Type: runway
Vertex 1: 15.97,8.34
Vertex 2: 16.20,8.45
Vertex 3: 16.18,8.56
Vertex 4: 15.95,8.45

Patch Num: 32
Patch Type: longgrass
Vertex 1: 16.04,8.04
Vertex 2: 16.33,8.09
Vertex 3: 16.31,8.23
Vertex 4: 16.03,8.18

Patch Num: 33
Patch Type: runway
Vertex 1: 16.46,8.59
Vertex 2: 16.68,8.69
Vertex 3: 16.65,8.80
Vertex 4: 16.44,8.70

Patch Num: 34
Patch Type: longgrass
Vertex 1: 16.56,8.31
Vertex 2: 16.80,8.36
Vertex 3: 16.77,8.51
```

Vertex 4: 16.54,8.44

Patch Num: 35
Patch Type: runway
Vertex 1: 16.96,8.84
Vertex 2: 17.18,8.93
Vertex 3: 17.15,9.05
Vertex 4: 16.95,8.95

Patch Num: 36
Patch Type: longgrass
Vertex 1: 17.04,8.54
Vertex 2: 17.27,8.58
Vertex 3: 17.25,8.74
Vertex 4: 17.03,8.71

Patch Num: 37
Patch Type: runway
Vertex 1: 17.46,9.10
Vertex 2: 17.66,9.20
Vertex 3: 17.63,9.30
Vertex 4: 17.42,9.20

Patch Num: 38
Patch Type: longgrass
Vertex 1: 17.57,8.71
Vertex 2: 17.80,8.77
Vertex 3: 17.78,8.91
Vertex 4: 17.54,8.86

Patch Num: 39
Patch Type: taxiway
Vertex 1: 8.19,5.52
Vertex 2: 8.46,5.67
Vertex 3: 8.43,5.79
Vertex 4: 8.17,5.65

Patch Num: 40
Patch Type: longgrass
Vertex 1: 8.26,5.34
Vertex 2: 8.51,5.48
Vertex 3: 8.50,5.56
Vertex 4: 8.25,5.44

Patch Num: 41
Patch Type: fence
Vertex 1: 8.55,6.75
Vertex 2: 8.69,6.82
Vertex 3: 8.65,6.90
Vertex 4: 8.52,6.81

Patch Num: 42
Patch Type: fence
Vertex 1: 10.41,8.03
Vertex 2: 10.54,8.10
Vertex 3: 10.50,8.18
Vertex 4: 10.38,8.09

Patch Num: 43
Patch Type: profile

```
Vertex 1: 11.54,5.70
Vertex 2: 11.8,5.82
Vertex 3: 11.61,6.672
Vertex 4: 11.35,6.53

Patch Num: 44
Patch Type: profile
Vertex 1: 14.19,6.885
Vertex 2: 14.45,7.02
Vertex 3: 14.18,8.1
Vertex 4: 13.91,7.95

Patch Num: 45
Patch Type: profile
Vertex 1: 16.72,8.038
Vertex 2: 16.98,8.171
Vertex 3: 16.6,9.48
Vertex 4: 16.35,9.32

Patch Num: 46
Patch Type: corner
Vertex 1: 10.31,6.14
Vertex 2: 10.45,6.14
Vertex 3: 10.45,6.24
Vertex 4: 10.31,6.24

Patch Num: 47
Patch Type: corner
Vertex 1: 16.15,7.37
Vertex 2: 16.41,7.32
Vertex 3: 16.51,7.62
Vertex 4: 16.15,7.67

C/N Ratios:
Number of C/N Pairs: 0
C/N Pair:
C/N Elements:

T/C Ratios:
Number of T/C Pairs: 20
T/C Pair: 1
T/C Elements: 1,2
T/C Pair: 2
T/C Elements: 3,4
T/C Pair: 3
T/C Elements: 5,6
T/C Pair: 4
T/C Elements: 7,8
T/C Pair: 5
T/C Elements: 9,10
T/C Pair: 6
T/C Elements: 11,12
T/C Pair: 7
T/C Elements: 13,14
T/C Pair: 8
T/C Elements: 15,16
T/C Pair: 9
T/C Elements: 17,18
T/C Pair: 10
T/C Elements: 19,20
```

T/C Pair: 11
T/C Elements: 21,22
T/C Pair: 12
T/C Elements: 23,24
T/C Pair: 13
T/C Elements: 25,26
T/C Pair: 14
T/C Elements: 27,28
T/C Pair: 15
T/C Elements: 29,30
T/C Pair: 16
T/C Elements: 31,32
T/C Pair: 17
T/C Elements: 33,34
T/C Pair: 18
T/C Elements: 35,36
T/C Pair: 19
T/C Elements: 37,38
T/C Pair: 20
T/C Elements: 39,40

C/C Ratios:
Number of C/C Pairs: 0
C/C Pair:
C/C Elements:

APPENDIX C
PRODUCTION IMAGES

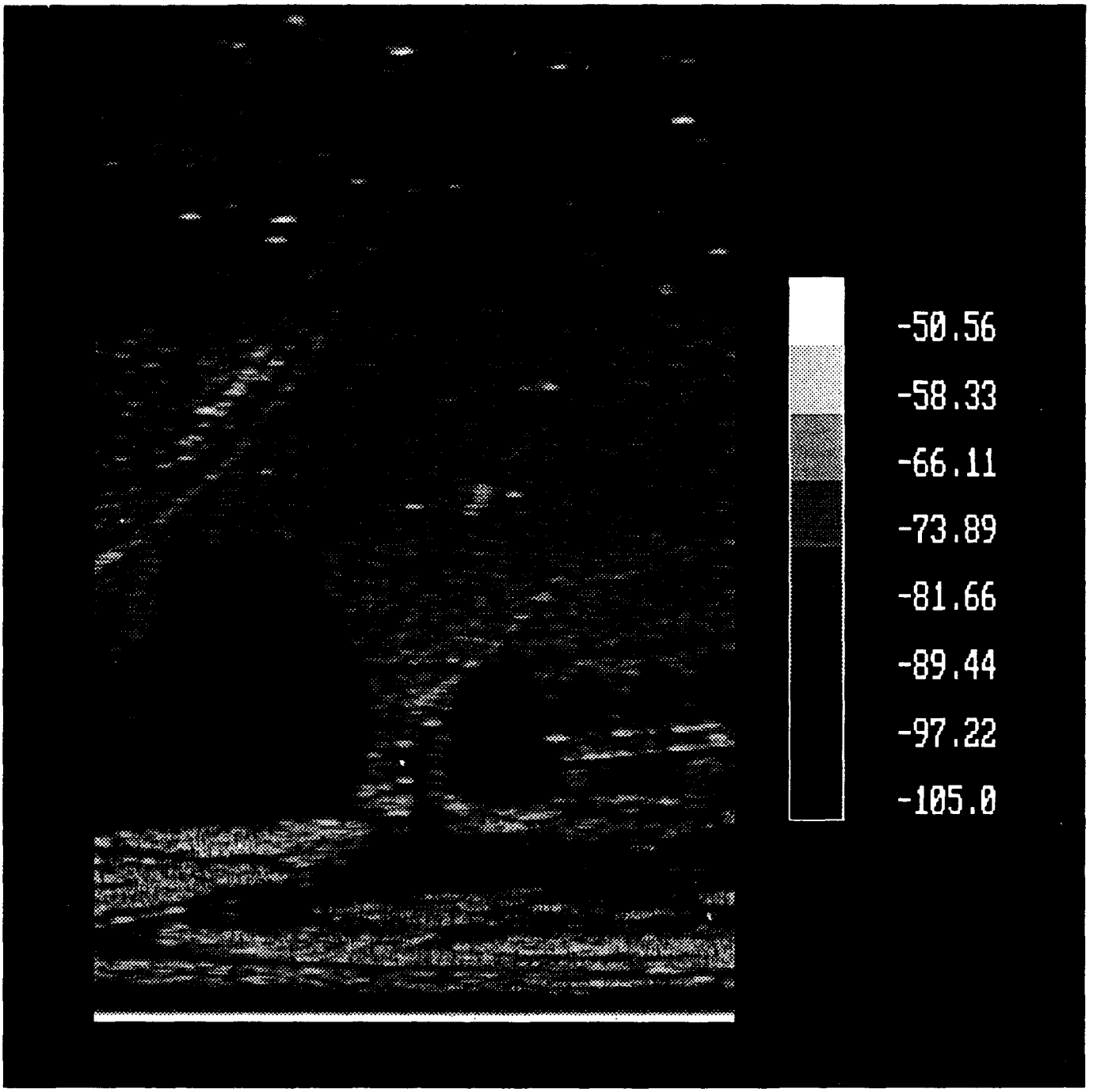

Figure C-1. Production image of 35 GHz system in fog (RVR 1.3 miles). (Run HI2R18)

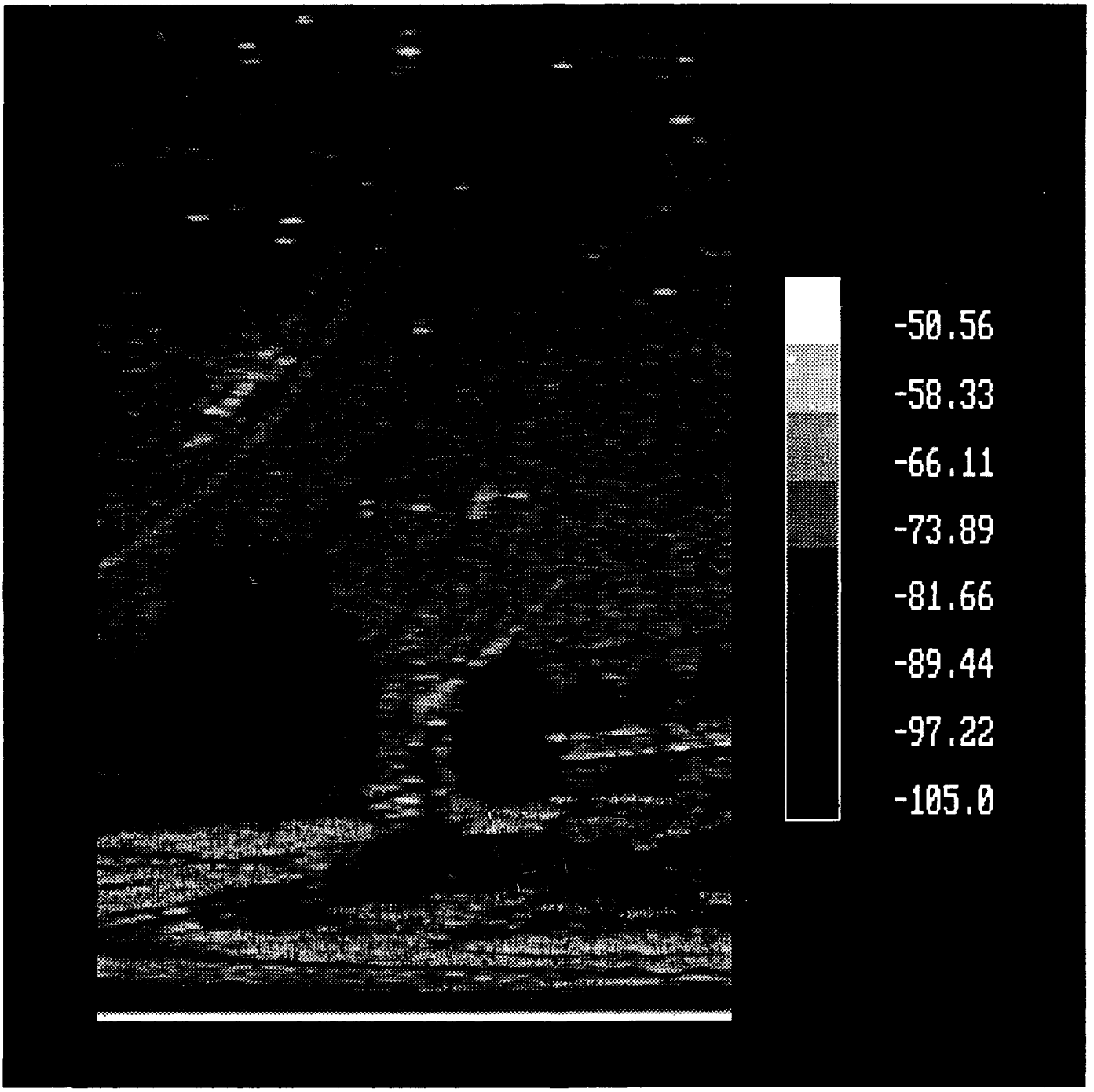

Figure C-2. Production image of 35 GHz system in medium snow. (Run HI2T09)

T09

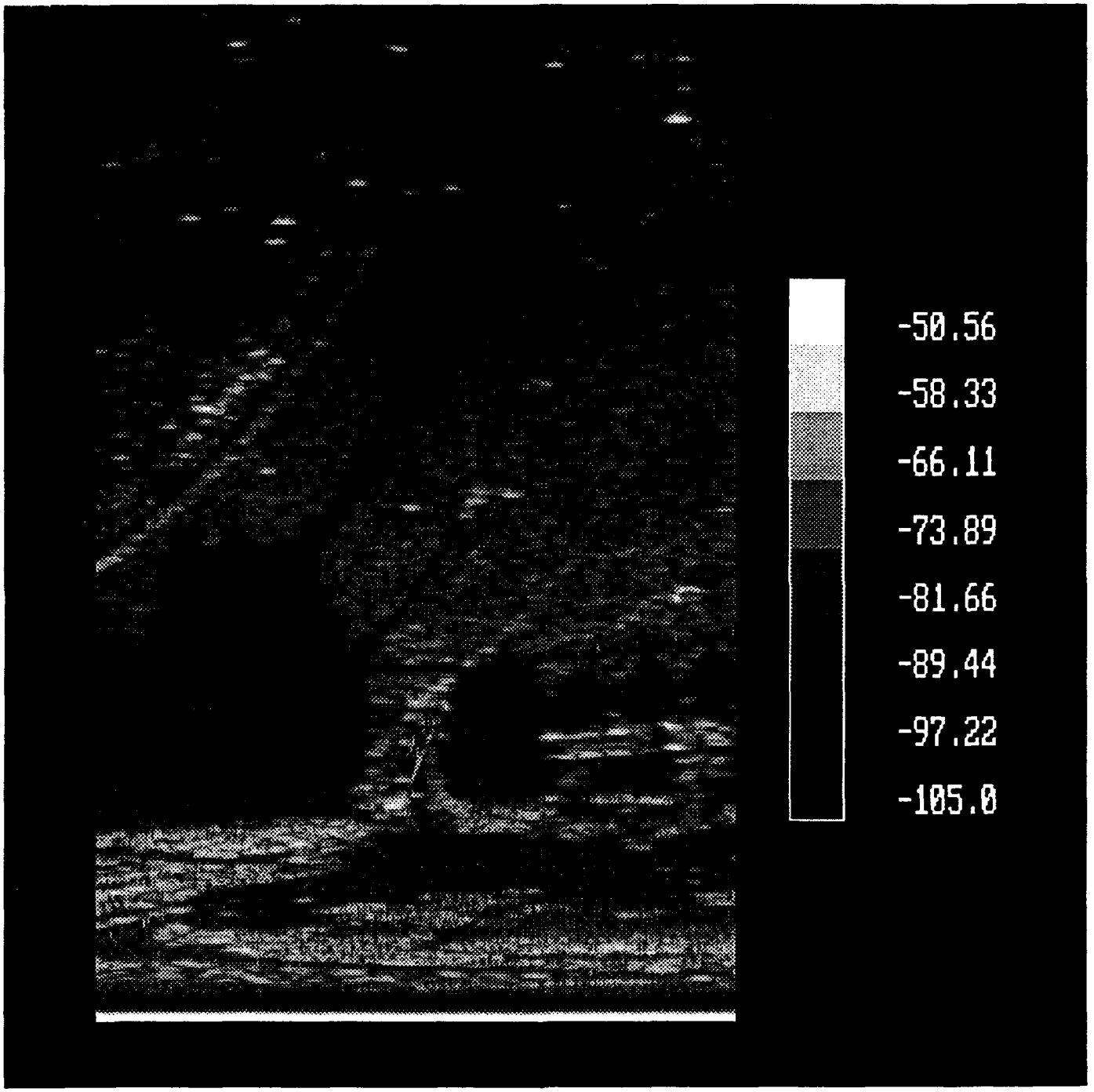

Figure C-3. Production image of 35 GHz system in light rain (1.2 mm/hr). (Run HI2R09)

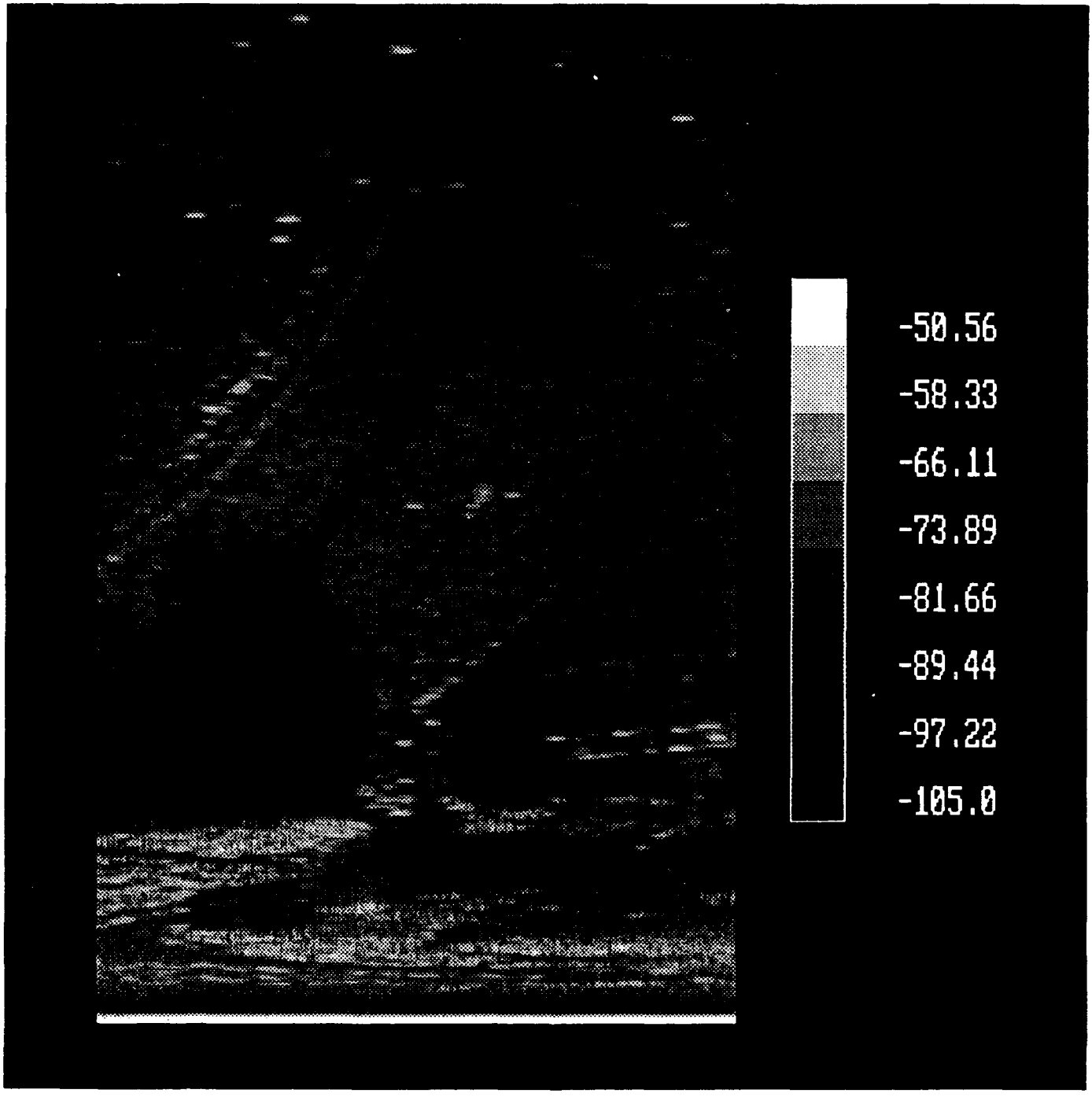

Figure C-4. Production image of 35 GHz system in medium rain (5.3 mm/hr). (Run HI2R23)

HI2R23

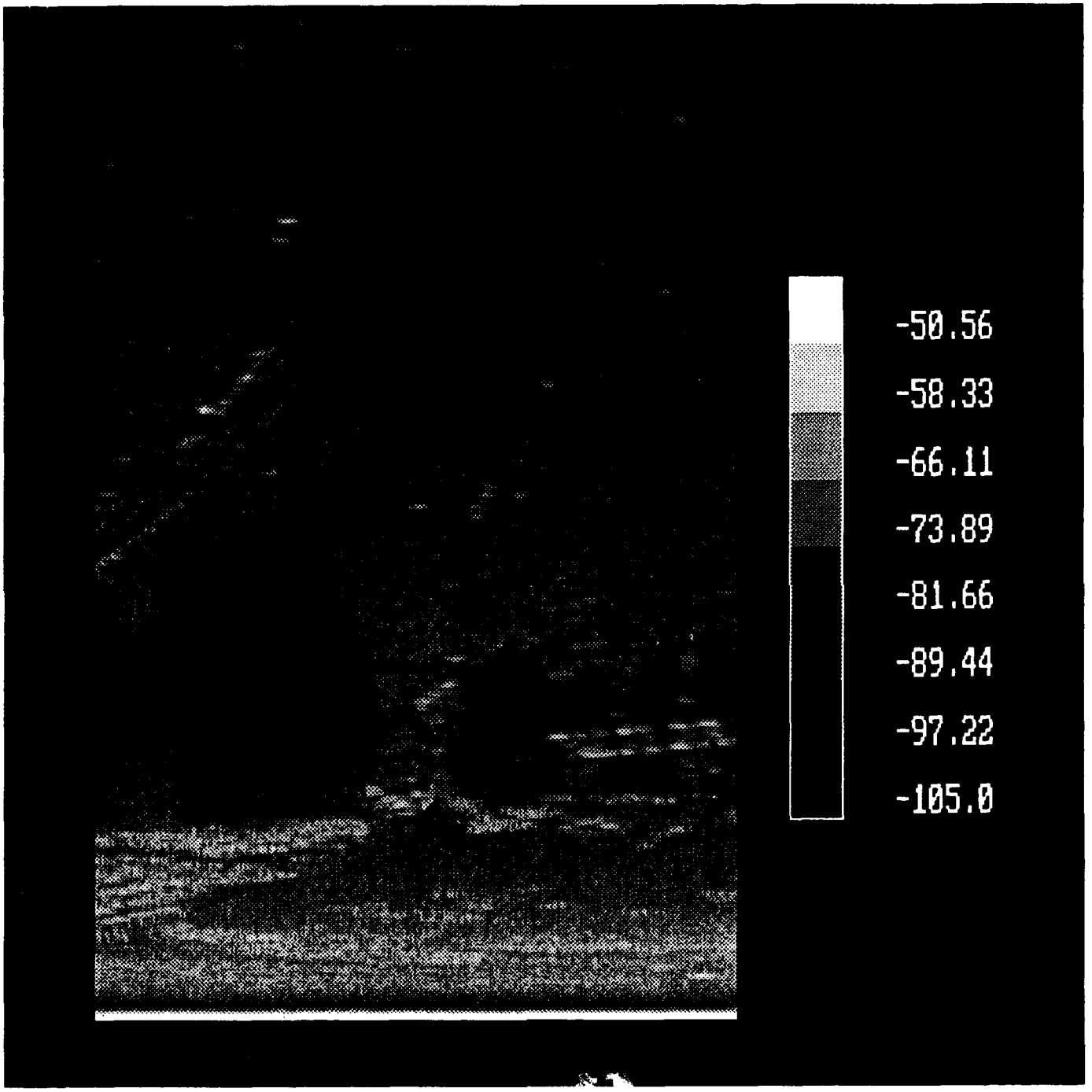

Figure C-5. Production image of 35 GHz system in heavy rain (12.9 mm/hr). (Run HI2R31)

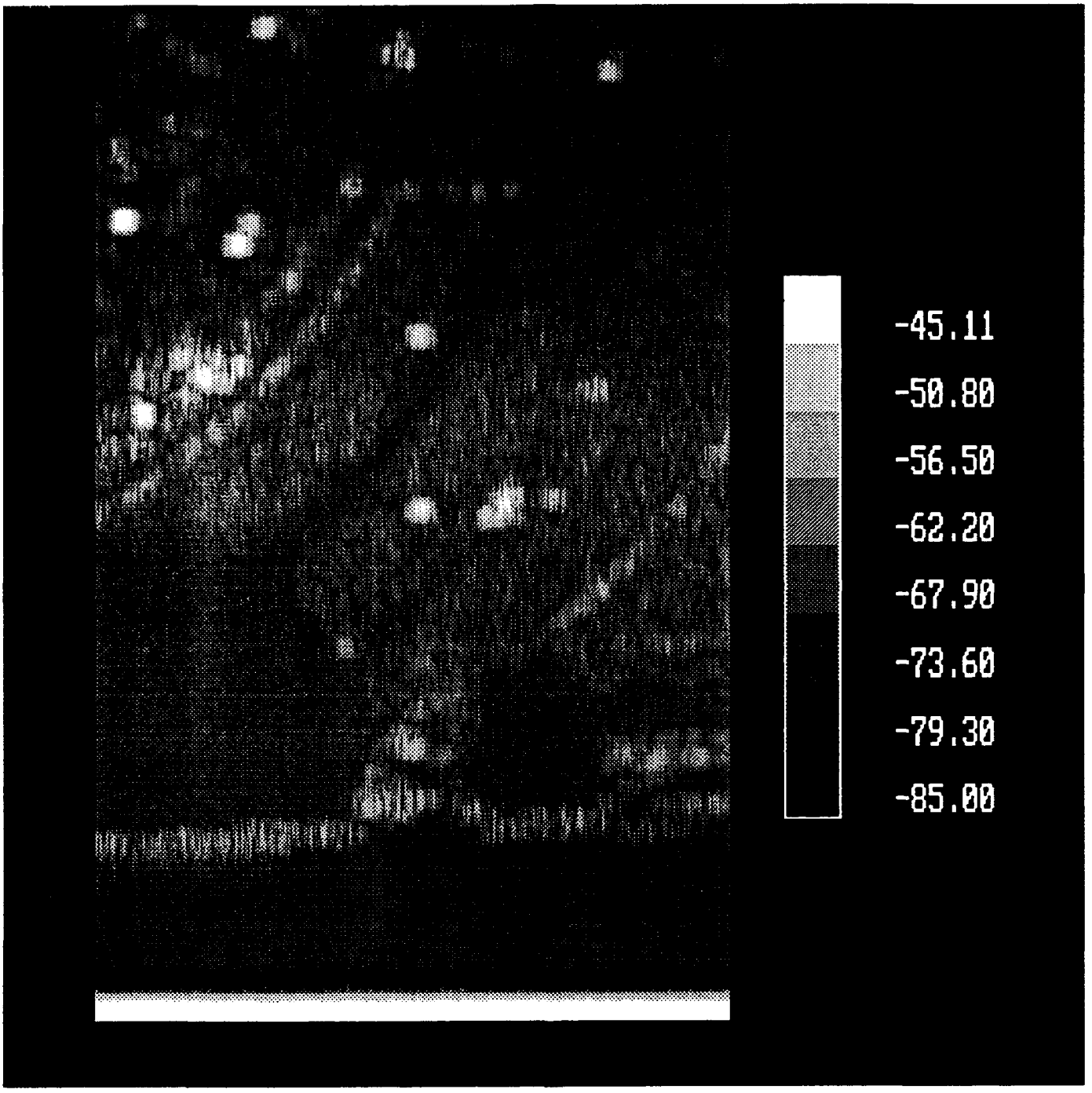

Figure C-6. Production image of 95 GHz system in clear weather (RVR 26 miles). (Run NS1R77D)

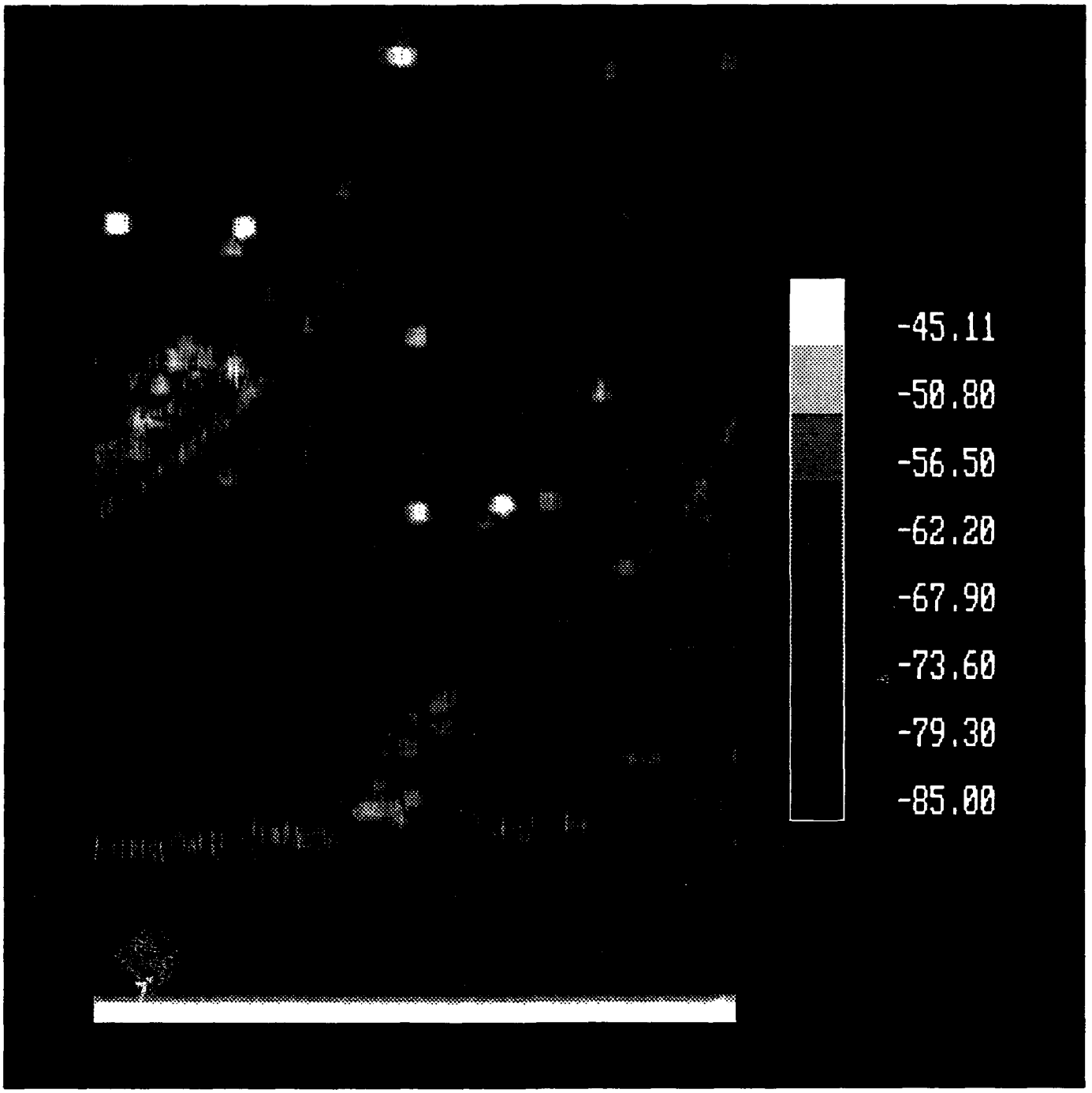

Figure C-7. Production image of 95 GHz system in fog (RVR 1.3 miles). (Run NS1R106D)

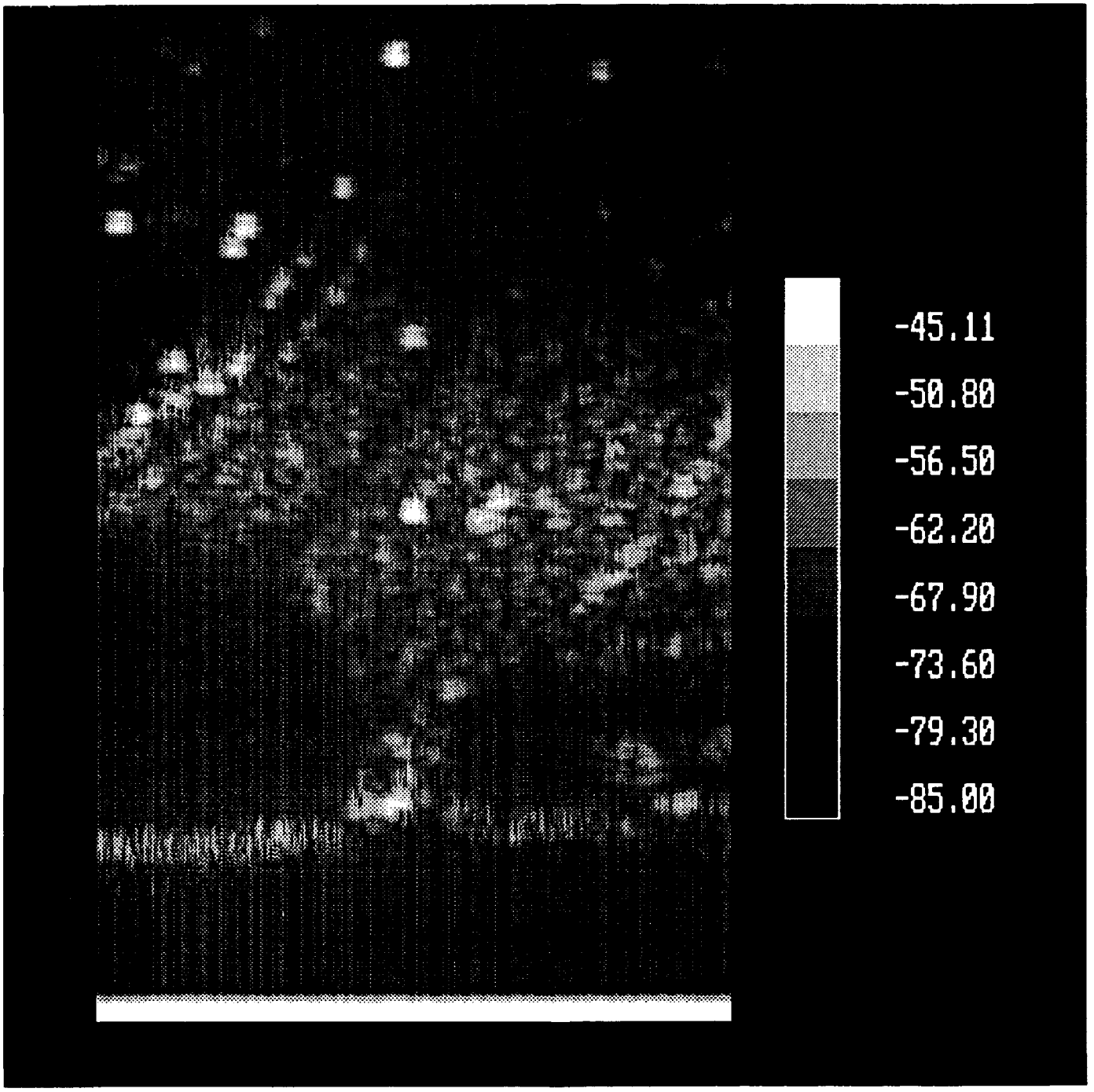

Figure C-8. Production image of 95 GHz system in medium snow. (Run NS1R151D)

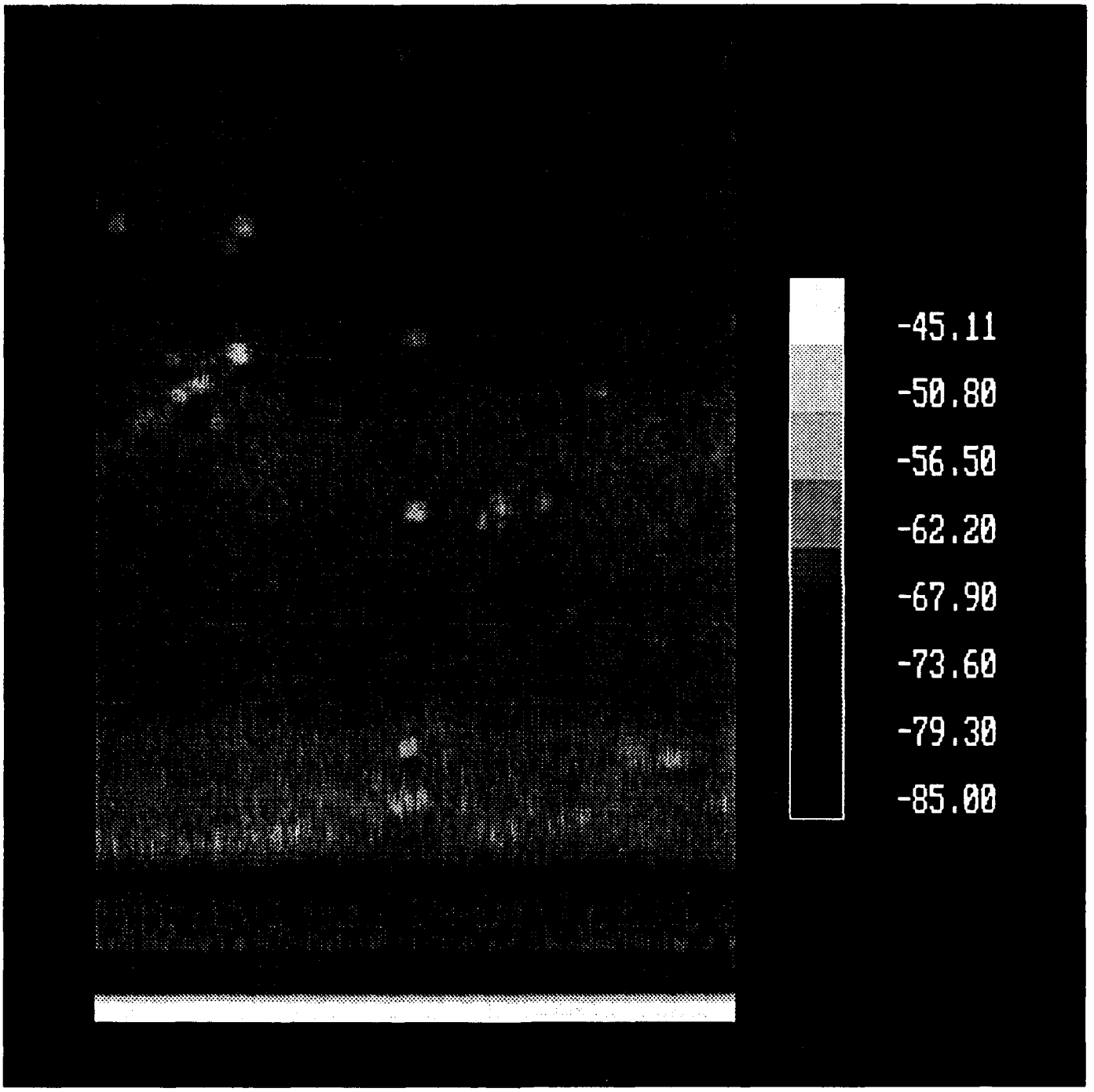

Figure C-9. Production image of 95 GHz system in light rain (1.2 mm/hr). (Run NS1R122D)

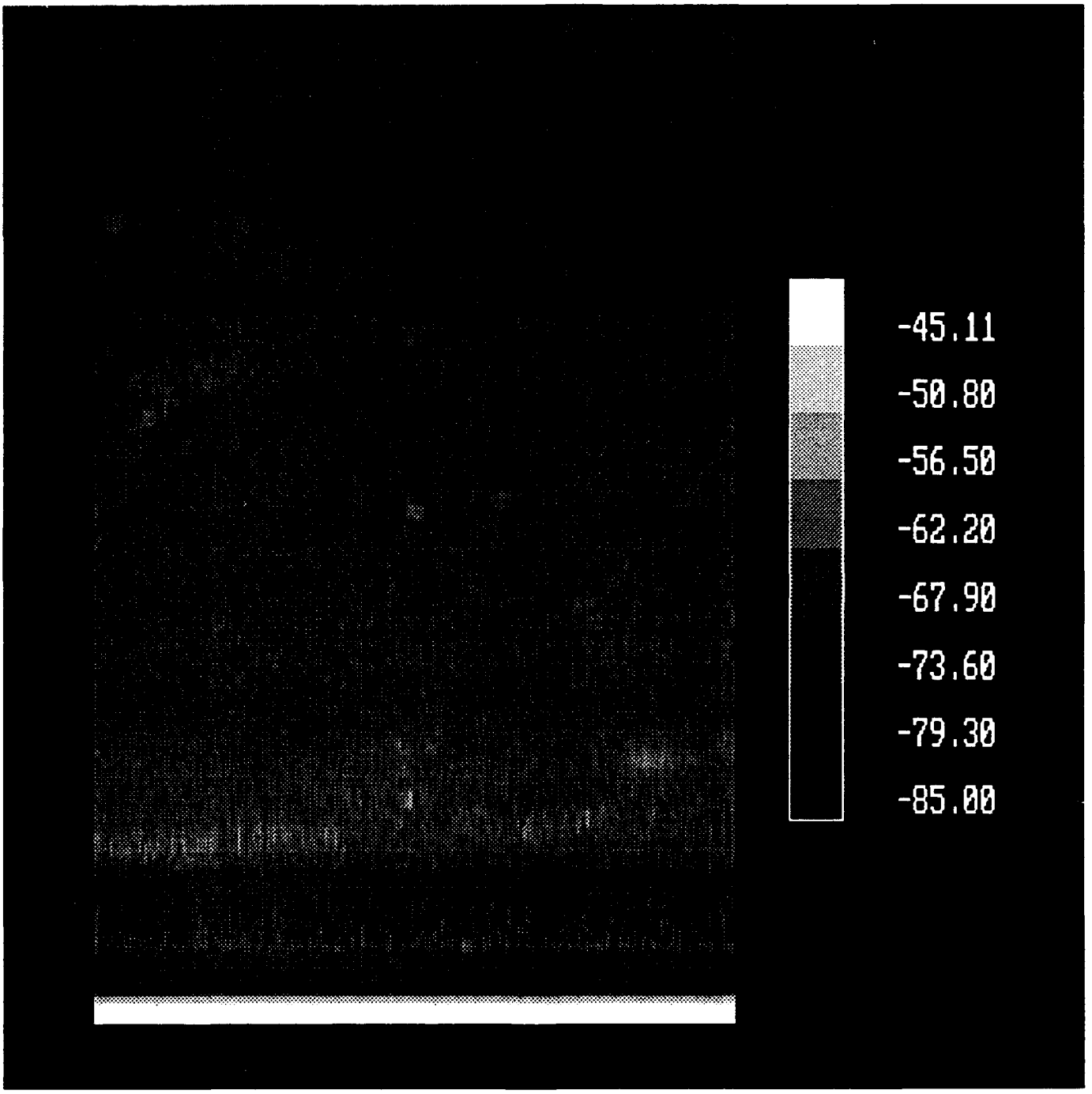

Figure C-10. Production image of 95 GHz system in medium rain (8.8 mm/hr). (Run NS1R90D)

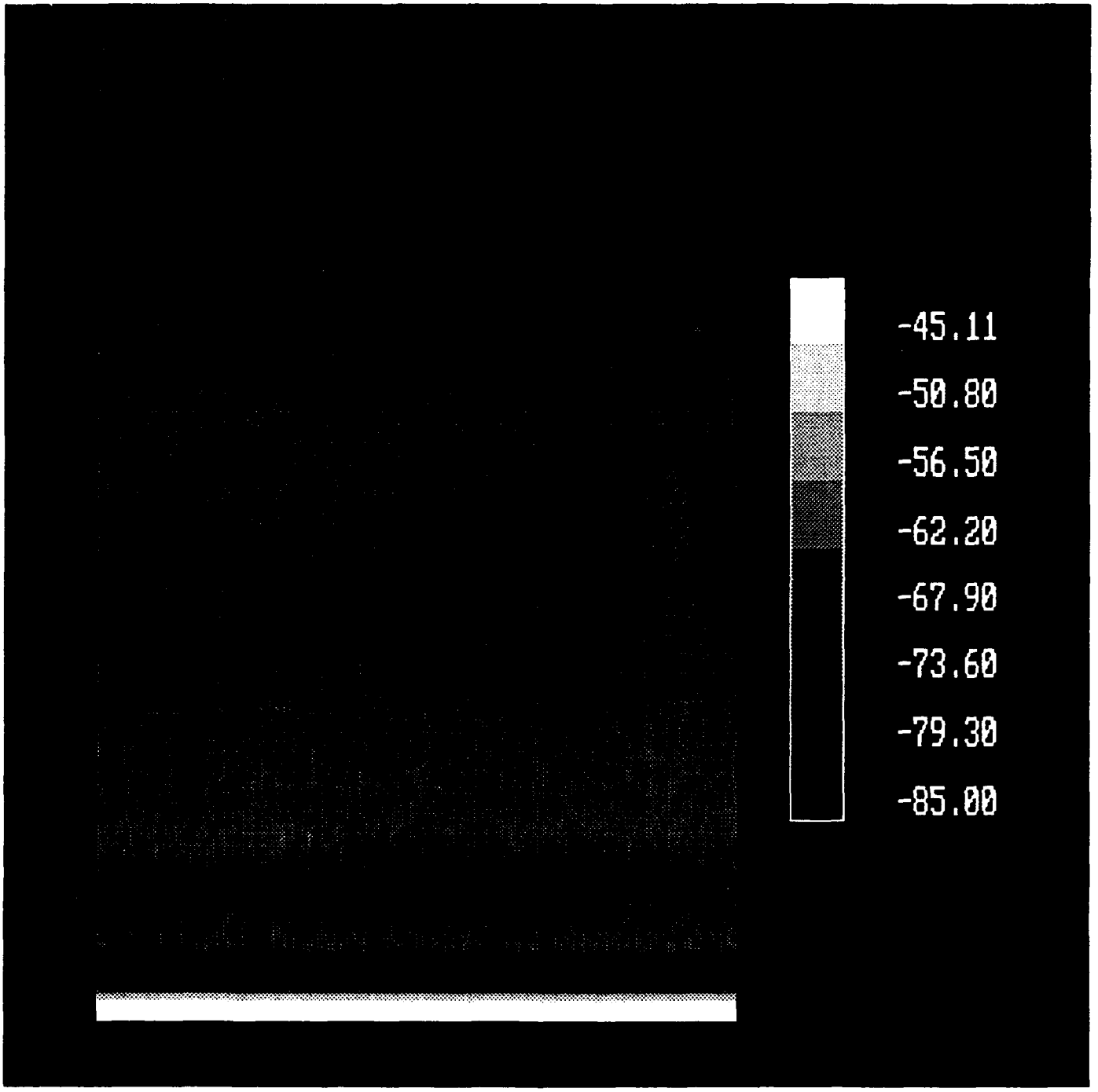

Figure C-11. Production image of 95 GHz system in heavy rain (20 mm/hr). (Run NS1R93D)

APPENDIX D
CONVERSION OF MAP COORDINATES TO DATA RESOLUTION CELLS

The question addressed in the following discussion is: given a patch which lies on top of a group of data resolution cells (see Figure D-1), which data resolution cells are totally within the boundaries of the patch?

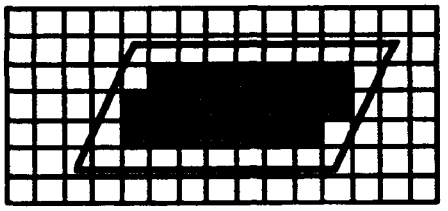

Figure D-1. Patch shape overlaying data resolution cell group.

The following procedure was used to convert from map coordinates data resolution cells.

1. input four vertices of each patch in map coordinates
2. translate map to radar coordinates x,y => r, θ
3. determine radar steps δr, $\delta\theta$
4. transform patch vertices to radar coordinates
   a. translate map coordinates into distances on the ground; i.e., use map scale factor (182.8 m / map division)
   b. perform axis translation to sensor location

      $$x' = x - x_o$$

      $$y' = y - y_o$$

      where x_o and y_o are the coordinates of the sensor.

   c. perform axis rotation to scene centerline (left-handed coordinate system) (see Figure D-2)

      $$x' = r \cos \theta$$

      $$y' = r \sin \theta$$

      where x' and y' refer to the map coordinates and r and θ refer to the radar range and angle.

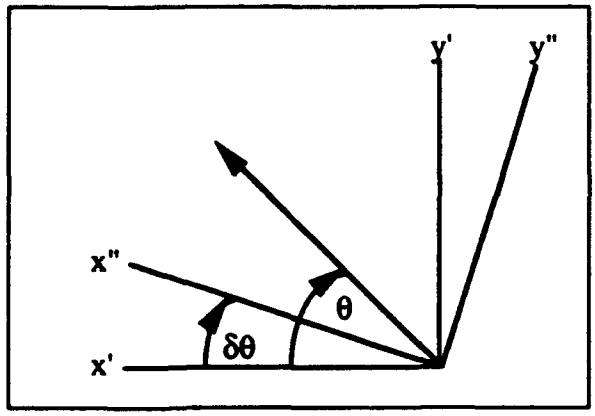

Figure D-2. Axis rotation definition.

$$x'' = r \cos(\theta - \delta\theta)$$

$$y'' = r \sin(\theta - \delta\theta)$$

where x" and y" refer to the rotated coordinate system

$$x'' = x' \cos \delta\theta + y' \sin \delta\theta$$

$$y'' = y' \cos \delta\theta - x' \sin \delta\theta$$

d. convert to polar coordinates

$$r = ((x'')^2 + (y'')^2)^{1/2}$$

if $x'' = 0 : \theta = \text{atan}(y''/x'')$

if $y'' > 0 : \theta = \pi/2$

if $y'' < 0 : \theta = 3\pi/2$

if $y'' = 0 : \theta = 0.$

5. determine radar cells to be included in patch

   a. Patch now defined by 4 vertices (v_1, v_2, v_3, v_4) in r, θ space

   b. Determine minimum and maximum values for r and θ. These values describe an annular segment within which all the valid cells must lie. (see Figure D-3)

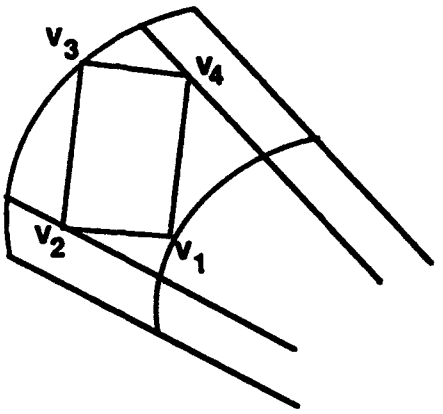

Figure D-3. Annular segment representation.

c. scan through candidate cells and determine which of these cells lie within the polygon defined by the four vertices. Method detailed in "Fundamentals of Interactive Computer Graphics" by J. D. Foley and A. van Dam, pp. 450-455.

   i. vertices must be specified in a clockwise rotation about the patch as $v_1 = x_1 , y_1 ; v_2 = x_2 , y_2 ; v_3 = x_3 , y_3 ; v_4 = x_4 , y_4$

   ii. point is defined as being inside the patch if it is to the right of the four line segments : $[v_1\ v_2]$, $[v_2\ v_3]$, $[v_3\ v_4]$, $[v_1\ v_4]$

   iii. point, p, is to the right of line segment (in left-hand coordinate system) if cross-product $[v_1\ v_2] \times [v_1\ p]$ is positive.

APPENDIX E
95 GHZ PROFILES IN WEATHER

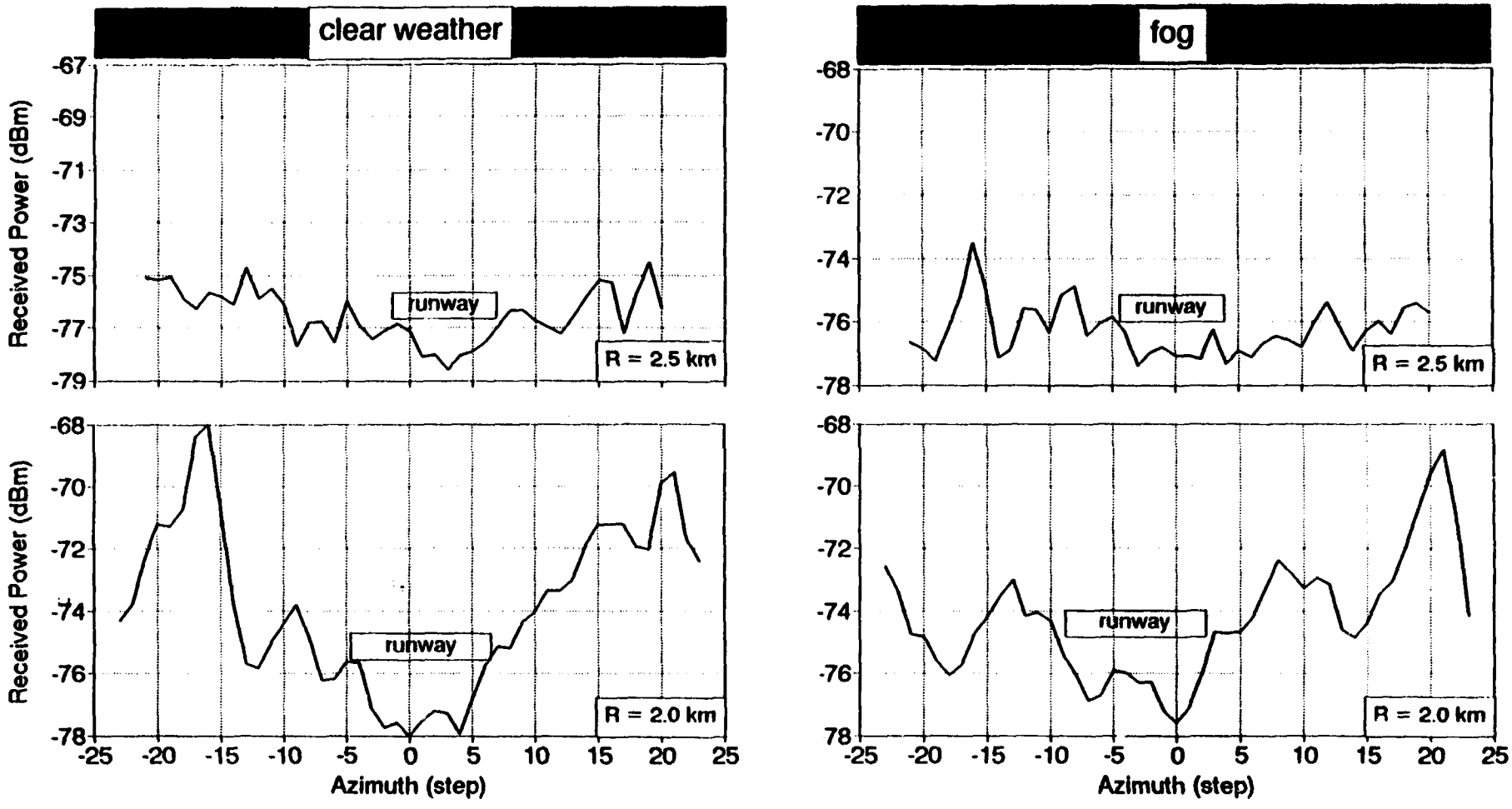

Figure E-1. Cross-range profiles for the 95 GHz radar in clear weather and fog at 2.0 and 2.5 km.

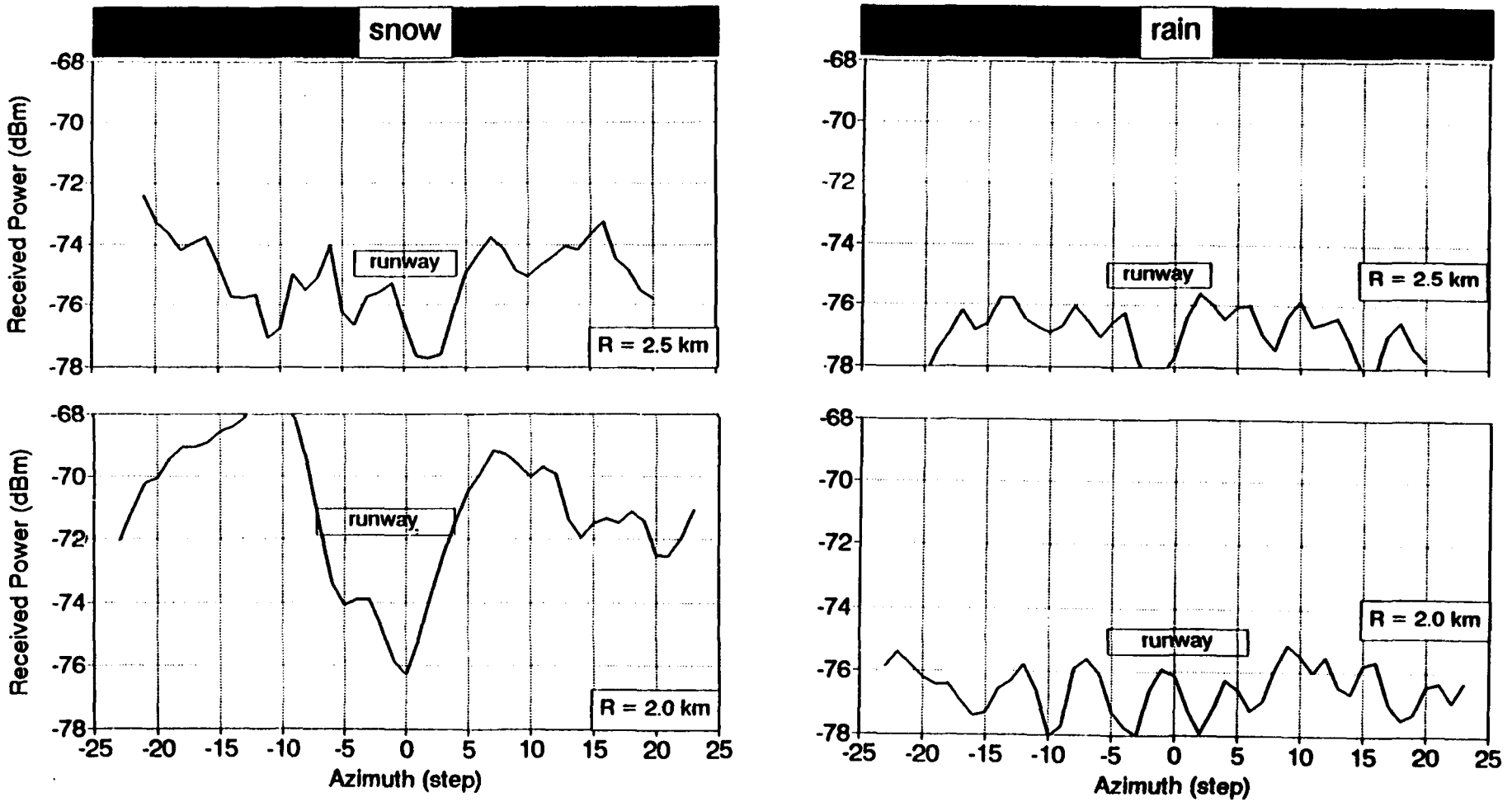

Figure E-2. Cross-range profiles for the 95 GHz radar in rain and snow at 2.0 and 2.5 km.

APPENDIX F
IR CONTRAST AND SIGNAL-VARIABILITY RATIOS
TABULAR RESULTS

TABLE F-1. CONTRAST AND SVR VALUES COMPUTED FROM IR IMAGE DATA

case	date	time	range 1710 m contrast	range 1710 m SVR	range 2380 m contrast	range 2380 m SVR	range 3300 m contrast	range 3300 m SVR
kod21	03/12	06:05	0.203	5.803	0.194	5.440	0.158	4.264
kod22	03/12	06:18	0.239	7.769	0.188	4.453	0.169	3.364
kod23	03/12	06:27	0.171	4.927	0.148	3.381	0.112	3.143
kod24	03/12	06:36	0.196	5.761	0.148	3.979	0.118	2.826
kod25	03/12	06:45	0.189	5.656	0.143	3.289	0.105	2.843
kod26	03/12	06:55	0.232	6.720	0.187	4.973	0.121	3.046
kod27	03/12	07:05	0.156	4.408	0.118	3.199	0.081	1.583
kod28	03/12	07:15	0.179	7.041	0.154	4.562	0.157	4.483
kod29	03/12	07:25	0.181	5.118	0.136	3.673	0.168	5.462
kod30	03/12	07:35	0.183	5.487	0.140	5.107	0.154	4.816
kod31	03/12	07:45	0.104	3.828	0.097	3.779	0.081	2.826
kod32	03/12	07:55	0.191	6.150	0.165	3.931	0.149	4.658
kod33	03/12	08:05	0.209	6.438	0.181	4.448	0.156	5.105
kod34	03/12	08:30	0.182	5.654	0.173	6.343	0.150	5.308
kod35	03/12	09:00	0.300	10.222	0.151	5.296	0.052	1.327
kod36	03/12	09:32	0.180	7.498	0.236	8.031	0.175	7.015
kod37	03/12	10:03	0.299	11.871	0.339	12.496	0.304	13.629
kod38	03/12	11:01	0.534	20.472	0.441	14.037	0.406	17.738
kod39	03/12	11:56	0.647	20.890	0.596	16.105	0.599	21.222
kod40	03/12	13:06	0.778	44.347	0.708	17.170	0.580	10.823
kod41	03/12	14:06	1.053	33.586	0.859	24.533	0.798	11.746
kod42	03/12	15:05	1.557	57.463	1.203	15.825	0.874	18.100
kod43	03/12	16:00	0.838	26.171	0.689	22.647	2.147	23.562
kod44*	03/12	16:59	1.783	28.530				
kod44	03/12	16:59	1.061	19.282	0.588	11.648	0.777	16.805
kod45	03/12	17:31	6.808	89.647	3.874	10.073	0.518	3.983
kod46	03/12	18:06	7.313	109.526	6.552	68.767	7.729	17.793
kod47	03/12	18:30	0.549	14.709	0.471	10.111	0.438	12.253
kod48	03/12	18:51	0.482	12.297	0.441	10.786	0.394	9.477
kod49	03/12	19:06	0.457	13.603	0.397	13.418	0.350	10.033
kod50	03/12	19:45	0.406	10.822	0.337	9.057	0.319	9.139
kod51	03/12	20:02	0.346	12.456	0.318	8.151	0.277	7.363
kod52	03/12	21:00	0.328	9.815	0.290	9.520	0.285	8.629
kod53	03/12	22:00	0.495	10.496	0.343	7.225	0.267	5.629
kod54	03/12	23:00	0.276	6.911	0.245	6.698	0.192	6.183
kod55	03/13	00:00	0.252	8.495	0.231	5.771	0.209	5.411
kod56	03/13	01:00	0.306	9.566	0.250	5.481	0.227	5.417
kod57	03/13	02:00	0.330	7.179	0.280	7.437	0.232	4.805
kod58	03/13	03:00	0.164	4.367	0.153	3.577	0.138	3.299
kod59	03/13	04:00	0.325	8.381	0.265	5.548	0.220	5.046
kod60	03/13	05:00	0.256	4.674	0.177	3.443	0.200	5.646
kod61	03/13	06:00	0.330	5.135	0.266	5.275	0.206	4.414

* measured within solar glint patch at range = 1710 meters

TABLE F-1. CONTRAST AND SVR VALUES COMPUTED FROM IR IMAGE DATA (CONTINUED)

case	date	time	range 1710 m contrast	range 1710 m SVR	range 2380 m contrast	range 2380 m SVR	range 3300 m contrast	range 3300 m SVR
kod62	03/18	11:13	0.509	14.533	0.416	14.658	0.299	4.625
kod63	03/18	11:15	0.101	7.303	0.083	6.658	0.067	3.741
kod64	03/18	11:46	0.060	3.657	0.061	5.124	0.053	2.593
kod65	03/18	13:02	0.058	3.099	0.051	3.001	0.045	1.695
kod66	03/18	13:18	0.037	2.048	0.026	1.888	0.005	0.271
kod67	03/18	13:45	0.026	1.555	0.010	0.721	-0.004	-0.146
kod68	03/18	14:00	-0.005	-0.343	0.013	0.941	-0.004	-0.207
kod69	03/18	14:15	-0.002	-0.185	0.009	0.680	0.010	0.353
kod70	03/18	14:30	0.014	0.608	0.003	0.215	-0.000	-0.009
kod72	03/30	08:38	0.000	0.000	0.000	0.000	0.000	0.000
kod73	03/30	08:51	0.000	0.000	0.000	0.000	0.000	0.000
kod74	03/30	09:04	0.000	0.000	0.000	0.000	0.000	0.000
kod75	03/30	09:52	0.000	0.000	0.000	0.000	0.000	0.000
kod76	03/30	10:18	-0.013	-0.746	-0.013	-0.746	-0.013	-0.746
kod77	03/30	10:33	0.000	0.000	0.000	0.000	0.000	0.000
kod78	03/30	10:53	0.000	0.000	0.000	0.000	0.000	0.000
kod79	03/30	11:16	0.000	0.000	0.000	0.000	0.000	0.000
kod80	03/30	11:33	0.012	0.702	0.029	1.538	0.023	1.138
kod81	03/30	11:47	0.017	1.273	0.022	1.167	0.010	0.623
kod82	03/30	12:03	0.000	0.000	0.000	0.000	0.000	0.000
kod83	03/30	12:17	0.000	0.000	0.000	0.000	0.000	0.000
kod84	03/30	13:41	-0.000	-0.029	-0.000	-0.029	-0.000	-0.029
kod85	03/30	14:15	-0.004	-0.311	0.013	0.527	0.004	0.172
kod86	03/30	14:31	0.003	0.224	0.003	0.224	0.003	0.224
kod87	03/30	14:47	0.008	0.578	0.008	0.578	0.008	0.578
kod88	04/18	08:45	0.016	2.388	0.000	0.000	0.009	0.785
kod89	04/18	09:03		1.256		1.979		1.847
kod90	04/18	09:21		1.613		2.890		3.813
kod91	04/18	09:42		1.820		1.886		1.715
kod94	04/18	10:51	-0.018	-0.353	-0.015	-2.334	-0.011	-1.559
kod95	04/18	11:45		-2.983		-2.792		-1.831
kod97	04/21	06:57	0.000	0.000	0.000	0.000	0.000	0.000
kod98	04/21	07:16	0.000	0.000	0.000	0.000	0.000	0.000
kod99	04/21	07:40	0.013	2.109	0.017	1.911	0.011	1.689
kod101	04/21	09:33	-0.043	-6.401	-0.040	-5.208	-0.021	-2.338
kod102	04/21	10:32		2.095		-0.019		0.792
kod103	04/21	10:44		4.361		5.227		2.842
kod110	05/27	07:01	0.274	22.692	0.281	24.811	0.260	14.237
kod112	05/27	08:47	0.315	31.155	0.326	31.464	0.293	25.438
kod115	05/27	11:30	0.766	43.992	0.748	54.857	0.664	24.811
kod117	05/27	13:01	1.057	114.346	1.092	78.059	0.906	45.719
kod119	05/27	15:07	1.207	127.533	1.139	101.291	1.460	22.521
kod129	05/27	20:41	0.550	42.494	0.556	64.880	0.528	16.871
kod130	05/27	21:03	0.877	46.795	0.860	38.218	0.803	35.892
kod131	05/27	21:30	0.691	49.867	0.869	29.976	0.703	36.394
kod134	05/28	00:00	0.687	28.255	0.798	28.701	0.722	31.671
kod137	05/28	03:00	0.606	19.537	0.710	49.657	0.592	12.125
kod140	05/28	06:00	0.604	29.700	0.671	46.492	0.571	14.765

TABLE F-2. RESULTS OF DATA ANALYSIS FOR BASELINE IR MEASUREMENTS

date	03/12/92		SVR Range			
name	time	vis (km)	1710 m	2380 m	3300 m	dT degC
k021	06:05	22.5	5.803	5.440	4.264	-1.64
k022	06:18	27.2	7.769	4.453	3.364	-1.91
k023	06:27	20.1	4.927	3.381	3.143	x
k024	06:36	19.2	5.761	3.979	2.826	-2.16
k025	06:45	13.8	5.656	3.289	2.843	-2.23
k026	06:55	19.6	6.720	4.973	3.046	-2.44
k027	07:05	12.4	4.408	3.199	1.583	-2.38
k028	07:15	32.1	7.041	4.562	4.483	-2.20
k029	07:25	39.8	5.118	3.673	5.462	-1.97
k030	07:35	38.8	5.487	5.107	4.816	-1.61
k031	07:45	36.6	3.828	3.779	2.826	-1.07
k032	07:55	35.5	6.150	3.931	4.658	-0.90
k033	08:05	41.4	6.438	4.448	5.105	-0.52
k034	08:30	30.8	5.654	6.343	5.308	0.17
k035	09:00	55.5	10.222	5.296	1.327	1.37
k036	09:32	75.6	7.498	8.031	7.015	4.24
k037	10:03	59.1	11.871	12.496	13.629	5.43
k038	11:01		20.472	14.037	17.738	5.92
k039	11:56	79.7	20.890	16.105	21.222	4.49
k040	13:06	94.8	44.347	17.170	10.823	6.18
k041	14:06	76.6	33.586	24.533	11.746	7.22
k042	15:05	95.4	57.463	15.825	18.100	7.52
k043	16:00	62.9	26.171	22.647	23.562	3.55
k044s	16:59	77.6	28.530	x	x	2.56
k044n	16:59	77.6	19.282	11.648	16.805	2.56
k045	17:31	73.6	89.647	10.073	3.983	2.98
k046	18:06	72.2	109.526	68.767	17.793	1.34
k047	18:30	77.6	14.709	10.111	12.253	1.34
k048	18:51	71.2	12.297	10.786	9.477	0.87
k049	19:06	74.0	13.603	13.418	10.033	0.95
k050	19:45	64.4	10.822	9.057	9.139	0.22
k051	20:02	78.8	12.456	8.151	7.363	-0.05
k052	21:00	61.9	9.815	9.520	8.629	-1.45
k053	22:00	53.9	10.496	7.225	5.629	-1.21
k054	23:00	54.8	6.911	6.698	6.183	-1.41
k055	24:00	77.6	8.495	5.771	5.411	-1.80
k056	25:00	46.4	9.566	5.481	5.417	-2.61
k057	26:00	34.8	7.179	7.437	4.805	-2.70
k058	27:00	15.4	4.367	3.577	3.299	-2.57
k059	28:00	43.0	8.381	5.548	5.046	-3.17
k060	29:00	46.1	4.674	3.443	5.646	-3.32
k061	30:00	46.9	5.135	5.275	4.414	-3.42

TABLE F-2. RESULTS OF DATA ANALYSIS FOR BASELINE IR MEASUREMENTS (CONT)

date 05/27/92			SVR			
		vis		Range		dT
name	time	(km)	1710 m	2380 m	3300 m	degC
k110	07:01	2.7	22.692	24.811	14.237	1.44
k112	08:47	11.9	31.155	31.464	25.438	3.01
k115	11:30	22.8	43.992	54.857	24.811	8.26
k117	13:01	32.5	114.346	78.059	45.719	11.63
k119	15:07	41.0	127.533	101.291	22.521	12.49
k129	20:41	63.2	42.494	64.880	16.871	6.86
k130	21:03	63.7	46.795	38.218	35.892	7.11
k131	21:30	41.2	49.867	29.976	36.394	7.09
k134	24:00	25.8	28.255	28.701	31.671	5.25
k137	27:00	12.0	19.537	49.657	12.125	5.09
k140	30:00	8.1	29.700	46.492	14.765	4.25

TABLE F-3. TABULATED RESULTS OF ANALYSIS OF LOW VISIBILITY DATA

date	03/18/92		rain	--- fog ----		--- rain ----		-------SVR--------			
name	time	vis km	rate mm/hr	kext (1/km)	rng98 (km)	kext (1/km)	rng98 (km)	1710	2380	3300	dT deg C
k062	11:13	10.22	0.59	0.015	253.0	0.257	15.2	14.53	14.65	4.62	0.57
k063	11:15	9.99	0.00	0.017	222.7	0.000	inf	7.30	6.65	3.74	0.42
k064	11:46	8.13		0.017	221.6			3.65	5.12	2.59	0.08
k065	13:02	4.27	1.76			0.515	7.5	3.09	3.00	1.69	0.03
k066	13:18	3.23						2.04	1.88	0.27	-0.09
k067	13:45	2.37	5.87			1.102	3.5	1.55	0.72	-0.14	-0.28
k068	14:00	2.28	9.39			1.477	2.6	-0.34	0.94	-0.20	-0.11
k069	14:15	2.20	9.39			1.477	2.6	-0.18	0.68	0.35	-0.31
k070	14:30	2.57	8.22			1.360	2.8	0.60	0.21	-0.01	-0.22

date	03/30/92		rain	--- fog ----		--- rain ----		-------SVR--------			
name	time	vis	rate	kext	rng98	kext	rng98	1710	2380	3300	dT
k072	08:38	1.50*						0.00	0.00	0.00	0.11
k073	08:51	0.61*						0.00	0.00	0.00	0.18
k074	09:04	0.59						0.00	0.00	0.00	0.23
k075	09:52	0.94	2.93					0.00	0.00	0.00	0.52
k076	10:18	2.82	4.69			0.957	4.1	-0.74	-0.74	-0.74	0.16
k077	10:33	3.16	5.28			1.031	3.7	0.00	0.00	0.00	0.51
k078	10:53	4.18	1.76			0.515	7.5	0.00	0.00	0.00	0.42
k079	11:16	4.45	0.00			0.000	inf	0.00	0.00	0.00	0.25
k080	11:33	7.42						0.70	1.53	1.13	0.09
k081	11:47	8.20	0.59			0.257	15.2	1.27	1.16	0.62	0.13
k082	12:03	3.53	8.22			1.360	2.8	0.00	0.00	0.00	-0.01
k083	12:17	4.27	6.46			1.170	3.3	0.00	0.00	0.00	0.52
k084	13:41	5.04	6.46			1.170	3.3	-0.02	-0.02	-0.02	0.03
k085	14:15	5.36	3.52			0.799	4.8	0.31	0.52	0.17	0.28
k086	14:31	5.41	2.93			0.712	5.4	0.22	0.22	0.22	0.19
k087	14:47	4.49						0.57	0.57	0.57	-0.10

date	04/18/92		rain	--- fog ----		--- rain ----		-------SVR--------			
name	time	vis	rate	kext	rng98	kext	rng98	1710	2380	3300	dT
k088	08:45							2.38	0.00	0.78	
k089	09:03							1.25	1.97	1.84	
k090	09:27							1.61	2.89	3.81	
k091	09:42							1.82	1.88	1.71	
k094	10:51	3.5	1.89	0.298	13.1	0.540	7.2	-0.35	-2.33	-1.55	2.03
k095	11:45	2.9	0.50	0.348	11.2	0.231	16.9	-2.98	-2.79	-1.83	2.29

date	04/21/92		rain	--- fog ----		--- rain ----		-------SVR--------			
name	time	vis	rate	kext	rng98	kext	rng98	1710	2380	3300	dT
k096	06:43	14.41	0.22	0.006	601.6	0.139	28.2				2.05
k097	06:57	10.92	3.28	0.006	630.2	0.764	5.1	0.00	0.00	0.00	1.79
k098	07:16	9.77	2.69	0.012	313.6	0.676	5.7	0.00	0.00	0.00	1.60
k099	07:40	24.18	0.29	0.001	2283.5	0.163	23.9	2.10	1.91	1.68	1.69
k100	08:30	11.93	3.02	0.001	2014.7	0.726	5.3				1.66
k101	09:33	12.12	0.82	0.001	2800.8	0.318	12.3	-6.40	-5.20	-2.33	1.69
k102	10:32	22.84	0.69	0.000	6036.7	0.284	13.7	2.09	-0.01	0.79	1.68
k103	10:44	27.75	0.04	0.000	4545.9	0.050	78.9	4.36	5.22	2.84	2.04

* visibility from hssvis - all other visibility values from lpv

APPENDIX G

TOWER TEST PLAN
FOR
EVALUATION OF IMAGING SENSORS

Tower Test Plan

for

Evaluation of Imaging Sensors

Autonomous Landing Guidance (ALG) Program
Synthetic Vision Technology Demonstration (SVTD) Program

Prepared By:

Controls Systems Development Branch
Flight Control Division
Flight Dynamics Directorate
Wright Laboratory OH

Date Prepared: 3 May 1991

TABLE OF CONTENTS

1.0 Test Program Information

Principle Programs	Job Order Number
Autonomous Landing Guidance Tower Tests	24030700
Synthetic Vision Sensor Program	24030744

Responsible Test Organization: WL/FIGL, WPAFB OH

Participating Test Organization: WL/AARI, WL/WEA

2.0 Introduction/Background

One of the major limitations of aircraft is the difficulty of conducting terminal area operations in adverse weather environments. Conditions involving high, gusting or rapidly changing winds may impose almost insurmountable physical restrictions, however, operations in fog, rain, snow, smoke and haze are limited primarily by the lack of pilot vision. At established airports the visibility limitation for approach and landing operations is partially overcome by the excellent landing guidance systems now available albeit very expensive, but at unequipped facilities and for specialized missions, (particularly military) the pilot must still rely primarily on his ability to see. Also, aircraft taxi and ground operations are severely hampered by low visibility conditions with no current operational systems available to assist the pilot.

In the recent past, several programs have undertaken to augment the pilots' vision by providing them with a real-time forward view generated by video systems such as Low Light Level Television and Infrared Cameras. One series of experiments was conducted with a millimeter wavelength (MMW) imaging system. At least one of these systems is now being applied in different forms on specialized aircraft. The advent of the Head Up Display where the images can be superimposed over the outside scene, along with new advances in imaging technology have caused renewed interest in using imaging sensors to augment pilot vision.

Results from these experiments along with simulations and other studies have indicated that those imaging sensors operating in the MMW band offer the best weather penetration capability but, in practice, exhibit limited resolution (due to practical antenna aperture limits). Those operating in the Infrared (and visible) wavelengths show good resolution but appear to have comparatively poor weather penetration. Choice of the sensor system features, i.e. wavelength, for a particular application, therefore, involves compromises which are best resolved by a scientifically documented comparison of the performance of the systems in relevant weather scenarios.

The experiments described in this document are intended to contribute to the database needed by the aviation community for their use in identifying requirements and technology capability for landing guidance application(s) and to assist in further development of imaging sensors. This will be accomplished by gathering and comparing definitive sensor performance data at different wavelengths of specific "targets" under documented meteorological conditions, and by providing resultant engineering test data to the aviation community to aid in the design and optimization of the next generation of real-time sensors.

Testing will be carried out at the Air Force Avionics Directorate, Wright-Patterson AFB on the tenth floor of building 620. The test site is a fully enclosed 18 foot by 18 foot room that provides an opportunity to test landing systems in a "suspended approach position" overlooking an active runway and taxiway. Analysis of the data will be performed by a tower test contractor familiar with millimeter wave technology.

3.0 Test Objectives

3.1 Program Objective

The program objective is to conduct a carefully documented comparative evaluation of existing brassboard or prototype imaging sensors under low visibility weather conditions and to establish a sensor performance database providing a benchmark of the capability for the technology state for use by the operational, manufacturing and regulatory elements of the aviation community. This work, to be accomplished in an instrumented tower test facility and range, involves collection of sensor output data (sensor performance and imagery) and atmospheric parameters which characterize the visibility between the sensor and various targets being viewed. The data analysis and evaluation results will be based on analyses of sensor performance data (and, if available, processed image quality) and meteorological data collected by the government in low visibility weather conditions caused by fog, rain and snow (with and without accumulation).

3.2 Test Objectives

A. Collect uniform sets of sensor return data on runways, taxiways and other relevant targets such as calibration targets and runway obstructions under a spectrum of low visibility weather conditions and at low grazing angles.

B. Collect meteorological data from multiple locations on the test range simultaneously during sensor system operation.

C. Analyze and compare relevant system parameters in terms of the fundamental sensor data and the processed image quality to determine the performance of the sensor in low visibility weather conditions; to measure and better define the sensor performance degradation caused by fog, rain and snow; to compare the sensor performance achieved against the landing system requirements specified in the Program Research and Development Announcement (PRDA) #89-04-PMRN; and to compare the sensor performance achieved among the sensors tested.

4. 0 Test Approach & Operations

4.1 Test Philosophy

These tests are intended to benefit all participants (the Air Force, the SVTD Program Office, all Sensor Vendors and elements of the aviation community including operators, manufacturers and regulators). In addition to satisfying the test objectives, the aviation community will find the data useful in determining system parameters that are influenced by specific weather conditions, and in determining basic parameters, e.g. cross section and emissivity of relevant materials, to more accurately predict system performance. The Air Force and the SVTD Program Office will use the data to evaluate systems and to acquire data that can be used to extrapolate the results to common weather conditions and compare image quality of various sensor technologies.

This test plan identifies certain tests and measurements which are required to assure that data from each tower test is taken under known conditions and can be evaluated with known references. In addition, data formats and media are delineated so that all participants will have access to the equivalent "raw" data.

Test conclusions will be based on an evaluation of the sensor performance data acquired from each sensor obtained under a variety of weather conditions. In addition, fundamental physical data about the scene materials at low depression angles will be obtained. Past studies have indicated the imaging systems of interest operate at millimeter wave (MMW) or infrared (IR) wavelengths so the test plan considers only those wavelengths.

4.2 Test Program

The Tower Test Program will be directed by a government Tower Test Director (TTD) designated by the Wright Laboratory Flight Control Division Chief (WL/FIG). The TTD will be in charge of all sensor tests conducted under this plan and will be responsible for ensuring compliance with all specified testing procedures and will ensure that the needs of the ALG and SVTD programs are met. A Tower Test Contractor (TTC) will support the TTD and will be tasked to conduct all tower testing operations required to collect the sensor performance data and to analyze and report the test results.

There are several types of testing that will be accomplished under this plan. Some initial informal testing using existing Air Force owned sensors will be conducted to establish baseline performance of test equipment, calibration targets, environmental sensors and activation procedures. This testing will also help in refining procedures, data recording methodology, data reduction and analysis. The formal testing addressed in this plan will last about one year and is designed to support the objectives of both the Autonomous Landing Guidance (ALG) program and the Synthetic Vision Technology Demonstration (SVTD) program.

The first type of formal testing involves millimeter wave sensors being developed for the joint DoD/FAA/Industry Synthetic Vision project.

The second type of formal testing involves promising sensors provided by Vendors selected to participate through a Fixed-Price sub-contract which provides only limited funds to offset any sensor vendor incurred expenses. By early 1992, the SVTD project must decide on a sensor to be used as a functional prototype. Testing of promising sensors will continue until the end of the Test Program to allow collection of as much data as possible in low visibility weather conditions and to collect data to contribute to the engineering performance data base.

The Tower Test Director (TTD) will coordinate the scheduling of all testing and resolve any conflicts. The TTD will maintain a tower test schedule that will include specific dates and vendors consistant with contractual commitments.

4.3 Test Approach

The complete ALG/SVTD Tower Test Program will be referred to in a single term as the EVALUATION and will consist of several individual sensor TESTS lasting up to 12 months. Each TEST will consist of a nominal two week baseline recording period followed by several DATA RUNS of the same sensor under varying weather conditions. The test procedures outlined below will be followed completely. This is a firm requirement to ensure a consistent and equally thorough evaluation of each representative test item. Due to the lack of space in the tower and limited data collection capability, tests of each sensor will normally be conducted individually.

4.3.1 Measurements

There are two major groups of measurements that will be recorded during each test period. The first group consists of system particular measurements and can be further broken down into one-time system descriptive measurements (ie power output, receiver sensitivity, etc..) and sensor performance data acquired during each data run. The second group consists of data on the atmospheric and ground surface conditions that are required to completely describe the environment over which the system is being tested.

Sensor data will be recorded only by the Tower Test Contractor during sensor testing. All data will be submitted to the Air Force for distribution to appropriate government and participating vendors. In addition, the Air Force will supply to the Sensor Vendor a copy of the weather information acquired during testing.

4.3.2 Minimum Test Requirements

For a successful test of a sensor system, sensor performance data must be gathered simultaneously with the meteorological data as listed in Section 9.1. The sensor test will, at a minimum, document 12 complete data runs for four different weather conditions at 3 data runs each. A minimum of 5 images/scans will be recorded for each data run within a 30 minute period. The first weather condition is in clear air for baseline testing. The second condition is during fog, the third is during rain and the fourth is during snow. For the last three conditions, the

prevailing visibility needs to be between 0 to 1 1/2 miles. The calibration of the sensor and scene will be made so that fundamental data and image evaluations can be produced as listed in Section 9.4.

4.4 Test Operation

The Tower Test Director (TTD) is responsible for all phases of sensor system testing. The Tower Test Contractor (TTC) is responsible for carrying out the directions from the TTD and must follow the test sequences and procedures outlined in this document while using Sensor Vendor supplied checklists. Sensor Vendor representatives will be visitors in the tower facility and may serve as technical experts on their sensor system. If any questions arise before or during testing, they should be directed to the TTD's attention.

4.5 Baseline Testing

4.5.1 Sensor/Weather Equipment Inspection

The TTC, prior to baseline testing, will prepare the tower test site for two weeks of testing using sensor/weather equipment. This preparation will include ensuring data gathering equipment is available, within calibration and fully operational. Also, an internal test must be accomplished to ensure all weather sites are properly feeding weather data to the tower facility for simultaneous recording in data gathering equipment.

4.5.2 Sensor Vendor Orientation

The Sensor Vendor is to report to the TTD the day prior to baseline testing, to confirm testing and to receive a safety, facility and access procedures briefings.

4.5.3 Sensor Connection

The TTC, with assistance from the Sensor Vendor, will unpack and connect the sensor to the data gathering equipment and tilt table (50 lb capacity) in accordance with the Sensor Vendor supplied sensor connection checklist. The TTC will validate the checklist to ensure it is sufficiently detailed to be understood and applied independently. Then the TTC and Sensor Vendor will perform a preliminary checkout of the sensor to ensure proper operation.

4.5.4 Sensor System Parameters

The TTC will validate the Vendor supplied system measurement checklist and record the following system specific parameters by direct measurement at the beginning and end of each data run, if parameters are subject to change. The measurements will indicate any system degradation and confirm first readings.

Radar: Operating Frequency/Modulation Techniques
Power (Peak/Ave)
Pulse Repetition Frequency (PRF)

Pulse Width/Pulse Compression Ratio
Antenna Az & El Beamwidth
Receiver Sensitivity
Antenna Polarization
LRU Size/Weight/Pwr Requirements
If Applicable, FOV and Scan Speed

Infrared: Operating Frequency
Minimum Resolvable Temperature (MRT)
Detector Type
Detector Dimensions
Frame Rate
FOV
Focal Length
LRU Size/Weight /Pwr Requirements
Cooler Type

Radiometer: Operating Frequency/Modulation Technique
Minimum Resolvable Temperature (MRT)
Detector Type
Detector Dimensions
Frame Rate
Receiver Sensitivity
Antenna Polarization
LRU Size/Weight/Pwr Requirements
If Applicable, FOV and Scan Speed

4.5.5 Sensor Calibration

The TTC will calibrate the sensor using the Vendor supplied sensor calibration checklist. The TTC will validate this checklist to ensure it is sufficiently detailed to be understood and applied independently. Calibration equipment (ie. black body sources and corner reflectors) will be available and positioned, IAW Appendix A2.

During periods of high atmospheric attenuation, an alternate calibration method may be needed. Direct RF signal injection or an echo box will be used, if available. This alternate calibration procedure should be addressed in the Sensor Vendor's checklist together with any peculiar test equipment requirements.

The final task in calibrating the imaging sensor is to bore-sight the center-line of the sensor to the position identified in Appendix A2. This is necessary to ensure captured imagery is standard for all systems for equal evaluation. Therefore, once the imaging sensor has been calibrated, the only allowable movement of the sensor will be while positioned on the FIGL provided tilt-table.

4.5.6 Baseline Sensor Testing/Operation

The TTC, with minimal assistance from the Sensor Vendor, will operate the sensor by following procedures outlined in the Vendor supplied sensor operations

checklist. The TTC will validate this checklist to ensure it is sufficiently detailed to be understood and applied independently.

The TTD will direct the start of the first data run under clear, daylight conditions to determine if the sensor under test is functioning satisfactorily. Additional clear-air data runs will continue during the two week Baseline Sensor Operation to collect sufficient baseline data (at least three useable runs) and to ensure the TTC is properly trained and prepared to operate the sensor using the Sensor Vendor provided checklists. The Baseline Sensor Operation will be terminated by the TTD only when both of these conditions have been met.

If the system malfunctions, the Sensor Vendor must troubleshoot and advise TTD on estimate repair time within 24 hours; otherwise the TTD will terminate that Baseline Sensor Operation. Further, if the TTC and Sensor Vendor determine that the system is operating properly but cannot "see" the runway or designated targets in a clear weather environment, then the TTD will terminate the test.

4.6 In-Weather Sensor Testing/Operation

Low Visibility weather conditions are random and infrequent events. Therefore, the following test scheduling procedures are established to provide maximum flexibility and responsiveness, and to ensure sensor data runs are accomplished whenever the visibility is reduced to 0 to 1 1/2 miles due to fog, rain or snow.

The TTD will schedule sensor test data runs through a series of planning, operations and alerting procedures. The TTD will be responsible for publishing Test Planning Schedules and Test Operations Schedules, and for activating Test Alert Operations. The Test Planning Schedule provides a 5 day outlook, the Test Operations Schedule provides a 24-48 hour confirmation and commitment to testing, and the Test Alert Operations provides for a 12 hour response for testing when low visibility weather conditions occur that were not reflected in the Test Operations Schedule.

WL/WEA will provide (or arrange for) weather forecasts of low visibility weather conditions over the test range as follows:

Daily:	24-48 hour forecasts
Daily:	24 Hr/Day alert notification (Metwatch) whenever low visibility weather conditions are forecast and/or observed.
Mon-Fri:	Extended outlook (5 day) forecasts.

The TTD will publish a bi-weekly Test Planning Schedule based on the extended outlook weather forecast. The day prior to any scheduled in-weather testing of a sensor system, the TTD will verify the following day's forecasted weather conditions, adjust the schedule (as necessary), and advise all necessary personnel (e.g. TTC, Sensor Vendor, WL/AA) of the specific Test Operations Schedule. The TTD will activate the Test Alert Operations whenever low visibility weather conditions occur unexpectedly and a sensor system(s) is available and ready for

testing. The TTD will establish an alert or standby schedule to cover the Test Alert Operations during non-duty hours (evenings, nights and weekends).

4.6.1 Sensor/Weather Equipment Inspection

The TTC will prepare the tower test site for testing. This preparation will include ensuring data gathering equipment is available, within calibration and fully operational. Also, an internal test must be accomplished to ensure all weather sites are properly feeding weather data to the tower facility for simultaneous recording in data gathering equipment.

4.6.2 Sensor Connection

The TTC will connect the imaging sensor to the data gathering equipment and tilt table (50 lb capacity) in accordance with the Sensor Vendor supplied sensor connection checklist. Then the TTC and Sensor Vendor, if on-site, will perform a preliminary checkout of the sensor to verify proper operation.

4.6.3 Sensor Operating Parameter Verification

The TTC will validate and record the following system specific parameters by direct measurement at the beginning and end of each data run, only if parameters are subject to change. The two measurements will be made to identify any system degradation.

Radar:	Operating Frequency/Modulation Techniques Power (Peak/Ave) Pulse Repetition Frequency (PRF) Pulse Width/Pulse Compression Ratio Antenna Az & El Beamwidth Receiver Sensitivity Antenna Polarization If Applicable, FOV and Scan Speed
Infrared:	Operating Frequency Minimum Resolvable Temperature (MRT) Detector Type & Dimensions Frame Rate FOV Focal Length
Radiometer:	Operating Frequency/Modulation Technique Minimum Resolvable Temperature (MRT) Detector Type & Dimensions Frame Rate Receiver Sensitivity Antenna Polarization If Applicable, FOV and Scan Speed

4.6.4 Sensor Calibration/Alignment

The TTC will calibrate the sensor using the Vendor supplied sensor calibration checklist. Calibration equipment (ie. black body sources and corner reflectors) will be available and positioned, IAW Appendix A2.

During periods of high atmospheric attenuation, an alternate calibration method may be needed. Direct RF signal injection or an echo box will be used, if available. This alternate calibration procedure should be addressed in the Sensor Vendor's checklist together with any peculiar test equipment requirements.

The final task in calibrating the imaging sensor is to bore-sight the center-line of the sensor to the position identified in the Appendix A2. This is necessary to ensure captured imagery is standard for all systems for equal evaluation. Therefore, once the imaging sensor has been calibrated, the only allowable movement of the sensor will be while positioned on the FIGL provided tilt-table.

4.6.5 Sensor Operation

The TTD will direct the start of first data run. The TTC, with minimal assistance from the Sensor Vendor, will operate the sensor by following procedures outlined in the Vendor supplied sensor operations checklist. If the system malfunctions, the Sensor Vendor must troubleshoot then advise the TTD of the estimated repair time within 24 hours. If repair time is lengthy, the TTD will terminate the test.

4.7 Test Logs

The TTD will maintain a Daily Test Log recording general weather conditions, unusual test events, problems encountered and lessons learned. The log will serve as a historical reference for the evaluation and will be used to preserve program continuity by informing an Acting TTD whenever the TTD is unable to attend a data run. If the TTC maintains a log, it will be openly accessible to TTD.

5.0 Test Items

5.1 General Description

The test articles consist of sensor systems including radars, radiometers and infrared devices operating at millimeter wave and infrared frequencies. The test articles include both active and passive systems that are expected to "see" through most low visibility weather conditions.

The test items are, at a minimum, immobile front-end sensor systems with the capability of producing a representative analog image. The sensor performance data and the images obtained under varying weather conditions will be analyzed and compared to assess their potential applicability for use in on-board landing guidance systems.

Some test articles may include real-time image processing and display of the real world scene. For others, signal processing to produce an image will be accomplished off-line and recorded. The Sensor Vendor supplied test articles may be in a brassboard configuration but will be completely enclosed and compatible with standard interconnections (ie. RS-170, RS-232) and power requirements (ie . 28VDC, 115VAC @ 60Hz) to the data gathering equipment. Also, all equipment used for this test will be properly grounded.

The Sensor Vendor will provide data on the test sensor system characteristics and parameters. These system characteristics and parameters will be reduced out of the sensor performance test data during the data analysis to allow sensor comparisons based on non-proprietary fundamental data.

6.0 Instrumentation

The following equipment is available to support testing. A list of required test equipment must accompany the Vendor's checklists to ensure a timely test. If there are questions or other support equipment requirements, these should be addressed to the Tower Test Director. See figure below for block-diagram representation of data collection suite.

6.1 Test Equipment

1 - AT compatible PC w/ Monitor,
  640k RAM,
  20Mb hard disk & 5 1/4" floppy drive
  Serial port
  IEEE-488 port
  Video RGB output
  Digital tape drive (Colorado DJ-10 - DC 2000 / QIC-40 or compatible)
  Video frame grabber board (Data Translation DT-2803)
1 - VHS Video camera
1 - VCR and magnetic tape compatible with video camera
1 - Color still camera with film
1 - Baseline IR Camera (If available)
1 - VCR and magnetic tape compatible with IR
1 - LeCroy digital data acquisition system w/"Waveform-Catalyst" software
1 - 2 axis tilt-table with automatic/manual controller

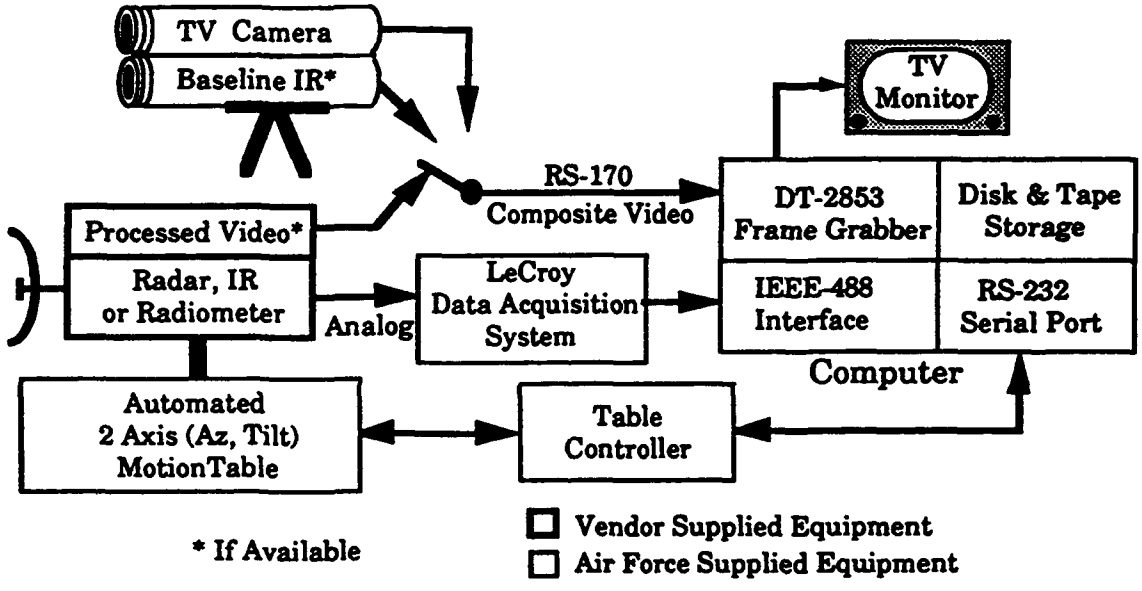

Tower Test Data Collection Instrumentation

6.2 Meteorological Instrumentation

Parameter Measured	Interval	Site	Equipment
Air Temperature	10 Min	T/FOV	1200 MPS
Dewpoint	10 Min	T/FOV	1200 MPS
Surface Pressure	10 Min	FOV	Weathertronics 7105-A
Wind Direction/Speed	1 Min	FOV	Weathertronics 2020/2031
Slant Visual Range	1 Min	T	LPV
Rainfall Rate	10 Sec	FOV	Wallop Rain gauge
Snowfall Rate *	1 Min	FOV	Tipping Bucket Gauge
Rain Drop Size Distribution	1 Min	FOV	Knollenberg
Liquid Water Content (Fog)	1 Min	FOV	Knollenberg
Freezing Level/Vert Profile	12 Hr	ARPT	GMD-5 Radiosonde
Snow Free Liq H2O Content *	1/Test	FOV	Calorimeter
Runway Visual Range	1 Min	FOV	HSS
Global Solar Radiance	10 Min	FOV	Eppley PSP
Global Terrestrial Radiance	10 Min	FOV	Eppley PIR
Fog Drop Size Distribution	1 Min	FOV	Knollenberg
Soil Temperature	10 Min	FOV	Yellow Springs 418
Surface Observation	1 Hr +	ARPT	Base Wx
Synoptic Weather	1 Day	FOV	WL/WE

FOV - located on the ground near the center of the sensor's field of view
T - located on tenth floor of tower facility unless otherwise indicated
ARPT - located at local airport
* - Measurements may be taken under future instrumentation contract

Data from these systems will be recorded on paper printout or computer diskettes (5.25", ASCII format).

7.0 Test Schedule

Testing will be accomplished between October 1991 - June 1992 and will consist of several individual sensor tests. Each sensor test will begin with a nominal two week clear weather baseline test. The two week baseline test will generally follow this sequence:

Day 0 - TTC inspects measurement equipment operation & interface
Day 1 - Set-up,initial readings and calibration of Sensor Vendor's system
Day 2 - Day 13 TTC operates Sensor Vendor's system gathering data
Day 14 - Discuss sensor teardown procedure, close Baseline Testing

The remaining period of the test, the TTC will operate each Vendor's sensor in specific low visibility weather conditions. Testing of each vendor provided sensor will continue until sufficient data has been gathered under each low visibility weather condition (fog, rain and snow) to support the required sensor performance data analysis. The sensor test will, at a minimum, document 12 complete data runs for four different weather conditions at 3 data runs each. A minimum of 5 images/scans will be recorded for each data run within 30 minutes. The first weather condition is in clear air for baseline testing. The second condition is during fog, the third is during rain and the fourth is during snow. For the last three conditions, the prevailing visibility needs to be between 0 to 1 1/2 miles.

The scheduling of sensor operation for data gathering will be determined by the Tower Test Director and will be governed, in part, by the environmental conditions, mission requirements, and the availability of essential equipment. There will be no restrictions on when the testing will be scheduled. This means that operations may be conducted during weekends and at night throughout the test period.

The Tower Test Director (TTD) will schedule the two week test when the Sensor Vendor has accomplished the following tasks:

1. Accepted the terms of testing, signified by signed contract
2. Received frequency allocation approval in WPAFB area
3. Provide TTD/TTC with 4 acceptable checklists that describe sensor connection, calibration, system measurements and operation

8.0 Facilities

8.1 General Description

Testing will be carried out at the Air Force Avionics Directorate, Wright-Patterson AFB on the tenth floor of building 620. The test site is a fully enclosed 18 foot by 18 foot room serviced by a large freight elevator and overlooks an inactive runway and taxiway. The far end of the runway is 10200 ft (3109 m) from the tower and the close end is 4100 ft (1250 m) The elevation of the tenth floor is such that it permits a 3.5° glideslope to the runway while positioned approximately 28° off of the centerline.

Surrounding the runway and taxiways is long bent grass. This contrasts well with the runway that is made of pitted asphalt and the taxiway of weathered concrete. At different locations on the runway various size vehicles can be placed as targets. This range offers a realistic representation of an aircraft approach to landing.

The Tower complex, runways and targets are located in Area B at Wright-Patterson Air Force Base, near Dayton, Ohio. The tower overlooks runways and targets immediately behind the Air Force Museum.

8.2 Test Site Elevation and Distances

Elevations:

Tower Base	965 ft (294 m) MSL
Tower Level 10	1098 ft (335 m) MSL
Runway Threshold	824 ft (251 m) MSL
Runway End	785 ft (239 m) MSL

Distances:

East-West black-top runway	150 ft (46 m) X 7147 ft (2178 m)
East-West cement taxiway	75 ft (23 m) X 6500 ft (1981 m)
Taxi turn-offs relative to near end	2200, 4400, 5800 ft (671, 1341, 1768 m)

Horizontal Range to near end of runway	3830 ft (1167 m)
Slant Range from level 10 to near end of runway	3842 ft (1171 m)
Horiz Angle from level 10 to near end of runway	28°
Slant Angle from level 10 to near end of runway	4.09°

Horizontal Range to far end of runway	10820 ft (3298 m)
Slant Range from level 10 to far end of runway	10828 ft (3300 m)
Horizontal Angle from level 10 to far end of runway	10°
Slant Angle from level 10 to far end of runway	1.45°

The antenna platform can be aligned by an optical sight. In addition, corner reflectors, diplanes and reflecting mirrors will be located in the target area to provide alignment targets for system antennas and optics prior to each test.

8.3 Tower Electrical Support

The following electrical power is available at the sensor platform:

110 VAC single phase 60 Hz, 200 Amps
208 VAC three phase 60 Hz, 30 Amps
208 VAC three phase 60 Hz, 60 Amps
120 VAC single phase 400 Hz, 200 Amps
208 VAC three phase 400 Hz, 200 Amps
28 VDC, 50 Amps

9.0 Data Reduction and Test Analysis

9.1 Meteorological

The meteorological and sensor data shall be time correlated, with imaging data time tagged to the prevailing weather conditions data through the WWV standard. In addition, a scan of the scene shall be made with a camcorder to record the visibility in the visual spectrum. The visual scene shall also be time correlated to the respective meteorological and sensor data. The recorded weather data shall be provided to the Test Director in binary or ASCII format on 5.25" floppy disks. Extensive use of a log book shall be made to indicate any meteorological condition judged not to be captured properly from the data provided by the meteorological sensors. See section 6.2 for a complete list of meteorological data being collected, with locations and intervals of measurements.

9.2 Sensor Data

9.2.1 Tower Test Contractor

The sensor data will be digitized by a LeCroy Data Acquisition System and recorded on 5.25" floppy disks and in binary or ASCII format. The recorded data will be accomplished in a pixel format, recording the accompanying horizontal and vertical rates and resolutions used to scan the image. The formatted digital image will be recorded in a fashion that allows the scanned scene to be replayed on the computer display with correct orientation for a quick-look. Each test will record and document all relevant information; the day, the time, the Sensor Vendor, etc. In the event the Sensor Vendor has a data collection system that is an integral part of their sensor, they shall provide to the Air Force a data set that is on 5.25" floppy disks and in binary or ASCII format.

9.2.2 Sensor Vendor

The Sensor Vendor will supply the following pertinent data and any other parameters that will be useful in describing sensor performance as part of the Sensor Vendor's System Parameter Measurement Checklist

RADAR :
- Range Profiles
- Power peak and average
- Transmitter waveform (pulse, FM, CW, etc.)
- Pulse Repetition Rate (PRF)/Pulse Width
- Radar mode, status, gains/ Pulse compression ratio
- Receiver bandwidths I & Q
- Total receiver dynamic range
- Calibrated peak video & Automatic Gain Control (AGC) levels
- Range distance - start and stop
- Antenna azimuth and elevation beamwidth, polarization
- Scanning azimuth and elevation (Az, El) and speed
- Receiver power transfer curve
- Antenna gain and beam pattern

RADIOMETER: Calibration temperature (Hot and Cold)
Total receiver bandwidths (RF, IF, Video)
Total receiver dynamic range
Antenna beamwidth (azimuth and elevation)
Scanning table azimuth and elevation (Az, El)
Minimum detectable temperature

FLIR : Calibration Temperature
Total receiver dynamic range
Integration time constant
Optics Aperture and Magnification Factor
Minimum detectable temperature

IMAGE: Shades of gray
Gain control
Enhancement principle, linear line interpolation, adjacent cell average, coordinates, etc.

9.3 Camcorder Data

A VHS recording will be made of the measured scene. Additional information, such as date, time, Sensor Vendor, and weather conditions, can be printed on the frame by overlaying messages or recording to an audio track.

9.4 Data Reduction

Data reduction will consist of combining sensor and weather data with other pieces of pertinent data into a single product. This product will provide a vehicle to evaluate and compare the capabilities of the tested sensors to penetrate the prevailing weather conditions and to identify objects and surfaces under a similar set of circumstances and conditions, for each sensor involved in the testing. Attention will be given to sensor viewing angles, range, and surface normals.

9.4.1 Fundamental Values

Radar cross section of point targets in scene (hard targets)
Radar cross section per unit area for expanded area targets runways, grass, rain covered grass, snow, water
Radar cross section per unit volume for rain, fog, snow
Radiometric values of transmissivity & emissivity for all surfaces and targets in scene
Losses due to material in path between sensor and reference targets for, clear air, rain, fog, snow, smoke, etc.
Resolution of sensors in azimuth, elevation, range

9.4.2 Images

Resolution in range, in azimuth, in elevation
Coordinate transformation, B-Scope, C-Scope
Real-time, update-rate, revisit time per scan
Off-line construction

9.5 Test Analysis

The Tower Test Contractor (TTC) will analyze the fundamental data obtained after data reduction (Section 9.4) to determine the sensor performance in low visibility weather conditions. Based on these analyses, the TTC will also provide assessments and recommendations to support the SVTD program decision on selection of a functional prototype Synthetic Vision sensor.

9.5.1 Sensor Performance vs PRDA # 89-04-PMRN Requirements

Compare sensor performance to the landing system requirements specified in the Program Research and Development Announcement (PRDA) # 89-04-PMRN. Specifically: Runway detection at 5km; runway identification at 3km; clear image of landing at 2km; and rollout, takeoff and taxi operations at very short ranges.

For runway detection, identification and landing, it is anticipated that at a minimum the sensor must be able to detect a 5% contrast between the runway edge and the adjoining edge material (grass, dirt, snow covered surface, etc). For rollout and taxi operations, it is anticipated that the sensor must be able to detect at a minimum a 5% contrast between the runway/taxiway and any runway/taxiway obstructions.

The Sensor Performance should be illustrated as graphs for each of the low visibility weather conditions (fog, rain and snow). These graphs will contain plots of performance measures/PRDA requirements vs the fundamental atmospheric and surface parameter that is causing the performance degradation (e.g. liquid water content, rain rate, drop size distribution, temperature, relative humidity).

9.5.2 Sensor Performance vs Theoretical Performance

Compare sensor performance to theoretical performance. These analyses will compare the measured fundamental snesor performance parameter values (Section 9.4) to those calculated from scientific theory using the measured atmospheric and surface conditions (Section 9.1).

The TTC will present the analyses in graphs and/or tables illustrating how the performance of each class of sensors is affected by each type of low visibility weather condition (fog, rain and snow). The TTC will determine the specific format of presentation. The scientific theory and supporting equations will also be included in the final report.

9.5.3 Millimeter Wave Extinction vs Optical Extinction (If RVR Capability Exists)

Compare the measured extinction of the millimeter wave and/or infrared signal to the measured optical extinction (runway visual range-RVR) to determine if RVR can be used to predict the sensor performance range of a millimeter wave or infrared SV sensor. The TTC will determine the format for presentation.

9.5.4 Sensor Performance Assessments and Recommendations

Based on the results of Sections 9.5.1 and 9.5.2, the TTC will compare the performance of all sensors tested and provide assessments and recommendations on the following:

a. The advantages and disadvantages of each type of sensor and each wavelength tested.

b. The extent of which each sensor meets the PRDA requirements for Synthetic Vision.

c. Estimate of the optimum Synthetic Vision sensor characteristics.

10.0 Reports

Sensor data analysis results will be documented in individual sensor reports and a final evaluation report. These reports will meet the format specified by the standard, ANSI Z39.18-1987. The Tower Test Contractor will provide the following specific test reports:

1. Individual sensor performance data analyses within 30 days after data collection. The analyses will be done as the data is collected for each low visibility weather condition.

2. An interim report which compares the performance and results of all classes of vendor sensors tested to date.

3. A final report within 60 days after completion of all vendor sensor testing. This report will compare the performance and results of all the classes of sensors tested.

The TTC generated reports and all supporting sensor test data, including calibration target and atmospheric and ground surface condition data, will be forwarded to WL/FIGL. FIGL will serve as the focal point for distribution of all data and reports generated by this program. All sensor data provided or gathered during sensor testing will be strictly controlled by FIGL.

Those reports and data analyses which contain only non-proprietary fundamental data will be made available to all Tower Test participants and may be made available to the scientific community at large. FIGL may also provide the non-proprietary fundamental data to update existing DOD data banks that compare wavelengths and concepts and to establish evaluation criteria to be used in future programs.

11.0 Responsibilities & Support Agreements

11.1 Responsibilities

Tower Test Director (TTD) - Lt Jeff Campbell / (513) 255-5531 / WL/FIGL

1. Coordinate all tests with Tower Test Contractor, Sensor Vendors, Staff Meteorologist, Test Facility and Test Range Managers.
2. Ensure all resources required to implement the ALG/SVTD Tower Test Plan are identified and in place.
3. Complete all pretest schedules, safety and environmental procedures.
4. Direct each test as outlined in this document, (ALG/SVTD Tower Test Plan).
5. Maintain and annotate a test log, recording significant information, ie. weather conditions, problem areas and improvements, for use in documenting results of the tests.
6. Direct starting, extending and terminating tests based on consultation with support organizations and existing weather conditions.
7. Represent the Synthetic Vision Technology Development (SVTD) Program Office.
8. Coordinate publication and manage implementation of the ALG/SVTD Tower Test Plan.
9. Ensure all Tower Test Plan objectives of the SVTD project are met.

Tower Test Contractor (TTC) - Mr Brian Hudson / (404) 528-7740 / GTRI

1. Comply with all directions from TTD.
2. Ensure all equipment is in working order and within calibration.
3. Validate Vendor supplied checklists for accuracy and completeness.
4. Compile data (sensor & weather) for baseline sensor tests.
5. Analyze data and deliver individual reports of each sensor test within 30 days after data collection for each low visibility weather condition.
6. Analyze, compare and document results of each sensor tested to date in an interim report.
7. Analyze, compare and document results of each sensor tested in a single final report within 60 days of final sensor testing.

Sensor Vendors - (TBD)

1. Provide 4 procedural checklists for sensor connection, calibration, system measurements and operation.
2. Deliver a functioning front-end sensor system to the Building 620 at Wright-Patterson AFB.
3. Provide 24 hour "on-call" technical assistance and sensor maintenance.

Staff Meteorology - Ms Sandra Weaver / (513) 255-5496 / WL/WE

1. Provides climatological studies for use in planning tests.
2. Serves as consultant for atmospheric effects on millimeter wave, infrared and visual systems.
3. Provides advice on meteorological measurements and instrumentation for EO/IR/MMW testing.

12.0 Safety

12.1 WL Facility Safety Plan

Safety planning will be accomplished IAW WL 127-1, Lab Director Safety Plan 127-2 and completion of AFSC form 2750 and associated supplements as required. The WL Laboratory Directors are charged with the responsibility to implement and support the safety program plan, WL Regulation 127-1, within their laboratories and ensure that their subordinates actively participate in the safety program. This responsibility includes assuring that contractors performing services for WL organizations comply with Air Force safety directives as specified on the terms of an Air Force contract with the Sensor Vendor. The Air Force supports the Occupational Safety and Health Administration (OSHA) through its own occupational safety and health program. The Air Force standards are equal to or more stringent than the OSHA standards and must be complied with.

12.2 Safety Approval Procedures

The Laboratory Safety Office (LSO) will act as the program focal point for safety during all tower test programs and will interface with the contractor's safety personnel on system safety matters.

The Tower Test Director will inform the LSO of an upcoming test by initiating the appropriate WL Safety Permit/Request (AFSC Form 2750). This request includes contractual safety data (e.g., analyses, plans) which are provided to the LSO for technical review and a recommendation for approval /disapproval. It is the responsibility of the contractor to provide to the Tower Test Director information needed for this request.

A Technical Safety Committee (TSC) exists to review planned experiments and tests to ensure that all safety aspects are considered. The LSO will establish a date and time to conduct a review of the test by members of the TSC. The TSC will perform a hazard analysis and provide guidance to reduce the risks identified during the analysis. The results of the evaluation will be documented by a Safety Permit/Request and the LSO will forward the completed permit along with recommendations to the appropriate chain of command.

After approvals, the Tower Test Director may authorize the project to proceed. A copy of the approved safety permit will be posted in the vicinity of the test and Bioenvironmental Engineering (MEDCEN/SGB) will be given more than a weeks notice to test each new radar system.

12.3 Personnel Safety

The following are examples of safety requirements normally affecting the kind of experiments anticipated:

a. Equipment containing high voltage or microwave emissions will be roped off to prevent inadvertent contact with dangerous signals.

b. Electrical distribution shall be reviewed prior to turning on any equipment to ensure switch, circuit breakers, extension cords, sockets and other electrical equipment are adequately rated and safe.

c. All equipment shall be adequately secured on/in stable tables, racks, or other supports.

d. Necessary controls shall be installed to ensure adequate cooling, temperature, and environmental protection.

e. Labels and signs warning of high voltage and microwave radiation shall be prominently displayed in accordance with applicable safety requirements.

13 .0 Security

Access to the tower will be controlled by WL/AAWP and WL/FIGL in coordination with the facilities Real Property Building Manager (RPBM). Sensor Vendor or other test personnel will not be allowed to enter without the proper security approval and escort.

A security clearance will be required of all test personnel in order to have access to the test facility in building 620 . Appropriate clearance documentation shall be forward to WL/FIGL, Wright-Patterson AFB, OH 45433-6553.

Calibrated data collected by the tower test program will be considered unclassified.

Appendix A1

ACRONYMS

ALG	Autonomous Landing Guidance
ANSI	American National Standard Institute
ARPT	Airport
AZ	Azimuth
EL	Elevation
EO	Elected Optics
FIGL	Flight Control Systems Branch Of Wright Lab
FOV	Field Of View
IAW	In Accordance With
IR	Infrared
LRU	Line Replaceable Unit
LSO	Laboratory Safety Office
MMW	Millimeter Wave
MRT	Minimum Resolvable Temperature
OSHA	Occupational Safety And Health Administration
PRDA	Program Research And Development Announcement
PRF	Pulse Repetition Frequency
RPBM	Real Property Business Manager
RVR	Runway Visual Range
SVTD	Synthetic Vision Technology Demonstration
T	Tower
TSC	Technical Safety Committee
TSCF	Targeting System Characterization Facility
TTC	Tower Test Contractor
TTD	Tower Test Director
VAC	Volts AC
VDC	Volts DC
WEA	Staff Meteorology Office Of WL
WL	Wright Laboratory
WL/AA	ionics Directorate Of Wright Lab
WPAFB	ight Patterson Air Force Base

Appendix A2

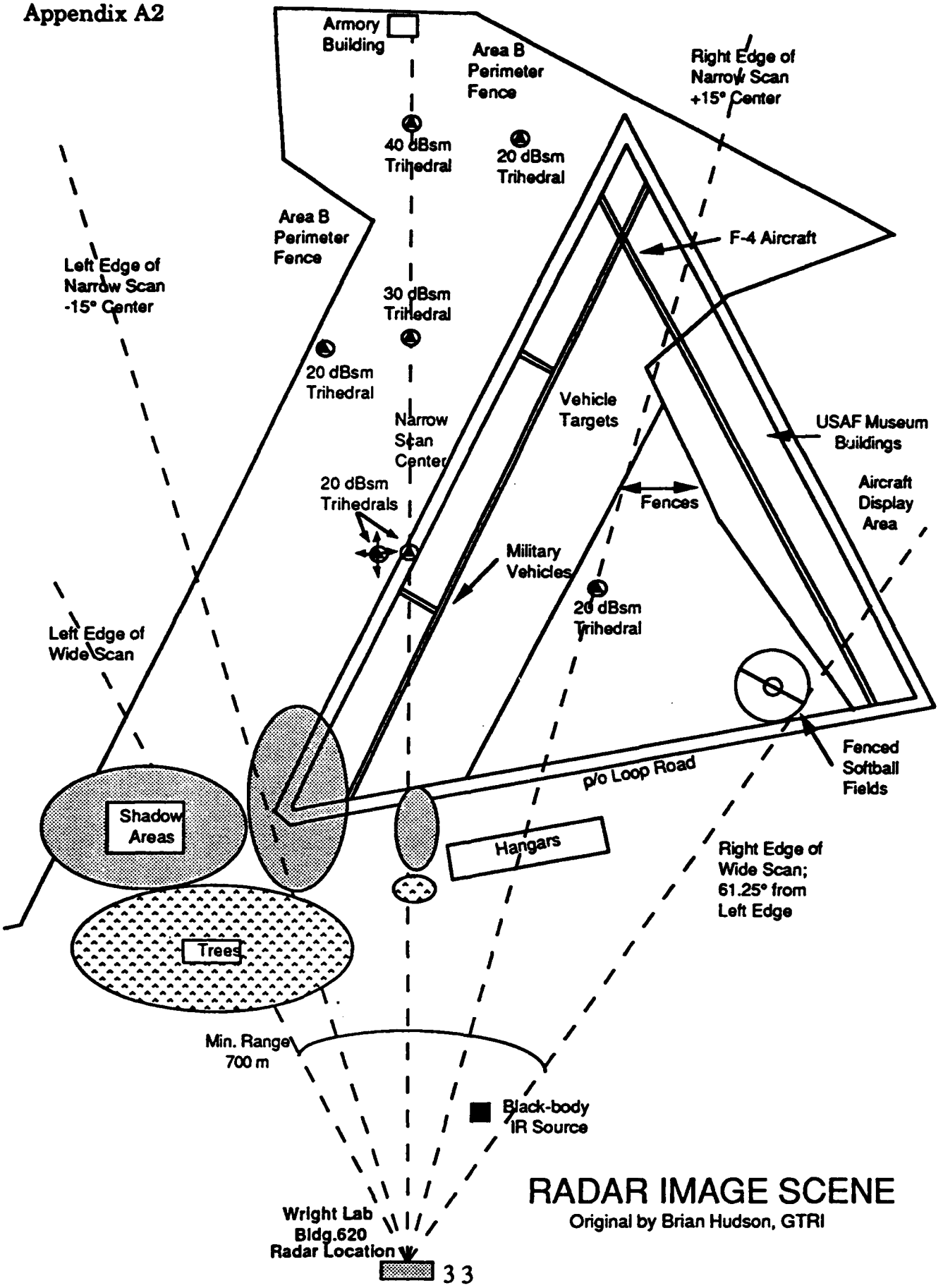

RADAR IMAGE SCENE

Original by Brian Hudson, GTRI

APPENDIX A3

METHOD OF TEST FOR MILLIMETER WAVE SENSORS

A3.1 Introduction

The following paragraphs describe the testing methodology to be followed by the tower test contractor (TTC) in satisfying the objectives of thew tower test program as delineated in the Tower Test Plan. The flow of data from creation to reporting will be described to illustrate the testing elements, including data sources, data collection methods, processing, calibration, data reduction, analyses, performance evaluation and reporting.

A3.2 Sensor Data Processing

The TTC has developed an automated data collection system, using government-owned equipment, that will record the primary output signals from the SV brassboard sensors under test. The sensor vendors will also record sensor data on a non-interference basis using their own data collection equipment. The "raw" test sensor data will be processed on site by the TTC only for the purposes of data quality verification, and all additional data processing will be performed off site at the TTC facility. Additional support test equipment provided by the government, TTC, and the sensor vendor will be used on-site during test sensor system characterization measurements. Meteorological data collection and calibration will be performed by a government subcontractor, and the formatted meteorological data will be delivered on a periodic basis. Meteorological data will be integrated with the reduced test sensor data by the TTC during the data analysis process.

Data collection, reduction, and analysis software will be developed and run by the TTC on IBM PC/AT compatible personal computers to maintain compatibility with government-owned equipment. Programs will be developed using the Microsoft "C" compiler version 5.0, running under the MS-DOS version 5.0 operating system. Pre-programmed software libraries are available for the National Instruments GPIB-PCII controller board, the Data Translation Video frame grabber board, and the FFT data reformatting function. Custom software subroutines will be written to control the LeCroy DAS and the Klinger Scientific MC-2 stepper table controller. Quick-look graphics software will convert raw sensor data into images to verify collected data quality. Data reduction and analysis software will be developed to reformat the raw sensor data and calibrate for RCS. The programs will automatically extract from the processed sensor data arrays the performance features and engineering values needed for performance analysis. Extracted features and reduced meteorological data will be combined in a database that will be exercised during sensor performance analysis.

A3.3 Data Evolution

Data from the SV sensor under test and from weather sensors will be recorded, reduced, and analyzed to produce qualitative results of imaging sensor performance in adverse weather. A flowchart has been drawn to describe the evolution of recorded data through the intervening processing stages. Figure A3-1 presents this data evolution flowchart from the sensors at the top to the

processed results at the bottom. Physical devices and processing operations are shown as rectangles, and the data in various intermediate formats are shown as rounded rectangles. There are four parallel data acquisition and processing paths that are merged during the data reduction process. The final data reduction step extracts sensor performance features and weather data into a relational data base that is exercised to develop analytical results. Sensor image data recording, processing, and display image generation provides for visual evaluation of sensor performance.

A3.3.1 Data Collection Sources

The primary data output from an electronic imaging sensor is a signal whose amplitude, frequency, or phase is a measure of the reflectivity or emissivity from a small portion of the observed scene, called a resolution cell. To develop a two-dimensional image of the scene, the sensor system provides this output signal over a span of azimuth angles and slant ranges (or elevation angles), defined as the coverage area. Data collection equipment will time sample, digitize, and record the sensor output signal with sufficient resolution to maintain the information content. Sensor data collected from the coverage area are stored in a two-dimensional data array with elements representing sensor resolution cells, and dimensions equal the number of resolution cells in azimuth by the number of cells in range, or elevation. Digital data fill the storage array one line at a time in a raster fashion. Radar sensor data fill each range line of the data array before the azimuth is incremented. Television format data are loaded along azimuth lines, and the elevation is incremented. The loaded data array becomes a recorded data file representing a single view, frame, or "snapshot" of the observed scene made by the test sensor.

Secondary data collected from an imaging sensor include parameters such as operating mode and antenna elevation that are constant over a measurement frame, and dynamic parameters such as automatic gain control and antenna azimuth that change during a frame. The data collection equipment and procedures provide for recording these additional sensor data items in registration with the primary sensor data. Constant parameters will be manually entered into a data collection system computer file or entered into the Daily Test Log. Dynamic sensor parameters will be imbedded with the primary sensor data or captured by an additional digital data acquisition channel. Sensor characterization measurements, including output power and receiver transfer function, or minimum detectable temperature, may only be made once during the tower tests. Sensor performance measurements such as noise level or response to a calibration source are recorded through the primary sensor output, and will be performed daily.

Meteorological sensors, television cameras, and scene photography are examples of supporting data sources for the sensor tower testing. Results of site surveys and any important personal observations made during testing should also be recorded to assist sensor performance analysis. These supporting data must be time marked for correlation with the primary and secondary sensor data.

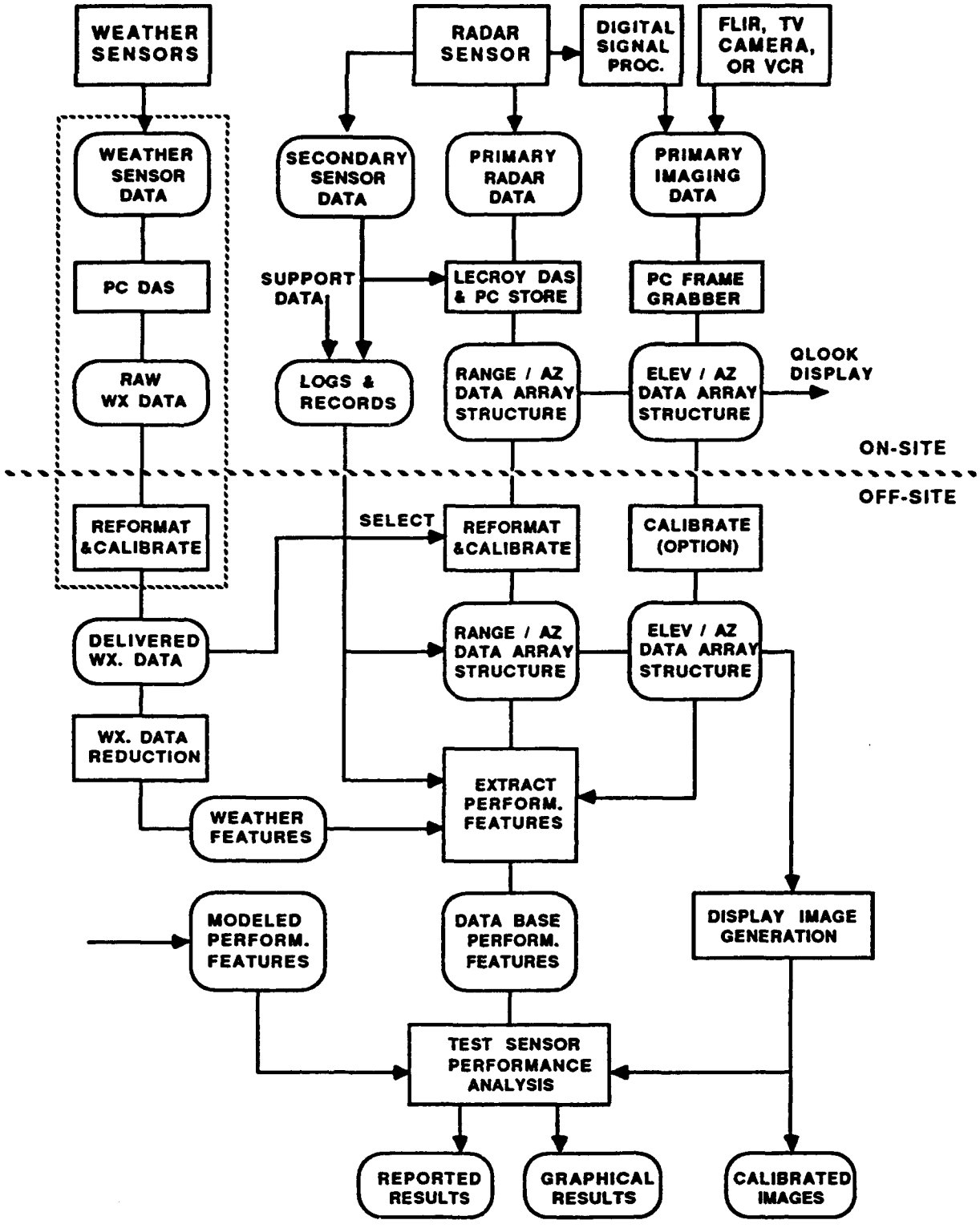

Figure A3-1. Flowchart of Data Evolution

A3.3.2 Data Reformatting

Primary sensor data will be recorded by the LeCroy data acquisition system (DAS), a vendor-supplied DAS, and a video cassette recorder. Digital data are stored in MS-DOS file format on fixed disk, floppy diskette, and DC-2000 tape cartridges. The video cassette storage format is monochrome RS-170 television video on S-VHS tape at standard recording speed. Sensor data from these different formats will be reduced to common digital file formats for performance analysis, one for radar range-angle data and one for perspective view (angle-angle) sensor data.

Sensor data processing by the TTC, including amplitude calibration, performance feature extraction, and image generation, will be based on a standardized data array structure stored in computer files with a common format. Each element of a data array will correspond to one sensor resolution cell in a fixed coordinate structure defined by the sensor coverage area. The sensor coverage area dimensions for tower test data collection have been specified to match the 30° azimuth by 20° elevation coverage available on a Head-Up Display (HUD). Radar sensor data collection and TV/FLIR framing will be adjusted to match these HUD dimensions.

Radar data arrays will have the coordinates slant range and azimuth angle. The coverage area dimensions have been defined as 6 km range by 30° azimuth, but actual slant range dimensions for a given radar sensor will fall between zero and 6 km range. The number of range resolution cells in the range dimension depends on sensor parameters and the sample clock rate, but 500 to 1000 range cells are typical. The number of azimuth resolution cells in 30° coverage is a function of the antenna beamwidth and scanning step size, but 0.1° stepping will give 300 azimuth cells. Recorded FMCW radar data will be computer processed with a fast-Fourier transform (FFT) to convert from beat frequency to range profile dimensions. Pulsed radar data are already in range profile dimensions. If enough radar data are recorded at each azimuth step position, then range cells from multiple range profiles will be integrated into a single range profile.

Perspective data arrays will have the coordinates elevation angle and azimuth angle, with dimensions 20° elevation by 30° azimuth. The Data Translation DT-2853 video frame grabber board digitizes RS-170 video to a resolution of 480 vertical picture elements (pixels) by 512 horizontal pixels. The frame grabber will digitize selected video frames from the video tape recordings of the FLIR sensor, any real-time radar perspective images, or the television camera. The achievable sensor data capture resolution is a function of all analog components prior to digital frame capture, including the sensor and video cassette recorder. The displayed resolution is also a function of the television monitor performance. RS-170 video has a 3:4 display aspect ratio and the frame grabber data array dimensions have a 2:3 aspect ratio, so some format adjustment may be needed. If the individual sensor pixels have "square" aspect ratio, the data array only needs 341 vertical pixels for 512 horizontal pixels.

A3.3.3 On-Site Data Processing

Example portions of the recorded sensor data will be processed by the PC-AT computer on site into display images within minutes of data collection. "Quick-look" images check the test sensor performance, and validate the recorded data quality. Sensor perspective images that were captured directly by the video frame grabber board will be reviewed on a TV monitor connected to the frame grabber video output. Quick-look data processing will include the minimum amount of sensor data reformatting necessary to accomplish these functions. Data calibration, perspective conversions, and display factor adjustments will be performed later, during post-mission data reduction and analysis at the TTC facility.

A3.3.4 Off-Site Data Processing

Recorded sensor data and supporting data will be transported off site to the TTC facility for post-mission data processing and sensor performance analysis. This approach reduces the number of TTC personnel needed on site, and allows data processing to be performed concurrently with the ongoing sensor tower testing. Sensor data processing steps include data selection, calibration, error analysis, data reformatting, and extraction of sensor performance features. The selected primary sensor data files, either before or after the calibration, will be converted into B-scope or C-scope display image files for viewing and photographing. Secondary sensor data is needed to develop sensor performance models, to perform data reformatting, and to calculate data calibration tables. Meteorological data will be time correlated with each processed sensor data file, and the necessary parameters extracted to support analysis of sensor performance in weather. Other supporting data, such as photographs, television camera images, and test logs, will be examined during sensor performance evaluations.

A3.3.4.1 Data Calibration

Sensor data calibration converts "raw" recorded sensor output data into standard engineering units. The analyst utilizes sensor data collected from reference sources, measured sensor parameters, and mathematical formulas for electromagnetic sensors to develop a computerized calibration conversion table. Besides engineering conversion constants, the calibration table includes factors for slant range, sensor non-linearity, and antenna beam taper. Automatic gain control (AGC) and sensitivity time control (STC) correction factors will also be accommodated. The calibration table is used to convert each "raw" sensor data point value into its calibrated equivalent. This one-to-one relationship means that the calibration output data file is equal in size to the "raw" input data file. The calibrated sensor data files are available for further processing, including performance feature extraction and display format conversion.

A3.3.4.2 Error Sources

The analyst will determine the possible sources of measurement error and their degree of effect on the results, to improve confidence in the performance analysis results. Comparison of measured results with predicted sensor performance is a good check for measurement or calibration errors. Radar sensor performance modeling using measured radar parameters, including

transmit power, antenna gain, and receiver sensitivity, will predict the sensor response to a precision reflector located within the measurement scene. Radar data are then collected from the reflector, processed through the calibration table, and the two results are compared. A small difference in the values, or small "closure" error, lends credibility to the measurement and calibration process. A large closure error indicates that a measurement or analysis system problem exists, and the error source will be isolated and corrected.

A3.3.4.3 Data Reduction (and Feature Extraction)

Data reduction is the process of converting a large volume of measured sensor data into a smaller data set in the form needed to support sensor performance analysis. Data reduction will include data selection, calibration, reformatting, and feature extraction. Data reduction is necessary, since an analysis effort typically cannot afford to exhaustively analyze all of the collected sensor data. Data selection is the process of indexing sensor data files by type and measurement conditions, and identifying those files containing the data needed to support a particular analysis process. For example, all the rain condition data files for a particular sensor would be reviewed to select those presenting the best distribution of rainfall rates from light to heavy. The selected data files will be calibrated against the appropriate calibration table, and reformatted, if necessary.

Feature extraction isolates data in test scene areas of interest from a sensor data file and develops numeric values from that data. Extracted features can be grouped into performance features that measure sensor effectiveness and fundamental engineering values that characterize the test scene environment. Examples of extracted engineering values are radar cross section for a target or clutter area, volumetric radar cross section for rain, and transmission path attenuation. Received power ratios and sensor resolution are examples of sensor performance features. The most important extracted radar performance feature is the received power contrast between the runway pavement and adjacent grass clutter areas. This feature will be determined by comparing the received power from small clutter areas (patches) on the pavement to clutter patches on the grass. Radar contrast will be measured for pavement/grass patch pairs over the runway range extent. Sensor performance features such as contrast and angular resolution of targets will also be extracted from the perspective image sensor data files.

The meteorological data collected by the weather system contractor will be calibrated and delivered to the TTC in MS-DOS compatible ASCII data file format. The TTC meteorological data processing software will 1) time search the meteorological data files for data matching specific sensor data collection events, 2) develop statistical parameters from the meteorological data, and 3) plot histograms of the selected meteorological data. The reduced meteorological data will support the selection and categorization of sensor data files for feature extraction. Meteorological data will be merged in the computerized data base with extracted performance features. The data base will be indexed by meteorological conditions to assist data searches for sensor performance analysis.

A3.3.5 Analysis and Performance Evaluation

Sensor performance analysis will use the sensor performance feature data base to evaluate sensor operation in a variety of weather conditions. The data base will be exercised to explore sensor performance in clear weather and range deterioration in adverse weather. Data from each test sensor will be examined to determine the detected contrast under different weather conditions between the runway and adjoining edge material. The analyst will look for interactions between the sensor and the test environment conditions, and will attempt to establish the performance limitations of each sensor evaluated. The analyst will explore the relationship between test sensor extinction range and the instrumented optical extinction range. Measured performance features will be used to support any conclusions reached in the evaluation process.

A mathematical model based on published sensor specifications, an estimation of test scene characteristics, and meteorological physics will be developed to predict a sensor's performance against the test scene under several different weather conditions. The model's output data files will be formatted as calibrated sensor data arrays for the full measurement scene, if image generation is needed from the model, or as extracted sensor performance features for analysis comparisons. The measured sensor performance in weather will be compared with the results from the computerized performance models having the same weather conditions and measurement scene characteristics. The performance model may be adjusted if any discrepancies between modeled and measured results are not attributable to measurement errors.

A3.3.6 Presentation and Reporting

Sensor measurements and analysis results will be presented in an interim and final technical reports, including the test and analysis methods used and the conclusions reached. Conclusions will be supported by extensive use of sensor performance graphs and tables of numeric results. Examples are plots of runway-grass contrast versus range, and tables of millimeter wave extinction ranges. Photographs will be delivered of the raw, processed, and modeled sensor data image displays in B-scope and C-scope formats and for a variety of weather conditions. These photographed images will include calibration grey scales to assist the observer in performing visual comparisons of the sensor images. An index will be provided for the library of raw, processed, and modeled data to support future analysis efforts. Since the photographs cannot reproduce the full dynamic range of the image displays, a library of sensor performance files will be saved in image display format for rapid recall and presentation on a television monitor.

A3.4 Test Procedures

Once a test sensor system has been installed and baseline measurements completed, a straight-forward daily test procedure will be followed. The tower test director (TTD) will rely on short-term weather forecasts to initiate a data collection exercise. The TDD and at least one operator will proceed to the avionics tower laboratory, and the weather data collection contractor will be notified. The test sensor and data acquisition system (DAS) will be powered on, operationally verified, and placed in a standby mode. When the TDD determines that the

desired weather conditions exist, a measurement run will be performed. An entry is made into the written test log, and a data filename is is keyed into the DAS computer. Radar sensor data are recorded by the DAS as the positioning table is automatically step-scanned across the 30° measurement azimuth sector in about 3-5 minutes. One time-tagged sensor data file containing all the recorded sensor data, including a DAS configuration header, is created on the DAS computer's fixed disk drive for each measurement run. The TDD will choose to perform another sensor data run, or to develop a quick-look image from the sensor data just recorded. Data collection will be interrupted for about 10 minutes if a sensor data file is selected for B-scope or C-scope display. All data files recorded during a measurement exercise will be copied to backup tape at the conclusion of the exercise. The sensor and DAS will be powered down and secured until the next measurement exercise.

A3.5 Calibration

A radar sensor's response to targets and clutter in a measurement scene must be fully characterized to permit calibration of the collected data into standard engineering units. Radar data collected from known stimuli (active signal sources and passive reflector targets) are used to develop calibration factors for the data collected from targets and clutter of unknown reflectivity. The three major steps for radar data calibration are 1) collect data from known calibrated sources, 2) develop a table of calibration correction factors from that data, and 3) process the "raw" radar data from subsequent data collection runs through the calibration correction table. Additional calculations use measured radar specifications to convert received power into absolute radar cross section (RCS) values. The first calibration step is performed daily on site, and the remaining steps will be accomplished at a later date during data reduction and analysis.

A3.5.1 Calibration Data Sources

Radar calibration sources include active sources, such as a signal generator or a coherent repeater, and passive sources, such as precision reflectors or echo boxes. The sensor tower tests will utilize signal generator injection signals and in-scene reflector targets to develop the calibration data needed to calibrate the brassboard radar sensors. Additionally, a series of measurements will be performed once to verify the radar sensor characteristics, such as transmit power and range resolution, that are needed to convert received power values into radar cross section (RCS) values.

A3.5.1.1 Signal Generator Injection

The most comprehensive radar sensor specification is the receiver transfer function, a measure of receiver output voltage to RF input power. In a bench test of the radar receiver, an RF signal at the transmit frequency will be injected directly into the receiver waveguide. The injected RF power level will be adjusted in 5 dB steps over the receiver's full dynamic range, and one set of radar video data will be digitized and recorded at each power step.

A3.5.1.2 Calibration Reflectors

Radar reflectors located within the measurement scene area will be used as RCS references for calibrating the recorded sensor data during data reduction

processing. As the recorded sensor data are processed, those resolution cell data points corresponding to the reflector locations will be separated from the clutter data. The magnitude of those reflector data points will verify the accuracy of radar transfer function calibration method.

A3.5.1.3 Sensor Specifications

The complete operating specifications for each test sensor will be determined at least once during the testing period. Some characterization activities may require partial disassembly of the test sensor and the use of special purpose test equipment, so more-frequent measurement of these parameters would not be practical. Some of the specifications may have to be ascertained from previous off-site measurements or from manufacturer's test data. Table A3-1 lists radar sensor specifications and suggested methods for measurement. Specifications for an infrared sensor will be covered separately. The TTC will use the measured radar sensor specifications for performance estimation calculations, to determine sizing and placement of calibration reflectors, and in the computation of calibration correction factors. These specifications will also be used to configure the LeCroy data acquisition system and to select an appropriate angular increment (step size) for Klinger table azimuth scanning.

TABLE A3-1. RADAR SENSOR SPECIFICATIONS

Specification	Symbol	Units	Meas. Method	Comments
Transmit Frequency	F_t	GHz	Wavemeter	or spectrum analyzer
Transmit Power (average)	P_{ta}	W	RF Power Meter	w. waveguide thermistor
Transmit Power (peak)	P_{tp}	W	RF Power Meter	Calculated from P_{ta}
Transmit Waveform	-	-	Various	Pulsed, PC, or FMCW
Transmit Pulse Rep. Rate	PRF	kHz	Oscilloscope	or FM sweep rate
Transmit Pulsewidth	τ	ns	Detector & Oscilloscope	or FM sweep width
Transmit Path Loss	α_t	dB	RF Source & Power Meter	
Waveform Timing Delay	t_0	μs	Oscilloscope	For A/D synchronization
Receiver Method	-	-	Vendor	Homodyne or superhet.
Pulse Compression Ratio	PC	none	Vendor	If PC mode used
Receiver Bandwidth	BW	MHz	Sweep Oscillator	or vendor data
Receiver Noise Figure	NF	dB	Noise Bridge	or vendor data
Receiver Path Loss	α_r	dB	RF Source & Power Meter	
Video Output Level	-	V	Oscilloscope	Saturated receiver level
Receiver Transfer Function	-	V/dB	Signal Injection	Receiver dynamic range
AGC/STC Factors	-	dB	Signal Injection	Dynamic variable
Antenna Beamwidths	-	deg.(°)	Antenna range	(V&H) (3 dB one-way)
Antenna Gain	G	dBi	Antenna range	Manufacturer data
Antenna Polarization	Pol.	-	Antenna range	Manufacturer data
Antenna Scan Rate	-	Hz	Period counter	Rapid scan only
Antenna Scan Width	-	deg.(°)	Antenna Range	Vendor data
Antenna Beam Centering	-	deg.(°)	Antenna Range	Vendor data

A3.5.2 Receiver Transfer Function

The recorded signal generator injection calibration data will be digitally processed to produce a calibration table relating received power to digitized receiver output. This table describing the receiver's output response to received power levels is called the receiver transfer function. Calibration data from an FMCW radar will be FFT converted to remove d-c and near-carrier noise from the amplitude value. Pulsed radar calibration data will be averaged to improve the accuracy of each table value. The calculations will also compensate for any AGC, STC, or signal processing gain factors involved.

A3.5.3 Calibration Conversion

The calibration conversion process will reduce raw radar reflectivity data to different degrees, depending on how the results are to be used in analysis. All raw data files for analysis will be converted into received power values using the receiver transfer function table. Most performance evaluation will involve comparisons of received power from different resolution cells within the measurement scene. Selected sensor data files will be further processed into calibrated RCS, and for clutter areas, into normalized RCS. This additional data reduction processing will provide the "engineering" data that characterizes the MMW radar reflectivity of the test measurement scene.

A raw data file consists of an array of data values collected during one antenna scan for the resolution cells within the measurement scene. Receiver transfer table calibration of the raw data files is accomplished by interpolating each uncalibrated data point between adjacent steps in the calibration table. There should be a one-to-one correspondence between the raw digital counts and received power. Raw data values in amplitude counts are converted into received power in milliwatts. For the baseline measurement files, the received power values will be further converted into RCS using the standard radar range equation solved for RCS (s). The data array entries for received power and slant range are substituted into the equation, along with the appropriate radar parameters from the specification table. The resulting RCS file is an array of resolution cells containing calibrated RCS values in square meters. The resolution cells that match locations of the calibration reflectors will be used as calibration check points. RCS values from those resolution cells covering clutter areas in the scene will be normalized to the area in the cell. The processed RCS files will be available for feature extraction or image generation purposes.

A3.6 Test Data Matrix

A test data matrix has been developed to address the sensor performance analysis objectives of image generation capability under a variety of weather conditions. Table A3-2 presents five classes of parameters, or test variables, in the order of decreasing dominance to the test schedule. The brassboard test sensors will be installed and tested one at a time, so this parameter will vary the least often. A given sensor will be tested under the maximum number of weather conditions available during the installation period. Variability is desired for the degree of each specific weather condition, so each condition is subdivided into light, medium, and heavy ranges, bounded by the limits of likely weather conditions. This weather variability is the most difficult parameter for the TTD to monitor in the decision process of when to collect sensor data. A variety of targets and clutter are present in every sensor data file collected. The measurement scene coverage area is fixed, so every data file contains returns for all ranges and scan angles within the scene area.

TABLE A3-2 DATA MATRIX PARAMETERS

Parameter	Selections
Sensor	Radars - Lear 94 GHz, Honeywell 35 GHz, Norden 94 GHz, Hughes 35 GHz
	Passive Infrared - Kodak
Weather	Clear, fog, rain, snow
Variability	Fog visibility - < 0.5, 0.5 to 1, 1 to 1.5 mi. (related to drop size distribution)
	Rain rate - 1, 5, >10 mm/hr (w. short-term variability) (related to drop size distributions)
	Snow fall rate - 2, 5, 10, 20 mm/hr (using optical gauge)
Targets	Runway, taxiway, calibration targets, & obstructions (extracted from scene data)
Geometry	Slant range 0.7 to 6 km (grazing angles 7° to 1°)

A3.7 Data Reduction

The recorded radar sensor data will be processed through several steps, including reformatting and calibration, before the performance features are extracted. The data reduction process converts the raw sensor data files into the performance feature data base, as detailed in Figure A3-2.

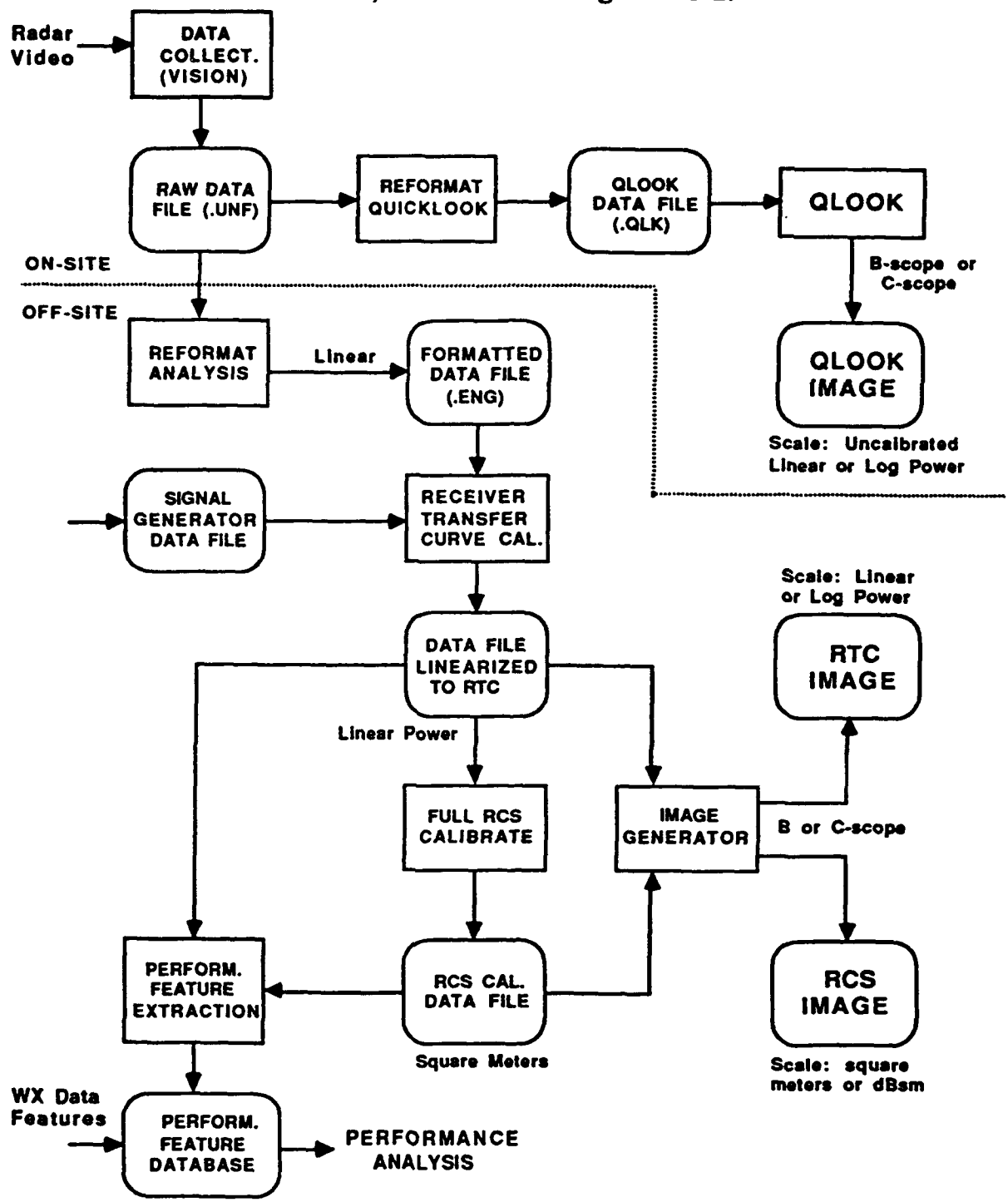

Figure A3-2 Sensor Data Reduction Process

Sensor display images will be generated on-site with quick-look graphics software, or off-site during sensor data analysis. Display images are the best way to present total sensor performance for comparison over a variety weather conditions. Quick-look processing performed on-site requires data reduction steps similar to those performed off-site, but limited to producing quick-look images. In both cases, the raw sensor data must be reformatted before additional processing. Quick-look images will be uncalibrated, but the off-site data reduction process includes two stages of calibration, receiver transfer curve correction and full RCS calibration. Sensor performance features will be extracted from reduced data files in each of these two calibration formats, and processed images will be generated from each file format.

As described in Section A3.3, the primary radar data and primary imaging data will follow parallel processing and storage paths until the sensor performance features are extracted into a performance data base. The extracted features will be combined in the data base with secondary sensor data, supporting data, and reduced meteorological data. The data base will support the analysis of test sensor performance in various weather conditions, with tabular and graphical output formats.

A3.7.1 Data Reformatting

Primary radar data recorded with the LeCroy DAS will have to be reformatted and calibrated prior to extraction of sensor performance features and combination with supporting data. Primary imaging data from a radar Digital Signal Processor (DSP) or a FLIR sensor will be in perspective format, and will not need to be reformatted. Radar data reformatting will be tailored to the type of radar sensor under test. Data reformatting will reduce the size of the data files through data integration and removal of any redundant data. The resulting data arrays will have a standardized format to be compatible with later processing stages.

Data recorded from an FMCW radar are in frequency-amplitude format, and must be converted into slant range-amplitude format before further processing. Data reformatting will use the Fast Fourier Transform (FFT) to accomplish this conversion. The FFT process provides coherent integration that improves signal-to-noise ratio (S/N) of the FMCW radar data. To equalize this signal processing advantage, the pulsed radar data will be pulse-to-pulse averaged to give a comparable S/N improvement. The actual data integration period for each radar sensor should be equal to the expected antenna beam dwell time on a point target during scanning. At equal antenna scan rates, an antenna with a wider azimuth beamwidth will have a longer dwell time on target than an antenna with a narrower beam. So, a longer data integration period should be allowed for the radar having a greater dwell time on target. A non-coherent pulsed radar produces data in range vs. amplitude format, so no conversion is needed. A coherent pulsed radar provides two quadrature data channels that will be combined during reformatting into a single amplitude channel.

A3.7.2 Feature Extraction

Performance feature extraction is the last sensor data processing step prior to the sensor performance database. This step is necessary to reduce the volume of data that has to be managed by the performance database. Extracted features are numeric values developed from the processed sensor data arrays that provide specific measures of sensor performance, such as scene contrast or resolution. Reformatted sensor data files are arrays of received power values for each resolution cell over the entire instrumented scene area. The whole array is needed to develop scene images that map every resolution cell into display image pixels,.but only small subsets of the data array are needed to compute sensor performance in weather. The small array subsets, called patches, are clusters of contiguous resolution cells from which a local average value of received power can be calculated. Table A3-2 presents ten major radar features that will be extracted into the performance data base. The averaged receive power values in RTC calibrated files are then used to compute the five radar performance features. Radar engineering values are similarly computed, but after applying RCS calibration correction to the averaged power values from the patches. Engineering values are the five features that will be extracted from the RCS calibrated files. The engineering values characterize the measurement scene phenomenology, while the performance features describe sensor response to the measurement scene in weather.

TABLE A3-3 EXTRACTED RADAR FEATURES

Name	Symbol	Units	Factors	Analysis Use
Radar Performance Features				
Noise Power	P_n	A/D counts	none	Min. detectable signal
Clutter/Noise Ratio	C/N	none (or dB)	P_C/P_n	Scene contrast
Clutter Contrast	C/C	none (or dB)	P_{c1}/P_{c2}	Image contrast
Range Resolution	ΔR	meters	P_{r2}, P_{r4}	Resolution cell area
Azimuth Resolution	ΔA	degrees or meters	P_{r4}, P_{r5}	Resolution cell area
Radar Engineering Values				
Radar Cross Section	σ	square meters (m^2)	calibration	Detection range
Normalized Area RCS	σ_0	m^2/m^2 (none)	cal. & resolution	Performance estimate
RCS Contrast*	T/C	none (or dB)	σ or σ_0	Scene contrast
Norm.Volume RCS*	σ_v	m^2/m^3 (m^{-1})	cal. & resolution	Performance estimate
Path Attenuation*	α	dB/km	σ_1, σ_2, σ_3	Detection range

* These features also indicate radar sensor performance.

A3.8.0 Sensor Performance Analysis

The sensor tower tests and subsequent data analysis will establish basic performance for the prototype and brassboard Synthetic Vision sensor systems against engineering standard targets and an example airport scene under a variety of weather conditions. Sensor data collection and data analysis requirements have been developed to satisfy the sensor tower test program

objectives. Those objectives are 1) assessments and recommendations of sensor suitability for flight testing, 2) documenting absolute performance in observed weather, and 3) documenting sensor performance versus optical extinction.

A3.8.1 Sensor Suitability

To be suitable for flight testing, the test sensor must produce a runway scene image with sufficient resolution and contrast to serve as a landing aid. This sensor imaging capability can be demonstrated in the tower test environment for the weather conditions experienced during the test period. The vendor's scan converter, if available for the tower tests, will provide real time imaging of the measurement scene on a television monitor. Additionally, the TTC will produce evaluation images from the raw radar sensor data in a process that emulates the sensor vendor's scan converter. Quick-look images will be available on site within minutes of data collection, and calibrated images will be generated at the TTC facility during performance analysis activities. The monochrome television monitor images can be photographed or recorded on videotape for later review and comparisons. To aid in image evaluation, the TTC will provide weather condition summaries from the raw meteorological data to correspond with each processed image. When determining suitability for flight testing, the test sensor's electrical and mechanical configuration and construction will also be considered.

A3.8.2 Absolute Performance

Absolute sensor performance in weather will be documented through detailed analysis of the recorded sensor data and time-correlated meteorological data. Sensor performance will be evaluated against the #89-04-PMRN requirements for runway imaging, and also, evaluated against the theoretical limits of operation. Numeric evaluation of sensor performance requires establishing figures of merit (FOM) related to mission requirements, and include image contrast, image resolution, and weather penetration. FAA guidelines for human visual performance state that a 5% image contrast ratio is necessary for runway detection. Raw sensor contrast will be measured as the difference in received power from the runway and surrounding grass areas of the scene. The same scene areas will be compared in the processed display image to establish a signal processing improvement factor. Optimum contrast and resolution will likely be achieved in clear weather conditions, when there are no airborne particles to attenuate and mask returns from the scene areas of interest. This baseline sensor performance will be compared with scene imaging capability in adverse weather to determine the degradation due to specific meteorological conditions. Further, the measured in-weather sensor performance will be compared with that calculated from a theoretical mathematical model of electromagnetic propagation.

A3.8.3 Optical Extinction

For Synthetic Vision to be a viable adverse weather landing aid, the SV sensor image must provide an improvement in runway detection range over the pilot's own vision. The range to optical extinction, or runway visual range (RVR), will be compared to the SV sensor's maximum detection range to establish a figure of SV improvement. An SV radar sensor's maximum detection range in weather will be the range at which the image contrast ratio between runway and

grass drops to 5%, or some other minimum detectable value. This "MMW extinction" range will be extracted from either the raw sensor data or the processed images. If RVR cannot be measured with the normal long-baseline optical gauge, the RVR will be calculated from the liquid water content and drop size distribution meteorological data.

A3.8.4 Performance Prediction

Radar sensor response in clear weather to clutter and in-scene reflector targets will be predicted using the measured radar specifications and the radar range equation. Estimating the normalized RCS (s_0) for clutter will permit calculation of the expected target-to-clutter and clutter-to-noise received power ratios. The effects of volumetric RCS (s_v) for precipitation and atmospheric attenuation (a) will also be included, using available mathematical models for those environmental effects on radar. The in-scene reflector targets will be sized and placed, based on estimated radar performance. The radar sensor performance prediction for a specified test scene will be compared with the measured results to verify correct operation of the sensor and data collection system.

A3.9 Presentation of Results

Sensor data analysis results will present measured sensor performance for all the weather conditions under which measurements were made. Engineering data describing the radar reflectivity of the measurement scene will be included to establish the sensor performance capabilities described for this example airport scene. The end products will include interim and final technical reports, and any significant intermediate results will be presented in technical memoranda or briefings to the government. Primary sensor performance will be plotted as detected scene contrast versus range for light, medium and heavy weather conditions. Calibrated engineering data will be formatted in tables and graphs, including RCS of surfaces, volumetric backscatter RCS, and atmospheric attenuation. Photographs of the calibrated B-scope and C-scope images generated during data processing will be presented for visual comparisons with the matching photographs of the visual scene. Conclusions will include strengths and limitations of sensor performance in weather, and recommendations for continuing the evaluation of each sensor into flight testing.

APPENDIX A4

TEST PLAN FOR INFRARED SENSORS

A4.1 Introduction

The Synthetic Vision Technology Demonstration Project is testing various sensors, including a millimeter wave radar and a PtSi focal plane array camera operating in the 3 to 5 micron infrared band, for detecting runways in poor visibility conditions. This plan establishes test procedures for evaluating the performance and suitability of the infrared sensor for detecting a runway under a variety of conditions. It is intended as a supplement to the original Tower Test Plan (WL/FIGL, 3 May 1991). Conditions such as measurement geometries and available instrumentation and calibration sources constrain the test possibilities. These limitations have been incorporated into the plan.

A4.2 Goals

The test is designed to demonstrate the performance of the IR sensor under carefully documented low visibility conditions and compare it with clear weather baseline performance and the performance of the millimeter wave system. Low visibility conditions should include fog, rain, and snow as conditions permit. A key issue in the performance of the IR system is the atmospheric contrast attenuation under various weather conditions. Analysis will attempt to quantify the available contrast under both standard linear response operation and with manufacturer supplier image enhancement algorithms. A further goal will be to compare these contrasts with the millimeter wave data under identical weather conditions and determine the preferred system for various types of adverse weather conditions.

A4.3 Test Site

The runway and taxiway which serve as the objects for the camera are located in area B of Wright Patterson Air Force Base, Ohio. The camera and other instruments are located on the 10th floor of the tower of building 620 at WPAFB at a level of about 84 meters above the runway. The slant range from the camera to the closest point on the runway is approximately 1250 meters and to the far end of the runway is about 3100 meters. The angle of the runway is such that it spans a horizontal angle of 18 degrees and a vertical angle of 2.5 degrees from the tower test chamber. The runway is about 50 meters wide by 2400 meters long. It is paralleled by a taxiway 25 meters wide by 2150 meters long. The runway surface is pitted asphalt, the taxiway is weathered concrete, and the adjacent background area is long bent grass, currently dormant.

A4.4 Meteorological Data

The Tower Test Plan (WL/FIGL, 3 May 1991) defines a set of meteorological data which will be collected to support the evaluation of sensors under various weather conditions. In the case of infrared radiation, weather conditions have a twofold impact on the observed scene. Atmospheric transmission of the radiation from runway and adjacent background areas will be diminished in poor visibility conditions resulting in a lowered apparent contrast at the sensor. In addition, changes in weather conditions will impact the inherent temperatures and

contrast between the runway and background at zero range. There will be conditions and times of day when the zero range contrast between runway and background is minimal even for high atmospheric transmission. It is important that the baseline set of clear weather tests include a sufficient variety of times of day, cloud cover conditions, and wind speeds and air temperatures to determine the extent of these zero inherent contrast situations.

In addition to the meteorological data defined in the tower test plan, it is necessary to know the approximate cloud cover and height, and the variance of the runway/taxiway area from clean and dry conditions. Therefore, the logbook must contain an estimate of the amount in eighths and height for low (0-6,000 ft), middle (6,000-18,000 ft) and high (above 18,000 ft) clouds at hourly intervals during the test or more often if conditions are changing rapidly. the logbook will also be annotated to describe the scene in terms of wet surfaces from rain, standing water, dew, frost, snow, etc.

A4.5 Calibration Sources

In an ideal test situation, a minimum of two large area temperature controlled reference sources would be placed within the scene and their temperatures monitored as part of the ground truth data. These known sources would help separate atmospheric transmission effects from weather induced changes in runway and background temperatures.

A more realistic alternative and the method to be used is to place a single large area high emissivity passive element in the scene and monitor the temperature with a thermocouple. The temperature of this reference element will fluctuate with environmental conditions, but shall be available for analysis purposes from the ground truth log.

In addition, a dual point calibration of the infrared camera tem will be obtained with a smaller fast reacting laboratory blackbody source ated in the tower near the camera positioned to fill the aperture with the camera focused at infinity. This will require turning the camera before and after each runway measurement sequence to record the indoor reference source. The temperatures of the blackbody shall be set to span the range of temperatures encountered in the outdoor scene. This may require some iterative adjustments to the blackbody source temperature and comparisons with the outdoor scene.

The combination of the controlled source at near zero range and the one large uniform ambient temperature reference point within the scene will permit a quantitative analysis of the scene imagery.

A4.6 Data Collection

A4.6.1 Types of Data Recorded

Each measurement series shall include a set of indoor reference source measurements to characterize the functioning of the infrared camera. These measurements shall be performed before and after each change of camera settings and no less than once every 8 hours. The specific procedures for initiating

the camera system parameters will be as follows:

(a) Turn on Auto Gain, Level and any desired contrast enhancement.

(b) Record a 30 second image of the test site, plus 3 digital frames.

(c) Reset camera to manual gain, level, enhancement off.

(d) Recalibrate with lens cap on.

(e) Remove lens cap and record a 30 second image of the test site, plus 3 digital frames.

(f) Aim camera at the blackbody.

(g) Record a 30 second image of the blackbody, plus 3 digital frames.

(h) Change the blackbody temperature and repeat step (g).

When runway tests from a moving vehicle are conducted, the two reference sources shall be moved to a location where they can be viewed from the vehicle prior to driving along the intended path. Configure sensor on a moving platform shielded from weather, but with an unobstructed view of at least 30 degrees azimuth. The procedure will be to drive the vehicle onto the beginning of runway (closest to tower), accelerate to 10 mph along center of runway, turn off the runway at the last exit, proceed along the center of the exit ramp, turn at the taxiway parallel to the runway, and proceed at 10 mph down the center of the taxiway. Follow procedures 6.1 (a) through (h) in collecting data, but record video data continuously.

A4.6.2 Data Recording Intervals

A4.6.2.1 Clear Weather Baseline

During the baseline clear weather period, imagery of the runway scene should be recorded at five minute to one hour intervals depending on runway-grass contrast to establish the variation of scene element temperatures with environmental conditions, particularly insolation. If data are recorded on video tape, about 30 seconds of imagery each interval should be sufficient. Direct digital readout is available from the camera, therefore, three frames of data will be recorded during each of the hourly readouts. The reason for three frames instead of one is to permit averaging of several frames to approximate the human visual system integration time of about 0.1 second. Scene variations will be minimal from about midnight to just before dawn. Data may be recorded at less frequent intervals during this period unless other environmental conditions such as cloud cover or winds are changing rapidly. Record data for a 24 hour period to cover the range of diurnal variation.

The clear weather baseline data shall include days with no clouds, days with partial overcast, and days with complete overcast. If abnormal winds or air

temperature variations are anticipated, data should be recorded under these conditions also.

Finally, record periods with wet ground from previous rain and snow covered ground. Follow procedures in 6.1 (a) through (h).

A4.6.2.2 In Weather

During low visibility weather, scene imagery shall be recorded at a frequency determined by the rate of changes in environmental parameters but at least once per hour. Each data point shall consist of about 30 seconds of video tape imagery and three digitized frames. Procedure 6.1 (a) through (h) will be followed to collect data.

A4.7 Data Analysis

The data reduction and analysis procedures will extract statistical parameters from various parts of the infrared image. The parameters and image regions will be selected to provide information on the available contrast between runway and background or other obstructions on the runway. They will include the mean and standard deviation of intensity values in each of the selected image regions, as well as maximum and minimum values.

Data reduction will be performed using directly captured digital outputs. However, in the case where only a video tape of the scene is available, digital frames will be extracted from several parts of the 30 second segment using a commercial frame digitizing device with a 512 x 512 pixel output.

The indoor blackbody reference source will establish a scale so that contrast can be described in terms of effective temperature differences or radiance differences. If automatic gain adjustments or image enhancement algorithms were invoked during the measurement of a particular frame, contrasts will be reported in relative image intensity units.

For the runway contrast analysis, the software shall permit the user to identify a number of small areas within the image and remember their locations within the frame for analysis of later frames. Because the camera is turned indoors between scene measurements, it is possible that the selected areas will not align with the intended features in a later image. The analysis software should include the possibility of specifying offset parameters to realign the polygons with the desired features in the new image if necessary.

Selected areas within the image shall include portions of the runway at various ranges from the tower. Because a single image will contain runway elements at ranges from 1200 to 3100 meters, at least four runway segments will be defined corresponding to ranges of approximately 1200, 1800, 2400, and 3000 meters slant range. Another set of polygons will outline background segments adjacent to the runway at about the same slant ranges. These pairs of polygons will be used to determine the contrast between runway and background as a function of slant range. If obstructions or other features of interest are present in the scene, they will also be marked by polygons for analysis. Although there is no

minimum polygon size for analysis, the areas should include enough pixels to lend significance to the statistical parameters extracted.

The tower blackbody can be analyzed in a similar manner. Intensity values from the controlled surfaces shall show a minimal standard deviation if the temperature distribution across the reference source was uniform. Mean intensity values can be associated with the temperature of each source to provide a two point calibration. The output of the infrared detectors in the camera system is linear with respect to irradiance, rather than object temperature. A two point linear calibration based upon the indoor blackbody source requires that the radiance values be calculated from their physical temperatures by the Planck equation. A linear irradiance versus intensity curve can be derived from these two points and used to calibrate the system response. Over small temperature intervals the non linearity of the temperature to radiance relation may be neglected and a first order linear temperature calibration established from the blackbody source.

Contrast values between runway and adjacent background shall be plotted as a function of slant range for each of the adverse weather conditions. Contrast shall be reported as apparent temperature difference if the camera was operated in the non automated mode and calibration source measurements are available at the same settings. For comparison with visible and millimeter wave data, however, a relative contrast value shall be more relevant. This is defined as

$$C_r = (I_r - I_b) / (I_r + I_b)/2$$

where I_r is the mean intensity from a segment of the runway and I_b is the intensity from an adjacent area of background. Meteorologists define the visible range as the point at which the contrast is less than 5%. This contrast can be negative as defined. Since runway detection does not depend upon the polarity of the image, the absolute value of the relative contrast may be the most useful parameter for performance evaluation.

Appendix A5

FUNCTIONAL TESTS AND PERFORMANCE TESTS
FOR LEAR ASTRONICS SENSOR

The radar system shall successfully demonstrate the below functional and performance features prior to continuing to task 3.

A. Functional Tests

1. Antenna Scan

Antenna shall scan +/- 15 degrees at 5 Hz minimum. Antenna shall respond to antenna control demands between -15 and +15 degrees in elevation while scanning in azimuth.

2. Transmitter Control

Each transmitter mode shall be demonstrated (using a spectrum analyzer) and the bandwidth measured.

3. Receiver Gain Control

The following tests shall be performed to verify that gain can be controlled manually, using an oscilloscope and spectrum analyzer connected to the video output:

- With the radar transmitting CW and the antenna pointed skyward, the video output shall be noted with the Radar Controller requesting 78 dB under manual gain control and repeated with the gain reduced in increments of 6 dB down to a value of 30 dB gain.

- To verify that the AGC function can be selected and that it has the expected effect of reducing the variation of the amplitude of the video signals while the antenna is scanning, the system shall be set with the antenna pointed down to approximately -5 deg. while scanning +/- 15 deg. in azimuth, manual gain control and 72 dB gain. The variation in the video signal on the oscilloscope shall be noted as the antenna scans. It shall then be switched to automatic gain control and the new limits on the video voltage noted.

4. Real-Time Display Control

To determine that image contrast and brightness can be controlled and to establish the limits of this control, ~~the antenna elevation angle will be adjusted to zero degrees~~, the antenna shall be set to azimuth scan at -5 degrees, the radar shall be set to transmit in the FM-2 mode, the AGC shall be set to automatic, and the values of GMIN and GMAX shall be adjusted while the effects on image contrast and brightness are measured.

The antenna elevation angle shall then be adjusted and the effects of elevation angle on the region of the image best illuminated by the antenna shall be determined. The optimal elevation angle for scene illumination shall also be determined.

Each of the programmed Sensitivity Time Constant (STC) values shall be tested to determine which one produces the best image.

B. Performance Tests

1. Image

The receive/transmitter, antenna, DSP and radar control unit which comprise the enhanced sensor system shall be demonstrated to be capable of operating to produce an image from which features such as the runway, taxiway, roads, fences, grass and buildings are discernible and sufficient to permit runway identification at a minimum range of 2 km, to support a pilot's decision to land at 2 km, and to support landing of an aircraft.

Specific tests to be performed are described below.

2. Signal-to-Noise Ratio

Demonstrate that a 10 m^2 corner target signal-to-noise ratio is 15 dB or better at approximately 3000 meters. This demonstration shall include an analysis of the noise floor. S/N measurement tolerance for this test is +/- 3 dB. The reflector is GFE.

To perform this test, measure the radar return at a fixed azimuth from a top hat radar reflector placed in a scene area of low reflectivity on the runway. Compare the power received from a 1 m^2 reflector target at 3 km range with the radar receiver noise floor. Alternately, use a larger radar reflector and subtract the difference in RCS between the reflector and 1 m^2 when calculating the S/N ratio. Measure the S/N power ratio with a spectrum analyzer connected to the radar receiver FM video output. Alternately, collect radar data using the GFE DAS or Lear Astronics DAS. Compare the magnitude of radar data in the resolution cell containing the reflector with the radar data from an adjacent cell having a magnitude determined by the noise floor of the receiver. Calibrate the data magnitude differences by collecting data from two radar reflectors having a known difference in RCS. Data averaging may be necessary to improve measurement accuracy with the data collection method. Averaging time must be identified for the calibration from two reflectors in adjacent cells.

3. Scan Rate

Demonstrate that the scan rate is >5Hz full cycle across a 30 degree field of view. Tolerance for this test is 10%.

To perform this test, measure the period of the antenna scan by monitoring scanner control signals on an oscilloscope. Calibrate the oscilloscope horizontal time base. Verify the scan width is 30 degrees by the scene geometry presented in the image. Convert the scan period into scan frequency.

4. Range Resolution

Demonstrate that the range resolutions for FM1, FM2, FM3 do not exceed 21 meters, 10 meters, and 5m respectively.

To perform this test, measure at fixed azimuth the return from two equal size reflectors placed one predicted range resolution cell apart. The reflector RCS should be significantly greater than the clutter in the area. Measure the depth of the amplitude null between the two

reflector returns using a spectrum analyzer connected to the receiver video. The spectrum analyzer should be set on the 1 mHz band with a frequency resolution of 1 kHz (one-half a radar resolution cell) or less. Increase the range separation of the reflectors by 25-50% of the predicted range resolution, and repeat the measurement. Determine at what range separation a 3 dB amplitude null if achieved.

5. Azimuth Resolution

Demonstrate that the azimuth resolution is consistent with a 0.38 degree beam width.

To perform this test, measure the return from a single reflector using a spectrum analyzer and slow pedestal scanning to determine the antenna beamwidth. The radar's azimuth resolution is defined by the antenna two-way 3 dB azimuth beamwidth. The reflector RCS should be significantly greater than the clutter in the area to reduce measurement errors. The spectrum analyzer should be set on the 1 mHz band with a frequency resolution of 2 kHz or less. The antenna should be moved left and right of the peak azimuth until the received amplitude is down 3 dB. Alternately, measure the return from two equal size reflectors placed one predicted azimuth resolution cell apart. Measure the depth of the amplitude null as the antenna azimuth is moved between the two reflector returns using a spectrum analyzer connected to the receiver video. Increase the azimuth separation of the reflectors by 25-50% of the predicted azimuth resolution, and repeat the measurement. Determine the azimuth separation at which a 3 dB amplitude null is achieved.

6. Signal Power Loss

Confirm that the loss in signal power varies as $1/R^4$ in clear air as proposed (0.4 dB per km attenuation assumed). Tolerance for this test is +/-3 dB.

Two or more radar reflectors will be placed at different ranges and the difference in measured received power will be compared with calculated values. The reflector RCS should be significantly greater than the clutter in the areas to reduce measurement errors. Either the spectrum analyzer or the DAS system can be used as the analysis tool.

7. Contrast

Determine the range at which a contrast of 3 dB between the runway and grass can be found in clear air. The minimum requirement is 2 km; the goal is 3 km or greater.

In measuring contrast, the grass will be defined as the "background" and at least 7 points in azimuth (at a given range) shall be averaged to determine the "average background" and the variance. These samples shall contain grass only.

8. Scene Registration

Confirm that scene registration is accurate within one beamwidth and does not vary with changes in left/right antenna scan direction.

9. Scene Geometry

Confirm that the geometric relationships of the objects within the image presented in the C scope presentation are accurate and that the lines are straight. Tests shall be carried out with the antenna mount in a level condition and tilted +/- 10 degrees in roll.

10. Sidelobe Management

Confirm that antenna azimuth first side lobes are less than 13 dB near to the main lobe and range side lobes shall be less than 20 dB, to prevent smearing.

11. Radar Power

The transmitter shall be connected to test equipment as determined to be appropriate by the Air Force Test Team and the power output of the transmitter measured at the flange of the wave guide and recorded. This measurement shall be made at the same port at which the gain of the antenna is measured. Absolute power level measurement accuracy is estimated to be +/- 1dB with the currently available HP power meter. The contractor may conduct this test at their facility prior to initiation of Task 1. In this case, the test must be witnessed by the Government or their representatives and data provided to the Government.

12. Receiver Sensitivity

Using a test configuration as determined to be appropriate by the Air Force Test Team, and with the transceiver set to CW mode and maximum gain, a signal will be injected into the receiver pass band. The frequency will be adjusted to maintain the signal in-band while the signal amplitude is adjusted to give 10 dB signal-to-noise ratio in a 150 kHz bandwidth. If a measurement cannot be accomplished at 150 kHz bandwidth, a different bandwidth may be used, subject to approval of the Air Force Tower Test Director. The minimum detectable signal shall be defined as being 10 dB less than this signal amplitude. The minimum detectable signal shall be measured and recorded at an initial receiver gain of 78 dB and at subsequent receiver gain levels decreasing in 6 dB increments to a value of 30 dB. Test accuracy is +/- 3 dB. The contractor may conduct this test at their facility prior to initiation of Task 1. In this case, the test must be witnessed by the Government or their representatives and data provided to the Government.

These measurements will be performed with the radar transmitting so that the homodyne mixer will be operating under near normal conditions. The antenna shall be disconnected so that any contributions to the noise floor from spill-over via the antenna will not be observed. The signal level shall be measured at the transceiver output with a spectrum analyzer.

13. Latency

Latency, defined as the period of time from the start of an antenna sweep until the time its complete video frame is displayed, shall be determined. Representative image patterns, that fully exercise the image processing algorithms, will be stored in a DSP EPROM. A change from one image to another will be commanded by a discrete signal, at which time the image data will be fed

to the DSP, not all at once, but piece wise at the rate of the FFT process working with a scanning antenna. The time period from the discrete signal command to the resulting change in RS-170 output pattern shall be measured. Total system latency shall be confirmed to be less than 200 milliseconds.